UNIVERSIDAD
Ð CÓRDOBA

Doctorado en Biociencias y Ciencias Agroalimentarias

Structure and dynamics of chromosomes: role in the genomic and pathogenic plasticity of *Fusarium oxysporum*

Estructura y dinámica de los cromosomas: papel en la plasticidad genómica y patogénica de *Fusarium oxysporum*

Lucía Gómez Gil

Dirigido por:

Dr. Antonio Di Pietro

Catedrático de Universidad

Córdoba, Mayo 2022

TITULO: *Structure and dynamics of chromosomes: role in the genomic and pathogenic plasticity of Fusarium oxysporum*

AUTOR: *Lucía Gómez Gil*

Campus de Rabanales
Ctra. Nacional IV, Km. 396 A
14071 Córdoba

https://www.uco.es/ucopress/index.php/es/
ucopress@uco.es

TÍTULO DE LA TESIS: Structure and dynamics of chromosomes: Role in the genomic and pathogenic plasticity of *Fusarium oxysporum*

DOCTORANDO/A: Lucía Gómez Gil

INFORME RAZONADO DEL/DE LOS DIRECTOR/ES DE LA TESIS

(se hará mención a la evolución y desarrollo de la tesis, así como a trabajos y publicaciones derivados de la misma).

La Tesis Doctoral de Dña. Lucía Gómez Gil se ha llevado a cabo en el Departamento de Genética de la Universidad de Córdoba, en el seno del Grupo "Genética molecular de la patogénesis fúngica" (BIO-138). Su desarrollo ha permitido a la doctoranda adquirir una sólida formación en Genética y Biología Molecular. Durante la realización de la Tesis, Dña. Lucía ha mostrado tener una gran capacidad de trabajo y aptitud para la investigación científica. En el trabajo se ha llevado a cabo, por primera vez, una caracterización detallada de las regiones teloméricas en el hongo fitopatógeno *Fusarium oxysporum*. Además, se han investigado los mecanismos subyacentes a la elevada plasticidad cromosómica en este organismo que favorece la rápida adaptación a nuevas condiciones ambientales, incluyendo la planta huésped. Los resultados obtenidos se han comunicado en varios congresos internacionales, y una parte de ellos se ha recogido en un artículo publicado en la revista Current Genetics.

Por todo ello, se autoriza la presentación de la tesis doctoral.

Córdoba, 24 de Mayo de 2022

Firma del director

DI PIETRO ANTONIO COSTANTE - X1583221Q

Digitally signed by DI PIETRO ANTONIO COSTANTE - X1583221Q
Date: 2022.05.24 13:17:04 +02'00'

Fdo.: Antonio Di Pietro

INDEX

LIST OF FIGURES

LIST OF TABLES

ABSTRACT

Fungal pathogens have developed a wide range of mechanisms allowing rapid adaptation to different environments. The vascular wilt pathogen *Fusarium oxysporum* f. sp. *lycopersici* (*Fol4287*) infects the roots of tomato plants by activating a series of mechanisms that are induced in the presence of nitrate, the most abundant form of inorganic nitrogen in soils. Here we characterized knockout mutants in nitrate assimilation genes and found that Nit1 as accounts for the major nitrate reductase activity, while Nit2 and Nit3 only have minor contributions. During growth on different nitrogen sources, we observed the formation of colony sectors which appeared to be the result of genomic instability. Following these findings, a study was initiated to understand the physical structure and dynamics of chromosomes in *Fol4287*. Previous studies had revealed that the genome of this isolate is compartmentalized into core regions and accessory regions, which are highly dynamic and have been associated with host adaptation. We found that the subtelomeric regions of *Fol4287* are highly conserved and contain two genes of unknown function, *FOXG_15616* and *FOXG_15617* genes as well as a *copia*-type retrotransposon, similar to those reported previously in the rice blast fungus *Magnaporthe oryzae*. Since previous whole-genome sequencing of serially passaged strains had detected recurrent copy number variations (CNVs) in certain accessory chromosomal regions, we performed karyotype analysis by CHEF and Southern blot to monitor chromosomal dynamics and molecularly characterize CNVs. This revealed the presence of previously unrecognized duplicated regions that are shared between accessory chromosomes in *Fol4287*. Different methodologies were set up for measuring the frequency of chromosome loss in *Fol4287*, both in the wild type strain and in mutants affected in DNA repair or chromatin structure. Our results indicate that the spontaneous mitotic loss frequency of an accessory mini chromosome in *Fol4287* can be as high as 1%, and that the stability of such accessory regions may be promoted by H3k9me3 histone methylation.

RESUMEN

Los patógenos fúngicos han desarrollado una amplia gama de mecanismos que les permiten una rápida adaptación a diferentes ambientes. El patógeno *Fusarium oxysporum* f. sp. *lycopersici* (*Fol4287*) causante del marchitamiento vascular infecta las raíces de las plantas de tomate activando una serie de mecanismos que se inducen en presencia de nitrato, la forma de nitrógeno inorgánico más abundante en los suelos. Aquí caracterizamos los mutantes knockout en los genes de asimilación de nitrato y descubrimos que Nit1 representa la principal actividad de la nitrato reductasa, mientras que Nit2 y Nit3 solo tienen contribuciones menores. Durante el crecimiento en diferentes fuentes de nitrógeno, observamos la formación de sectores de colonias que parecían ser el resultado de inestabilidad genómica. Tras estos hallazgos, se inició un estudio para comprender la estructura física y la dinámica de los cromosomas en *Fol4287*. Estudios previos habían revelado que el genoma de este aislado está compartimentado en regiones centrales y regiones accesorias, que son altamente dinámicas y se han asociado con la adaptación al huésped. Encontramos que las regiones subteloméricas de *Fol4287* están altamente conservadas y contienen dos genes de función desconocida, los genes *FOXG_15616* y *FOXG_15617*, así como un retrotransposón de tipo-*copia*, similar a los informados previamente en el hongo del añublo del arroz *Magnaporthe oryzae*. Dado que la secuenciación anterior del genoma completo de cepas sometidas a pasajes en serie había detectado variaciones recurrentes en el número de copias (CNVs) en ciertas regiones cromosómicas accesorias, realizamos análisis de cariotipo por CHEF y Southern blot para monitorear la dinámica cromosómica y caracterizar molecularmente las CNVs. Esto reveló la presencia de regiones duplicadas previamente no reconocidas que se comparten entre los cromosomas accesorios en *Fol4287*. Se establecieron diferentes metodologías para medir la frecuencia de pérdida cromosómica en *Fol4287*, tanto en la cepa de tipo silvestre como en mutantes afectados en la reparación del ADN o en la estructura de la cromatina. Nuestros resultados indican que la frecuencia de pérdida mitótica espontánea de un mini-cromosoma accesorio en *Fol4287* puede llegar al 1%, y que la estabilidad de tales regiones accesorias puede ser promovida por la metilación de la histona H3k9me3.

INTRODUCTION

INTRODUCTION

1. Fungal pathogens

One of the most significant economic factors affecting crop production is the occurrence of infectious diseases in plants. Among the potential infectious agents, such as bacteria, viruses, fungi and nematodes, fungal plant are by far the most devastating. The search for productivity and cost-effectiveness in agriculture has led to a reduced species diversity, which favours the spread of a single adapted fungal pathogen lineages and massive crop damage (Covo, 2020). For instance, in the first half of XXth century, the banana cultivar Gros Michel, which was attacked by a new race of the ascomycete fungus *Fusarium oxysporum* f. sp. *cubense* (Tropical Race 1), was globally replaced by the resistant cultivar Cavendish. In the last decade, a new aggressive strain of *F. oxysporum* f. sp. *cubense* Tropical Race 4 emerged that can infect the previously resistant clone Cavendish, representing a severe threat to the global banana industry (Garcia-Bastidas *et al.*, 2014). Although the use of fungicides has helped to mitigate fungal pathogen infections, it is increasingly controversial due to the potential adverse effects on human health and biodiversity as well as the emergence of fungicide-resistant strains (Korolev *et al.*, 2011), which can decrease the effectiveness of medical treatments to fungal infections in humans and animals.

Fungi are a large and diverse group of eukaryotic organisms that differ from plants and animals in how they obtain nutrients. Since fungi lack chloroplasts, they can only obtain energy through organic compounds. Moreover, fungi are osmotrophic, which means that they absorb nutrients from the surrounding environment (Dyakov and Zinovyeva, 2007). These features have determined their characteristic mycelial structure, with branched hyphae that maximise their ability of absorption and substrate occupation. Most fungal plant pathogens belong to the Ascomycete and Basidiomycete phyla, which can infect a wide range of crop species. Plant pathogens use different infection strategies, allowing to categorize them into biotrophs, necrotrophs and hemibiotrophs. Biotrophs are those pathogens that manipulate plant defences to obtain the nutrients from living cells by using specialized structures called haustoria, formed within the host cell. On the other hand, necrotrophs obtain the nutrients needed to grow and reproduce from dead plant cells, which have been killed through the release of toxins and enzymes secreted by the pathogen. The third group, hemibiotrophs start their life cycle as biotrophs and later switch to a necrotrophic lifestyle (Möller and Stukenbrock, 2017).

The colonization of plants by fungal pathogens is the net result of the plant defence response and the action of virulence effectors secreted by the pathogen. In addition to different physical and chemical barriers used by plants, specific defense proteins are produced in response to effector-mediated signals to avoid pathogen infections. Fungal pathogens use different strategies to overcome plant defences, which range from manipulating host gene transcription to interfering with plant metabolism. As a result of these interactions, both the host and the pathogen are subjected to a co-evolution process, which can differ depending on the type of ecosystem where the interaction takes place.

Our knowledge of plant-fungus interactions has considerable advanced in the past two decades thanks to genetic and genomic approaches (Crous *et al*., 2015; Zhang *et al*., 2017). The estimated number of fungal species is around 3 million and only 100,000 are recognized. With the advent of light microscopy in the XIXth century, the morphological characterization of fungal spores was used to classify similar fungal pathogens based on the plant species they infect. Some fungi such as *Fusarium*, that are morphologically identical but are host-specific, were named using the term 'special forms' (*formae speciales*, f.sp.). But the morphological characterization of fungi was not completed until the mid XXth century, when Transmission Electron Microscopy (TEM) and Scanning Electron Microscopy (SEM) were developed. The advances in computing technology together with the use of DNA data in the 1990s made possible to establish phylogenetic relationships between different fungi species, although some events such as species hybridization or horizontal transfer events, or full or partial loss of chromosomes, are often not reflected in the phylogenetic trees. The use of genome analysis can help to solve these shortcomings, as it will be shown below in the results obtained in this PhD Thesis.

2. Fusarium oxysporum

The genus *Fusarium* comprises a group of ascomycete filamentous fungi from the class Sordariomycetes, order Hypocreales, family Nectriceae, that encompasses mycotoxin producers and plant pathogens that sometimes are capable of infecting humans as opportunistic pathogens to cause fusariosis (Ma *et al.*, 2013). Plant diseases associated with these fungi encompass wilts, blights, rots, and cankers on different crops. During their action, *Fusaria* produce secondary metabolites named mycotoxins, such as trichothecenes and fumonisins. The consumption of food products contaminated with these mycotoxins poses a sevee risk for human health, owing to their carcinogenic and teratogenic effects (Qu *et al*., 2022). The reproduction in *Fusaria* can be sexual (meiotic spores) or asexual (mitotic spores)

depending on the species complex, although less than 20% have a known sexual stage (Ma *et al.*, 2013)

A robust phylogenetic analysis of the genus revealed 20 *Fusarium* species complexes with economic relevance that include about 300 species (O'Donnell *et al.*, 2013). These fungi originated ca. 91.3 Mya ago, at the same time as flowering plants (Smith *et al.*, 2010). Figure 1 shows the age estimates for the origin and diversification of the 20 Fusarium species complexes. Highlighted in blue are those for which the ability to infect humans has been reported at least for one species of the complex.

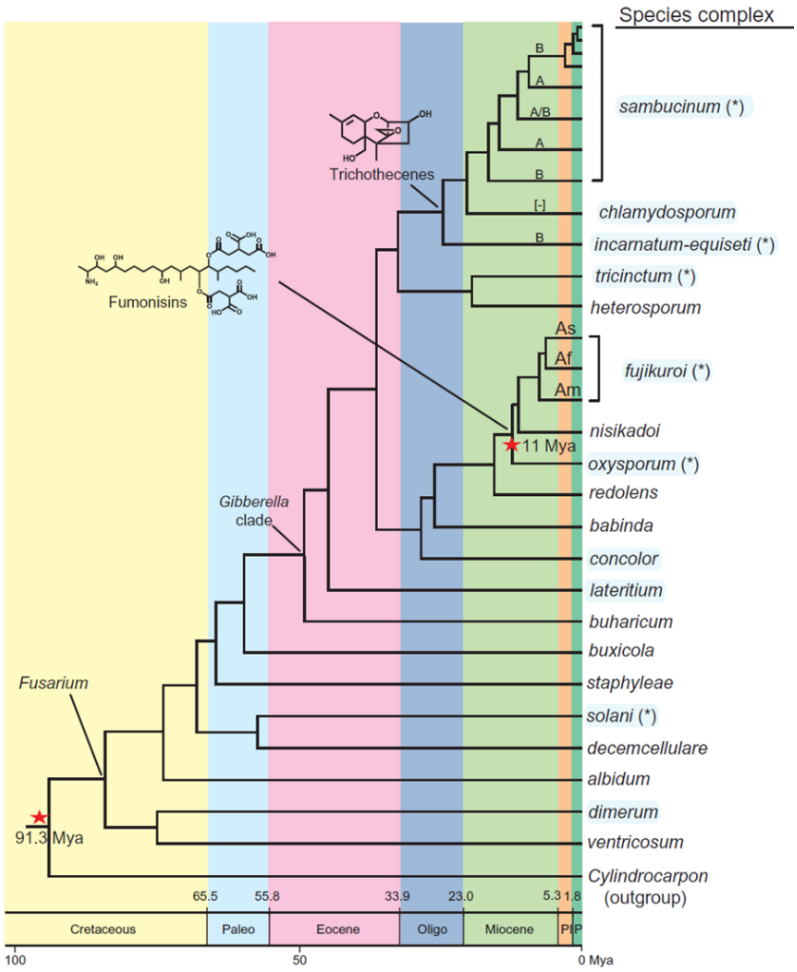

Figure 1. Chronogram of divergence time and origins of the 20 *Fusarium* species complexes. (Zhang *et al.*, 2017).

The *F. oxysporum* species complex constitutes a broad family of fungi widely distributed in soils and aquatic environments (Bell and Khabbaz, 2013) that can infect more than 150 plant species (Rana *et al.*, 2017). *F. oxysporum* can also infect immunocompromised

patients causing fusariosis disease that show corneal (O'Donnell *et al.*, 2004) and dermal (Veiga *et al.*, 2022) infections in humans.

Plant infection by *F. oxysporum* is host-specific, with a given isolate causing disease only a single single plant species. This has led to a particular classification system for members of the *F. oxysporum* species complex that incorporates the term *forma specialis* (abbreviated as f.sp.). Table 1 lists *formae speciales* infecting some food producing crops (Rana *et al.,* 2017). The list also includes *F. oxysporum* f. sp. *lycopersici (Fol)*, which infects tomato and whose chromosome structure and dynamics has been studied in this work.

Table1. List of *F. oxysporum* formae speciales (ff. spp.) infecting some food crops, (Adapted from Rana *et al.*, 2017).

	Crop host	
f. sp.	Botanical name	Common name
albedinis	*Phoenix dactylifera*	Date palm
asparagi	*Asparagus officinalis*	Asparagus
batatas	*Ipomoea batatas*	Sweet potato
cepae	*Allium spp.*	Onion
Ciceris	*Cicerarietinum*	Chickpea
cubense	*Musa spp.*	Banana
cucumerinum	*Cucumis sativus L.*	Cucumber
lycopersici	***Lycopersicon esculentum***	**Tomato**
meloni	*Cucumis melo L.*	Muskmelon
Pisi	*Pisum spp.*	Pea
spinaciae	*H Spinacia oleracea L.*	Spinach
tuberosis	*Solanum tuberosum L.*	Potato

Each *forma specialis* may originate from a single ancestor (monophyletic *forma specialis*) or from different clades (polyphyletic *forma specialis*) and can be further subdivided into pathogenic races that are classified according to differential virulence on different host cultivars (Rana *et al.,* 2017). *Fol* has three different races with virulence/avirulence phenotypes that have successively evolved (e.g. race 2 originated from race 1), but the origin of the ancestral *Fol* race remains unknown (Biju *et al.,* 2017).

2.1 Life cycle

F. oxysporum grows as a hyphal colony with a delicate white to pink mycelium, often with chlamydospores, microconidia and macroconidia spores which are mitotic and asexual (Figure 2.1). Chlamydospores are one- or two-cell spherical soilborne spores originated from hyphae or macroconidia modification that can survive for long time as dormant propagules owing to their thick cell wall. *F. oxysporum* may propagate through the air as microconidia, which are small and abundant, oval-ellipsoid shaped and uninucleate spores

produced on structures called conidiophores. Macroconidia are sparse to abundant, produced mainly on the surface of the plants killed by the pathogen, and borne as aggregates in the sporodochium or on branched conidiophores on the aerial mycelium, with three- to five septae, pointed at both ends, with a pedicellate base. Three-septate macrospores are most common (Ma *et al.*, 2013; Srinivas *et al.*, 2019, Toussoun and Nelson, 1976). The infection by *F. oxysporum* starts with root colonization after triggering the germination of fungal spores and chemotropic sensing of peroxidase signals released by plant roots and the invasion occurs mainly between root surface cells. The initial colonization happens through a biotrophic phase, where hyphae growing mainly intercellularly in the root cortex (Figure 2.2) (Redkar *et al.*, 2022).

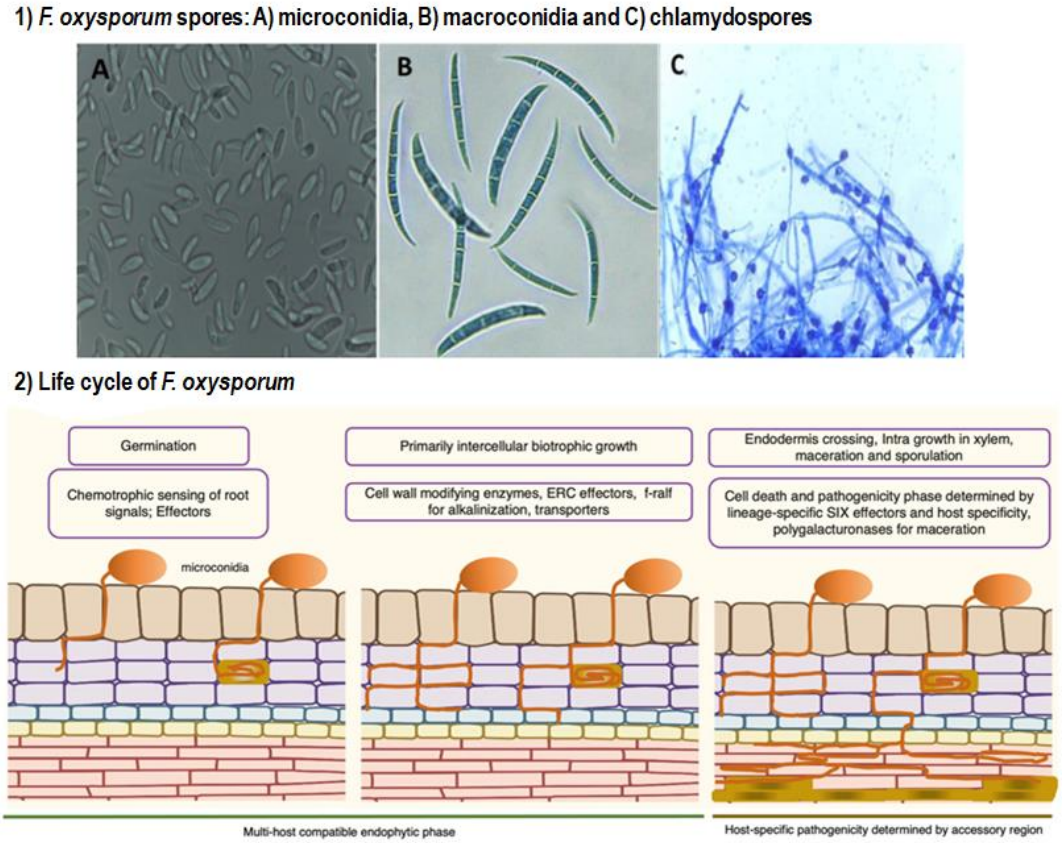

Figure 2. In (1) *F. oxysporum* spores and in (2) life cycle. (Fig. 2.1 adapted from Cardona-Piedrahita *et al.,* 2019 and Fig 2.2 adapted from Redkar *et al.,* 2022).

Then, the fungus follows a path of colonization through the xylem vessels by entering through the xylem pits, resulting in rapid plant colonization. Within the xylem, the fungus produces hyphae and microconidia, which germinate and colonize the upper vascular vessels, leading to disease symptoms such as wilting. In the later stages of infection, the fungus propagates through parenchymatous tissue and begins to sporulate abundantly on the

macerating host tissue, enhancing its propagation by though the soil, transplants, etc. This second step is characterized by a transition from endophytic to pathogenic growth starting with endodermis crossing and colonization of xylem vessels. All these steps are conditioned by the extent of the defence response by the host plant and the action of pathogen virulence effectors. Although extensive research has been performed to elucidate plant-pathogen interactions, there are still many unknowns, such as how the fungus obtains nutrients from the plants in the initial biotroph phase.

2.2. Pathogenicity mechanisms

Plant-pathogen interactions are governed by pathogenicity factors of the fungus and defence mechanisms of the host (Figure 3). Either plant or pathogen use a series of factors to defend and colonize, respectively (Ma *et al.*, 2013; Rana *et al.*, 2017).

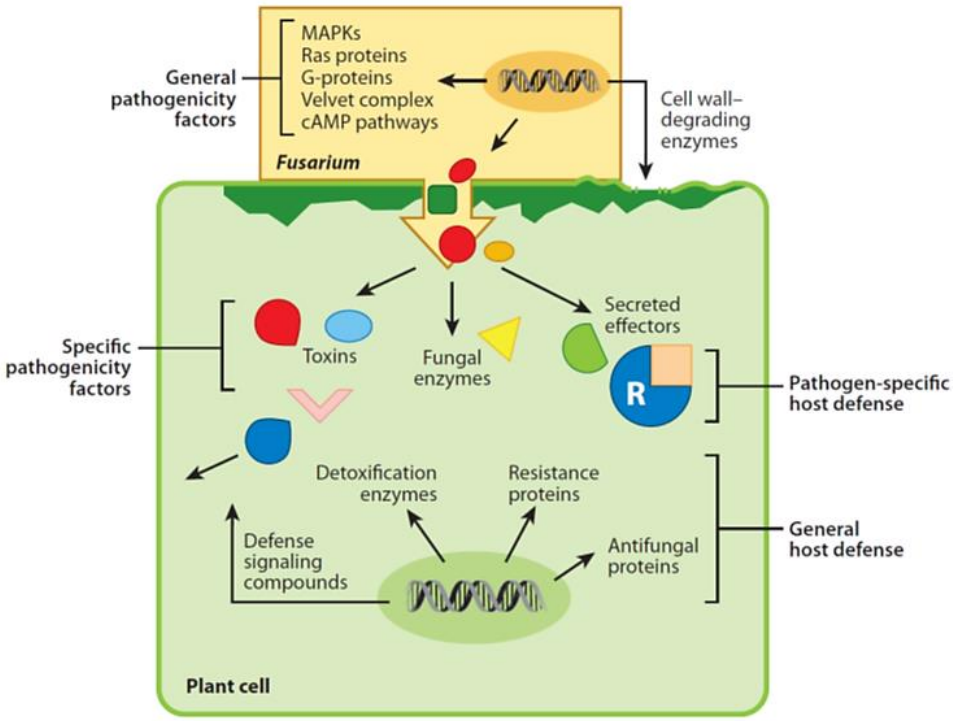

Figure 3. Fusarium pathogenicity and host defence mechanisms (from Ma *et al.*, 2013)

The factors involved in *Fusarium* infection include the secretion of lytic enzymes to break the physical barriers of the plant cell wall as well as the fungal cellular signalling pathways that regulate invasive growth and adaptation to the host niche. Additional pathogenicity factors are the secretion of fungal effectors and host-specific phytotoxins. Plant defence mechanisms which play a significant role in pathogenesis include the

production of antifungal proteins, the activation of defence signalling pathways, the recognition of fungal effectors by resistance genes or the detoxification of phytotoxins.

2.2.1. Effector proteins

Fungal pathogens secrete small proteins that deregulate plant immune responses and facilitate host colonization. There are two types of fungal effectors: 1) apoplastic, when they are secreted into the extracellular space around the plant cells, and 2) cytoplasmic, when they are translocated into the plant cell. Apoplastic effectors include inhibitors that inactivate plant proteases or chitinases. Pathogens also secrete proteases such as serine protease 1, which inactivates extracellular tomato chitinases (Jashni *et al.*, 2015). *Fol* encodes a tomatinase enzyme that cleaves α-tomatine, a plant compound that disrupts the fungal plasma membrane (Pareja-Jaime *et al.*, 2008).

Virulence-determining effectors typically reside in the accessory chromosomes of fungal plant pathogens. Some of the best characterized effector proteins in *Fol* are the "secreted in xylem" (SIX) proteins. *Fol* secretes 14 different small cysteine-rich SIX proteins (Rep *et al.*, 2003; Rep *et al.*, 2004; van Dam *et al.*, 2016). These effector genes reside on accessory chromosome 14, also known as the "pathogenicity" chromosome, which can be transferred between strains, determining their virulence capacity. The proteins SIX1, SIX3, SIX5 and SIX6 are essential for full virulence of *Fol*. SIX1 and SIX3 are directly involved in root colonization and hyphal growth in the xylem. The effector genes that encode SIX proteins have shown to be *forma specialis*-specific, and some SIX proteins are recognized by the plant as race-specific avirulence (AVR) factors (van Dam *et al.*, 2016). For example, SIX4 is AVR1, while SIX3 is AVR2 and SIX 1 is AVR3, the avirulence factors that interact with the resistance genes of tomato I-1, I-2 and I-3, respectively. Thus, the *Fol* proteins SIX1 and SIX3 are recognized by the tomato receptor-like kinases I-3 and I-2 in the nucleus and function as resistance proteins to induce tomato defences (Rep, 2005; Rep *et al.*, 2005).

2.3. Pathogen-host arms race

The use of genomic data contributes to understanding the evolution of fungal pathogens, since they allow the identification of the genes subjected to selective pressure by identifying polymorphism and the distribution of substitutions and the proportions of non-synonymous and synonymous mutations in coding sequences (Möller and Stukenbrock, 2017). This allows to estimate alterations in translated proteins derived from nucleotide changes in the coding sequence. Bearing this in mind, two different types of co-evolution, namely 'trench warfare' and 'arms race' may be responsible for the pathogen genetic

variation. The 'trench warfare' scenario usually occurs in natural ecosystems where natural selection favours the presence of different alleles in pathogen populations that are spatially separated (Möller and Stukenbrock, 2017). This set of alleles is maintained at the co-evolving locus at balanced frequencies in the population. Similarly, genetic variation of resistance genes is maintained by balancing selection. The 'arms race' scenario involves the successive and rapid replacement of pathogen alleles (selective sweep) in the population because of the development of new resistance alleles in the host. Selective sweeps generally provoke a decrease of genetic variation and a homozygosity excess owing to the accumulation of new unique mutations.

The gene-for-gene interaction between *Fol* and tomato fit the 'arm race' model as depicted in Figure 4 (Takken and Rep, 2010). Thus, non-specialized strains of *F. oxysporum* which colonize roots are recognized by plant receptor-like kinases that trigger PAMP (Pathogen associated Molecular Pattern)-triggered immunity (Figure 4a). Host-specific fungal effectors such as SIX3 (AVR2), SIX1 (AVR3) or SIX6 promote the disease in tomato. Then, tomato plants evolve the I-2 and I-3 resistance receptors AVR2 and AVR3 which specifically recognize the virulence effectors (Figure 4b). The pathogen then may use one two approaches: (i) AVR2 mutates to avoid recognition by the tomato resistance protein without changing its virulence effector properties or (ii) a new effector, AVR1, evolves to suppress I-2 and I-3 resistance action (Figure 4c). Finally, tomato I and I-1 resistance proteins evolve to recognize AVR1 so the plant is again protected (Figure 4d). This scenario appears to have occurred over millions of years, although so far only a few polymorphisms have been found in SIX genes from *Fol* strains worldwide. This homogeneity seemed to be contradictory with the proposed genome adaptation scenario. However, the fact that all *six* genes are contained in a single chromosome that can be transferred between clonal lines may contribute to explain this homogeneous distribution (Van Der Does *et al.*, 2008).

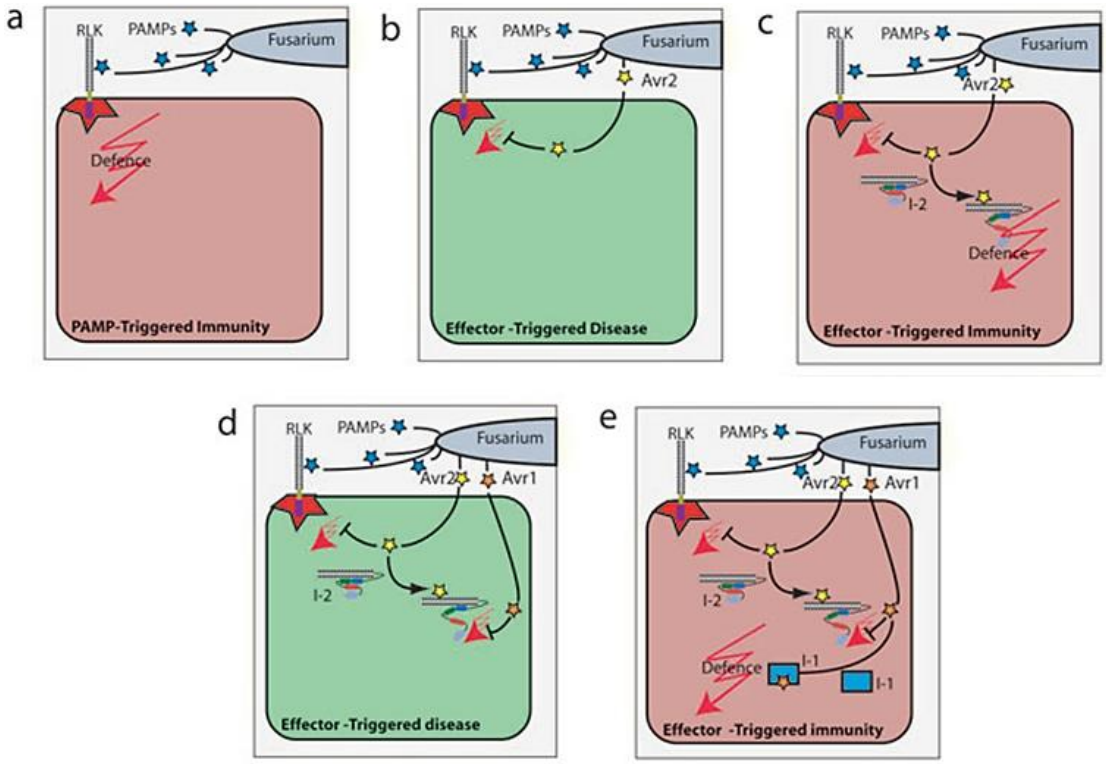

Figure 4. Arms race between *F. oxysporum* and tomato. (Adapted from Takken and Rep, 2010).

3. Genome organization in fungal pathogens

Fungal pathogen genomes are compartmentalized into two structurally separate regions: the core and the accessory region. The core region, necessary to carry out housekeeping functions in the organism, is highly conserved among isolates of the same species and even among closely related species. The accessory region, unlike the core region, shows high variability, so the degree of conservation between species differs. These regions have features that differentiate them from the core regions such as a lower number of genes, abundance of repeated elements (including transposable elements) and different histone methylation patterns (Ma *et al.,* 2010; de Jonge *et al.,* 2013; Yang *et al.,* 2020; Fokkens *et al.,* 2018). It has been widely described that these features are responsible for the accessory regions to accumulate chromosomal rearrangements and mutations more quickly than the core regions. Based on this, it has been suggested that these accessory regions present a faster rate of evolution, influencing the adaptive capacity of the fungus, a term known as a "two-speed" genome (Raffaele and Kamoun, 2012; Dong *et al.,* 2015). However, recently, this concept has been questioned, showing that the effector genes present in these accessory regions do not always have a faster rate of evolution and finding that two-speed genome evolution does not have an exclusive benefit for plant pathogens (Torres *et al.,* 2020).

A comparative genome sequencing and analysis of three different *Fusarium* species, *F. graminearum* (*Fg*), *F. verticillioides* (*Fv*) and *Fol* isolate 4287 revealed that the size of *Fol4287* genome was about 60 Mb, containing 17,735 genes located on 15 chromosomes, while the number of chromosomes in *Fv* and *Fg* was 11 and 4, respectively. The smaller number of chromosomes in *Fg* in comparison to *Fv* and *Fo* was explained by chromosome fusion, while the higher number of genes in *Fol* was explained by unique sequences present in the accessory genome region. It was found that the core genome shared by the of the three *Fusarium* species occupied 11 out of the 15 chromosomes of *Fol*.

The *Fol* lineage specific (LS) or accessory chromosomes are constituted by unique sequences, which make up about 40% of the *Fol* genome assembly (Ma *et al.*, 2010). This accessory genome is constituted by chromosomes 3, 6, 14 and 15, as well as by scaffold 27 of chromosome 1 and scaffold 31 of chromosome 2 and some unpositioned scaffolds not included in the chromosome assembly. These accessory regions include a huge number of transposable elements (TEs), selfish genetic elements with the ability to insert into new regions of the genome. Depending on the types, TEs use a cut-and-paste or a copy-and-paste mechanism to propagate in the genome and their activity is a main factor of genome expansions (Fouché *et al.*, 2022). The accessory chromosome 14 was shown to be transferred from *Fol* to a non-pathogenic *F. oxysporum* isolate thereby conferring virulence toward tomato plants (Ma *et al.*, 2010). Horizontal gene transfer can be defined as the stable integration of DNA elements from one individual to another, and the transfer of full chromosomes between pathogenic as well as non-pathogenic fungi can occur (Mehrabi *et al.*, 2017). It was later shown that the pathogenicity functions transferred are located only the short arm of chromosome 14 of *Fol* (Vlaardingerbroek *et al.*, 2016). Further experiments using partial deletion strains were used to narrow down the regions that are essential for tomato infection, showing that virulence was even higher after partial than for the complete pathogenicity chromosome transfer (Li *et al.*, 2020b).

A recent re-sequencing of the genome of the *Fol4287* strain (Ayhan *et al.,* 2018) revealed divergences with the first sequencing deposited in the database (Ma *et al.,* 2010), which fundamentally affected the accessory regions of the chromosomes 1, 3, 6 and 15 and also at one end of chromosome 13. A high degree of homology was detected between the 0.7 Mb accessory region present on chromosome 1 and a region on chromosome 15, both regions being noted separately as 1&15. In the same way, a common region was detected between accessory chromosomes 3 and 6 and whose difficulty in assigning it to one of the two chromosomes caused it to be annotated separately as region 3&6. Finally, the presence

of a duplicated region corresponding to the right end of chromosome 13 was detected. A more in-depth analysis of these events is discussed in this phD work.

4. Mechanisms of genome plasticity

Fungal pathogens exhibit a high genomic plasticity that implies changes in the structure and organization of the genome. When the organism faces stressful situations, instability of the genome is produced that leads to an increase in genetic diversity and confers an adaptive advantage to the new environment. The biggest source of genetic variability is the existence of a sexual cycle. However, many organisms, including some fungal pathogens, lack a sexual cycle. This could indicate that these organisms have a lower evolutionary potential, however, many mechanisms have been described that contribute to the increase in genomic plasticity and an increased adaptive capacity (Seidl and Thomma, 2014; Mat Razali *et al.,* 2019; Buscaino, 2019). Here we describe the main mechanisms underlying this variability.

4.1. Structural variations: aneuploidy and polyploidy

A mechanism responsible for the genomic variability detected with increasing frequency in the genomes of fungal pathogens is the presence of structural variations (SVs) (Stranger *et al.,* 2007; Zhang *et al.,* 2009; de Jonge *et al.,* 2013; Wang *et al.,* 2020). SV events can involve partial or full chromosomes. The first group includes balanced SVs that do not involve gain or loss of DNA, such as reciprocal translocations, inversions and fusions. However, some SVs are unbalanced leading to a loss or gain of genetic material and therefore to copy number variation (CNV). Examples of this type of SVs are large insertions, deletions, non-reciprocal translocations and duplications. Aneuploidy and polyploidy are the most extreme cases of SVs, that produce CNVs at a large scale involving entire chromosomes (Gorkovskiy and Verstrepen, 2021).

CNVs involve insertions and deletions ranging from 50 bp to complete chromosomes and constitute an essential mechanism of adaptive evolution through the establishment of genotypic and phenotypic diversity (Steenwyk *et al.,* 2018). On a small scale, variability in stress-related genes has been reported in numerous organisms. Wine yeast cells can form aggregates to increase their survival in conditions of lack of oxygen, being able to float in the medium and thus achieve a greater supply of oxygen. This process known as flocculation is controlled by the FLO gene family, with both duplication and deletion of these genes reported as a strategy to favour survival (Fidalgo *et al.,* 2006; Steenwyk and Rokas, 2017).

At large-scale, ploidy changes involve alterations in chromosome copy number. Aneuploidy is an imbalance of the genome due to the loss of large chromosome segments or entire chromosomes. It has been reported in several fungi that in certain stress situations, aneuploidy can be a quick and transitory solution to adapt to these conditions (Naranjo-Ortiz and Gabaldón, 2020; Yona *et al.,* 2012). In yeast populations, it has been described that in the presence of high concentrations of copper, the cells are capable of duplicating large chromosomal regions to increase the number of copies of the genes responsible for copper regulation, thus increasing tolerance to this toxic compound. Furthermore, this type of aneuploidy was observed to reverse when the yeasts are grown under less selective conditions (Chang *et al.,* 2013).

Another type of large-scale CNV is polyploidy, the process by which an organism has two or more complete sets of chromosomes relative to the haploid karyotype. When an organism duplicates its own chromosomes, it is called autopolyploidy (same genotype), while if this increase in the number of chromosomes is produced by the combination between two species, it is referred to as allopolyploidy (different genotype) (Otto, 2007; Todd et al., 2017). In fungi, fewer cases of polyploidization than in plants or animals have been detected because they show a faster evolution rate and greater genomic variability, making it difficult to trace polyploidy (Soltis *et al.,* 2015; Kenny *et al.,* 2016; Naranjo-Ortiz and Gabaldón, 2020). One hundred million years ago, the genus *Saccharomyces* arose through an allopolyploidization process that involved the duplication of the whole genome and hybridization between different species (Wolfe and Shields, 1997). A pathogenic fungus that shows high chromosomal copy number plasticity is *Candida albicans*. Normally, it is in a diploid state, however, in response to certain conditions, it can alter its ploidy, reaching a tetraploid state that can later revert to the initial diploid state through a process known as "concerted chromosome loss" (Hull *et al.,* 2000; Bennett and Johnson, 2003). Many organisms that have undergone whole-genome duplication show chromosomal instability due to an abnormal mitosis process. Recently, a high rate of DNA damage during S-interphase has been shown in human cells due to their tetraploid state, showing a direct link to tumorigenesis (Gemble *et al.,* 2022).

4.2. DNA damage

One of the main causes of genome instability is DNA damage, either spontaneously or induced, resulting in DNA double-strand breaks (DSBs). To maintain genome integrity, different DSB repair pathways are activated, with Homologous Recombination (HR) and Non-Homologous End Joining (NHEJ) DNA repair pathways constituting the two main

mechanisms. The HR pathway is based on the existence of homology between two sequences and involves the invasion of broken DNA strands in a homologous DNA duplex molecule (Krejci *et al.,* 2012). On the other hand, the NHEJ pathway directly joins the two ends of the DNA without requiring the existence of homology and can generate errors during repair that include small insertions or deletions (Lieber, 2010). Alternatively, the DSBs can be repaired by Single-Strand Annealing (SSA) pathway, that also requires homologous sequences and that entails the remove of the region between both repeats (Featherstone and Jackson, 1999; Bhargava *et al.,* 2016). If DSBs cannot be repaired, loss of genetic material and shorter chromosome versions will occur (Mehrabi *et al.,* 2017).

A recent study in *Streptomyces* revealed that the repair mechanisms of DSBs increase the diversity of the genome contributing to its evolution (Hoff *et al.,* 2018). Inducing the formation of DSBs, it was found that during the repair mechanism, loss of chromosome ends and extensive deletions were produced, suggesting that DSBs underlie genomic plasticity. It has also been reported that knockout mutants in some genes involved in DNA repair in *S. cerevisiae* show increased genomic instability that manifests itself in many ways, including structural variations, point mutations and aneuploidies (Serero *et al.,* 2014).

4.3. Epigenetic mechanisms

Organisms with a higher and faster capacity to adapt to environmental conditions usually show differences in the structure of their genome, presenting stable core genomic regions and accessory regions with a more dynamic behavior. Epigenetic changes play a critical role in the establishment and maintenance of genomic compartments and contribute to genome plasticity and evolution. Thus, the dynamic compartments are enriched in heterochromatin which is generally characterized by reduced transcriptional activity and appears to contribute to the suppression of recombination (Grewal and Jia, 2007; Harr *et al.,* 2016). Despite this, the accessory regions of many fungal pathogens enriched in heterochromatin marks are the ones that show the greatest instability (Seidl *et al.,* 2016; Möller *et al.,* 2019). It has been suggested that the greater genetic variation in these regions is due to the existence of polymorphisms and DNA mutations that cannot be repaired efficiently due to the greater compactness of the chromatin. This makes it difficult for proteins involved in DNA repair mechanisms to access, making these regions more susceptible to DNA breakage, which in turn contributes to a higher rate of chromosome rearrangements and CNVs (Sasaki *et al.,* 2014; Sun *et al.,* 2016).

Heterochromatin in fungal pathogens is associated with histone modifications that include the trimethylation of lysines 9 and 27 of histone 3 (H3K9me3, H3K27me3) (Freitag,

2017). In *Z. tritici* it has been shown that, although both epigenetic marks contribute to the formation of heterochromatin, they influence the stability of the genome in different ways (Möller *et al.,* 2019). Knockout mutants in the *kmt1* and *kmt6* genes, which encode the methyltransferases responsible for H3K9me3 and H3K27me3, respectively, were generated. The Δ*kmt1* mutant showed higher genomic instability due to a higher frequency of chromosomal rearrangements and transposon activation. In contrast, the Δ*kmt6* mutant showed greater genomic stability, suggesting that the presence of the H3K9me3 mark is necessary to maintain genomic stability, while H3K27me3 leads to chromosomal instability. Another study with knockout mutants in these same genes confirmed that the spontaneous mutation rate in the *Z. tritici* genome is increased in the presence of the H3K27me3 epigenetic mark (Habig *et al.,* 2021).

4.4. Telomeric and subtelomeric regions

Telomeres are nucleoprotein structures found at the ends of chromosomes and are made up of short tandem repeats (Zakian, 1996; Blackburn, 2001). The sequence that makes up the telomere is highly conserved from vertebrates to fungi such as *Aspergillus nidulans*, *Neurospora crassa* and also *Fusarium oxysporum* and consists of a tandem repeat of the hexameric sequence "TTAGGG" (Moyzis *et al.,* 1988; Bhattacharyya and Blackburn, 1997; Wu *et al.,* 2009; Garcia-Pedrajas & Roncero, 1996). The presence of telomeric regions is essential to ensure genome stability by preventing DNA loss during the conservative replication process (Vodenicharov and Wellinger, 2006). It has been reported that their shortening can lead to chromosomal instability and their total loss generates DNA damage and chromosomal fusions caused by double-strand breaks (DSBs) that are not efficiently repaired by the previously discussed HR and NHEJ pathways (Heacock *et al.,* 2007; Longhese, 2008). Another mechanism that causes telomere instability is the presence of retrotransposable elements called MoTeRs that are inserted within the tandem repeats, as has been described in *M. oryzae* (Starnes *et al.,* 2012; Rahnama *et al.,* 2020).

The regions adjacent to the telomeres are known as subtelomeres and are characterized by having a region more proximal to the telomere with the presence of genes duplicated at multiple chromosomal ends and another distal region that contains short tandem repeats (Pryde *et al.,* 1997). The subtelomeric regions, and to a lesser extent, the telomeric regions, constitute gene reservoirs, among which are contingency genes and species-specific genes, that allow rapid adaptation of organisms to different environmental conditions. Contingency genes are common in pathogenic organisms, being found in species of the *Fusarium* genus regions with avirulence genes close to telomeres and whose structure

has been maintained due to the existence of chromosomal rearrangements (Barry *et al.,* 2003; Cuomo *et al.,* 2007). These subtelomeric genes can undergo mutations and modulate their expression to overcome the immune barrier imposed by the host, revealing their great involvement in adaptation processes (Barry *et al.,* 2003).

The other genes involved in this adaptive process are species-specific genes that appear to arise by duplication and then diverge so that they are shorter than the core genes. In *Aspergillus fumigatus*, the existence of genomic islands enriched in this type of genes and transposable elements has been described, facilitating the adaptation of the fungus to very diverse environmental conditions, from the soil to the animal host (Fedorova *et al.,* 2008).

4.5. Transposable elements

Repetitive DNA elements constitute one of the main sources of variability in the genomes. Due to the high degree of homology, they enhance recombination and genomic rearrangements (Hedges and Deininger, 2007). There are several types of repetitive DNA elements, among which transposable elements (TEs) stand out, although we can also find mini and microsatellites (tandem repeats), multicopy gene families, segmental genomic duplications and pseudogenes (Mehrabi *et al.,* 2017).

Many fungal genomes have a high content of TEs, some of which are capable of transposing to other regions of the genome while others lack mobility. Those TEs that encode the enzymes necessary for transposition are known as autonomous TEs while non-autonomous TEs lack these enzymes and thus depend on other elements for transposition (Wessler, 2006; Mat Razali *et al.,* 2019). Depending on the nature of the mechanism used for mobilization and transposition, TEs can be classified into different classes and subclasses (Finnegan, 1989; Wicker *et al.,* 2007). Class I or retrotransposons use an RNA sequence as an intermediate that is reverse transcribed by the enzyme reverse transcriptase to cDNA, which subsequently integrates into the genome. As new copies of TEs are generated during this process, it is known as "copy and paste" mechanism. Within the class I TEs we find two main groups depending on whether they carry long terminal repeats (LTR-retrotransposons) or not (non-LTR retrotransposons). Within this last group the SINE and LINE retrotransposons are short or long intercalated nuclear elements, respectively (Wessler, 2006; Pray, 2008).

Class II includes DNA transposons that integrate into the target site either by direct excision ("cut and paste", subclass I) or by generating a copy ("copy and paste", subclass II). The inverted terminal repeats (ITR) that some members of this class of TEs present, are

recognized by the enzyme transposase responsible for their excision later insertion in another region of the genome, leaving a gap that is filled by repair enzymes generating a short duplicated sequence, characteristic of this type of TEs (Craig *et al.,* 2002; Mat Razali *et al.,* 2019).

As a result of transposition, TEs can generate small-scale changes such as modulation of gene expression when inserted into promoter regions or even gene inactivation due to insertion into the coding region (Seidl and Thomma, 2014). However, TEs also involve large-scale changes and chromosome rearrangements including translocations, duplications, inversions, and deletions (Gray, 2000; de Jonge *et al.,* 2013; Torres *et al.,* 2021; Lorrain *et al.,* 2021). The variability generated by TEs has contributed to shaping and configuring the architecture of fungal genomes, originating regions through the invasion and subsequent expansion of TEs that lead to an increase in the genome size (Stukenbrock and Croll, 2014; Möller and Stukenbrock, 2017; Fouché *et al.,* 2022). This phenomenon could have occurred in *Fol*4287, whose genome consists of 15 chromosomes and a total size of 60 Mb with a high content of repetitive sequences, including TEs. In contrast, as previously commented, the genomes of *F. verticillioides* and *F. graminearum* are smaller in size with 42 Mb and 36 Mb and a total of 11 and 4 chromosomes, respectively. Importantly, 74% of the TEs detected in Fol4287 are in the accessory regions of the genome, indicating that this compartmentalization and expansion of the genome may have been the result of the TE activity (Ma *et al.,* 2010; Stukenbrock and Croll, 2014).

It is considered that the activation and mobilization of TEs occurs in response to stress conditions to favour the adaptation of fungi to new environments (Capy *et al.,* 2000). Fungal plant pathogens experience stress during the host plant infection process, secreting effector molecules to overcome immune barriers (Ferreira *et al.,* 2006; Hernández-Chávez *et al.,* 2017). In stable environments, TEs are subject to epigenetic silencing; however, under stress situation such as the plant infection process, chromatin remodelling occurs, leading to increased expression of TEs and associated effector molecules (Figure 5). Thus, pathogenic fungi can overcome the host's immune barriers and penetrate their cells (Fouché *et al.,* 2022).

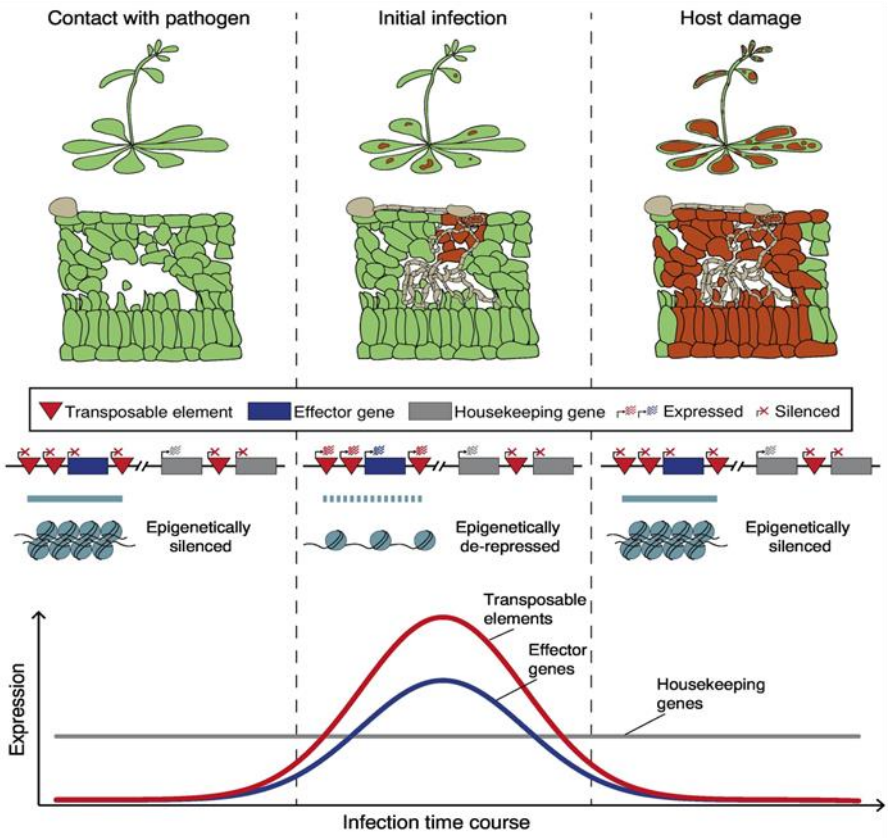

Figure 5. Epigenetic de-repression mediates transposable element activity. During the initial stages of infection, an epigenetic de-repression occurs that leads to increased expression of TEs and associated effectors necessary to ensure colonization of the host plant. (Adapted from Fouché *et al.,* 2022).

4.6. Parasexual recombination

While these are the main reported mechanisms for genome variability, others may be used by fungal pathogens to adapt to new environments including horizontal gene and chromosome transfer and parasexual recombination. Parasexual recombination has been reported as an adaptation mechanism for ineffective meiotic processes (Sherwood and Bennett, 2009). The parasexual cycle is a recombination process alternative to meiosis, where two compatible strains fuse their hyphae to share nuclei and cytoplasmic components in such a way that recombination of genetic material can happen. This behaviour has also been reported in fungi from the genus *Fusarium* that lack sexual cycle, such as *Fol4287* and involves the transfer of pathogenicity among different *Fol4287* strains (Teunissen *et al.,* 2002).

4.7. Horizontal gene or chromosome transfer

This mechanism allows the integration of DNA fragments or chromosomes from an individual to another individual of the same or different species. This exchange of genetic

material can facilitate adaptation to novel niches. For example, the transfer of chromosome 14 of *Fol4287* can convert a non-pathogenic strain into a virulent pathogen (Ma *et al.*, 2010). This behaviour is unique for chromosome 14 of *Fol4287* and it has been suggested that it occurs by hyphal fusion and parasexual recombination. For other accessory chromosomes, the transfer frequency is negligible or much lower than for chromosome 14. Core chromosomes could also exhibit horizontal transfer but always when chromosome 14 is involved (Vlaardingerbroek *et al.*, 2016).

Collectively, the above mechanisms affect genome diversity that can explain the rapid evolution of fungal pathogens as well as provide information on pathogenicity factors.

AIMS OF THE STUDY
OBJETIVOS DEL ESTUDIO

AIMS OF THE STUDY

The goal of the present study was to generate new knowledge on different aspects related to genome plasticity in the fungal pathogen *Fusarium oxysporum* f. sp. l*ycopersici* (*Fol4287*). For this purpose, the following topics were addressed:

1) Effect of environmental factors such as nitrogen content of culture media, on the generation of spontaneous colony growth variants in *Fol4287* as an indicator of genome plasticity.
2) Structural characterization of chromosome ends including telomeres and subtelomeres to assess their contribution to chromosome stability. Characterization of their physical structure and role of the subtelomeric genes in chromosome stability.
3) Characterization of chromosome rearrangements associated with genome plasticity of *Fol4287*.
4) Identification of changes in the copy number of accessory regions and monitoring frequencies of chromosome loss and gain using different experimental approaches under several environmental conditions.
5) Identification of the mechanisms underlying copy number variations and chromosome rearrangements.

OBJETIVOS DEL ESTUDIO

El objetivo del presente estudio fue generar nuevo conocimiento sobre diferentes aspectos relacionados con la plasticidad del genoma en el hongo patógeno *Fusarium oxysporum* f. sp. *lycopersici* (*Fol4287*). Para ello, se abordaron los siguientes temas:

1) Efecto de factores ambientales como el contenido de nitrógeno de los medios de cultivo, sobre la generación de variantes de crecimiento espontáneo de colonias en Fol4287 como indicador de la plasticidad del genoma.
2) Caracterización estructural de los extremos cromosómicos, incluidos los telómeros y subtelómeros, para evaluar su contribución a la estabilidad cromosómica. Caracterización de su estructura física y papel de los genes subteloméricos en la estabilidad cromosómica.
3) Caracterización de los reordenamientos cromosómicos asociados con la plasticidad del genoma de Fol4287.
4) Identificación de cambios en el número de copias de regiones accesorias y seguimiento de frecuencias de pérdida y ganancia de cromosomas utilizando diferentes enfoques experimentales en varias condiciones ambientales.
5) Identificación de los mecanismos subyacentes a las variaciones del número de copias y reordenamientos cromosómicos.

MATERIALS AND METHODS

MATERIALS AND METHODS

1. Strains and plasmids

Fungal and bacterial strains, as well as the plant cultivars used in this work are described in (Table 2).

Table 2. Fungal and bacterial strains and plant cultivars used in this study.

Specie	Strain	Features	Reference
Fusarium oxysporum	Fol4287	Wild type (f.sp. lycopersici, Race 2)	FGS(1)
	Δ*nit1*	Deletion of nitrate reductase gene *nit1*. Hyg^R	(Gómez-Gil *et al.*, 2018)
	Δ*nit2*	Deletion of nitrate reductase gene *nit2*. Hyg^R	(Gómez-Gil *et al.*, 2018)
	Δ*nit3*	Deletion of nitrate reductase gene *nit3*. Hyg^R	(Gómez-Gil *et al.*, 2018)
	Δ*nit1*Δ*nit2*	Deletion of nitrate reductase gene *nit2* in Δ*nit1* background. Hyg^R-$Phleo^R$	(Gómez-Gil *et al.*, 2018)
	Δ*ntr1*	Deletion of nitrate transporter gene *ntr1*. Nat^R	(Gómez-Gil *et al.*, 2018)
	NitFG	Spontaneous chlorate-resistant mutant	(Gómez-Gil *et al.*, 2018)
	Com1	Complementation of NitFG mutant with an areA+ allele	(Gómez-Gil *et al.*, 2018)
	Δ*areA*	Deletion of nitrogen regulator gene *areA*. Hyg^R	(López-Berges *et al.*, 2010)
	P*act*::*FOXG_15617*	*FOXG_15617* gene fused to actin promoter. Overexpression. Hyg^R	This study
	Chr13::GFP-ChFP	Insertion of H1::ChFP and H2::GFP constructs in the duplicated region of Chr13. Neo^R	(López-Díaz, unpublished)
	Δ*rad1*	Deletion of DNA excision repair gene *rad1*. Hyg^R	(López-Díaz, unpublished)
	Δ*lig4*	Deletion of DNA ligase 4 gene *lig4*. Hyg^R	(López-Díaz, unpublished)
	Δ*ku70*	Deletion of DNA helicase II subunit I gene *ku70*. Hyg^R	(López-Díaz, unpublished)
	wt-RFLP13	RFLP marker in the duplicated region of Chr13. Nat^R	(Franco-Cano, 2021)
	Δ*rad1*-RFLP13	Deletion of the *rad1* gene in wt-RFLP13 background. Hyg^R	This study
	Δkmt*1*-RFLP13	Deletion of the histone methyltransferase *kmt1* gene in wt-RFLP13 background. Hyg^R	This study
Escherichia coli	DH5α	*supE44, ΔlacU169 (Φ80lacZΔM15), hsdR17, recA1 endA1, gyrA96, thi-1, relA1*	Invitrogen™

Saccharomyces cerevisiae	BY4741	*MATa his3Δ1 leu2Δ0 met15Δ0 ura3Δ0*	Euroscarf
	P*gal*::*FOXG_15617*	*FOXG_15617* cDNA cloned into the galactose-inducible p426 expression vector	This study
Tomato *(Solanum lycopersicum)*	Monika	Susceptible to *F. oxysporum* f. sp. *Lycopersici,* Race 2	Syngenta, Almería, Spain

(1)*Fusarium* Genetics Stock Center

The plasmids used in this study are listed in Table 3.

Table 3. Plasmids used in this study.

Plasmid	Features	Reference
pGEM® - T	Derived from plasmid pGEM®-5Zf(+), linearized with EcoRV and with a T added in both 3' ends.	Promega
pAN7-1	Derived from pUC18. Carrier of the phosphotransferase *hygromycin* B (*hph*) gene from *Streptomyces spp*., under control of the *gpdA* gene and the terminator of the *trpC* gene of *A. nidulans*.	(Punt *et al.,* 1987)
pGEMT - *hph*BB	Derived from pAN7-1 plasmid with shorter version of *gpdA* and *trpC*.	Our group
pAN8-1	Carrier of the phleomycin resistance gene under control of the promoter of the *gpdA* gene and the terminator of the *trpC* gene of *A. nidulans* cloned in pUC18 *Eco*RI-*Sal*I.	(Mattern *et al.,* 1988)
pDNat	Carrier of the *nat1* gene under the control of the promoter of trpC gene from *A. nidulans*.	(Kopke *et al.,* 2010)
pGEMT-Neo^R	Carrier of the neomycin resistance gene under control of the promoter of the *gpdA* gene and the terminator of the *trpC* gene of *A. nidulans*.	(Fernandes, unpublished)
pSpark® I	Linearized with *Eco*RV, allows cloning of PCR fragments with blunt ends. Confers resistance to ampicillin.	Canvax, Biotech
P*act*/pGEMT	Promoter of the actin gene from Fol4287 amplified with primers incorporating a *Pst*I site and cloned into pGEMT.	This study
FOXG_15617/pGEMT	*FOXG_15617* gene from Fol4287, including endogenous terminator sequence, cloned into pGEMT.	This study
Pact::*FOXG_15617*/ pGEMT	*FOXG_15617* gene under the control of actin promoter cloned in pGEMT.	This study
p426GAL	Yeast expression vector carrying the galactokinase (GAL1) promoter induced by gaactose.	ATCC(1)
FOXG_15617/p426	cDNA of *FOXG_15617* cloned into p426 expression vector.	This study

(1)American Type Culture Collection.

2. Culture media

Media were prepared with RO deionized or RO ultrapure water (Direct-Q® 8 UV remote water purification system, Merck Millipore) and sterilized by autoclaving (120°C, 1.2 atmosphere of pressure, 20 minutes) or by filtration (0.22 µm pore size, Millipore). The media used for growth are shown below, while for each experimental protocol, the compounds and media used will be described in the respective section.

2.1. Culture media for *F. oxysporum*

- Potato Dextrose Broth (PDB): Boil 200 g of peeled potatoes in 1 L of deionized water for 1 hour. Crush, filter the potatoes and add 20 g of glucose and deionized water up to 1 L.

- Potato Dextrose Agar (PDA): 3.9% (w/v) of a commercial preparation of potato, dextrose and agar (BD Difco™).

- Yeast extract Peptone Dextrose/Agar (YPD/YPDA): Yeast extract (3 g/L), peptone (10 g/L) and glucose (20 g/L). For solid medium, add 15 g/L agar.

- Puhalla's Minimal Medium (PMM): $MgSO_4 \cdot 7H_20$ (0.5 g/L), KH_2PO_4 (1 g/L), KCl (0.5 g/L), $NaNO_3$ (2 g/L) and sucrose (30 g/L). For solid medium, add 15 g/L agar. (Puhalla, 1968).

- Synthetic Medium (SM): $MgSO_4 \cdot 7H_20$ (0.2 g/L), KH_2PO_4 (0.4 g/L), KCl (0.2 g/L), glucose (10 g/L), $FeSO_4$ (0.01 g/L), $ZnSO_4$ (0.01 g/L) and $MnSO_4$ (0.01 g/L). This medium was supplemented with different nitrogen sources. For solid medium, add 15 g/L agar. (Di Pietro and Roncero, 1996a).

- Regeneration Minimal Medium (RMM): $MgSO_4 \cdot 7H_20$ (0.5 g/L), KH_2PO_4 (1 g/L), KCl (0.5 g/L), $NaNO_3$ (2 g/L), glucose (20 g/L) and sucrose (200 g/L). Add 12.5 g/L agar for Petri dishes and 4 g/L for Top agar.

2.2. Culture media for *S. cerevisiae*

- Yeast extract Peptone Dextrose/Agar (YPD/YPDA): Yeast extract (10 g/L), peptone (20 g/L) and glucose (20 g/L). For solid medium, add 15 g/L agar.

- Synthetic Defined medium (SD): Yeast nitrogen base without amino acids and ammonium sulfate (1.7 g/L), ammonium sulfate (5 g/L), glucose (20 g/L), Drop-out mix (2 g/L). For solid medium, add 15 g/L agar.

2.3. Culture media for *E. coli*

- Luria-Bertani medium (LB/LA): Tryptone (10 g/L), yeast extract (5 g/L) and NaCl (5 g/L). For solid medium, add 15 g/L agar (Miller, 1972). This medium was supplemented with ampicillin (50 µg/ml) for the selection of resistant bacteria. In gene cloning experiments, for the selection of bacteria that carry the plasmid of interest, the medium was supplemented with IPTG (134 µM) and X-Gal ((0.005% (w/v) dissolved in formamide)).

3. Synthetic oligonucleotides

The synthetic oligonucleotides used as primers in amplification and sequencing reactions are detailed in (Tables 4-11). Internal stability, duplex and hairpin formation, and different physicochemical parameters (Tm: Temperature of melting; calculated through the [2(A+T)°+4(G+C)°] method) were determined using the software "Oligo V7.0" (Molecular Biology Insights, Inc., USA). Oligonucleotides were synthesized by Isogen Life Science (Netherlands).

Table 4. Primers used for targeted gene deletion and knockout mutants analysis. The terminal sequences included to favor hybridization with the 3 'or 5' end of the hygromycin, nourseothricin or phleomycin resistance cassettes in lowercase.

Gene	Name	Sequence (5' → 3')	Tm	Use
nit1	Nit1-10	GGCGGGTCACGGTATGATTG	64°C	Split marker
	Nit1-11	CGGTATGATTGGAGGCGATTC	64°C	Split marker
	Nit1-13	gaatgcacaggtacacttgtttCAGGAGATAGAG GCGATGGG	64°C	Split marker
	Nit1-15	aggggctgtattaggtctcgTACTTTACAGGGAG GCGTGAG	64°C	Split marker
	Nit1-16	GCCTCATGTCTTGGGTGTCC	64°C	Split marker
	Nit1-17	CAGATGCTATGCCCGATAATCA	64°C	Split marker
	Nit1-18	CATAGTGGTGAAGAAGAGCCT	62°C	Southern
	Nit1-19	CGTCGTCGTTCGTCTTGGTA	62°C	Southern
	Nit1-For	CGGCTACTGGGGTGAGAAGG	66°C	RT-qPCR
	Nit1-Rev	GGAACACTTCTCGGTCTGCG	64°C	RT-qPCR
nit2	Nit2-10	CCCTCAATGCTTCAACCTCAAA	64°C	Split marker
	Nit2-11	TATTCTCTTCAACCTCTACACGA	64°C	Split marker
	Nit2-13	gaatgcacaggtacacttgtttAGACTCTGAGAAG AAGTTTTACAA	64°C	Split marker
	Nit2-15	aggggctgtattaggtctcgGCAGACCTCCTATC GCAGATT	64°C	Split marker Southern
	Nit2-16	TGAGGCTATCCAGAGTGTTGC	64°C	Split marker Southern
	Nit2-17	GCACCAACGAGACCCTCAAC	64°C	Split marker
	Nit2-18	TCAGAAGGAGTTTACCCGAGA	62°C	RT-qPCR
	Nit2-19	TTTTGTTTGATGAAGTTGGCGG	62°C	RT-qPCR
nit3	Nit3-10	CGTAAACATCAAGTCGGAATGG	64°C	Split marker
	Nit3-11	TGATAGATGAGCCGACAGACAA	64°C	Split marker

	Nit3-13	gaatgcacaggtacacttgtttCGCAATGGATGG CTACGCAAT	64°C	Split marker
	Nit3-15	aggggctgtattaggtctcgTCATTCTTCTTT CTGCCATAACAA	64°C	Split marker
	Nit3-16	GCTCTCCTTCTTTTCTCTTTGG	64°C	Split marker
	Nit3-17	CCGTCAACCGTGATGAGATAC	64°C	Split marker
	Nit3-18	TACTGGGACACAAAGGATGGA	62°C	Southern
	Nit3-19	TGTCTTTGGTGATTTGGATGAG	62°C	Southern
ntr1	Ntr-1	GAGCATTCCACAGAGATTTAGA	62°C	Split marker
	Ntr-2	ATTGAGAAGCATGGTAGTAATCA	62°C	Split marker
	Ntr-3	tacaacgtcgtgactgggaaaaccctggcgATTGGGA AATATCAAGACAACTAA	62°C	Split marker
	Ntr-4	AACCCCATCAGCCGAAAAGC	62°C	Split marker Southern
	Ntr-5	CAAACCGCCAAGTTCAACGC	62°C	Split marker Southern
	Ntr-6	gctgtttcctgtgtgaaattgttatccgctTGGAAAAG GGAAAAATACGAATG	62°C	Split marker Southern
	Ntr-7	TCGTTTCTTCAGGTATGGAGC	62°C	Split marker RT-qPCR
	Ntr-8	CATACGTTGCTTCTTTTGTTGG	62°C	Split marker RT-qPCR
	Ntr-9	CCTCGCACCACTTGTCAACA	62°C	RT-qPCR
	Ntr-10	AAGACGGCAGGCATAATGAAG	62°C	RT-qPCR
Area	AreA-1n	TGAATGCTCGTCCCTGCTCC	64°C	Complementation
	AreA-2n	ACTCGGAAACTGATGCGGGC	64°C	Complementation
	AreA-4	AGAGCAGCAGCAGAGGCAAG	64°C	Southern RT-qPCR
	AreA-5	CTGGTGAACTGGCTGGACGG	66°C	Southern RT-qPCR
Cnx	CnxABC-1	TCATACTTGCGTATTTGACCTATT	64°C	Sequence analysis
	CnxABC-2	ATTTTTACAGGGGAGAGTTGTCA	64°C	Sequence analysis
	CnxABC-3	CACCAAGTCAGCTTATTCTTTCA	64°C	Sequence analysis
	CnxABC-4	ATCACTGGGTGGAGAAGGAGA	64°C	Sequence analysis
	CnxABC-5	ACCAAGAGATGCTGGACCTCA	64°C	Sequence analysis
	CnxABC-6	ATGGCGAGTATTGGAGAAGAGT	64°C	Sequence analysis
	CnxE-3	GGAAGCTGTATCTTTTGATAACTA	64°C	Sequence analysis
	CnxE-4	GGGGTGTGCATTGTATATTTGG	64°C	Sequence analysis
	CnxF-1	CTTCTTCACACATCTCGTTCAC	64°C	Sequence analysis
	CnxF-2	AGACCAAAAGGCATTCAACAAAAA	64°C	Sequence analysis
	CnxF-3	CTCGTTCACACTCATGCAATAAT	64°C	Sequence analysis
	CnxF-4	GCCAACTTCGTGTAAAAAAAGAAA	64°C	Sequence analysis
	CnxG-1	ATTCATTTCTTGTTTTCTCCGTG	62°C	Sequence analysis
	CnxG-2	AATGTGGCTGGTGTCCTTTTGT	64°C	Sequence analysis
	CnxG-3	CAGGCAAGAAAAGATCATACCG	64°C	Sequence analysis
	CnxG-4	CAAACCATATCGCTTCAAGTAGT	64°C	Sequence analysis
	CnxH-1	TCCTCTGCCACTCCGCTTGT	64°C	Sequence analysis
	CnxH-2	TGTTTCTGTGTATTATTGGAATTA	60°C	Sequence analysis
	CnxH-3	TCGTTGCCCTTGATCGTTGCT	64°C	Sequence analysis
	CnxH-4	GGTTTGGCGATTGTGGGACG	64°C	Sequence analysis

	CnxH-5	TGGGCGGAGACCTGGAATGA	64°C	Sequence analysis
	CnxH-6	GAGATAAGAGTTTATTACCCGCA	64°C	Sequence analysis
rad1	Rad1-PF	CCTTGATGGGTTGGATGGAG	62°C	Split marker
	Rad1-PFN	TTGCTCGGTGCCAGTCATTC	62°C	Split marker
	Rad1-PR	tttacccagaatgcacaggtacacttgtttaAGACGAT GTGTTGAAGGGGG	62°C	Split marker
	Rad1-TF	tggtcgttgtaggggctgtattaggtctcgCCAAGCCA ATGTCAAAGCGG	62°C	Split marker
	Radd1-TR	GGACCTTGATGGCACCTTGT	62°C	Split marker
	Rad1-TRN	GGAAGGGAAAATCAGCGGAG	62°C	Split marker
	Rad1-SOF	CAAGCCCAAGACGGAGAAAC	62°C	PCR analysis
	Rad1-SOR	TCTTCTTTCTGCTGTGCTTCC	62°C	PCR analysis
	Rad1-STF	CCTTCCCCTATCCTTTCTCAA	62°C	Southern
	Rad1-STR	CTACCTTCTTCTTCCTGTCTC	62°C	Southern
lig4	Lig4-PF	TGGTCGGTTTAGGGGAGTAG	62°C	Split marker
	Lig4-PFN	AATCTCCACGCCAATCGCTG	62°C	Split marker
	Lig4-PR	tttacccagaatgcacaggtacacttgtttaGTTGTAA GCTAGGCGGTTGC	62°C	Split marker
	Lig4-TF	tggtcgttgtaggggctgtattaggtctcgGAGAATAC AACGCCCAAAACC	62°C	Split marker
	Lig4-TR	CTCCGTCTTATCTTATCGCAC	62°C	Split marker
	Lig4-TRN	TCTCTCTTGGAACGACGATTG	62°C	Split marker
	Lig4-SOF	ATCAGAAGAATCCGCCATCAAA	62°C	PCR analysis
	Lig4-SOR	TTTGTCATCTCTCCCTTGAACT	62°C	PCR analysis
	Lig4-STF	TGCTGGGGAAGATTGTTGTAG	62°C	Southern
	Lig4-STR	CTCTCTGATTGTCTCTTGTGAA	62°C	Southern
ku70	Ku70-PF	AAGCGATAGGGATGAGCACG	62°C	Split marker
	Ku70-PFN2	ACCTGAGACTGCCAGCATAG	62°C	Split marker
	Ku70-PR	tttacccagaatgcacaggtacacttgtttaTGTGTGAT TGGTTGGCGATGT	62°C	Split marker
	Ku70-TF	tggtcgttgtaggggctgtattaggtctcgACAGGCGT TTTTGCTACTTTC	62°C	Split marker
	Ku70-TR	GTTGGATTCTTCGCATTCTGT	62°C	Split marker
	Ku70-TR1	GGTTAAAGGCAATCGTGATAGA	62°C	Split marker
	Ku70-SOF	TTACATTTGGCTGGACGGTGA	62°C	PCR analysis
	Ku70-SOR	ACACCAAGCGACACCCATTTT	62°C	PCR analysis
	Ku70-SPF	TGATTCGGGGGTCTCGGTG	62°C	Southern
	Ku70-SPR	CCTTCCACGCCTTGTCTCTT	62°C	Southern
kmt1	Kmt1-PF	GAAGAACGAGAGAGGCAGCA	62°C	Split marker PCR analysis
	Kmt1-PFN	GCCGTTGACCTGTGGATTGA	62°C	Split marker
	Kmt1-PR	ttacccagaatgcacaggtacacttgtttGGGTTGTTT GTTTTGGCTCAG	62°C	Split marker
	Kmt1-TF	tcgttgtaggggctgtattaggtctcggTCACTTTTAC TCCAATCTGCTC	62°C	Split marker
	Kmt1-TR	TTGAGACAGAGGAGAGAAAGG	62°C	Split marker PCR analysis
	Kmt1-TRN	TCTATCTTTTGTGCCTATTAAATG	62°C	Split marker
	Kmt1-STF	ATGGAATGGTATAACTTGCTGG	62°C	Southern

	Kmt1-STR	GTAACCAATCGTCCCAAACTC	62°C	Southern

Table 5. Primers used for molecular analysis of chromosome ends.

Region	Name	Sequence (5' → 3')	Tm	Use
Telomere	Tel-F	TTAGGGTTAGGGTTAGGG	54°C	Southern qPCR
	Tel-R	CCCTAACCCTAACCC	48°C	Southern qPCR
NextTel	Subtel-9	CCGTGTCCGTCGTTATTATTG	62°C	Southern qPCR
	Subtel-10	GGCAATATAAGGGGGTTGGG	62°C	Southern qPCR
FoRS	FoRS-1	GGTCTTCTGGGTGTTGATCG	62°C	qPCR RT-qPCR
	FoRS-2	AAGTTCAAGGCACGGCTGGT	62°C	qPCR RT-qPCR
FOXG_15616	Subtel-31	TACGGAATGAAGATTTGTTAATAG	62°C	Southern qPCR
	Subtel-32	ACCAATCAGAGCCATATCCAG	62°C	Southern qPCR
	FOXG_15616-1	GTCAATATGTGTTATCGTTTAGAA	62°C	RT-qPCR
	FOXG_15616-2	CCCTTCTTGTTGACATTTCTCT	62°C	RT-qPCR
FOXG_15617	Subtel-2	TCCTCCGTTGCTGGTATCGA	62°C	Southern qPCR
	Subtel-6	GCCCAATGGTGATGAAGAGC	62°C	Southern qPCR
	Subtel-17	ACCGCCCTCCATCAAAGCAA	62°C	RT-qPCR
	Subtel-18	CAATAGACGGGATGGATAGGA	62°C	RT-qPCR

Table 6. Primers used to obtain Pact::FOXG_15617 transformants. Complementary 5'-tails are indicated in lowercase.

Gene	Name	Sequence (5' → 3')	Tm	Use
Actin	Pact-2P	GGCTGCAGCATTAGAAAGTTC	62°C	DNA cloning Fusion PCR
	Pact-3	GGCTGTGGATTACGGTGTGT	62°C	DNA cloning
	Pact-4	gtagccccaagcacggcatGGCTGTGGATTACGGTGTGT	62°C	Fusion PCR
	Pact-5	CCGTCTCCTTCTCCATCCAA	62°C	PCR analysis
FOXG_15617	Subtel-11	GTCAGCCTCTTATCCTTCATTT	62°C	DNA cloning Fusion PCR
	Subtel-29	GTAATAATCGTCGTCCTCGCT	62°C	PCR analysis
	Subtel-30	GTTGTGACGGACGCTGAGAA	62°C	DNA cloning
	Subtel-36	acacaccgtaatccacagccATGCCGTGCTTGGGGCTAC	62°C	Fusion PCR

Table 7. Primers used to obtain Pgal::FOXG_15617 transformants. Complementary 5'-tails are indicated in lowercase.

Gene/ Vector	Name	Sequence (5' → 3')	Tm	Use
FOXG_15617	subtelF-2-p426	aaccccggattctagATGCCATGCTTAGGGCTACCA	64°C	DNA cloning
	subtelR-2-p426	cataactaattacatgaTCATGGACGTGGTTCACCGAT	64°C	DNA cloning
p426	p426-P-subtelF	ctaagcatggcatCTAGAATCCGGGGTTTTTTCTC	64°C	DNA cloning
	p426-T-subtelR	gccgcgtccatgaTCATGTAATTAGTTATGTCACGCT	64°C	DNA cloning
	Pura3(Sc)-2	CACCATACCACAGCTTTTCAAT	62°C	PCR analysis
	Tura3(Sc)-1	CTGATGCGGTATTTTCTCCTTA	62°C	PCR analysis

Table 8. Primers used to obtain Chr13::GFP::ChFP transformants.

Name	Sequence (5' → 3')	Tm	Use
Flank1Che-F	AATACCCTCTTGGTCCTCTCG	64°C	Fusion PCR
Flank1Che-FN	TTGCTTGATGATCTCGACCCC	64°C	Fusion PCR
Flank1Che-R	tcatttaggtgcttctttcgatctcttcGCCTCGCTTCACTTGTTCACT	64°C	Fusion PCR Southern
Hist1-F	GAAGAGATCGAAAGAAGCACC	62°C	Fusion PCR
Flank2Che-F	tgtacgttaaaagttccgtggagttaccAACCTACAACGAGATCCCCTC	64°C	Fusion PCR
Flank2Che-R	GAGATTGGTTGATGAGGGTCC	64°C	Fusion PCR
Flank2Che-RN	GCAGGCAAAACCACGAACAGT	64°C	Fusion PCR
Cherry-F	CCGACATCCCCGACTACTTG	64°C	Southern qPCR
Cherry-R	GATGGTGTAGTCCTCGTTGTG	64°C	Southern
Cherry-qPCR	CCCGTAATGCAGAAGAAGACC	64°C	qPCR
13GFP-cherry	TGCAGTGAATATCGAGCCTCTA	64°C	Southern
Flank3GFP-F	AGTGAACAAGTGAAGCGAGGC	64°C	Fusion PCR
Flank3GFP-FN	TTGTCATCGCCTCCAAATGCC	64°C	Fusion PCR
Flank3GFP-R	cacatctgcatccatttgagtcccgagaCACACTACGAAGAGGTCACTG	64°C	Fusion PCR
H2B-2	TCTCGGGACTCAAATGGATGC	64°C	Fusion PCR
terHYG-R	CCAAGCAGCAAAGAGTGCCTT	64°C	Fusion PCR
Flank4GFP-F	tcactagaaggcactctttgctgcttggGTAGGGCTGCATGATGGTTTC	64°C	Fusion PCR
Flank4GFP-R	AGGCAGGAGAGACAGTGATTG	64°C	Fusion PCR
Flank4GFP-RN	CCAAGTCCCAAAGCCTACCAA	64°C	Fusion PCR
GFP-F	CAACATACGGAAAACTTACCCTT	64°C	Southern
GFP-R	TTTGATGCCGTTCTTTTGCTTGT	64°C	Southern
GFP-16	CCAACACTTGTCACTACTTTCA	62°C	qPCR
GFP-qPCR	ATCCTGTTGACGAGGGTGTCT	64°C	qPCR

Table 9. Primers used to detect and quantify CNVs.

Chr	Name	Sequence (5' → 3')	Tm	Use
1&15	T4Chr15-F	TTGGAGGAGAAGTGGAAACGG	64°C	Southern T4 probe
	T4Chr15-R	CTGACTGACTCGTACTATCCG	64°C	Southern T4 probe
	T5Chr15-F	TCGCAATCTTCGGTCTCGCAA	64°C	Southern T5 probe qPCR
	T5Chr15-R	TGAAAGAACCCTGGACGTGGT	64°C	Southern T5 probe qPCR
	S1N15.3-WF	TCCAGCTACCAAAGTGATGCC	64°C	Southern W probe
	S1N15.3-WR	CCCTACTTTGGTACTGTGTGC	64°C	Southern W probe
	S15.15-1XF	TGGGCAGGGATTGAACCAGT	64°C	Southern X probe
	S15.15-1XR	CTGAAGATGTGTGAGCCCAGA	64°C	Southern X probe
	S15.10-ZF	AGTCGGGAGGAATGGTCACAA	64°C	Southern Z probe
	S15.10-ZR	GTGACTGAAAAGAACCTGCCC	64°C	Southern Z probe
3&6	S3N6.26-CF	CAGGTGGTGGAGCAATGACTT	64°C	Southern C3 probe
	S3N6.26-CR	AGAAGCGAAGCAGAAACCCCT	64°C	Southern C3 probe
14	Chr14DP1-F	GGTGCTTGTGAGGAGTGATGA	64°C	Southern C14 probe
	Chr14DP1-R	AACCGCAACACAACACGCTCT	64°C	Southern C14 probe
13	T2Chr13-F	GGAATCTTGGCTGAAACGCTG	64°C	qPCR
	T2Chr13-R	AGCGAAGCAAATCCAGCCCC	64°C	qPCR
	13GFP-cherry	TGCAGTGAATATCGAGCCTCTA	64°C	Southern C13 probe
	Flank1Che-R	tcatttaggtgcttctttcgatctcttcGCCTCG CTTCACTTGTTCACT	64°C	Southern C13 probe

Table 10. Primers used for RFLP insertion on chromosome 13.

Name	Sequence (5' → 3')	Tm	Use
Chr13SNP-F	TGCAGTGAATCTCGAGCCTCTA	64°C	Fusion PCR
Chr13Mut-R	CACCTCAAATCATCGGCGAAC	64°C	Fusion PCR
Chr13SNP-R	TAGAGGCTCGAGATTCACTGCA	64°C	Fusion PCR
Chr13Mut-F	CTCCGCTAGGCAGTAACATTG	64°C	Fusion PCR
Chr13Mut-RN	TGGCAGGACTATTCGAGAGAG	64°C	Fusion PCR
Chr13Mut-FN	CTTCTGCTCTCGATGCTTCTG	64°C	Fusion PCR

Table 11. Primers used to amplify reference genes and resistance cassettes.

Gene/ Vector	Name	Sequence (5' → 3')	Tm	Use
Hyg	Hyg-G	CGTTGCAAGACCTGCCTGAA	62°C	Split marker PCR analysis
	Hyg-Y	GGATGCCTCCGCTCGAAGTA	64°C	Split marker PCR analysis
Phl	Fle-5	CGGAGCGGTCGAGTTCTGG	64°C	Split marker
	Leo	GCCACGAAGTGCACGCAGTT	64°C	Split marker
Nat	Nat-3	TCCTTCACCACCGACACCG	62°C	Split marker
	Nat-4	ACCCCATCCGCCGGTACG	62°C	Split marker

hyg/phl/ neo/nat cassettes	PgpdA-15B	CCGAGACCTAATACAGCCCCT	66°C	Split marker
	PgpdA-16B	AGGGGCTGTATTAGGTCTCG	62°C	PCR analysis
	Ttrpc-4B	CCTGGGTTCGCAAAGATAATT	60°C	PCR analysis
	Ttrpc-8B	AAACAAGTGTACCTGTGCATTCTGG	72°C	Split marker
	M13-F	CGCCAGGGTTTTCCCAGTCACGAC	78°C	PCR analysis
	M13-R	AGCGGATAACAATTTCACACAGGA	68°C	PCR analysis
Actin	Act-q7	ATGTCACCACCTTCAACTCCA	62°C	qPCR qRT-PCR
	Act-q8	CTCTCGTCGTACTCCTGCTT	62°C	qPCR qRT-PCR

4. Instrumentation and apparatus

The scientific equipment used for this work is summarized in Tables 12 and 13.

Table 12. Apparatus used in this study.

Apparatus	Application
5804 Centrifuge (Eppendorf)	Centrifugation of samples
Autoclave (P-Selecta)	Sterilization of materials and media
AV-100 Vertical Laminar Flow (Telstar)	Operation in sterile and particle-free conditions
CFX Connect ™ Real-Time PCR System (Bio-Rad)	DNA quantification and gene expression using qPCR
FastPrep-24™ 5G Homogenizer (MP Biomedicals ™)	Homogenization of samples using glass beads
FreeZone 6Plus Freeze-Dry System (Labconco®)	Freeze drying of samples
Heraeus Incubator (Thermo scientific)	Variable temperature incubation
Hybridization Oven / Shaker Station SI30H (Stuart Scientific)	Membrane hybridization (Southern)
Infors HT Multitron Standard Incubator	Incubation with shaking and temperature of liquid samples
J2-HS Centrifuge (Beckman)	Centrifugation of samples
LE225D Balance (Sartorius)	Weigh compounds
MC-8 Magnetic Stirrer (Bunsen)	Media homogenizer
MiniSpin® Centrifuge (Eppendorf)	Centrifugation of samples
MJ Mini™ Thermal Cycler (Bio-Rad)	DNA amplification by PCR
OR-ST 1200 Fume Cupboard (Burdinola)	Toxic gas extraction
Perfection V500 Scanner (Epson)	Image scanning
Precision Balance (Cobos)	Weigh compounds
Savant DNA120 SpeedVac Concentrator (Thermo Scientific)	Concentration of samples by vacuum
ThermoStat Plus Thermoblock (Eppendorf)	Incubation of vials (1.5 or 2 ml)

Vortex MS3 Minishaker (IKA®)	Sample homogenizer

Table 13. Instruments used in this study.

Instruments	Application
Axio M2 Dual Cam Microscope (Zeiss)	Microscopy Imaging
BASIC 20+ pHmeter (Crison)	pH measurement
BH-2 Microscope (Olympus)	Microscopic conidia count
Cell Counting Chamber (Thoma)	Microscopic count
CHEF-DR® III Pulsed Field Electrophoresis System (Bio-Rad)	Resolving chromosome-sized DNAs
DC290 ZOOM Photographic Machine (Kodak)	Obtaining photographic images of agarose gels
LAS-3000 Imager (Fujifilm)	Reveal Hybridization Membranes
M200 Infinite Pro Fluorimeter (Tecan)	Absorbance measurement on 96-well microtiter plates
ND-1000 Spectrophotometer (NanoDrop®)	Nucleic acids quantification and absorbance measurement
SmartSpec ™ Plus Spectrophotometer (Bio-Rad)	Absorbance measurement

5. Microorganisms culture conditions

5.1. *F. oxysporum*

To obtain mycelia for DNA/RNA extraction and fresh microconidia for different assays, the fungal strains were cultured during 3-4 days in PDB medium at 28 °C with orbital shaking at 170 rpm. In the case of mutant and complemented strains, appropriate antibiotics (hygromycin B at 20 µg/ml, phleomycin at 4 µg/ml, nourseothricin at 2.5 µg/ml or geneticin at 10 µg/ml) were added to the culture medium. For transformants selection on solid medium, antibiotics were added at the following concentrations: 55 µg/ml of hygromycin B, 11 µg/ml of phleomycin, 50 µg/ml of nourseothricin or 27.5 µg/ml of geneticin.

Microconidia were obtained by filtration through a nylon filter (Monodur; mesh size 10 µm), harvested by centrifugation at 8,000 rpm for 10 min and resuspended in sterile Milli-Q water. After measurement with a hemocytometer (Thoma; Marienfield, Germany), the conidial suspension density was adjusted to proper concentration for subsequent assays.

For long-term preservation of the different strains, the collected microconidia were resuspended in glycerol at 30% (v/v) and stored at -80 °C. These suspensions are used as

stock to obtain fresh microconidia. Mycelium for subsequent DNA, RNA and protein extraction was stored at -80 °C.

5.2. *S. cerevisiae*

Yeast cells were grown at 30°C in both YPD complete medium. For the selection and cultivation of yeast transformants, minimal SD medium with drop-out supplements was used. SD/-Trp dropout allowed the selection of the wild-type strain BY4141 while SD/-Ura was used to select for transformants that had incorporated the expression vector p426 carrying the *ura3* gene. For long-term preservation of the different strains, yeast cells were resuspended in glycerol at 20% (v/v) and stored at -80 °C.

5.3. Bacteria

E. coli DH5α was cultured with shaking (250 rpm) and at 37 °C in LB liquid medium, or without shaking in LA solid medium at the same temperature. The medium was supplemented with the antibiotic ampicillin (100 µg/ml) for the selection of strains carrying plasmids with the resistance gene. Bacterial strains were preserved at -80 °C in LB medium with 30% glycerol (v/v).

5.4. Tomato plants

The seeds were sterilized by immersing them in 20% bleach (v/v) for 30 minutes. After this time, the seeds were washed 3 times for 10 minutes with ultrapure water. The seeds were sown in wet vermiculite and incubated for 14 days (until the first pair of true leaves appeared) in a growth chamber with determined conditions (temperature of 28 °C, relative humidity of 40-70% and a photoperiod of 14 hours of 36W white fluorescent light and 10 hours of darkness). For infection assays, the roots of the plants were introduced into a dilution of fresh *F. oxysporum* conidia.

6. Nucleic acids isolation

6.1. DNA isolation from F. oxysporum

6.1.1. CTAB method from lyophilized mycelium

Genomic DNA (gDNA) extraction was performed from *F. oxysporum* mycelium grown for 3-4 days and using the CTAB method (Torres *et al.,* 1993) with some modifications. The frozen mycelium was lyophilized using a freeze-drying system and then pulverized using a homogenizer and 1-5 mm diameter glass beads. Each sample was resuspended in 1 ml of CTAB extraction buffer[(1)], 4 µl of β-mercaptoethanol and chloroform:octanol 24: 1 (v/v) to make a final volume of 2 ml. This mix was homogenized

by inversion and incubated at 65 °C for 30 minutes. After incubating at RT for 15 minutes, the sample was centrifuged for 10 minutes at 13,400 rpm. The upper aqueous phase was transferred to a new Eppendorf tube, precipitated by adding 1 ml of 100% ice-cold ethanol and incubated at -20 °C for at least 1 hour (O/N preferred). Precipitated DNA was centrifuged for 10 minutes at 13,400 rpm and washed two times with 1 ml of 70% ethanol (v/v). DNA pellet was dried and resuspended in 50 µl of sterile Milli-Q water with 4 µl of RNase (10 mg/ml) and incubated at 37 °C for 45 minutes. The amount and quality of extracted DNA was monitored either by electrophoresis in a 0.7% agarose gel (w/v) or in a Nanodrop® ND-1000 using absorbance ratios (260/280 nm and 260/230 nm wavelength).

(1)**CTAB extraction buffer:** Trizma base (12.1 g/L), EDTA (7.44 g/L), NaCl (81.8 g/L) and Cetyltrimethylammonium bromide (20 g/L). Heat to 60 °C to dissolve and adjust to pH 8.0 with NaOH. Keep at 37 °C to avoid precipitation.

6.1.2 Direct DNA isolation from mycelium colonies

For colony PCR analysis, DNA isolation was performed using the *Phire Plant Direct PCR Master Mix* kit (Thermo Scientific™). A *F. oxysporum* colony was picked (in the most extreme part) with a toothpick and put into a 1,5 ml Eppendorf tube with 20 µl of sterile Milli-Q water. The mycelium was crushed against the Eppendorf tube for 5-6 times and 1 µl of this suspension was added to 4 µl of dilution buffer. The sample was incubated for 2 hours at RT and 0.5 µl of the mix were used for PCR (final volume: 10 µl).

6.2 DNA isolation from S. cerevisiae

Yeast DNA isolation was performed using the LiOAc-SDS method (Lõoke *et al.*, 2011). A yeast cell was picked with a toothpick and transferred into a 1,5 ml Eppendorf tube with 100 µl of lysis buffer (0.2M Lithium acetate and 1% SDS). The mix was incubated at 70 °C for 5 minutes and then precipitated by adding 300 µl of 100% ice-cold ethanol. DNA and cell debris were spin down for 3 minutes at 13,400 rpm and washed with 300 µl of 70% ice-cold ethanol (v/v). Pellet was dried and resuspended in 50 µl of sterile Milli-Q water with 1 µl of RNase (10 mg/ml). Finally, cell debris were spin down for 15 seconds at 13,400 rpm and 1 µl of supernatant was used for PCR (final volume: 10 µl).

6.3 Plasmid DNA isolation from E. coli

Plasmid DNA isolation was performed using the CTAB method (Murray and Thompson, 1980) with some modifications. An isolated colony carrying the plasmid of interest was inoculated in 5 ml of LB medium (containing the resistance antibiotic) and grown

O/N (12-14 hours) at 37 °C with orbital shaking of 250 rpm. The next day, the steady state culture was centrifuged for 2 minutes at 13,400 rpm to collect the bacterial cells. The cell pellet was resuspended in 200 µl of STET solution[1], 4 µl of lysozyme (50 mg/ml), 4 µl of RNase (10 mg/ml) and incubated 10 minutes at RT. The sample was boiled for 1 minute at 100 °C and centrifuged 10 minutes at 13,400 rpm. Mucous-like cell debris was removed with a sterile toothpick and 10 µl of 5% CTAB solution[2] was added to precipitate the plasmid DNA. After 10 minutes of incubation at RT, samples were centrifuged 10 minutes at 13,400 rpm and the pellet was resuspended in 350 µl of 1.2M NaCl and 750 µl of 100% ice-cold ethanol and incubated for 10 minutes at RT. The sample was centrifuged again at 13,400 rpm for 10 minutes and the precipitated DNA was washed with 70% ethanol (v/v). Finally, the pellet was dried and resuspended in 20 µl of sterile Milli-Q water.

[1]**STET:** 8% sucrose (w/v), 0.1% Triton X-100 (v/v), 50 mM EDTA and 50 mM Tris-HCl pH 8.0.

[2]**CTAB solution:** Cetyltrimethylammonium bromide (50 g/L). Keep at 37 °C to avoid precipitation.

6.4 RNA isolation from F. oxysporum

RNA isolation was carried out from mycelium obtained in the suitable induction conditions for each experiment. The frozen mycelium was lyophilized using a freeze-drying system and then pulverized using a homogenizer and 1-5 mm diameter glass beads. Each sample was resuspended in 1 ml of Tripure Isolation Reagent and centrifuged at 4 °C for 10 minutes at 13,000 rpm. The supernatant was transferred to a new Eppendorf tube and incubated for 5 minutes on ice to allow dissociation of nucleoprotein complexes. 200 µl of chloroform (per 1 ml of Tripure) were added and the mix was vortexed for 15 seconds. After incubated on ice for 5 minutes, the samples were centrifuged at 4 °C for 15 minutes at 13,000 rpm, resulting in the formation of three phases. The upper clear phase was transferred to a new clean Eppendorf tube with 500 µl of isopropanol, mixed by inversion and incubated for 10 minutes on ice. Subsequently, the samples were centrifuged at 4 °C for 10 minutes at 13,000 rpm. The RNA pellet was washed with 1 ml of 70% ice-cold ethanol (v/v) and centrifuged at 4°C for 5 minutes and 8,000 rpm. Finally, the pellet was dried, resuspended in 50 µl of sterile Milli-Q water (RNase free) and incubated for 15 minutes at 60 °C. The RNA obtained was stored at -80 °C. The amount and quality of extracted RNA was monitored either by electrophoresis in a 1% agarose gel (w/v) or in a Nanodrop® ND-1000 spectrophotometer using absorbance ratios (260/280 nm and 260/230 nm wavelength).

6.5 RNA isolation from infected tomato plants

RNA purification from infected plant roots or stems was carried out using the commercial *RNeasy Plant Mini* kit (Qiagen). Roots and stems were lyophilized using a freeze-drying system and then pulverized using a homogenizer. Each sample was resuspended in 450 µl of lysis buffer, and then, the cell debris were removed by filtration and centrifugation in a column supplied in the kit. Subsequently, 100% ethanol and adhesion buffer were added to allow the RNA to adhere to the membrane, and after several washes, the RNA was eluted in 30 µl of sterile Milli-Q water (RNase free) and stored at -80 °C.

7. DNA amplification reactions

7.1. Standard PCR

PCR amplification reactions were performed in a thermocycler using different thermostable Taq DNA polymerases depending on the objective of the experiment and the fragment size. For reactions where high fidelity in amplification was required, the enzyme *Expand High Fidelity PCR System* (Roche) or the enzyme *Phusion® High-Fidelity DNA Polymerase* (New England Biolabs) were used, following the manufacturer´s instructions. For knockout mutant confirmation and Southern blot probes, the thermostable *BioTaq™ DNA Polymerase* (Bioline) was used. Each PCR reaction contained 300nM of each primers, 2.5mM MgCl2, 0.8mM of dNTPs mix and 0.05 U/µl of polymerase. Genomic DNA was added at 5-10 ng/µl and plasmid DNA at 1-5 ng/µl final concentration. The amplification conditions are detailed in (Table 14).

Table 14. Standard PCR conditions.

Polymerase	Step	Temperature, Time	Cycles
Expand High Fidelity PCR System	Initial denaturation	94 °C, 2 minutes	1x
	Denaturation	94 °C, 15 seconds	35x
	Annealing	Tm(1), 30 seconds	
	Elongation	68 °C(2) / 72 °C, 1 minute/kb	
	Final elongation	68 °C(2) / 72 °C, 10 minutes	1x
	Hold	4 °C, unlimited time	
Phusion® High-Fidelity DNA Polymerase	Initial denaturation	98 °C, 30 seconds	1x
	Denaturation	98 °C, 10 seconds	35x
	Annealing	Tm(1), 30 seconds	
	Elongation	72 °C, 30 seconds/kb	

	Final elongation	72 °C, 10 minutes	1x
	Hold	4 °C, unlimited time	
BioTaq™ DNA Polymerase	Initial denaturation	94 °C, 5 minutes	1x
	Denaturation	94 °C, 35 seconds	35x
	Annealing	Tm(1), 35 seconds	
	Elongation	72 °C, 1 minute/kb	
	Final elongation	72 °C, 10 minutes	1x
	Hold	4 °C, unlimited time	

(1) Tm is the binding temperature of the primers to the template.

(2) For PCR products larger than 3 kb, elongation temperature should be 68 °C.

7.2. Colony PCR

Colony PCR was performed using the *Phire Plant Direct PCR Master Mix* kit (Thermo Scientific™) from isolated DNA (as described in section 6.1.2). Each PCR reaction contained 525nM of each primer, 1X Phire Plant Direct PCR Master Mix, and 0.5 µl of DNA. The amplification conditions are detailed in (Table 15).

Table 15. Colony PCR conditions.

Step	Temperature, Time	Cycles
Initial denaturation	98 °C, 5 minutes	1x
Denaturation	98 °C, 5 seconds	35x
Annealing	Tm, 5 seconds	
Elongation	72 °C, 20 seconds/kb	
Final elongation	72 °C, 1 minute	1x
Hold	4 °C, unlimited time	

7.3. Labelling PCR

Obtaining digoxigenin-labelled DNA probes for Southern blot analysis was performed using a standard PCR with *BioTaq™ DNA Polymerase* (Bioline), substituting the dNTPs for *DIG DNA Labelling Mix* (Roche), a mix of deoxyribonucleotides containing DIG-11-dUTP.

Purification of labelled probes, to remove the components of the PCR, was carried out by adding 0.1 volumes of 8M Lithium chloride and 2.5 volumes of 100% ice-cold ethanol. After an incubation at -20 °C for at least 1 hour (O/N preferred), precipitated DNA was

centrifuged for 30 minutes at 13,400 rpm and 4 °C and washed with 70% ethanol (v/v). DNA pellet was dried and resuspended in 11 µl of sterile Milli-Q water.

7.3.1 Telomer probe obtention

Telomere probe (TEL) was obtained by Gustavo Bravo-Ruiz as described (Starnes *et al.,* 2012). Labelling PCR using two complementary primers (Tel-F and Tel-R) with several copies of the telomeric sequence (TTAGGG) of Fol4287 was performed. The primers work as a zip obtaining as result a smear of DNA of different sizes with the repeated sequence TTAGGG. The region of 1-1.5 kb was purified from the gel and used as probe (Figure 6).

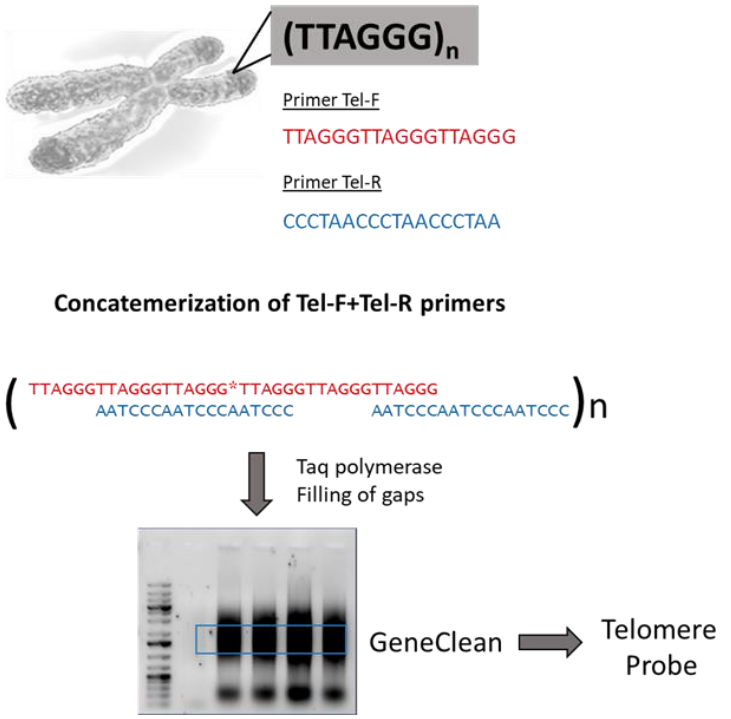

Figure 6. Telomere probe design. The telomeric probe was obtained by labeling PCR with two complementary primers (Tel-F and Tel-R) containing several copies of the TTAGGG telomeric sequence. The 1-1.5 Kb fragments obtained after PCR amplification were purified from the gel and used as a probe. Designed by Gustavo Bravo-Ruiz.

7.4. Fusion PCR for generating knockout mutants

The generation of knockout mutants of Fol4287 was carried out by targeted gene deletion using the Split-marker technique consisting of the replacement of the wild type allele of the gene with a resistance cassette (Catlett *et al.,* 2003). Gene deletion is performed by fusion PCR, a technique that allows the fusion of two or more PCR products with overlapping regions (Yang *et al.,* 2004) (Figure 7). For this, three consecutive rounds of PCR are required (Figure 7A). First (PCR I), two fragments of approximately 2 Kb located upstream (promoter) and downstream (terminator) of the target gene were amplified with

two primer pairs in which one of each pair has extensions at its 5' end that are complementary to the resistance cassette, which was also amplified with specific primers. The amplified fragments were then subjected to a fusion PCR (PCR II) without primers in which the overlapping ends anneal. Finally, the fused products were amplified by PCR using specific primers internal to the resistance cassette and to the flanking regions of the target gene (PCR III). Thus, we obtained two fragments carrying approximately 75% of the resistance cassette, including an overlapping region, and 1.5 Kb of the promoter or terminator region of the target gene. Both overlapping fragments were used for protoplast transformation and the replacement of the target gene by the resistance cassette occurred by a double homologous recombination event (Figure 7B).

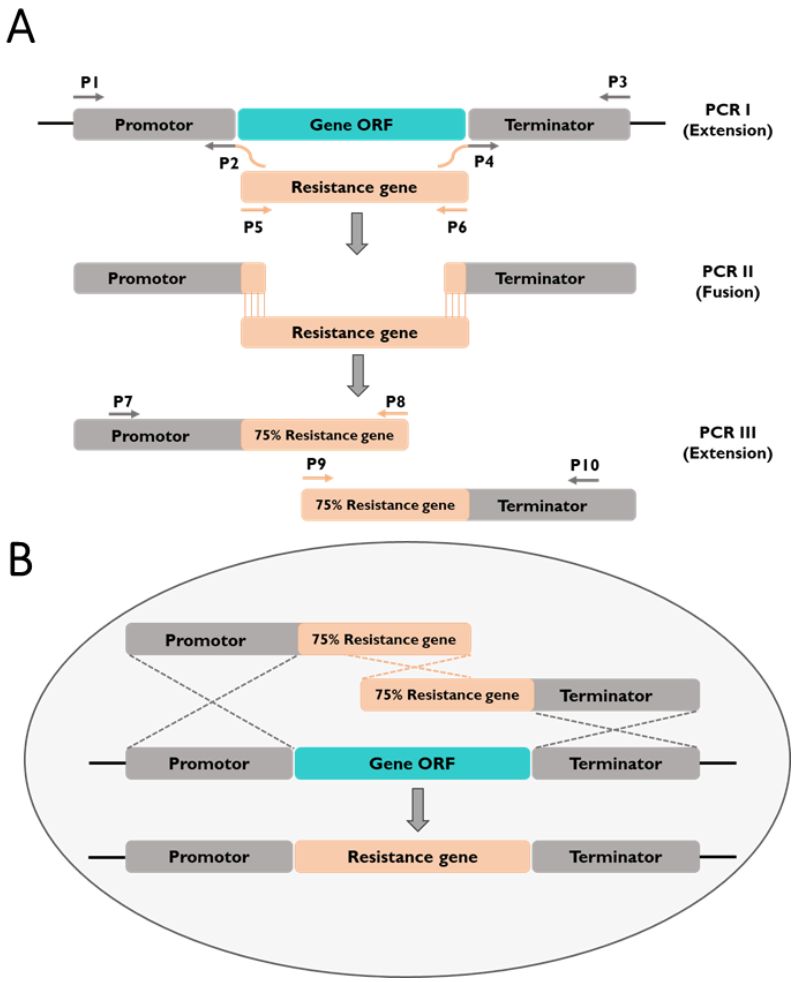

Figure 7. Schematic representation of the split-marker strategy for targeted gene deletion in Fol4287. (A) Amplification of the region upstream (promotor: P1/P2) and downstream (terminator: P3/P4) of the target gene with primers containing tails homologous to the resistance cassette (PCR I). Fusion PCR without primers (PCR II) in which the overlapping ends anneal. Obtaining both final constructs by amplification with specific primers internal to the resistance cassette and to the flanking regions of the target gene. **(B)** Protoplast transformation with the two PCR fragments resulting in homologous recombination and replacement of the target gene by the resistance cassette.

7.5. Reverse transcriptase PCR (RT-PCR)

Isolated RNA was treated for 30 minutes at 37 °C with *DNase I Recombinant* kit (Roche) to remove DNA debris. Thus, 1 µg of total RNA was mixed with 0.2 µl DNAse, 1 µl of 10X Incubation buffer and sterile Milli-Q water to final volume of 9.5 µl. To stop the reaction, the mix was incubated at 75 °C for 10 minutes, adding EDTA at a final concentration of 2.5 mM to prevent hydrolysis of RNA during heating.

The resulting treated RNA was reverse transcribed with the *Transcriptor Universal cDNA Master* kit to synthesize the cDNA. For this, to the 10 µl of RNA previously treated with DNase, 4 µl of buffer and 1 µl of reverse transcriptase were added and it was completed with sterile Milli-Q water to a final volume of 20 µl. The reverse transcription conditions are detailed in (Table 16).

Table 16. Reverse transcription conditions.

STEP	TEMPERATURE, TIME
Annealing	25 °C, 5 minutes
Reverse transcription	55 °C, 10 minutes
Denaturation	85 °C, 5 minutes
Hold	4 °C, unlimited time

7.6. Quantitative PCR

For each sample, three simultaneous technical replicates were performed using a CFX Connect ™ Real-Time PCR System (Bio-Rad).

For the measurement of gene expression, a quantitative reverse transcription PCR (RT-qPCR) was carried out using 5 µl of cDNA (diluted 1:1), 7.5 µl of *FastStart Essential DNA Green Master* (Roche), 300nM of each primer and sterile Milli-Q water was added to a final volume of 15 µl. The amplification conditions are detailed in (Table 17).

Table 17. Quantitative PCR conditions.

STEP	TEMPERATURE, TIME	CYCLES
Initial denaturation	95 °C, 10 minutes	1x
Denaturation	95 °C, 10 seconds	40x
Annealing	Tm, 10 seconds	
Elongation	72 °C, 20 seconds(1)	

Fluorescence measurement	80 °C, 5 seconds

(1) Elongation time for 200 bp amplicons.

To analyze the products obtained in the PCR, the denaturation curves (Melting Curves) were performed. For this, increments of 0.5 °C were programmed every 5 seconds, starting at 65 °C until reaching 95 °C, determining the fluorescence after each increase in temperature.

Once Ct values were obtained (Ct=number of cycles required for the fluorescent signal to cross the threshold), comparison of multiple samples was performed using relative quantification by the $2^{-\Delta\Delta Ct}$ method (Livak and Schmittgen, 2001; Pfaffl, 2001), normalizing the data against the actin gene as an endogenous reference.

$$RE = 2^{-\Delta\Delta Ct}$$

$$\Delta\Delta Ct = (Ct_t - Ct_c)_{Tto} - (Ct_t - Ct_c)_{Ref}$$

RE: Relative expression of the target gene with respect to the control gene

t: Target gene

c: Control gene

Tto: Treatment conditions

Ref: Reference conditions

8. Genetic transformation

8.1. Obtention of *F. oxysporum* transformants

8.1.1 Generation of F. oxysporum protoplasts

Protoplasts were obtained following the protocol described by (Powell and Kistler, 1990) with some modifications. First, $5x10^8$ fresh microconidia (obtained from a culture grown for 3 days at 28 °C and 170 rpm) were inoculated in 200 ml of PDB. After 14 hours of incubation, the obtained germlings were collected by filtration through a double layer of Monodur and washed first with sterile Milli-Q water and then with OM solution(1). Germlings were collected with a sterile spatula and transferred to a 50 ml Falcon tube containing 5% (w/v) of the *Extralyse*® enzyme preparation (Laffort) dissolved in OM. The mix of germlings and enzyme was incubated for at least 45 minutes at 30 °C with slow shaking (60 rpm). After this time, protoplasts generation was monitored every 10 minutes by microscopic observation until having an optimal number and quality of protoplasts. At this time, the

enzymatic digestion was stopped by adding ice-cold STC solution(2) to the mix. Protoplasts were filtered through a double layer of Monodur, in Corex (Pyrex) centrifuge tubes placed on ice and washed with ice-cold STC solution. Filtrates was centrifuged for 15 minutes at 3,000 rpm and 4 °C in a vasculating rotor, the pelleted protoplasts were carefully resuspended in 1 ml of STC and counted with a hemocytometer. The protoplast solution was adjusted to a final concentration of $3x10^7$ protoplasts/ml and stored at -80 °C in aliquots of 100 µl with 10% of PEG(3) (v/v) and 1% DMSO (v/v).

(1) **OM solution:** 1.2 M $MgSO_4$ and 0.1 M $N_{a2}HPO_4$; pH 5.8-6.0 adjusted with orthophosphoric acid. Sterilize by filtration.

(2) **STC solution:** 0.8 M sorbitol, 50 mM CaCl2 and 50 mM Tris-HCl pH 7.5.

(3) **PEG:** 60% polyethylene glycol 4000 (w/v) in 0.6 M MOPS.

8.1.2 Transformation of F. oxysporum protoplasts

Transformation was performed as described (Malardier *et al.,* 1989) with slight modifications. First, the transforming DNA (approximately 2 µg), aurintricarboxylic acid (ATA; 10 µl of a 0.1M stock previously centrifuged 3 minutes at 13,400 rpm) were mixed in an Eppendorf tube with TEC solution(1) to a final volume of 60 µl. Simultaneously, a transformation control without DNA was prepared. The mixtures were incubated for 20 minutes on ice, and after this time, they were carefully mixed with 100 µl of protoplasts ($3x10^7$) and incubated on ice another 20 minutes more. Then, 160 µl of PEG solution were added, mixed, and incubated for 15 minutes at RT. Next, 1 ml of STC was added and the samples were centrifuged for 5 minutes at 3,000 rpm to pellet the protoplasts that were finally resuspended in 200 µl of STC. In the case of the protoplasts incubated with the transforming DNA, 4 aliquots of 50 µl were mixed with 3 ml of Top agar (prewarmed to 45 °C) and spread on plates with regeneration minimal medium. In the case of the control, without DNA, 10^{-3} and 10^{-4} dilutions were made in STC, adding 100 µl of each one to 3 ml of Top agar and spread on plates with the same medium, to obtain different protoplast concentrations and determine the percentage of regeneration and its viability. In addition, a 10^{-4} dilution of the control solution was made in sterile Milli-Q water, which causes destabilization of the protoplasts and their consequent death, of which 100 µl were mixed with the Top agar, to determine the percentage of spores present. A final control was carried out by mixing 190 µl of the control solution with 3 ml of Top agar, to certify the absence of growth in selective medium. Plates were incubated at 28 °C for 90 minutes, 3 hours or 14 hours before adding the 3 ml of Top agar containing phleomycin (400 µg),

nourseothricin (1.625 mg) or hygromycin B (2 mg), respectively. No antibiotic was added to the regeneration and spore controls. Plates were incubated again at 28 °C for an additional 4-5 days until the appearance of transformant colonies that were transferred to selective medium and subjected to two consecutive rounds of single monoconidial purification.

(1) **TEC solution:** 10 mM Tris-HCl pH 7.5, 1 mM EDTA pH 8.0 and 40 mM $CaCl_2$.

8.2. Obtention of *S. cerevisiae* transformants

8.2.1 Generation of S. cerevisiae competent cells

Competent yeast cells were prepared using the LiAc method as described in "Yeastmaker™ Yeast Transformation System 2 manual" (Clontech, USA) with some modifications. First, it was necessary to refresh the yeast strain of interest, and for this, from a stock frozen at -80 °C, the strain was streaked on a YPDA plate and allowed to grow at 30 °C until the appearance of colonies (2-3 days). A single colony was inoculated into 3 ml of YPD liquid medium in a sterile 15 ml culture tube and incubated at 30 °C with orbital shaking at 250 rpm for 8 hours. After this time, 1-10 µl of the pre-culture (depending on the OD_{600}) are added to a 250 ml flask containing 50 ml of YPD and left incubating at 30 °C and orbital shaking at 250 rpm O/N (14-16 hours). When the OD_{600} reached 0.4-0.5, the culture was divided into two 50 ml sterile Falcon tubes and cells were centrifuged at 3,500 rpm during 5 minutes at RT. Each cell pellet was resuspended in 8 ml of sterile Milli-Q water and centrifuged again for 5 minutes at 3,500 rpm and RT. After removing the supernatant, each pellet was resuspended in 750 µl of fresh 1.1X TE/LiAc solution(1), transferred to two Eppendorf tubes, and centrifuged at 13,400 rpm for 15 seconds. Each pellet was resuspended in 350 µl of 1.1X TE/LiAc solution and kept on ice until transformation.

(1) **1.1X TE/LiAc solution:** 1.1 ml of 10X TE buffer, 1.1 ml of 1M LiAc (10X) and add sterile Milli-Q water until 10 ml.

8.2.2 Transformation of S. cerevisiae competent cells

Yeast transformation was carried out following the instructions of the "Yeastmaker™ Yeast Transformation System 2 manual" (Clontech, USA) with some modifications. First, plasmid DNA (approximately 100 ng), DNA fragment of interest (approximately 160 ng) and denatured carrier DNA (50 µg; heated at 100 °C for 5 minutes and cooled on ice another 5 minutes; Repeat once more just before use) were combined in an Eppendorf tube to a final volume of 10 µl with sterile Milli-Q water. A control without the DNA fragment of interest was included. Competent yeast cells (50 µl) were added and

mixed well by pipetting, after which, 450 µl of PEG/LiAc solution(1) was added. The mix was incubated for 30 minutes at 30 °C, vortexing well every 10 minutes. Then, 20 µl of DMSO was added to the mix and it was incubated for 15 minutes at 42 °C, remixing well by vortexing every 5 minutes. Cells were pelleted for 15 seconds at 13,400 rpm and resuspended in 500 µl of sterile Milli-Q water. 100 µl taken directly from the transformation mix and 100 µl of a 1/10 dilution were spread on plates with the appropriate selective medium and incubated upside down at 30 °C until colonies appear (3-5 days). Transformation efficiency was calculated by applying the following formula:

$$\textit{Transformation Efficiency} = \frac{cfu\ x\ Suspension\ Volume\ (ml)}{Vol.\ plated\ (ml)\ x\ amount\ of\ DNA\ (\mu g)}$$

(1) **PEG/LiAc solution:** 8 ml of 50% PEG 3350, 1 ml 10X TE buffer and 1ml of 1M LiAc (10x).

8.3. Obtention of *E. coli* transformants

8.3.1 Generation of E. coli competent cells

Bacterial competent cells were prepared using the method described by (Untergasser, 2008) with some modifications. First, *E. coli* DH5α strain was streaked on an LA plate and incubated O/N at 37 °C to obtain fresh cells. Different isolated colonies were inoculated into inoculum tubes with 5 ml of SOB medium(1). After 14 hours of incubation at 28 °C and orbital shaking at 250 rpm, 3 ml of these starter cultures were inoculated into 4 flasks of 1 L containing 250 ml of SOB medium. The next day, when the OD_{600} reached 0.45, the cultures were placed on ice for 10 minutes. Subsequently, the cells were pelleted by centrifugation at 4,000 rpm and 4 °C for 10 minutes, the supernatant was removed and each of the four pellets were resuspended in 80 ml of cold Inoue solution(2). The samples were centrifuged again under the same conditions, but the resulting pellets were resuspended this time in 20 ml each of Inoue solution. Then, the 4 aliquots were pooled and rapidly mixed with 6 ml of pre-warmed DMSO. While preparing 200 µl aliquots, the mix was left at RT for a maximum time of 10 minutes. Finally, the competent cells were frozen in liquid nitrogen and stored at -80 °C.

(1) **SOB medium:** 0.5% yeast extract (w/v), 2% tryptone (w/v), 10 mM NaCl, 2.5 mM KCl, 10 mM $MgSO_4$ and 10 mM $MgCl_2$.

(2) **Inoue solution:** $MnCl_2$ (10.9 g/L), $CaCl_2$ (2.2 g/L), KCl (18.7 g/L) and 20 ml 0.5 M PIPES(3). Add 1 L of water and filter-sterilize.

(3) **PIPES solution:** Dissolve 15.1 g PIPES (piperazine-1,2-bis[2-ethanesulfonic acid]) in 80 ml water by throwing in KOH until the solution clears up. The pH should be close to the desired pH 6.7. If it is too low, add KOH, if it is too high, add HCl. Add water until 100 ml and aliquot in 10 ml tubes. Store at -20 °C.

8.3.2 Transformation of E. coli competent cells

For transformation of *E. coli*, 100 µl of competent cells were combined with DTT (17 mM final concentration) and 5 µl of ligation mix (containing the DNA fragment of interest) or directly with 10-100 ng of plasmid DNA. The mix was incubated for 30 minutes on ice, heated at 42 °C for 1 minute and immediately left on ice for 5 minutes, thus allowing the DNA to enter through the pores of the plasma membrane. To allow gene expression, transformed cells were incubated for one hour at 37 °C and 250 rpm with 1 ml of SOC medium(1). Finally, the samples were centrifuged for 2 minutes at 5,000 rpm, 950 µl of supernatant were removed and the remaining volume was spread in LA plates containing the resistance antibiotic. When transformed with the pGEM-T vector, LA medium was supplemented with IPTG (134 µM) and X-Gal ((0.005% (w / v)), allowing the selection of transformed strains through the blue/white colonies method.

(1) **SOC medium:** Add 20 ml filter-sterilized 20% glucose solution to 1 L of SOB medium.

9. Nucleic acids identification and purification techniques

9.1. Standard nucleic acids electrophoresis

The separation and identification of DNA or RNA molecules was carried out by agarose gel electrophoresis dissolved in 1X TAE buffer(1). The agarose concentration ranged between 0.7-2% (w/v), depending on the size and nature of the molecule to be separated. Ethidium bromide stain (0.5 µg/ml final concentration) or *SYBR® Safe* stain (0.2X final concentration) were added to the agarose solution and poured into an electrophoresis tray for polymerization. Each sample was mixed with 6X loading buffer(2) in a 5:1 (v/v) ratio. Electrophoresis was carried out in horizontal chambers in 1X TAE buffer applying a constant voltage of 2-5 V/cm.

Nucleic acids visualization was carried out on an ultraviolet or blue light transilluminator (depending on staining) and the size of the DNA fragments was estimated by comparison with the *GeneRuler 1 kb Plus DNA Ladder* size marker (Thermo scientific), containing fragments from 75 bp to 20 kb.

(1) **50X TAE Buffer:** 242 g/L Trizma base, 100 ml 0.5M EDTA pH 8.0 and 57.1 ml glacial acetic acid.

(2) **6X loading Buffer:** 0.25% bromophenol blue (w/v), 0.25% xylencianol blue (w/v) and 40% sucrose (w/v) in 5X TAE buffer.

9.2. Contour-Clamped Homogeneous Electric Field (CHEF) electrophoresis

Separation and identification of *F. oxysporum* chromosomes was performed by Contour-Clamped Homogeneous Electric Field (CHEF) electrophoresis. For this, protoplasts were prepared following the protocol described in section 8.1.1 but with slight modifications in the solutions used. Thus, the OM solution was replaced by 1.2M $MgSO_4$ solution(1), and the STC solution was replaced by 1M Sorbitol solution(2). In addition, the samples were centrifuged at a lower speed, 2,500 rpm. Protoplast solution was adjusted to a final concentration of $8x10^8$ protoplasts/ml in STE solution(3) and mixed with a volume of 1.2% Low Melting agarose (NuSieve™ GTG™, Lonza) in STE containing 1 mg/ml of proteinase K. Subsequently, this mixture was added in molds (Bio-Rad) obtaining plugs that were allowed to solidify at 4 °C for 15 minutes. Once the plugs were solidified, they were removed from the mold and incubated O/N at 50 °C and 60 rpm in 5 volumes of NDS solution(4). The following day, NDS was removed and the protoplasts were washed 3 times with Wash Buffer (WB) solution(5) at RT and slight agitation for approximately 1 hour. Protoplast plugs were stored at 4 °C in WB, being stable for 3-6 months.

Once solid, the protoplast plugs were inserted into the wells of the gel and sealed with Low Melting agarose. Chromosomes were separated by pulsed-field electrophoresis in 1% Certified Megabase agarose (Bio-Rad) gel (w/v) in commercial 0.5X TBE buffer. Electrophoresis was carried out for 255 hours at 1.6 V/cm in a CHEF-DR® III system (Bio-Rad) in 0.5X TBE at 8 °C, with switch times between 1200 and 4800 s, an angle of 120° and a constant flow of 700 ml/min. The buffer was changed every two days. Gels were stained during 30 minutes with ethidium bromide (0.5 µg/ml final concentration) or with *GelRed*® (3X final concentration) in water, followed by two water washes of 10 minutes to remove excess staining. Chromosomes were visualized on an ultraviolet transilluminator.

(1) **$MgSO_4$ solution:** 1.2 M $MgSO_4$; pH 5.8 adjusted with orthophosphoric acid.

(2) **Sorbitol solution:** 1 M sorbitol.

(3) **STE solution:** 25 mM Tris-base, 50 mM EDTA and 1M Sorbitol; pH 7.5 adjusted with NaOH.

(4) **NDS solution:** 100 mM Tris-base, 500 mM EDTA and 1% Lauryl sarcosine (w/v); pH 9.5 adjusted with NaOH. Sterilize by filtration.

(5) **Wash buffer solution:** 50mM EDTA; pH 8.0 adjusted with NaOH.

9.3. Single chromosomes recovery from a CHEF gel

Chromosome DNA recovery from CHEF gels were performed according to the method described previously (Langner *et al.,* 2019; Langner *et al.,* 2021) with some

modifications. Chromosome bands of interest were excised from the gel and were placed in Eppendorf tubes at 4 °C. Mini-chromosomal DNA was eluted from the gel plugs by electroelution using a *D-Tube™ Dialyzer Midi, MWCO 3.5 kD* (Merck). To do this, first, the membrane was pre-hydrated with Milli-Q water for 5 minutes and, after this time, the water was removed with the help of a pipette and the agarose plug was introduced inside. The tube was filled with 0.5X TAE containing 1 mg/ml of proteinase K, placed in a Falcon tube with the same solution, and left for 1 hour at 55 °C in a water bath. Then, the tube was placed in an electrophoresis rack (*D-Tube™ Electroelution Accessory Kit,* Merck) and it was introduced into the electrophoresis chamber with 0.5X TAE warm buffer (previously heated to 65 °C). Electroelution was carried out at 120V for 3.5-4 hours in the electrophoresis chamber covered with thermal insulation to maintain a constant temperature of approximately 50 °C. Release of the DNA from the membrane was carried out by reversing the polarity for 3 minutes. Eluted DNA was carefully pipetted up and down at least 5 times on inner side of membrane and transferred to a clean microcentrifuge tube. DNA was precipitated by adding 2 vol 100% ice-cold ethanol, 0.1 vol 3M Sodium Acetate (pH 5.2) and incubated O/N at -20 °C. Precipitated DNA was centrifuged for 40 minutes at 10,000 rpm and 4 °C, washed with 1 ml of 70% ethanol (v/v) and centrifuged for 20 minutes at 10,000 rpm and 4 °C. DNA pellet was dried and resuspended in 20-30 µl of sterile Milli-Q water. The amount and quality of DNA extracted was monitored by Nanodrop® ND-1000 using absorbance ratios (260/280 nm and 260/230 nm wavelength).

9.4. Purification of DNA fragments from standard agarose gels

The purification of DNA fragments from agarose gels was performed using the *E.Z.N.A.® Gel Extraction Kit* (Omega Bio-Tek), following the manufacturer's recommendations. In this way, the DNA band of interest was excised from the gel, dissolved in Binding Buffer, and transferred to a column. Subsequently, the column was washed three times and the DNA was eluted in water. The amount and quality of extracted DNA was monitored by electrophoresis in a 0.7% agarose gel (w/v).

9.5. Southern blot

9.5.1 DNA transfer and fixation

For Southern analysis, approximately 1 µg of gDNA from the strains to be analyzed was treated with restriction endonucleases and the digested DNA was separated by electrophoresis in a 0.7% agarose gel (w/v) and 85V. Once the electrophoresis was finished, the gel was treated to denature the DNA before its hybridization, and for this, all the treatments were carried out at RT and shaking. First, an acid depurination (partial hydrolysis)

was carried out, immersing the gel in 0.25N HCl for 15 minutes in two consecutive washes. Subsequently, two 15-minute washes were made with the alkaline 0.5N NaOH:1.5M NaCl solution, to denature the DNA. Finally, the DNA was neutralized by immersing the gel in 0.5M Tris-HCl pH 7.5:1.5M NaCl solution, with two washes of 30 minutes each.

After the gel treatments were finished, the DNA was transferred by capillary to a positively charged nylon membrane (Roche). The transfer was carried out in a tray containing 10X SSC buffer(1) on which was placed an inverted electrophoresis support covered by a filter paper impregnated in 10X SSC. On this filter paper, 3 pieces of *Whatman™* paper (grade 3MM) impregnated in 10X SSC were placed, and then, the treated agarose gel was turned upside down. On top of the gel, the nylon membrane impregnated in 3X SSC, 3 pieces of *Whatman™* paper impregnated in this same buffer and 3 other dry pieces of *Whatman™* paper were successively placed. Finally, a stack of absorbent paper, a piece of glass and an approximate weight of 0.5 kg were placed. The transfer was carried out for at least 12 hours at RT, and finally, the DNA was fixed by introducing the membrane in an oven at 80 °C for 90 minutes.

(1) **10X SSC Buffer:** 1.5M NaCl and 0.17M sodium citrate.

9.5.2 Hybridization

The membrane with the fixed DNA was prehybridized for 1 hour at 50 °C with *DIG Easy Hyb™ Granules* (Roche) at a rate of 0.3 ml/cm^2 of membrane. Subsequently, it was hybridized for at least 12 hours at 50 °C with the same solution containing 20 ng/ml of double-stranded probe labeled with digoxigenin (see section 7.3). Previously, the probe was denatured at 100 °C for 10 minutes and rapidly chilled on ice for at least 5 minutes.

9.5.3 Washes and detection

After the hybridization solution was removed, the membrane was washed twice with a 2X SSC: 0.1% SDS (v/v) solution at RT for 5 minutes and with rotation. This was followed by two more 15-minute washes at 50 °C with a preheated solution of 0.5X SSC:0.1% SDS (v/v). All subsequent washes were done at RT. It was subsequently equilibrated with Buffer 1(1) for 5 minutes and treated with Buffer 2(2) for 30 minutes. The following incubation was carried out for 30 minutes with Buffer 2 containing anti-digoxigenin antibody conjugated to alkaline phosphatase (750 U/ml, Roche) diluted 1:20000. The membrane was then washed 2 times for 15 minutes with Buffer 1 containing 0.3% Tween 20 (v/v) and equilibrated in Buffer 3(3) for 5 minutes.

Detection was carried out by the enzymatic action of alkaline phosphatase on the *CDP-Star*® substrate (Roche), emitting a light signal detected by chemiluminescence. For this, the membrane was placed on a piece of acetate and diluted *CDP-Star*®(4) was added. Subsequently, the membrane was covered with another piece of acetate and the excess liquid was removed. Finally, the image was captured with the Fujifilm LAS-3000 camera.

(1) **Buffer 1:** 0.1M maleic acid pH 7.5 and 0.15M NaCl.

(2) **Buffer 2:** 1% *Blocking reagent* (w/v) (Roche) in Buffer 1.

(3) **Buffer 3:** 0.1M Tris-HCl pH 9.5 and 0.1M NaCl.

(4) ***CDP-Star*® solution:** 1% (v/v) in Buffer 3.

9.5.4 Stripping

When it was necessary to re-hybridize the membrane with a new probe, stripping was carried out to remove the previous one. For this, the membrane was washed twice with distilled water at RT for 5 minutes. It was then incubated twice with the stripping solution(1) at 37 °C for 10 minutes. Finally, it was washed twice with a 2X SSC solution for 5 minutes at RT. After the washes, the membrane is ready for prehybridization and hybridization with the probe.

(1) **Stripping solution:** 0.2M NaOH and 0.1% SDS.

9.6. DNA cloning with plasmid vectors

Cloning of PCR amplified DNA fragments was carried out using the commercial *pGEM®-T Easy Vector System Kit* (Promega) or the *pSparK® I DNA Cloning Kit* (Canvax) depending on whether the DNA fragments had cohesive or blunt ends, respectively, and following the manufacturer's instructions. Before cloning, the fragments were precipitated with 4M ammonium acetate pH 5.4 and 100% ice-cold ethanol, or they were purified using the *E.Z.N.A.® Gel Extraction Kit* (see section 9.4). For more complex cloning, in order to increase efficiency, it was necessary to dephosphorylate the DNA thus avoiding re-ligation. For this, the DNA was treated with *rAPid alkaline phosphatase* (Roche) for 1 hour at 37 °C, followed by its inactivation at 75 °C for 5 minutes.

10. Proteins identification and purification techniques

10.1. Protein isolation and quantification

To extract intracellular proteins, the mycelium obtained under induction conditions was lyophilized and pulverized. The resulting powder was transferred to a 2 ml Eppendorf tube and 1 ml of 0.05M phosphate buffer pH 6.0(1) was added. The resulting mixture was homogenized by vortexing and incubated for 2 minutes on ice. Subsequently, it was

centrifuged at 10,000 rpm and 4 °C for 30 minutes, the supernatant was collected and stored at -20 °C. Protein concentration was determined with the *DC™ Protein assay* (Bio-Rad), using bovine serum albumin (BSA) as a standard and following the manufacturer's instructions. Alternatively, protein extracts were loaded into a Coomassie gel to determine protein amount.

(1) **0.05M phosphate buffer pH 6.0:** 13.2 ml of K_2HPO_4 and 86.8 ml of KH_2PO_4. Take 10 ml of this mixture and take up to 200 ml of water to have the buffer at pH 6.0.

10.2. Protein electrophoresis

Protein separation was performed by SDS-PAGE electrophoresis under denaturing conditions (Sodium Dodecyl Sulphate-Polyacrylamide Gel Electrophoresis) (Laemmli, 1970). The samples were mixed with loading buffer(1), boiled for 10 minutes and loaded into a polyacrylamide gel (40% Acrylamide/Bis solution 37.5:1, Bio-Rad), consisting of two phases, a top gel or concentrating gel, with a polyacrylamide concentration of 4%, and a lower gel or separating gel with a polyacrylamide concentration of 8%. Electrophoresis was performed in Tris-Glycine(2) buffer at 15mA while the protein samples were introduced into the concentrating gel and then at 30mA into the separating gel. A vertical system (Mini-Protean II, Bio-Rad) was used and the *ProSieve Quadcolor* marker (Lonza) was used to obtain a molecular weight reference.

(1) **Loading buffer:** 50 mM Tris-HCl pH 6.8, 8% glycerol (v/v), 1.6% SDS (w/v), 4% ß-mercaptoethanol (v/v), 0.1% bromophenol blue (p/w).

(2) **Tris-Glycine buffer:** 25 mM Trizma base, 192 mM glycine, 0.1% SDS pH 8.3 (w/v).

10.3. Western blot

Once the electrophoresis was finished, the proteins were transferred to a nitrocellulose membrane using the *Trans-Blot® Turbo™ Transfer System* (Bio-Rad) following the manufacturer's instructions. After several washes with TBS-T(1), membrane blocking was performed using 20 ml of TBS-T supplemented with 5% skim milk (w/v) for 1 hour. The membrane was washed several times with TBS-T and incubated overnight at 4 °C with a 1/1000 dilution of the primary antibody (anti-Ynr1, José Manuel Siverio) in TBS-T with 1% skim milk. Membranes were washed three times with TBS-T for 10 minutes and incubated with the secondary antibody (anti-rabbit 1/5000) for 1 hour in TBS-T with 1% skim milk. Finally, the membrane was washed three times with TBS-T and the proteins were detected by chemiluminescence using *ECL Select™ Western blotting Detection reagent* (GE Healthcare, Amersham™) and Fujifilm LAS-3000 camera.

(1) **TBS-T:** 202 mM Trizma base, 137 mM NaCl and 0.1% Tween 20 (v/v). Adjust the pH to 7.6.

11. Biochemical assays

11.1. Nitrate reductase activity

Nitrate Reductase (NR) activity was determined by spectrophotometry as described by (Fujii and Takaya, 2008). The NR activity was determined in cell-free extracts of the mycelium obtained under induction conditions. Reaction mixtures adjusted to a final volume of 1 ml contained: 900 µl of a solution consisting of 100 mM potassium phosphate buffer pH 7.5, 10% (v/v) glycerol, 10 mM $NaNO_3$, 2.5 mM Na_2MoO_4, 0.01 mM FAD and 0.2 mM NADH; 100 µl of the crude extract of the strain to be analysed were added to this solution. The reaction blank was prepared by adding 100 µl of 0.05 mM potassium phosphate buffer pH 6.0 to the solution instead of the crude extract. The reaction mixtures were then incubated at 30 °C for 30 min at 200 rpm shaking. After the incubation time, 300 µl were taken from this mixture and 300 µl of the Griess reagent[1] were added and completed to a final volume of 900 µl with sterile Milli-Q water. After mixing with gentle agitation, the absorbance at 540 nm was determined. The micromoles of NO_2^- formed were determined by interpolation to a calibration curve prepared with $NaNO_2$ as standard, in a concentration range of 10-100 µM. The activity defines one Unit of enzyme activity as that amount of enzyme that produces 1 µmol of NO_2^-/min. The specific activity of the enzymes was expressed as Units/mg protein.

[1]**Griess reagent:** 1% sulphanilamide in 50 ml 1N HCl and 0.01% N-(1-naphthyl)ethylenediamine in 50 ml 0.1 M potassium phosphate buffer, pH 7.5.

11.2. Nitrite reductase activity

Nitrite Reductase (NiR) activity was measured as the rate of NO_2^- disappearance using the NADPH-nitrite reductase method described by (Ferrari and Varner, 1971). The NiR activity was determined in cell-free extracts and $NaNO_2$ at a final concentration of 2.5×10^{-4} M was added to start the assay. Immediately, a spectrophotometric measurement was made to determine the initial concentration of nitrite in the medium. After 40 minutes of incubation, the amount of nitrite present in the medium was measured again. The difference between the final and initial concentration of nitrite in the medium reflects the amount of nitrite reduced by the NiR enzyme. Nitrite was determined colorimetrically adding 300 µl of the Griess reagent. One unit of nitrite reductase is defined as the amount of enzyme causing the reduction of 1 µmol of NO_2^-/min. The specific activity of the enzymes was expressed as Units/mg protein.

11.3. In vitro mRNA translation assay

This assay was performed using the *Retic Lysate IVT™ kit* (Invitrogen) that contains reticulocytes isolated from rabbits that can efficiently translate exogenous RNAs from different organisms. 7.5 µg of RNA isolated from mycelium obtained under induction conditions was added to the reaction mixture containing: 1.25 µl of translation mix minus-methionine (with different salt concentration to optimize the efficiency), 2.5 µl of 500 µM methionine, 17 µl of retic lysate and sterile Milli-Q water (RNase free) was added to final volume of 25 µl. The mixture was incubated for 2 hours at 30 °C in a water bath for protein synthesis. Next, 2.5 microliters of RNase A (1mg/ml) were added and incubated at 30 °C for 10 minutes. To stop the reaction, the samples were placed on ice for 5 minutes and stored at -20 °C for subsequent analysis.

12. Phenotypic assays

12.1. Growth rate

To compare the growth speed between the different strains, 10 µl of a suspension of $1x10^8$ microconidia/ml were inoculated on the center of a Petri dish with YPDA medium. Plates were incubated for 3 days at 28 °C, scanning at 48h and 72h of growth. The growth rate was calculated by measuring the increase in the colony area in those 24 hours using the image editing program "MultiGauge V3.0". Growth rate was also determined by measuring hyphal density indicated as mean gray value using the image editing program "ImageJ".

12.2. Conidiation rate

To evaluate the conidiation capacity in solid medium, 10 µl of a suspension of $1x10^8$ microconidia/ml were inoculated on the center of a Petri dish with YPDA medium and the strains were allowed to grow at 28 °C for 7 days. After this time, the microconidia were collected from the whole colony. For this, 3 ml of Milli-Q water was added to the colony, scraped with a spatula and the volume was filtered through a system consisting of a 5 ml tip with cotton. Finally, the microconidia were counted to determine the conidiation rate.

12.3. Quantification of spontaneous colony growth variants

To quantify the frequency of colony growth sectors, we have developed an optimized method (Díaz *et al.,* 2022) which allows the systematic analysis and efficient quantification of these sectors in multiple colonies of *F. oxysporum.*

For this, Puhalla's Minimal Medium (PMM) was supplemented with methionine (50 mM) since this amino acid restricts the growth of the colony, allowing a more accurate quantification of the sectors generated (Figure 8). Two methods have been optimized for

the quantification of sectors, although in this project only the "line method" has been used. Firstly, the concentration was adjusted to $5x10^6$ microconidia/ml. Next, a drop of 5 µl was added to a bacterial loop, placed the loop carefully on the surface of the PMM plate, and spread the microconidia along a line of 5 cm. Plates were incubated at 28 °C for 5 days and the colony growth sectors were counted on days 3, 4, and 5 after inoculation (Figure 9).

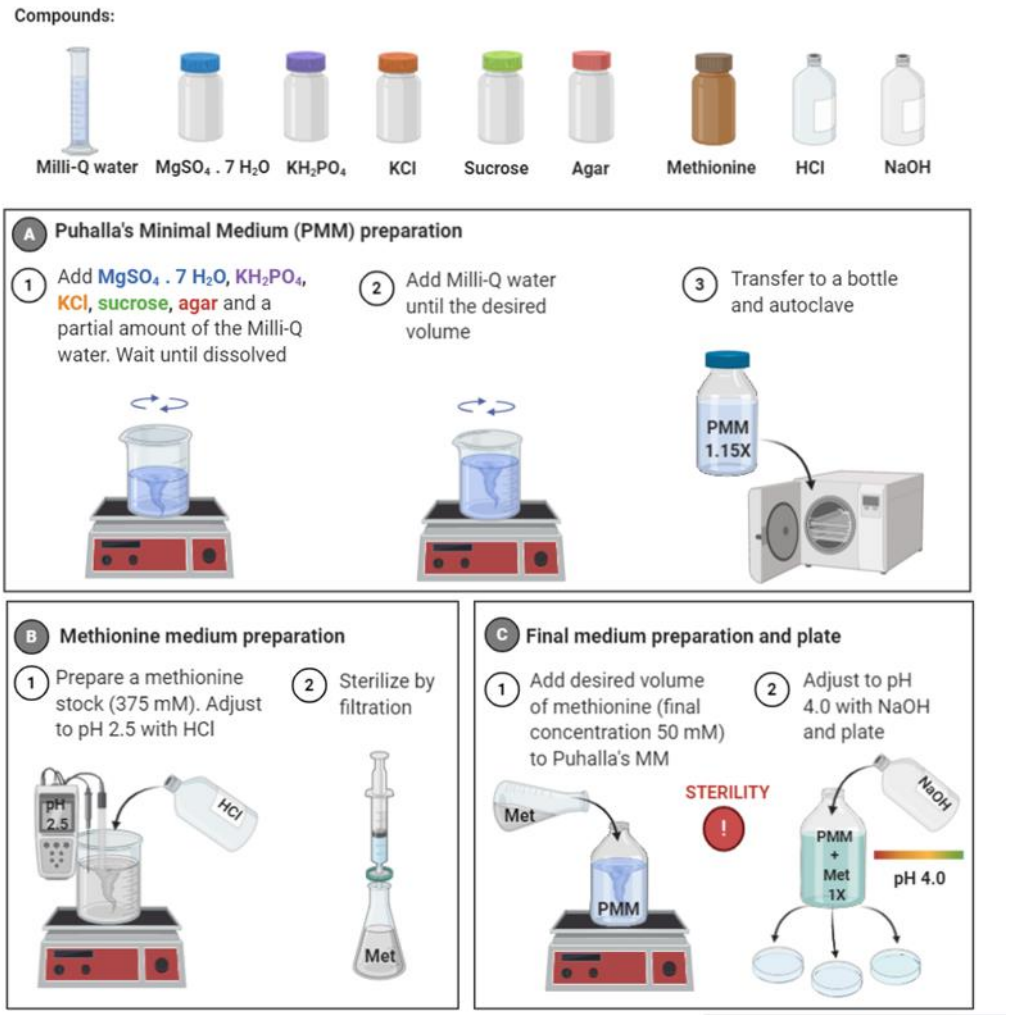

Figure 8. Preparation of Puhalla's Minimal Medium (PMM) supplemented with methionine. (A) Weigh the different ingredients of PMM, adjust with water to the desired final volume to obtain a 1.15X solution, and autoclave. **(B)** Prepare a 375 mM methionine stock solution in water, adjust the pH to 2.5 with 2.4 M HCl for solubilization, and filter-sterilize. **(C)** Add the appropriate volume of methionine stock to the autoclaved PMM cooled to 45 °C, adjust pH to 4.0 with 10 N NaOH, and pour into Petri dishes.

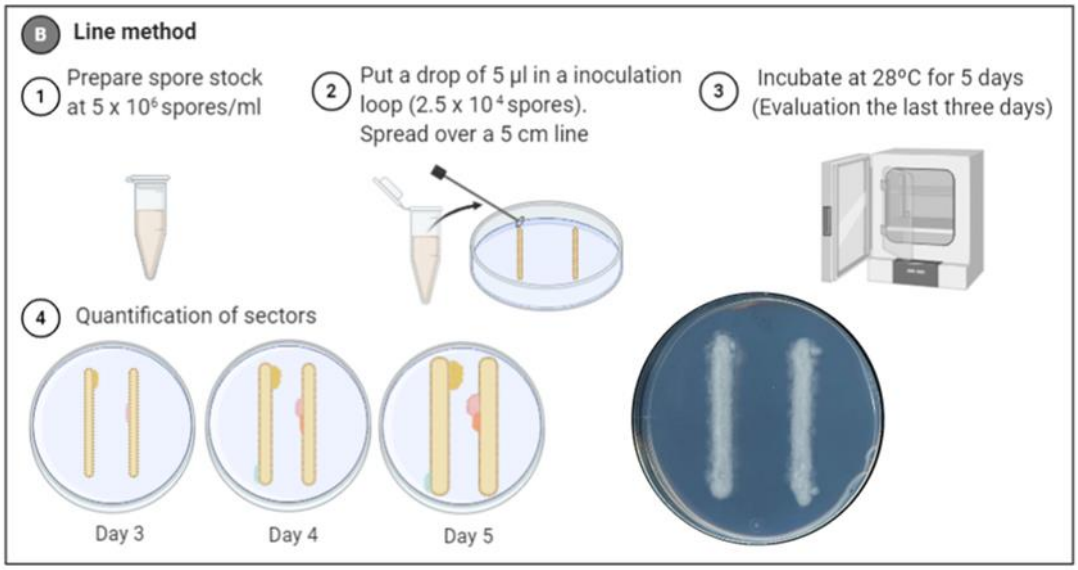

Figure 9. Quantification of colony growth sectors. Line method: Place a 5 µL drop containing $2.5x10^4$ microconidia in an inoculation loop and spread along a 5 cm line (2 lines per plate). Incubate at 28 °C and count the emerging colony growth sectors starting at day 3 until day 5. Perform at least 6 replicates for both methods.

12.4. Stress assays

12.4.1 Cell wall stress

To determine the capacity of the generated strains to growth in presence of cell wall-damaging agents, droplets from serial dilutions containing 10^4, 10^3 and $5x10^2$ fresh microconidia were spot-inoculated on MM plates with or without Calcofluor White (CFW; 40 µg/ml) or Congo Red (CR; 100 µg/ml). Plates were incubated at 28 °C for 3 days and scanned.

12.4.2 Toxicity to the methyl methanesulfonate compound

To establish the sensitivity level of the generated mutants to the DNA-damaging agent methyl methanesulfonate (MMS), aliquots of $1x10^7$ microconidia were inoculated in Milli-Q water, either treat or not (control) with 0.1% MMS for 1 or 2 hours at 28 °C and then incubated for 5 minutes at 50 °C. Droplets from serial dilutions containing 10^4, 10^3 and 10^2 microconidia were spot-inoculated on PDA plates, incubated at 28 °C for 2 days and scanned.

12.4.3 Toxicity to the 5-fluoroorotic acid compound

To determine the rate of spontaneous mutation and associated genomic instability, a toxicity assay to 5-fluoroorotic (5-FOA) compound was performed (Boeke *et al.,* 1984). For solid medium, yeast strains were spot-inoculated on SD medium plates under induction

conditions (2% galactose + 0.1% glucose) with or without Ura (0.005%) and 5-FOA (0.1%). After two days of incubation at 30 °C, the resistance degree of the colonies to the toxic compound was evaluated. For liquid condition, yeast strains were grown O/N at 30 °C and 200 rpm in SD medium. After 14 hours, the optical density (OD600) of the cultures was measured and adjusted to 0.03. Aliquots were added to wells of Microtiter™ plates containing SD medium supplemented with Ura and/or 5-FOA at the previously indicated concentrations. The growth rate was determined by measuring the optical density at 600nm.

12.5. Tomato plant infection

Tomato plant infection assays were performed as described (Di Pietro and Roncero, 1998). To analyze the pathotype of the different strains of *F. oxysporum*, tomato plants (*Lycopersicon esculentum* cultivar Monika) were used. For this, the two-week-old plants (see section 5.4) were inoculated with the different strains by immersing the roots in a suspension of $5x10^6$ microconidia/ml for 30 minutes. Then, the plants were transplanted into seed sockets with new vermiculite and grown in a growth chamber with the conditions previously described (see section 5.4). After 10 days of inoculation, the evolution of the disease began to be recorded and the survival percentage after 30-40 days was established. For this, the Kaplan-Meier method was used, comparing the differences between groups using the log-rank test with the software "GraphPad Prims V8.0" (López-Berges *et al.*, 2012).

13. Serial passaging experiments

13.1. Serial passaging experiment on solid YPDA medium

Serial passaging experiments on solid YPDA medium were performed both at medium-term (Figure 10) and long-term (Figure 11). Both assays started by spot-inoculating $1x10^6$ microconidia on the center of YPDA plates and incubating for one week at 28 °C. Then, 5 ml of sterile Milli-Q water was added to the colony and scraped with a sterile spatula. The supernatant was homogenized with a pipette to release the microconidia adhered to the mycelium and they were separated through a sterile filtering system consisting of a 5 ml tip with cotton. Finally, the microconidia were counted and an aliquot of $1x10^6$ microconidia was spot-inoculated on a new YPDA plate for the next passage. For the long-term experiment, gDNA from the mycelium of the evolved populations after the 10^{th} passage was isolated and analysed by qPCR to detect CNVs. In the medium-term experiment, gDNA isolation was performed at the level of monoconidial isolates and at each of the passages. The samples were also analysed by qPCR to detect CNVs.

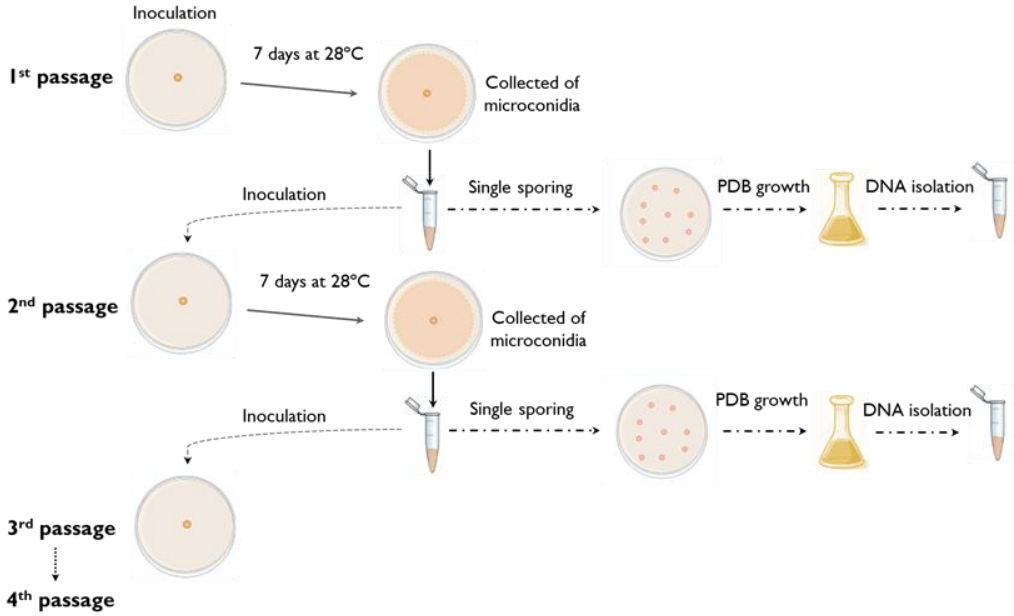

Figure 10. Schematic diagram of the medium-term serial passaging experiment on solid YPDA medium. $1x10^6$ microconidia of Fol4287 were spot-inoculated on YPDA plates and incubated for 7 days at 28 °C. Total conidia from the colony were collected and an aliquot of $1x10^6$ microconidia was spot-inoculated on a new YPDA plate for the next passage. In parallel, dilutions of collected microconidia were plated on YPDA and incubated for 2 days at 28 °C. gDNA from monoconidial isolates was isolated and analyzed by qPCR to detect CNVs. Four serial passages were performed.

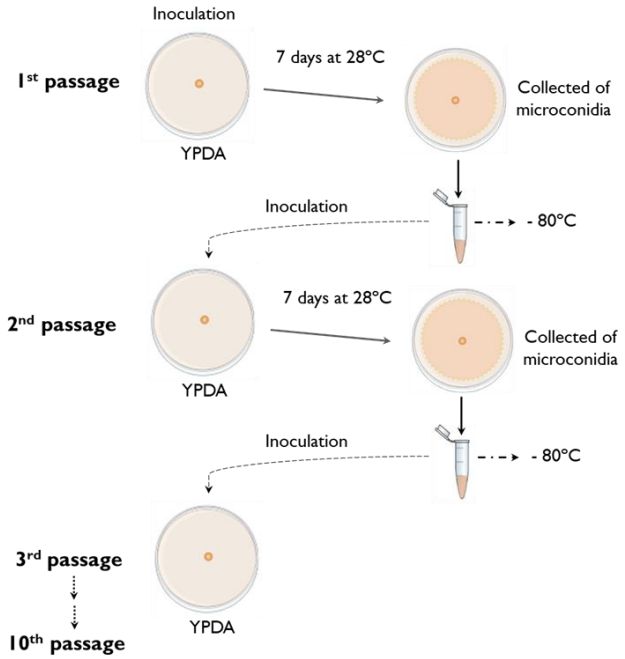

Figure 11. Schematic diagram of the long-term serial passaging experiment on solid YPDA medium. $1x10^6$ fresh microconidia of the wild type strain were spot-inoculated on the center of YPDA plates and incubated at 28 °C for 7 days. Total conidia from the colony were collected and $1x10^6$ microconidia was spot-inoculated on a new YPDA plate for the next passage. gDNA from the mycelium of the evolved lines after the 10^{th} passage was isolated and analyzed by qPCR to detect CNVs.

13.2. Serial passaging experiment on liquid YPD medium

1.25x10^7 fresh microconidia of the wild type strain *Fol4287* were inoculated in YPD liquid medium and grown for 3 days at 28 °C and 170 rpm orbital shaking. The culture was filtered through a double layer of Monodur and an aliquot with 1.25x10^7 microconidia was inoculated into a fresh flask with YPD for the next passage. In parallel, serial dilutions of the collected conidia were plated on YPDA to obtain monoconidial isolates and gDNA was isolated directly from the mycelium of colonies grown on plates. A qPCR analysis was performed to detect CNVs (Figure 12).

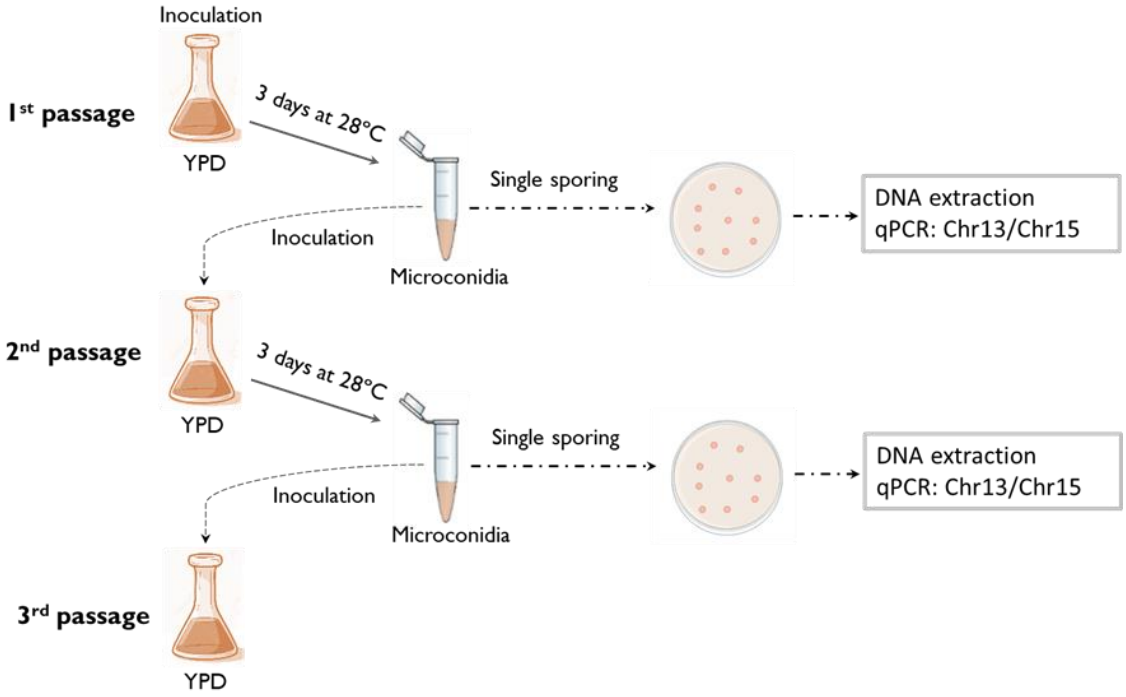

Figure 12. Schematic diagram of the medium-term serial passaging experiment in liquid YPD medium. 1.25x10^7 fresh microconidia of the wild type strain Fol4287 were cultured in liquid YPD medium at 28 °C for 3 days. 1.25x10^7 of collected microconidia were inoculated in a new flask (next passage). In parallel, dilutions of collected microconidia were plated on YPDA and incubated for 2 days at 28 °C. gDNA from individual colonies was isolated and analyzed by qPCR to detect CNVs.

14. Methods for CNVs quantification

To study chromosomal dynamics and quantify the loss rate of accessory chromosomal regions, different quantification methods were optimized.

14.1. Fluorescence-activated cell sorting

Fluorescence-activated cell sorting (FACS) experiments were performed as described (Vlaardingerbroek *et al.,* 2015) with some modifications. Conidia suspensions

were prepared by filtering cultures through 2 layers of Miracloth (Merck) and diluted in sterile Milli-Q water. The parameters used in the cytometric sorting were: 20,000 evt/s (number of drops per second containing a particle that generates a fluorescent signal), 70 µm nozzle at 70 psi pressure, λ=488nm (GFP), λ =561nm (mCherry). The conidial populations classified according to their fluorescent pattern were plated on YPDA and incubated for 2 days at 28 °C to obtain monoconidial isolates that were subsequent analyzed by fluorescence microscopy using an Evos FL inverted microscope (AMG). All FACS experiments were performed using a BD Facsaria III.

14.2. Quantitative PCR

For the quantification of copy number variations (CNVs), a quantitative PCR (qPCR) was carried out using 5 µl of gDNA diluted to 10 ng/µl (50 ng final concentration); 7.5 µl of *FastStart Essential DNA Green Master* (Roche), 300nM of each primer and sterile Milli-Q water was added to a final volume of 15 µl. Amplification conditions were the same as those detailed in section 7.6.

Copy number was established using the single copy actin gene as reference. A value of 2 indicates duplicated chromosomal regions and a value of 1 non-duplicated regions. In the case of loss of a copy, the coverage would go from a value of 2 to a value of 1.

14.3. Restriction Fragment Length Polymorphism (RFLP) method

14.3.1 Obtaining the DNA construct carrying the RFLP13 marker

To obtain transformants that had an RFLP marker in the duplicated region of chromosome 13, a DNA construct was designed in which a SNP was artificially included, giving rise to the RFLP marker. The transforming DNA construct was obtained by fusion PCR technique (Figure 13). In the first round of PCR (PCR I) the two ends of the DNA construct were amplified separately with primers carrying a SNP in the overlapping region. In the second round of PCR (PCR II) the amplified fragments were fused through overlapping ends. In the last round (PCR III) the previous fragment was amplified using nested primers obtaining a fragment carrying the RFLP marker that generates a restriction site for the enzyme *Xho*I. This DNA construct were used to transform protoplasts of the wild type strain *Fol4287* and transformants with this DNA construct inserted in their genome were obtained (wt-RFLP13 strain).

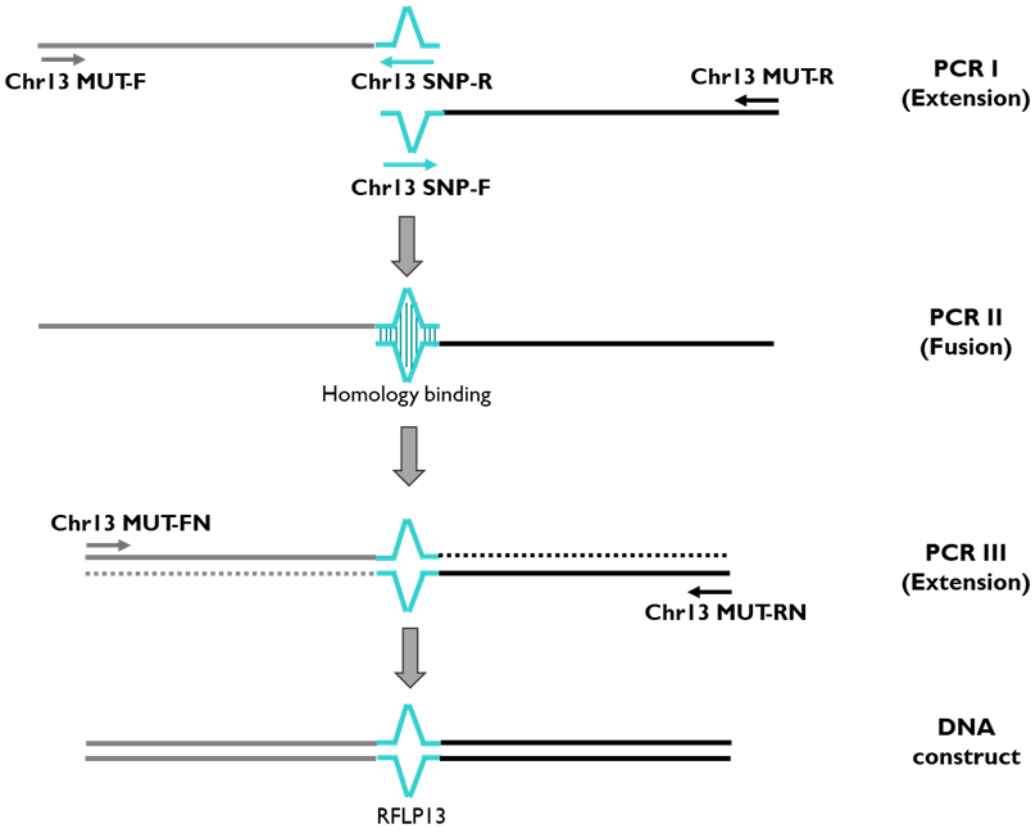

Figure 13. Obtaining DNA construction for chromosome labelling. In the first round of PCR (PCR I), the two ends of the DNA construct were amplified separately with primers carrying a SNP at their overlapping end. In the second round of PCR (PCR II) both fragments were fused. In the last round (PCR III) the fragment previously obtained was amplified using nested primers.

14.3.2 Detection and quantification of RFLP13 marker loss

A short-term serial passaging experiment was performed to quantify the loss rate of chromosome 13mini (Figure 14). Conidia of the wt-RFLP13 strain were plated on YPDA directly from stock at -80 ºC. After growing for two days, three random colonies (P1-P3) were picked and resuspended in Milli-Q water. Serial dilutions of the resulting conidia were plated on YPDA to obtain individual colonies and gDNA was isolated directly from the colony mycelium. 200 monoconidial isolates derived from each of the progenitor colonies were analyzed by PCR and enzymatic digestion with *Xho*I to determine if the loss of one of the duplicated regions of chromosome 13 had occurred.

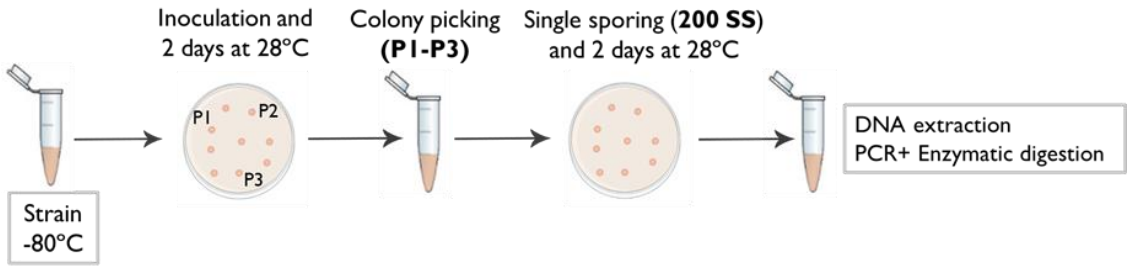

Figure 14. Short-term serial passaging experiment for RFLP13 marker loss detection. Microconidia of wt-RFLP13 from -80 °C were directly inoculated on YPDA plates and incubated for 2 days at 28 °C . Dilutions of three randomly colonies (P1-P3) were plated on YPDA and incubated at 28 °C for 2 days more. gDNA from 200 individual colonies of each one was isolated and analyzed by PCR and enzymatic digestion to determine absence or presence of chromosome loss.

15. Bioinformatic analysis

15.1. Gene search and sequence retrieval

In silico gene search of both Fol4287 and related fungal species was performed using the *BLAST* algorithm (Altschul *et al.,* 1990) from the *National Center for Biotechnology Information* (NCBI; http://www.ncbi.nlm.nih.gov), *Fungal and Oomycete genome database* (FungiDB; https://fungidb.org/fungidb/app) and *Saccharomyces Genome Database* (SGD; https://www.yeastgenome.org).

15.2. Domain prediction and MW calculation

Protein domains prediction was made using the Prosite (ExPASy; https://prosite.expasy.org/) and NCBI Conserved Domain Search (https://www.ncbi.nlm.nih.gov/Structure/cdd/wrpsb.cgi) algorithms. The molecular weight (MW) of the analyzed proteins was calculated using *ExPASy's Compute pI/Mw* tool (Gasteiger *et al.,* 1993; https://web.expasy.org/compute_pi/).

15.3. Illumina single chromosome sequencing

Illumina NovaSeq 6000 sequencing of a single chromosome recovered from a CHEF gel (section 9.3) was performed by STAB VIDA company, Portugal, obtaining a total of 23,446,092 paired reads with a mean length of 150 bp. Dilay Hazal Ayhan, of the University of Massachusetts Amherst, performed the subsequent bioinformatic analysis (Ayhan, 2021). The reads obtained in the Illumina sequencing were mapped to the last reference genome sequence of *Fol4287* (Ayhan *et al.,* 2018) obtaining a median coverage of 10.5X using *BWA mem v0.7.15* (Li and Durbin, 2009). The alignments were cleaned and sorted, after which the pair information was fixed, duplicate reads were marked, and alignment statistics were generated via *Samtools v1.4.1* (Li, *et al* 2009) and *Picard v2.0.1*

(http://broadinstitute.github.io/picard). The read coverages were calculated at single-base resolution via *BEDtools genomecov v2.26.0* (Quinlan *et al.,* 2010). To obtain the complete sequence of the isolated chromosome, the regions with high read mapping to the reference assembly were artificially joined and the PacBio reads of the wild type whole-genome sequencing were mapped to this artificially constructed chromosome using *BWA bwasw v0.7.15* (Li and Durbin, 2010).

15.4. CNV calling

Whole genome sequencing of wild type strain Fol4287 and evolved populations and subsequent bioinformatic analysis was performed by Dilay Hazal Ayhan (included in López-Díaz, 2019). Further analysis was performed to optimize the detection of CNVs present in the genome (Ayhan, 2021). The read depth at single nucleotide resolution was generated using the *BEDtools genomecov v2.26.0* tool. Median Illumina read depths calculated over 10 kb-window regions were normalized first to the median read coverage of the sample and then to wild type strain. The coverage of duplicate regions was artificially multiplied by 2 to reflect the real copy numbers.

16. Software and website

Prediction and processing of the data obtained in this work has been performed using the software and websites listed in (Table 18).

Table 18. Software and websites used in this study.

SOFTWARE	APPLICATION
Adobe Illustrator CS5	Figure design
Adobe Photoshop CS6	Image editing
AxioVision 4.7	Microscope imaging and analysis
BioEdit	Multiple sequence alignment
CFX Maestro 1.1 (Bio-Rad)	qPCR data acquisition and analysis
GraphPad Prism v8.0	Graph creating and statistical analysis
Image Reader LAS-3000	Capture, editing and analysis of images obtained after revealed by chemiluminescent detection
ImageJ	Image editing / Image quantification and measurement
Kodak 1D Image Analysis	Capturing photographic images of agarose gels

MultiGauge v3.0	Image editing / Image quantification and measurement
Oligo 7	Design and analysis of oligonucleotides
SeqBuilder	Editing and analysis of nucleotide and protein sequences
SeqMan	Assembling DNA sequences in contigs
SnapGene	Editing and analysis of nucleotide and protein sequences
WEBSITE	**APPLICATION**
National Center for Biotechnology Information (NCBI) https://www.ncbi.nlm.nih.gov	BLAST: Sequence alignment Genome database: Retrieval of gene and protein sequences
FungiDB https://fungidb.org/fungidb/app	BLAST: Sequence alignment Genome database: Retrieval of gene and protein sequences
Saccharomyces Genome Database (SGD) https://www.yeastgenome.org	BLAST: Sequence alignment Genome database: Retrieval of gene and protein sequences
ExPASY-Prosite database https://prosite.expasy.org/	Protein domain prediction
NCBI Conserved Domain Search https://www.ncbi.nlm.nih.gov/Structure/cdd/wrpsb.cgi	Protein domain prediction
ExPASY https://web.expasy.org/compute_pi/	Compute pI/Mw

CHAPTER 1

Elucidating the nitrate assimilation pathway (NAP) in Fol4287

CHAPTER 1: Elucidating the nitrate assimilation pathway (NAP) in *Fol4287*

1. Introduction

Nitrogen is one of the main components of the complex macromolecules required for the structure and function of living organisms. Therefore, such organisms have developed complex control mechanisms to guarantee a constant supply of nitrogen. Fungi can use a wide variety of nitrogenous compounds, although the primary or preferred sources are those that are in a reduced state such as ammonium, glutamate or glutamine. However, in the absence or under limitation of these compounds, other nitrogen sources such as nitrate, nitrite, amides, purines, amino acids and proteins can be used although the degree of assimilation is lower (Marzluf *et al.,* 1997).

Nitrate (NO_3^-) is the most abundant form of inorganic nitrogen in soils and most fungi possess genes for nitrate assimilation, indicative of the relevance of this process (Joergensen and Wichern, 2008; Gorfer *et al.,* 2011). The nitrate assimilation pathway (NAP) begins with the transport of nitrate into the cell by a specific transporter, followed by nitrate and nitrite reductase activities, which reduce it first to nitrite (NO_2^-) and then to ammonium (NH_4^+), respectively, the latter being converted to organic nitrogen for cell growth (Vidmar *et al.,* 2000; Unkles *et al.,* 2004).

The use of secondary nitrogen sources such as nitrate requires the activation and synthesis of structural genes that encode enzymes involved in the assimilation pathway (Marzluf *et al.,* 1997). The characterization of genes and proteins involved in this pathway has been carried out in fungal models such as *Aspergillus nidulans* and *Neurospora crassa*. Mutants deficient in nitrate assimilation are easily selected due to their resistance to chlorate (ClO_3^-) (Pateman *et al.,* 1967; Johnstone *et al.,* 1990; Fu and Marzluf, 1987). In *A. nidulans*, the nitrate assimilation pathway is mainly made up of three components: the specific nitrate transporter NtrA and the two enzymes that catalyze the reduction of nitrate to nitrite and then to ammonium (NiaD and NiiA). Additionally, the genome of this fungus has a second high-affinity nitrate transporter (NtrB) (Unkles *et al.,* 2001) as well as additional proteins homologous to NiaD with nitrate reductase-like activity.

In fungi, nitrogen metabolism is highly regulated to ensure that the genes required for utilization of alternative nitrogen sources are only transcribed in the absence of preferred sources. In the presence of primary nitrogen sources such as ammonium or glutamine, the expression of the nitrate assimilation cluster is repressed, a phenomenon known as

"Nitrogen Metabolite Repression" (NMR). However, in the absence of ammonium and the presence of nitrate, nitrate assimilation gene expression is induced (Arst and Cove, 1973; Marzluf *et al.,* 1997; Wong *et al.,* 2008). This complex transcriptional control in *A. nidulans* involves the action of the nitrate-specific activator NirA (Burger *et al.,* 1991; Strauss *et al.,* 1998) and the nitrogen status-sensing regulator AreA (Kudla *et al.,* 1990). In the presence of nitrate, both proteins act synergistically to activate the transcription of the nitrate and nitrite reductase genes, allowing efficient assimilation of this compound (Muro-Pastor *et al.,* 2004; Berger *et al.,* 2008). In other fungi, nitrogen assimilation is also highly regulated by AreA orthologs such as Nit-2 in *N. crassa* (Fu and Marzluf, 1987) or NUT1 in *Magnaporthe oryzae* (Froeliger and Carpenter, 1996).

The nitrate assimilation pathway as well as its regulation are highly conserved across fungi, including the tomato pathogen *Fol4287* (Figure 15). This fungus uses nitrate as the sole nitrogen source through a first step of intracellular transport mediated by the specific transporter Ntr, an ortholog of of *A. nidulans* NtrA. In addition, the *Fol4287* genome has three paralogs of nitrate reductases (Nit1, Nit2 and Nit3) involved in the reduction of nitrate to nitrite. The final step is catalyzed by the enzyme nitrite reductase (Nii1) responsible for the reduction of nitrite to ammonium, which is subsequently converted into organic nitrogen for growth. In *Fol4287*, the transcriptional control of the nitrate assimilation pathway genes is done by AreA and NirA, and a previous report showed that mutants lacking AreA are deficient in the induction of nitrate and nitrite reductase genes (López-Berges *et al.,* 2010).

Under anaerobic conditions, organisms undergo another key biological process in the nitrogen cycle: denitrification. This involves the reduction of nitrate to gaseous nitrogen (N_2) and its release into the atmosphere (Zumft, 1997). Despite being typically a prokaryotic process, several filamentous fungi with denitrifying activity have been described, although it is only partial since they are unable to reduce nitrous oxide (N_2O) to N_2 (Shoun and Tanimoto, 1991; Shoun *et al.,* 1992). Based on our *in-silico* analysis in *Fol4287*, the denitrification system could include two enzymes located in the mitochondria: NirK, which presumably encodes a disassimilating copper-containing nitrite reductase, and P450nor, responsible for a cytochrome P450 with nitric oxide reductase activity (Kobayashi *et al.,* 1996; Shoun *et al.,* 2012) (Figure 15).

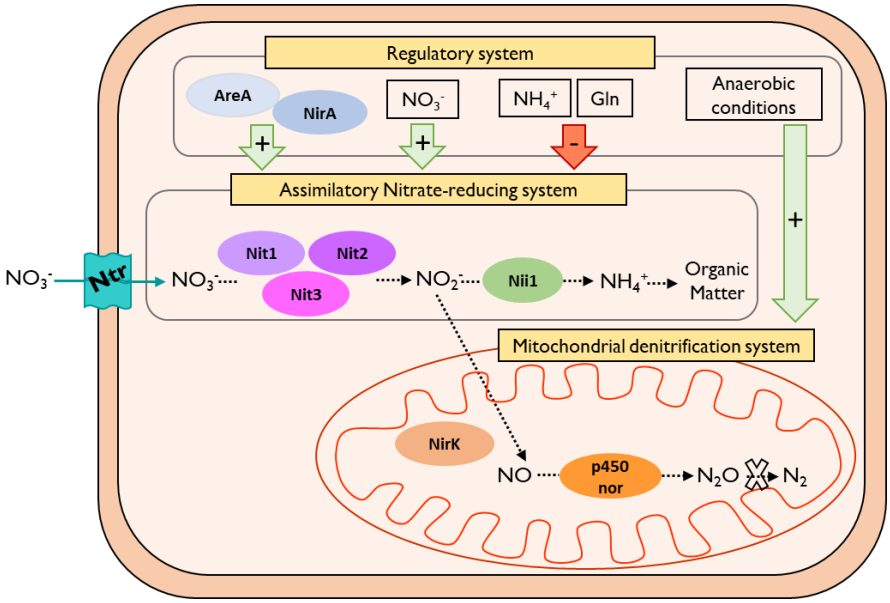

Figure 15. Model of the Nitrate Assimilation Pathway (NAP) and denitrification system in F. oxysporum. Import of extracellular nitrate (NO_3^-) by the Ntr transporter and subsequent reduction to nitrite (NO_2^-) by nitrate reductases (Nit1, Nit2 and Nit3). The action of nitrite reductase (Nii1) generates ammonium (NH_4^+) which undergoes a conversion process to form organic nitrogen compounds. Transcriptional activation is driven by the GATA factor AreA and the Zn binuclear cluster protein NirA. The activation of NAP requires the presence of nitrate and the absence of the repressing metabolites ammonium and glutamine (Gln). Fungal denitrification, in anaerobic conditions involves the conversion of NO_2^- to nitrous oxide (N_2O) through the action of a copper-containing nitrite reductase (NirK) and a cytochrome p450 with nitric oxide reductase activity (p450nor).

In this work we set out to clarify the role of the *nit1*, *nit2*, *nit3* and *ntr* genes in nitrate assimilation (Gómez-Gil *et al.*, 2018). To this aim, a detailed molecular and phenotypical characterization of knockout mutants in these different genes was performed. Our results show that only *nit1*, *nit2* and *ntr1* re significantly expressed during growth on nitrate as the sole nitrogen source. Targeted deletion of *nit1* and *ntr1* severely affected the growth of Fol4287 on nitrate, highlighting the relevance of the Nit1 and Ntr1 proteins in nitrate assimilation by the fungus. Biochemical analysis revealed that among the three nitrate reductases, Nit1 contributes 50% of the total NR activity. In addition to the knockout mutants, a spontaneous chlorate resistant mutant derived from *Fol4287*, named NitFG, was characterized, which is unable to grow in nitrate and shows low NR activity, although the transcript levels of *nit1* and *nit2* are significantly increased. Taken together, our results provided new insights into the nitrate assimilation process in the fungal pathogen *Fol4287*.

SUBCHAPTER 1.1: Role of different *nit* genes and of the *ntr1* gene in nitrate assimilation

2. Results

2.1. *In silico* identification of nitrate assimilation pathway (NAP) components in Fol4287

A *BLASTp* search of putative NAP components in the *Fol4287* genome identified predicted orthologs of *A. nidulans* genes, including at least three genes encoding NRs (*FOXG_04181*, *FOXG_03770*, *FOXG_02795*) and one gene (*FOXG_00635*) responsible for a nitrate/nitrite transporter (Table 19). *FOXG_04181*, located on chromosome 4, encodes Nit1, a protein with 904 amino acids and a calculated molecular weight of 101.8 kDa that exhibits 56.4% identity with *A. nidulans* NiaD (*AN1006*) and more than 90% identity with NR proteins from other *Fusaria* such as *F. fujikuroi* (*FFUJ_12277*, 95.4%) or *F. verticillioides* (*FVEG_07298*, 94.3%). The paralogous gene *FOXG_03370*, also located on chromosome 4, encodes Nit2, a protein with 1,025 amino acids and a molecular mass of 116.6 kDa exhibiting 53% identity with the second NRs (*AN8449*) from *A. nidulans,* and more than 90% identity with those from *F. fujikuroi* (*FFUJ_14513*, 93.1%) and *F. verticillioides* (*FVEG_12090*, 92.2%). The third NR paralog *FOXG_02795,* located on chromosome 8, encodes Nit3, a predicted protein of 951 amino acids and a molecular weight of 106.9 kDa that exhibits 63% identity with the third NR (AN9037) of *A. nidulans* and more than 90% identity with those from *F. fujikuroi* (*FFUJ_06561*, 97.2%) and *F. verticillioides* (*FVEG_01627*, 94.4%). Finally, the *FOXG_00635* gene located on chromosome 1, encodes a nitrate/nitrite transporter (Ntr) with 513 amino acids and a calculated molecular weight of 55.3 kDa. This protein exhibits significant identity to nitrate transporters of *F. verticillioides* (*FVEG_00877*, 98.1%) and *F. fujikuroi* (*FFUJ_00934*, 96.7%), while the identity with Ntr (AN1008) of *A. nidulans* is lower (49.1%).

Table 19. Nitrate assimilation pathway components from Fol4287 identified by BLASTp analysis. Molecular weight is indicated in KiloDaltons (KDa).

GENE	PROTEIN	LOCALIZATION	N° aa	MOLECULAR WEIGHT
FOXG_04181	Nit1	Chr4	904	101.8
FOXG_03770	Nit2	Chr4	1,025	116.6
FOXG_02795	Nit3	Chr8	951	106.9
FOXG_00635	Ntr	Chr1	513	55.3

2.2. Quantitative measurement of nit1, nit2, ntr and areA gene expression

To measure the transcript levels of the *nit1*, *nit2*, *ntr* and *areA* genes, RT-qPCR analysis with gene-specific primers was performed using cDNA from the wt, Δ*nit1*, Δ*nit2*, Δ*ntr1*, Δ*areA* mutants as well as the NitFG mutant and its Com1 strain complemented with the wild type *areA* allele, obtained under induction conditions (4 hours in synthetic medium supplemented with nitrate) (Figure 16). As expected, the expression level of the respective deleted gene in the different mutants was null. interestingly, Δ*nit1* and NitFG mutants showed an overexpression of the paralog *nit2*, possibly due to a compensatory mechanism to optimize nitrate assimilation. The highest expression levels for *nit1* and *nit2* were detected in the NitFG mutant (5-fold and 6-fold, respectively, relative to the wild type strain), followed by the Δ*nit1* mutant in which the expression level of the *nit2* gene was 4.5-fold that of the wild type strain. The Δ*nit2* and Δ*ntr* mutants showed similar *nit1* expression levels of 1.4-fold relative to the wild type strain. As previously described (López-Berges *et al.,* 2010), the Δ*areA* mutant showed a low *nit1* transcript level, and this reduction was fully restored in the Com1 strain. Finally, the Com1 strain recovered the expression level for the structural nit genes compared to the wild type strain. However, the expression level of *ntr* in Com1 strain increased instead of decreasing (more than 20-fold), reaching the highest transcript level detected among the tested strains.

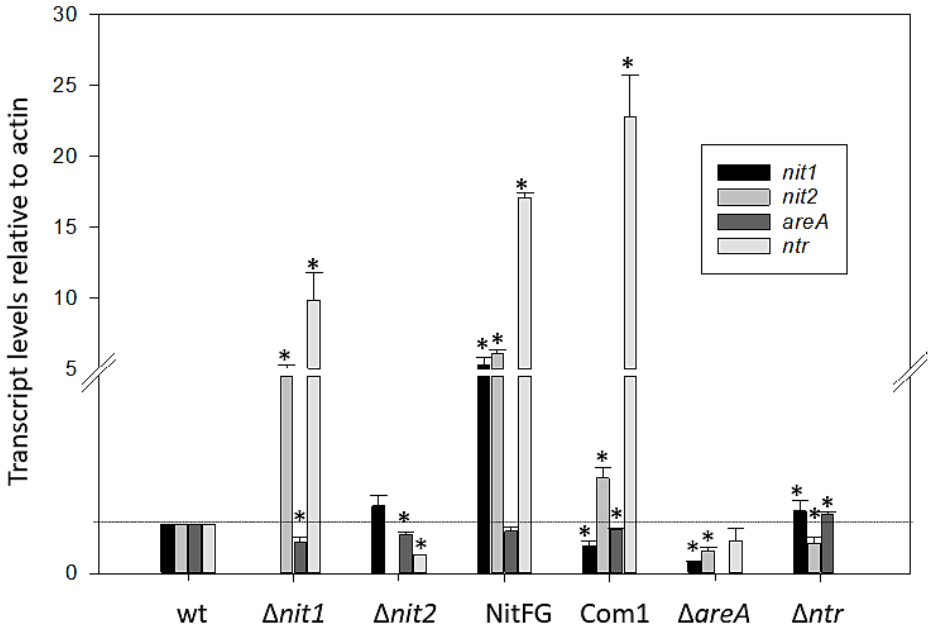

Figure 16. Relative transcript levels of genes encoding different nitrate reductases (nitl, nit2), a nitrate/nitrite transporter (ntr) and the transcriptional activation factor (areA) in NAP strains. RNA samples of the indicated strains were obtained from mycelia transferred for 4 h to synthetic medium (SM) containing 23.5 mM $NaNO_3$. Transcript levels were measured by real time RT-qPCR and are indicated relative to those of the actin gene. Bars represent standard errors calculated from three biological replicates, each including three technical replicates.

2.3. Nitrate and nitrite reductase activities in NAP strains

Measurement of nitrate and nitrite reductase activities (NR and NiR respectively), in the indicated strains was performed from cell-free extracts obtained under induction conditions (Figure 17). Individual deletion of each of the three *nit* genes affected total NR activity to different extents. The Δ*nit1* mutant showed the lowest NR activity with a 50% reduction compared to the wild type strain. The reduction in NR activity in the other two mutants was less, 30% in Δ*nit2* and 5% in Δ*nit3*. We speculate that the remaining 15% could be due to the presence of additional nitrate reductase-like proteins in Fol4287. In agreement with these results, in the Δ*nit1*Δ*nit2* double mutant only 20% NR activity was detected. The remaining strains (NitFG, Δ*ntr*, Δ*areA*, Com1) showed similar levels of NR activity between 35-45% compared to the wild type strain (Figure 17A).

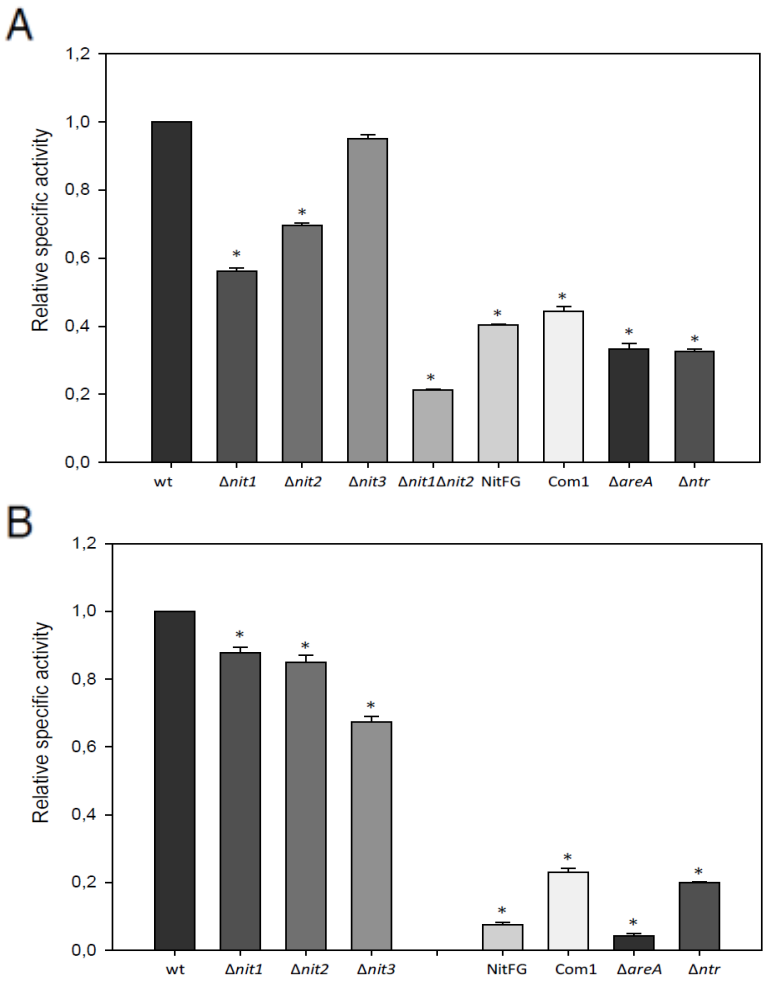

Figure 17. Nitrate and nitrite reductase activities in NAP strains. Cell-free extracts from cultures grown under induction conditions were used to measure nitrate **(A)**, or nitrite **(B)** reductase activity. The specific activity of the enzymes was expressed as Units/mg protein relative to wild type strain. Bars indicate standard errors calculated from three biological replicates each including three technical replicates.

NiR activity, determined as the rate of nitrite disappearance, was reduced between 10-30% in the three *nit* mutants. However, in NitFG, Δ*ntr*, Δ*areA* and Com1, a reduction in NiR activity of up to 80-90% was detected, probably due to the reduced NR activity that results in the formation of lower intracellular NO_2^- levels and, consequently, in reduced transcriptional activation of the *nii1* gene. Unexpectedly, the Δ*areA* complemented strain Com1 did not recover full levels of NR and NiR activities (Figure 17B).

2.4. Immunodetection of Nit1 reveals its absence in Δnit1 and NitFG mutants

Western blot analysis of protein extracts obtained from NO_3^-–induced and non-induced conditions was performed to determine the presence of Nit1 protein in the wild type strain and the Δ*nit1* and NitFG mutants (Figure 18). Under induction conditions, immunoblotting with polyclonal anti-nitrate reductase (anti-Ynr1) antibody from the yeast *Hansenula polymorpha* allowed the detection of a protein band of approximately 120 kDa in the wild type strain and in an ectopic transformant. This band most likely corresponds to the post-translationally modified nitrate reductase protein Nit1, reflected by its higher than expected molecular weight. This band was lacking in the protein extracts of the Δ*nit1* #10 and #30 mutants, confirming the replacement of the *nit1* gene by the Hyg^R cassette. In the spontaneous mutant NitFG, the protein band was also missing, confirming the lack of Nit1 production in this strain. The absence of immunodetection of Nit1 in all strains under non-induced conditions confirmed that the production of Nit1 is nitrate-inducible (Figure 18A). As a loading control, the polyclonal anti-α-tubulin antibody was used showing a similar signal in all the tested samples (Figure 18B).

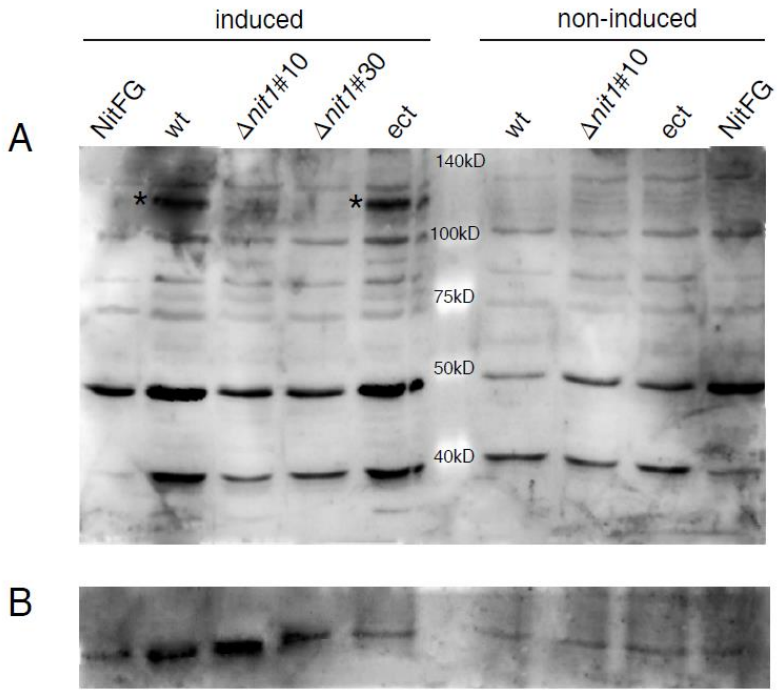

Figure 18. Immunodetection of the major F. oxysporum nitrate reductase (Nit1). Intracellular protein extracts obtained under NO_3^- induced and non-induced conditions were separated by SDS–PAGE and immunoblotted with polyclonal anti-nitrate reductase antibody from *Hansenula polymorpha* (anti-Ynr1) (Navarro *et al.,* 2003) **(A)**, or with comercial mouse polyclonal anti-α-tubulin antibody (Santa Cruz Biotechnology) **(B)**.

The lack of Nit1 protein in the NitFG mutant is consistent with the lower NR activity exhibited by this strain and its chlorate resistance phenotype. However, these results contrast with the observed overexpression of the *nit1* gene in this mutant (see Fig. 16). To elucidate the absence of Nit1 protein in this strain, we conducted an *in vitro* mRNA translation assay (Figure 19). Proteins obtained under NO_3^--induced conditions *in vitro* by translation of mRNA in a rabbit reticulocyte lysate system or *in vivo* (for comparative purpose), were separated by SDS-PAGE electrophoresis and visualized by Coomassie blue staining (Figure 19A). Immunoblotting with anti-Ynr1 antibody confirmed the absence of Nit1 in NitFG and Δ*nit1* #10, both *in vivo* and *in vitro*, whereas in the wild type strain the presence of the Nit1 protein was detected in both protein samples. The difference in the size of the bands confirmed the existence of a posttranslational *in vivo* modification that does not occur in the *in vitro* reticulocyte lysate system (Figure 19B). Therefore, the molecular basis for the NR-deficient phenotype of the NitFG mutant remains to be determined.

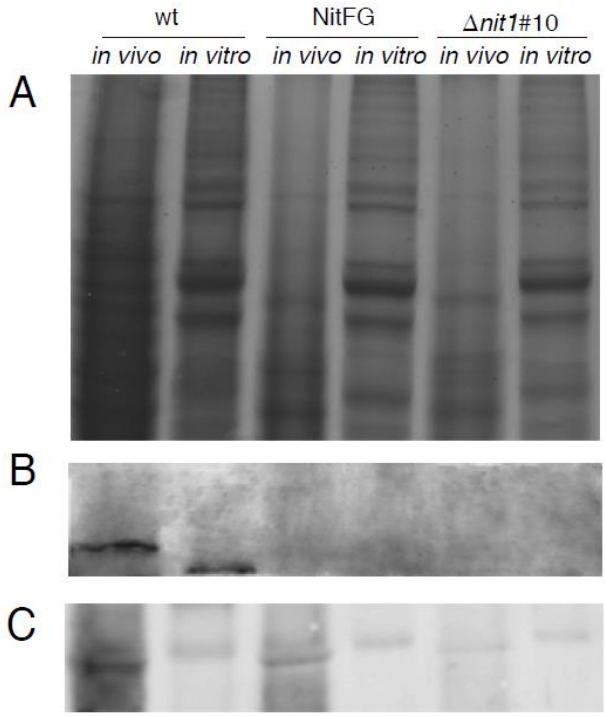

Figure 19. Immunodetection of the Nit1 nitrate reductase in cell-free extracts. Proteins were obtained under NO_3^- induced conditions *in vivo*, or *in vitro* by translation of mRNA in a rabbit reticulocyte lysate system (Invitrogene AM1200), separated by SDS–PAGE and stained with Coomassie blue **(A)**, immuno-blotted with polyclonal antinitrate reductase from *H. polymorpha* (Navarro *et al.,* 2003) **(B)**, or immuno-blotted with commercial mouse polyclonal α-tubulin antibody (Santa Cruz Biotechnology) **(C)**.

2.5. Colony growth phenotypes of NAP strains on different nitrogen sources

To determine the role of the different genes on nitrate assimilation and to link it with the results obtained in the previous assays, the NAP strains were subjected to a phenotypic characterization of growth in the presence of different primary and secondary nitrogen sources (Figure 20).

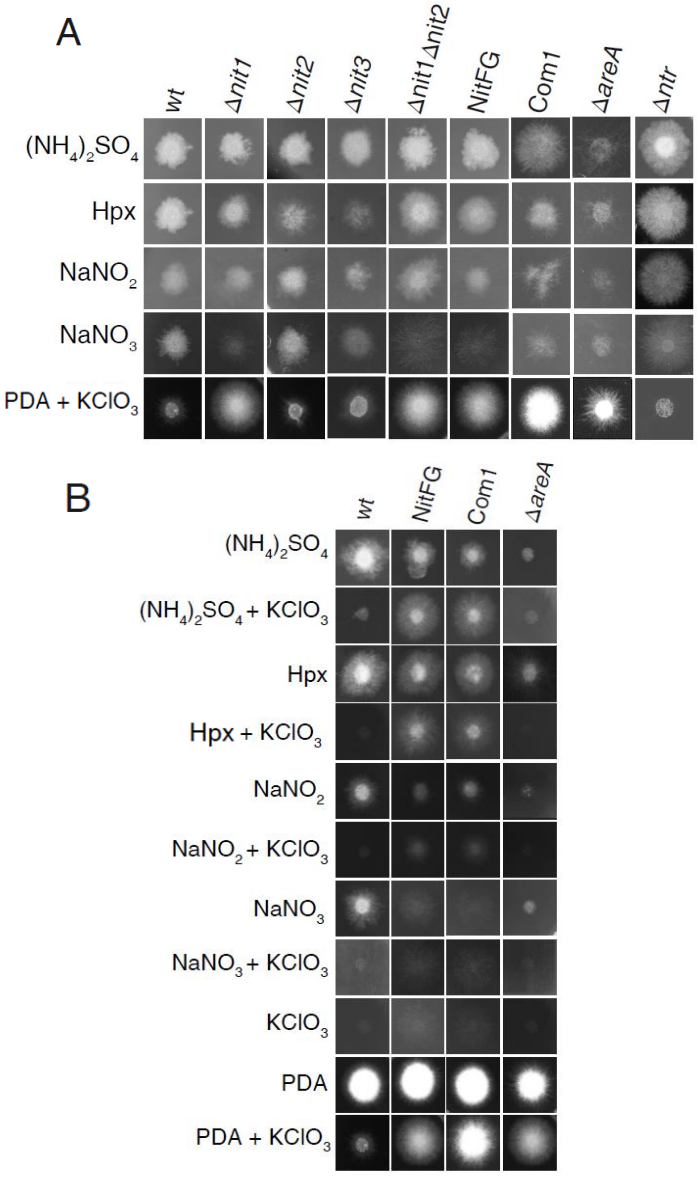

Figure 20. Colony growth phenotypes of mutants in NAP components on different nitrogen sources. (A) The indicated strains were grown for 3 days at 28 °C on synthetic media (SM) containing the indicated nitrogen source: ammonium sulfate ($(NH_4)_2SO_4$; 23 mM), hypoxanthine (Hpx; 7 mM), sodium nitrite ($NaNO_2$; 5 mM) or sodium nitrate ($NaNO_3$; 23 mM). Mutants were also grown in PDA medium supplemented with potassium chlorate ($KClO_3$; 122 mM) to confirm loss of nitrate reductase activity. **(B)** Growth of NitFG, Com1 and Δ*areA* strains on the indicated media with or w/o chlorate.

The Δ*nit1*, Δ*nit1*Δ*nit2*, NitFG mutants showed a drastic impairment to grow in the presence of nitrate and a normal growth capacity in the presence of other nitrogen sources such as ammonium, hypoxanthine and nitrite as compared to the wild type strain. The Δ*areA* mutant was deficient in growth on all nitrogen sources tested, highlighting the importance of AreA in nitrogen catabolic gene regulation. Furthermore, all these strains showed a chlorate-resistant phenotype. The growth phenotype shown of the NitFG mutant and the Com1 complemented strain seem to indicate that the areA gene mutation is not the only one reason for the defects shown by this mutant. These results were further confirmed by a growth assay in the presence of different nitrogen sources supplemented with chlorate (Figure 20B).

On the other hand, Δ*nit2* and Δ*nit3* mutants showed a growth phenotype similar to that of the wild type strain on all nitrogen sources, including nitrate, and were also chlorate-sensitive. Taken together, these results indicate that the main NR involved in nitrate assimilation of *Fol4287* is Nit1, while Nit2 and Nit3 act as accessory proteins that are not essential for this process. The Δ*ntr* mutant showed a chlorate-sensitive phenotype similar to the wild type strain and showed reduced growth in the presence of nitrate, likely due to the reduced ability to import this compound. However, growth was not completely inhibited, which indicates that the fungus has the ability to incorporate or use nitrate through another pathway (Figure 20A).

In this growth assay we observed that the reduced growth capacity exhibited by some of the NAP mutants in the presence of certain nitrogen sources did not imply a decrease in colony area. To further explore this, the phenotypic growth assay was repeated for some of the strains, increasing the growth time (5 and 7 days) to better quantify colony area as well as hyphal density (Figure 21). This assay confirmed the phenotypes observed in the previous experiment (Figure 21A). As expected, the different mutants did not show growth differences with respect to the wild type strain in the presence of ammonium. However, a more restricted colony growth was observed on this medium for all strains, as compared to the other nitrogen sources, despite being a preferred nitrogen source for the fungus. Indeed, quantification of the colony area in the wild type strain revealed a significant reduction of the growth area on ammonium, although this difference did not imply a lower hyphal density, indicating similar mycelial production of the wild type strain on the different media (Figure 21B, upper graphs). We next tested the growth of the different mutants on

nitrate and found that they did not show a decrease in colony area but did exhibit a lower hyphal density (Figure 21B, bottom graphs).

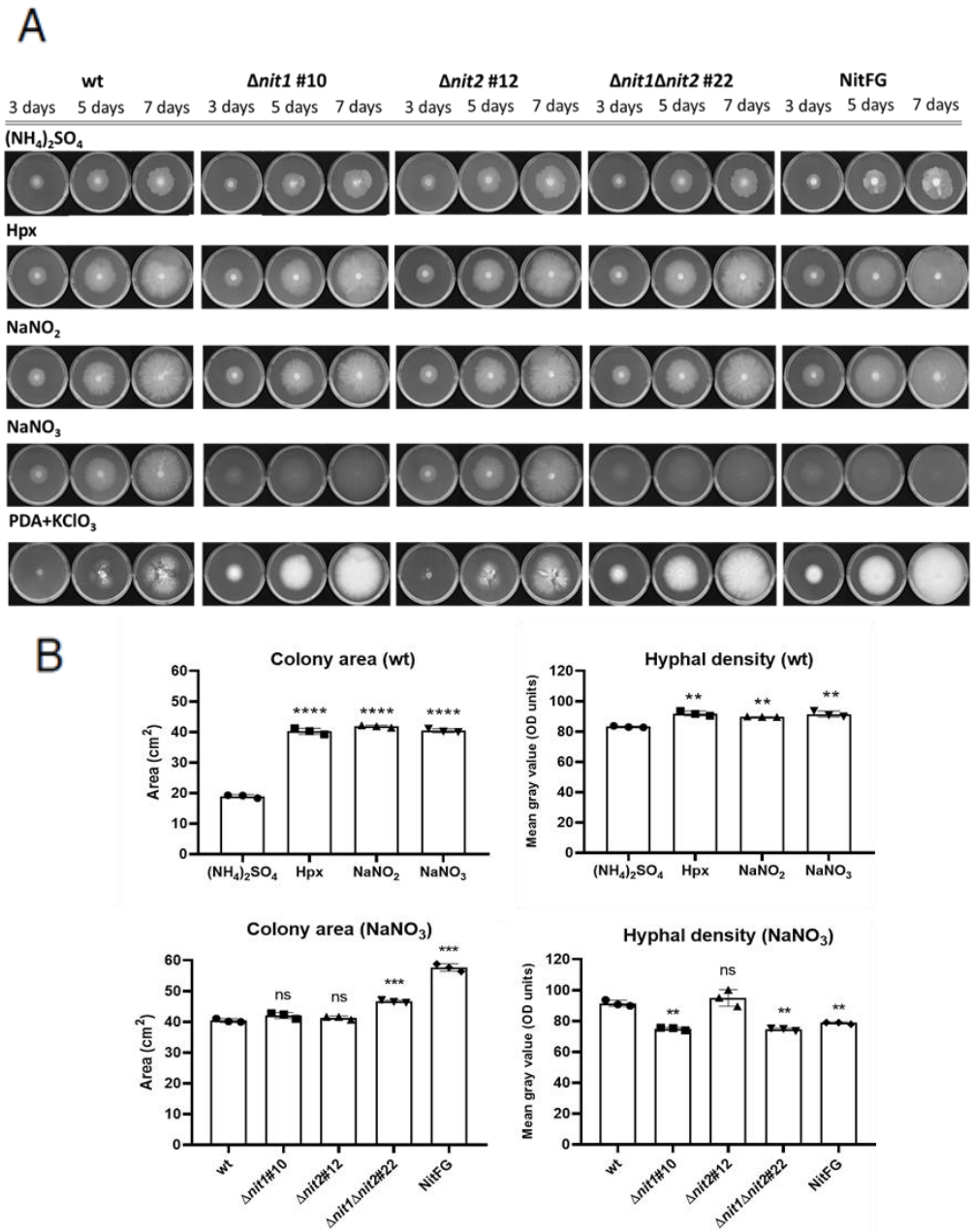

Figure 21. Reduced hyphal density correlates with reduced growth of NAP mutants. (A) Phenotypic characterization of the wild type strain and mutants affected in NR activity. Aliquots of 10^6 microconidia of the indicated strains were spot-inoculated on the center of synthetic medium (SM) plates containing the indicated nitrogen sources: ammonium sulfate ($(NH_4)_2SO_4$; 23 mM), hypoxanthine (Hpx; 7 mM), sodium nitrite ($NaNO_2$; 5 mM) or sodium nitrate ($NaNO_3$; 23 mM). NAP mutants were also grown in PDA medium supplemented with potassium chlorate ($KClO_3$; 122 mM) to confirm loss of nitrate reductase activity. Plates were incubated at 28 °C and scanned on days 3, 5 and 7 for quantification of the colony area and hyphal density. **(B)** (Upper graphs) Colony area (left) and hyphal density (mean gray value; right) in the wild type strain after 5 days of growth on SM supplemented with the indicated nitrogen sources. (Bottom graphs) Colony area and hyphal density of the wild type strain and the indicated mutants affected in NR activity on SM supplemented with 23 mM sodium nitrate. Data shown represent the mean and standard deviations of three independent

replicates for each strain. ** p<0.01, *** p<0.001, **** p<0.0001 versus wild type according to Welch's t-test; ns, non-significant.

In other words, the Δ*nit1*, Δ*nit1*Δ*nit2* and NitFG mutants showed lower mycelial production levels on nitrate than the wild type strain and the Δ*nit2* mutant, although their colony area was similar to that of the wild type strain or even larger such as in the spontaneous mutant NitFG. In summary, on nitrate as the sole nitrogen source, the mutants lack nutrients due to their inability to assimilate nitrate and this results in a less dense but more expansive colony growth that resembles that of fungal colonies inoculated on water agar-medium lacking nutrients.

SUBCHAPTER 1.2: Detection of colony sectors in *Fol4287*

2. Results

2.1. Fol4287 generates spontaneous colony sectors during growth on different media plates

During the phenotypic characterization of the NAP mutants, we observed the recurrent appearance of colony sectors. These are best visualized at longer growth times (5 and 7 days), with some representative examples of sectorized colonies shown in Figure 22. The sectors were easily detectable from the rest of the colony due to their differential growth, exhibiting in most cases an increased aerial mycelium. In addition, the sectors generally showed faster growth than the rest of the colony, which is why we called them colony growth variants.

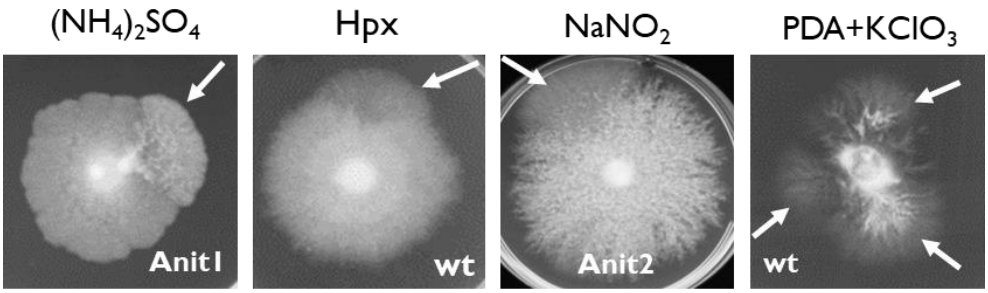

Figure 22. Representative examples of colony sectors on different nitrogen sources. Sectors are indicated with arrows. Note that the colony sectors present differential morphologies and growth capacity (Enlargements from Fig 21).

Previous experiments in our group had revealed that in nitrogenous media, sector formation was slightly increased and that it occurred both in the wild type strain and in different knockout mutants (Pérez-Nadales *et al.,* unpublished). Similar results were obtained in this work during the phenotypic characterization of mutants in genes involved in the nitrate assimilation pathway. The sectoring colonies shown as representative examples here correspond both to the wild type strain and to mutants in *nit* genes grown in the presence of different nitrogen sources. In addition, in the presence of the toxic compound chlorate, which induces mutations and DNA damage, sectors that may be associated with genomic instability were also detected (Figure 22). Based on these results, we conclude that the appearance of sectors is not exclusively due to the inactivation of certain genes involved in nitrate assimilation, since they were also detected in the wild type strain, indicating that sectoring is a recurrent phenomenon during plate growth of *Fol4287*.

Discussion

3.1. The nitrate assimilation genes are highly conserved among fungal species

In silico analysis of the *Fol4287* genome identified predicted orthologs to *A. nidulans* and *N. crassa* genes involved in the nitrate assimilation pathway. Thus, we identified a protein called Ntr (*FOXG_00635*) representing an ortholog of *A. nidulans* NtrA, a high-affinity nitrate transporter (Unkles *et al.,* 1991). However, *A. nidulans* has a second nitrate/nitrite transporter (NrtB), which does not seem to have an ortholog in Fol4287. We also found three paralogs (*FOXG_04181*, *FOXG_03770*, and *FOXG_02795*) encoding proteins Nit1, Nit2 and Nit3 respectively, with Nit1 showing the highest degree of identity with NiaD, the main NR identified in *A. nidulans* (Pateman *et al.,* 1964). The last step of the nitrate assimilation pathway is also conserved in Fol4287 through the action of the nitrite reductase Nii1 encoded by the *FOXG_03192* gene, an ortholog of *A. nidulans* NiiA (Pateman *et al.,* 1964; Unkles *et al.,* 1992).

In *A. nidulans*, the structural genes *ntrA*, *niaD* and *niiA* are grouped in a gene cluster located on chromosome 8 (Johnstone *et al.,* 1990). This synteny is maintained in other *Aspergilli spp.* such as *A. fumigatus,* where the cluster is located on chromosome 1 (Amaar and Moore, 1998). However, other species such as *N. crassa* and *F. oxysporum* do not show this synteny. In *N. crassa*, the nitrate transporter gene nit-10 is not physically linked to the nitrate and nitrite reductase genes nit-3 and nit-6, respectively (Gao-Rubinelli and Marzluf, 2004). In *F. oxysporum*, these three genes are located on different chromosomes: *ntr1* on chromosome 1, *nit1* on chromosome 4 and *nii1* on chromosome 8. The grouping of functionally related genes in so- called "selfish operons" may facilitate their coordinated expression (Price *et al.,* 2005). Thus, fungal species in which these genes are grouped in a same cluster could require fewer transcription factors since the three genes are close to each other and share bidirectional promoters, as in *niaD/niiA* in *Aspergillus*. In the case of Sordariomycetes such as *N. crassa* and *F. oxysporum*, the transcriptional regulation could be more complex due to the location of these genes on different chromosomes.

3.2. Nit1 is the main nitrate reductase of Fol4287

Phenotypic characterization of the single Δ*nit1* mutant and the double Δ*nit1*Δ*nit2* deletion mutant revealed a reduced growth in the presence of nitrate as the sole nitrogen source, due to their inability to assimilate the compound in the absence of one or both nitrate reductases. This has been previously described for a single *F. oxysporum* mutant in the major nitrate reductase Nit1 (Correll *et al.,* 1987), as well as in a Δ*niaD* mutant of *A.*

nidulans (Schinko et *al.,* 2010). On the contrary, the mutants Δ*nit2* and Δ*nit3* only presented a slightly decreased growth compared to the wild type strain. These results indicate that Nit1 is the main NR protein required for growth on nitrate as the sole nitrogen source and that Nit2 and Nit3 enzymes are not essential for this process. Biochemical measurements of nitrate reductase activity supported these results as deletion of the *nit1* gene caused a 50% reduction in total nitrate reductase activity relative to the wild type strain. Nit2 has the second highest NR activity, contributing 30% of the total, while the deletion of *nit3* only caused a 5% decrease in total NR activity. In addition, immunobloting assays revealed that in Fol4287 the production of Nit1 is nitrate-inducible, similarly to NiaD in *A. nidulans* or Nit3 in *N. crassa* (Downey *et al.,* 1987; Fu and Marzluf, 1987).

3.3. *Fol4287* exhibits a compensatory mechanism of gene expression to optimize nitrogen assimilation

The expression of *nit1*, *nit2* and *ntr* genes was measured in the wild type strain and NAP mutants. The highest expression levels for the *nit1* and *nit2* genes were detected in the NitFG mutant, followed by *nit2* gene expression in the Δ*nit1* mutant. The Δ*nit2* and Δ*ntr* mutants showed similar levels of expression of the *nit1* gene. In addition, an increased transcription of the *ntr* gene was detected in mutants Δ*nit1*, NitFG and complemented strain Com1. The increased expression of the *nit* and *ntr* genes in the different mutant backgrounds, compared to the wild type strain, indicates the existence of a compensatory mechanism of gene expression to optimize the availability and assimilation of nitrate. This is reminiscent of the "pseudo-constitutivity" phenotype described in *A. nidulans* mutants with low NR activity. It was shown that in NR null mutants, which cannot assimilate nitrate, the transporters remain functional, transporting nitrate to the intracellular space. The accumulation of significant intracellular levels of nitrate due to the low NR activity leads to nuclear accumulation of NirA and, consequently, increased expression of the assimilatory genes (Schinko *et al.,* 2013).

3.4. The NitFG mutant overexpresses the nit1 gene but lacks Nit1 protein and shows low levels of NR activity

The spontaneous NitFG mutant shows a physiological phenotype similar to that of the Δ*nit1* strain, i.e. very weak growth on nitrate and resistance to chlorate, which correlated with low levels of NR activity and a lack of Nit1 protein. However, the data obtained from the gene expression analysis were totally unexpected, with the NitFG mutant showing an overexpression of the *nit1* and *nit2* genes under induction conditions. Sequencing of the

three structural *nit* genes in this mutant showed 100% identity in the nucleotide sequence with the corresponding wild type alleles.

At the level of transcriptional regulation, sequencing of the *areA* gene in the NitFG mutant identified two nucleotide changes in the open reading frame resulting in a possible non-functional protein. However, this fails to explain the increased expression of the *nit1* and *nit2* genes or the growth pattern of this mutant, since it should be unable to grow in the presence of nitrite, hypoxanthine and ammonium similar to the Δ*areA* mutant. We complemented the NitFG mutant by inserting the wild type *areA* allele, however, the Com1 strain did not recover the wild type phenotype, still showing reduced levels of NR and NiR activity and a growth pattern characteristic of NR mutants, with resistance to chlorate and inability to grow on nitrate. Interestingly, overexpression of the *nit1* and *nit2* genes exhibited by the NitFG mutant was not detected in the Com1 strain, indicating the recovery of the wild type regulation for these genes. Thus, although complementation of NitFG with the wild type *areA* allele had no effect at the growth phenotype, it did reveal its involvement in transcriptional regulation by re-establishing normal expression levels of both *nit* genes.

An additional approach to determine the molecular basis of the NitFG phenotype was the analysis of the DNA sequences of the five genes *cnxABC*, *cnxE*, *cnxF*, *cnxG* and *cnxH* encoding subunits of the molybdenum-containing factor, which have been described in *A. nidulans* to function both in nitrate reductase and xanthine dehydrogenase activity (Arst *et al.,* 1970; Klitich and Leslie, 1988; Unkles *et al.,* 1999). However, no changes in the nucleotide sequence of any of these five loci were detected, as confirmed by the wild type growth of the NitFG mutant on hypoxanthine.

We hypothesized that the two-point mutations in the *areA* gene detected in the NitFG mutant could lead to a loss of function of this gene. However, in previous studies mutations in the *areA* gene did not imply a loss of function. The *areA1900* mutation in *A. nidulans*, consisting of a 9-bp deletion and loss of three amino acids in the basic region following the zinc finger in the DNA-binding domain (Muro-Pastor *et al.,* 2004) was reported as a partial loss-of-function mutation resulting in an increased affinity for some specific AreA sites in the niiA-niaD promoter, leading to overexpression of these genes in the presence of the inducer nitrate. A similar situation could be occurring in the NitFG mutant, where the two mutations flank the DNA-binding domain, albeit distantly. However, unlike NitFG the *areA1900* mutant was able to grow in the presence of nitrate. Further work is needed to elucidate the molecular and biochemical bases of the contradictory phenotypes of NitFG mutant.

3.5. Colony sectoring occurs frequently on plates and could be indicative of genomic instability

Fungi are prone to phenotypic plasticity reflected in the existence of different morphological alternatives and physiological behaviors in response to environmental conditions (West-Eberhard, 1989). Sometimes, under well-defined conditions, recurrent phenotypic changes are observed that always generate the same result. These changes seem are usually associated with endogenous characteristics of the fungus. These phenotypic changes are particularly frequent in filamentous fungi and can be readily observed with the appearance of colony growth sectors on plates (Silar *et al.,* 1999).

The phenomenon known as "sectoring" was observed in this study during the phenotypic characterization of the wild type strain and NAP mutants in the presence of different nitrogen sources. In addition, previous studies in our group had already indicated the ability of *Fol4287* to spontaneously produce sectors with differential growth on different media (Pérez-Nadales *et al.,* unpublished). Despite being a frequent phenomenon in fungi, the underlying molecular mechanisms remain poorly understood, although previous studies suggest both a genetic and epigenetic origin (Silar, 2019). In our group, the isolation and sequencing of sectors produced by *Fol4287* revealed large-scale genetic changes possibly related to chromosomal rearrangements (Pérez-Nadales *et al.,* unpublished; López-Díaz *et al.,* 2019). Such changes have been associated with genome and chromosome instability in other organisms. In *S. cerevisiae*, sequencing of variant colonies with a sectored phenotype revealed that they exhibited altered karyotypes due to *de novo* structural genomic variations, indicating that copy number variations provide the basis for this phenotypic plasticity (Heasley and Argueso, 2022). Moreover, the formation of colony sectors can also result from genomic instability caused by DNA damage. Mutants in genes involved in DNA damage repair in *S. cerevisiae* displayed a high frequency of multi-sectored colonies. Subsequent molecular analyses, including CHEF electrophoresis, revealed an increased chromosome loss and large-scale chromosomal rearrangements (Vasan *et al.,* 2014).

These observations served as a starting point for a more in-depth analysis of the molecular mechanisms underlying genomic and chromosomal instability in *Fol4287*, following two distinct, yet interrelated approaches.

In chapter 2 of the thesis, we focus on analysing the role of telomeric and subtelomeric regions in genome plasticity and chromosome structure maintenance in *Fol4287*. Telomeres are nucleoprotein structures located at the ends of chromosomes and whose integrity is essential to maintain genomic stability. Telomere shortening or loss can

lead to replicative senescence, apoptosis, chromosome fusions, and increased chromosome instability (Liu *et al.,* 2004; Capper *et al.,* 2007; Heacock *et al.,* 2007). Adjacent subtelomeric regions exhibit the highest instability in the genome due to the presence of blocks of homologous repeat sequences (Rudd *et al.,* 2007; Chen *et al.,* 2018).

Chapter 3 focuses on an attempt to elucidate the putative link between chromosome rearrangements and genomic instability in *Fol4287*. Results from a previous PhD work (López-Díaz, 2019), where events of duplication or deletion of specific chromosomal regions were recurrently detected after serial passages through different environmental conditions, served as a starting point. We investigated the origin, mechanism, and frequency of chromosomal rearrangements in *Fol4287* using a combination of serial passaging, karyotyping, FACs and genome re-sequencing.

CHAPTER 2

Physical structure of chromosome ends and their function in genome plasticity of Fol4287

CHAPTER 2: Physical structure of chromosome ends and their function in genome plasticity of *Fol4287*

1. Introduction

This chapter describes the study on the role of subtelomeric and telomeric regions on the maintenance of chromosome structure. The hypothesis supporting these investigations were the well-known genome plasticity of *Fol4287*, given the fact that subtelomeric regions have a large variability. The main aim of the studies included in this chapter were to relate the subtelomeric structure of *Fol4287* with its genomic stability.

2. Results

2.1. Subtelomeric regions appear to be conserved across *Fol4287* chromosomes

The telomeric sequence is highly conserved among filamentous fungi and consists of a repeat of the hexameric sequence TTAGGG. To investigate the physical structure of Fol4287 chromosome ends, we first performed a *BLASTn* search with the telomeric repeat sequence (TTAGGG)x5 against the Fol4287 genome and found matches on chromosomes 3, 5, 6, 14 and 15 (Figure 23). Although telomeric repeats are expected to be located exclusively at chromosome ends, we also found hits in the internal regions of chromosomes 3 and 6 suggesting the occurrence of chromosome fusions.

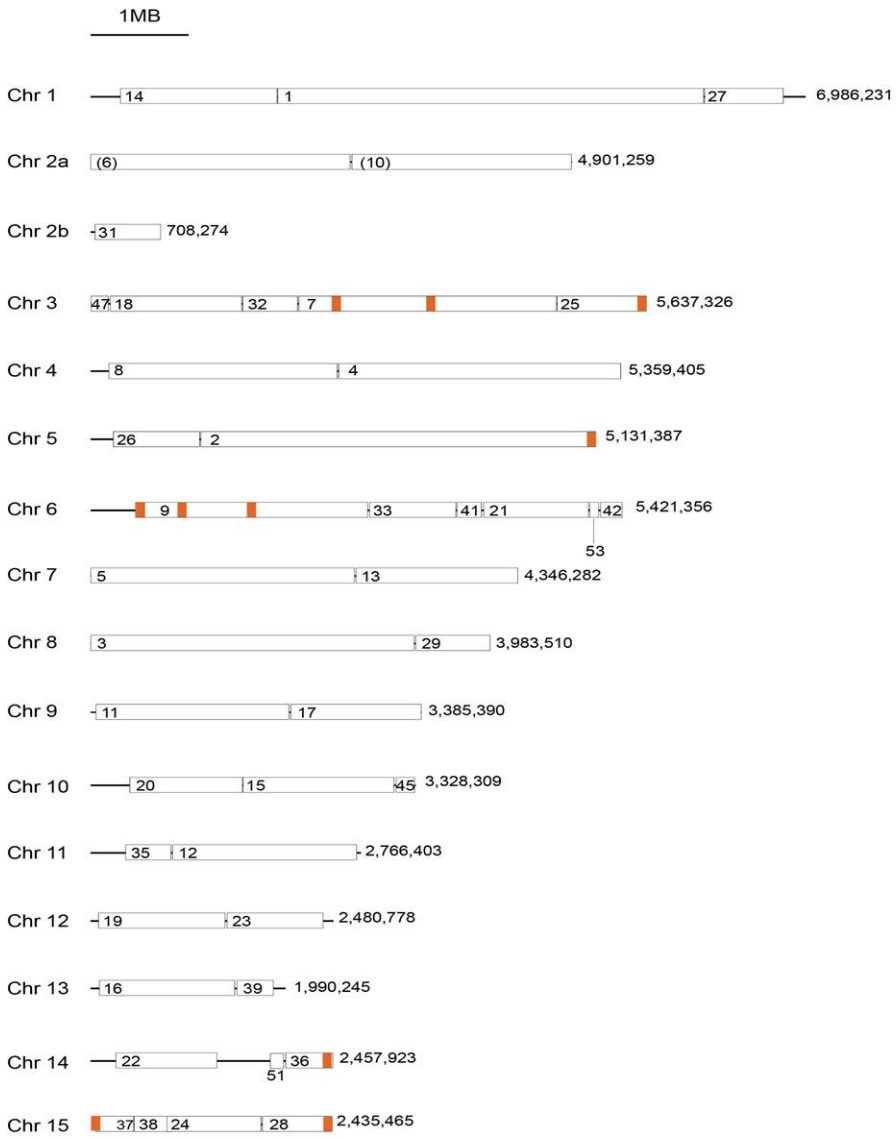

Figure 23. In silico analysis of Fol4287 telomeric regions. A *BLASTn* search with the telomeric repeat sequence (TTAGGG)x5 was performed against the Fol4287 genome in FungiDB. The chromosome map (modified from Ma *et al.,* 2010) shows the location of the identified telomeres (orange boxes) as well as the number of contigs and the total size of each chromosome. Note that most of the chromosome ends are not sequenced (indicated by a black line).

Chromosome 15 was the only chromosome for which both telomeric regions were retrieved in the genome database and was therefore selected for further analysis of the subtelomeric regions. We noted that the sequence of a region of around 10 Kb was highly conserved at both ends of the chromosome (Figure 24).

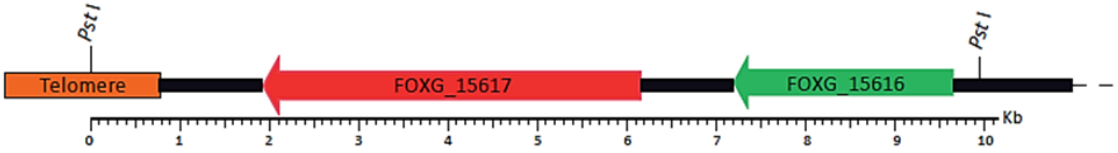

Figure 24. Schematic representation of the conserved subtelomeric region in Fol4287. Physical map of one end of chromosome 15 (supercontig SC28). The conserved region comprises approximately 10 Kb between two *Pst*I sites and includes two predicted open reading frames.

To test whether this conserved region is also present on other chromosomes, gDNA of *Fol4287* was treated with the restriction enzyme *Pst*I, which cuts at both ends of the conserved subtelomeric region (see Figure 24) and subjected to Southern blot analysis with a probe containing five tandem repeats of the telomeric sequence TTAGGG. If the restriction map of the chromosome ends differed for each of the 15 chromosomes, we would expect a hybridization pattern consisting of maximum 30 bands. Instead, we observed a single hybridyzing band of around 10 Kb, suggesting that the 10 kb *Pst*I fragment adjacent to the telomere is highly conserved across the chromosomes of Fol4287 (Figure 25A). By contrast, Southern blot using other restriction enzymes that cut at larger distances from the telomeric repeat revealed multiple hybridizing bands. This suggests that only 10 kb subtelomeric region is conserved on all chromosomes. and since not all chromosome ends have the same number of the TTAGGG hexamer repeats, the hybridizing band sizes were different

To further confirm these results, the entire chromosomes of *Fol4287* were separated by CHEF electrophoresis and subsequently performed Southern blot analysis with the telomeric probe containing the TTAGGG repeats (Bravo-Ruiz, unpublished). Strikingly, the pattern of hybridizing bands detected in the Southern blot was identical to that of the chromosomes in the CHEF gel, suggesting that the telomeric repeat sequence is present on all chromosomes (Figure 25B).

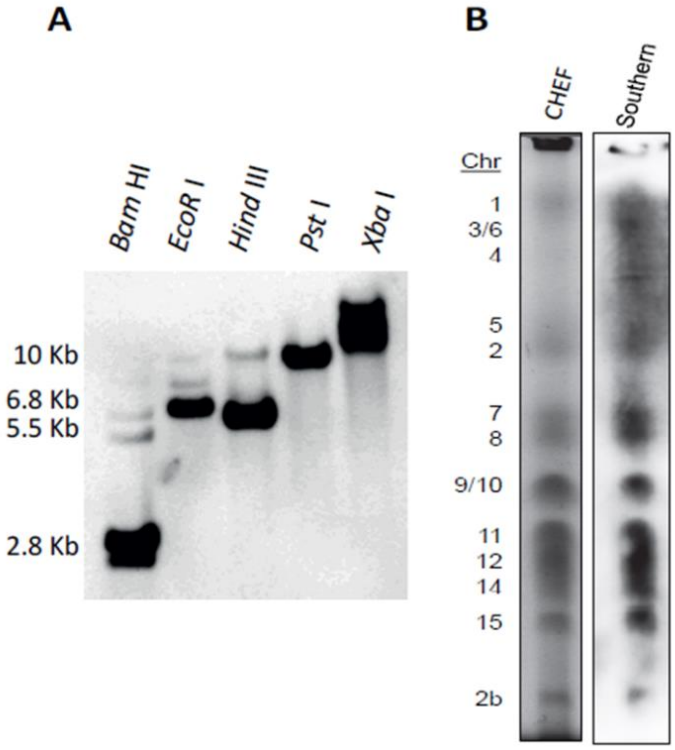

Figure 25. The chromosome ends in Fol4287 are highly conserved. (A) Southern blot of gDNA of Fol4287 treated with the indicated restriction enzymes was hybridized with a probe containing five tandem copies of the telomeric sequence TTAGGG. Sizes of hybridizing bands are indicated. Experiment performed by Gustavo Bravo-Ruiz. **(B)** Chromosomes of Fol4287 separated by contour-clamped homogeneous electric field (CHEF) electrophoresis were visualized by ethidiumm bromide staining (left panel) and submitted to Southern blot analysis with the telomeric probe. The putative positions of chromosome bands based on their sizes are indicated on the left.

2.1.1 The conserved 10 kb subtelomeric region contains two predicted open reading frames

Inspection of the conserved 10 Kb region located at both ends of chromosome 15 revealed the presence of two predicted open reading frames (ORFs), *FOXG_15617* and *FOXG_15616* (see Figure 2). To search for potential homologs of *FOXG_15617* and *FOXG_15616* in the genome of Fol4287, we performed a *BLASTp* search with the amino acid sequences of the two genes (Table 20). The search with *FOXG_15617* identified five hits, three of which correspond to predicted genes located on chromosomes 3, 14 and on the other end of chromosome 15. The other two hits mapped to unpositioned contig DS231739.1. All of these genes are located in subtelomeric regions as demonstrated by its position with respect to the total size of the chromosome. The first four homologs are very similar in length to *FOXG_15617* and encode proteins with high identities (88% to 90%), while the fifth, *FOXG_17278*, is longer and has a lower degree of identity (79%).

Table 20. Identification of putative homologs of the subtelomeric gene FOXG_15617 in the Fol4287 genome using BLASTp analysis.

GENE	LOCALIZATION	LENGTH	Nº aa	IDENTITY	COVERAGE	SCORE
FOXG_16462	(Chr14-SC36) 1,812,546	4,020 bp	1,339	90%	99%	2,279
FOXG_16652	(Chr 15-SC37) 1,838	4,257 bp	1,418	88%	99%	2,240
FOXG_14987	(Chr 3-SC25) 5,551,022	4,070 bp	1,356	88%	99%	2,236
FOXG_17281	DS231739.1 28,166	4,071 bp	1,356	88%	98%	2,196
FOXG_17278	DS231739.1 4,410 -11,367	5,292 bp	1,763	79%	98%	1,947

A search with the amino acid sequence of *FOXG_15616* identified six putative homologs (Table 21). Four of these (*FOXG_16653*, *FOXG_16461*, *FOXG_17282* and *FOXG_14986*) are annotated in the database with numbers that are consecutive to the homologs of *FOXG_15617* and are thus contiguous.

Table 21. Identification of putative homologs of the subtelomeric gene FOXG_15616 in the Fol4287 genome using BLASTp analysis.

GENE	LOCALIZATION	LENGTH	Nº aa	IDENTITY	COVERAGE	SCORE
FOXG_05570	Chr 2a 2,496	2,859 bp	952	100%	100%	1,667
FOXG_16653	(Chr 15-SC27) 7,423	2,418 bp	805	100%	100%	1,666
FOXG_16461	(Chr 14-SC36) 1,808,832	2,418 bp	805	100%	100%	1,666
FOXG_17282	DS231739.1 33,588	2,835 bp	944	100%	93%	1,560
FOXG_14986	(Chr3-SC25) 5,547,636	2,331 bp	776	89%	100%	1,449
FOXG_17278	DS231739.1 4,410-11,367	5,292 bp	1,763	95%	61%	956

Moreover, another putative homolog (*FOXG_05570*) is located on chromosome 2a, apparently only 2,500 bp from the chromosome end. Since this chromosome did not contain hits in the previous search with the telomeric repeat sequence (see Figure 23), we speculate that the end of chromosome 2a is not completely sequenced and therefore the *FOXG_15617* ortholog associated with this chromosome end was not detected in the *BLASTp* search. Notably, all five detected homologs were similar length to *FOXG_15616* and the encoded proteins exhibit identities between 89% and 100%. Interestingly, both *BLASTp* searches with *FOXG_15617* and *FOXG_15616* gave hits with the same predicted gene, *FOXG_17278,* located on an unpositioned contig. Although both ORFs are annotated in the database as a single gene, they appear to correspond to two independent genes, since a detailed sequence analysis detected the existence of an intergenic region with high identity to the region located between *FOXG_15616* and *FOXG_15617* on chromosome 15.

The results obtained from *in silico* analysis are schematically represented in Figure 26, indicating the chromosomal localization of the different homologs of *FOXG_15616* and *FOXG_15617* (Figure 26A) and the structural organization of the corresponding subtelomeric regions (Figure 26B).

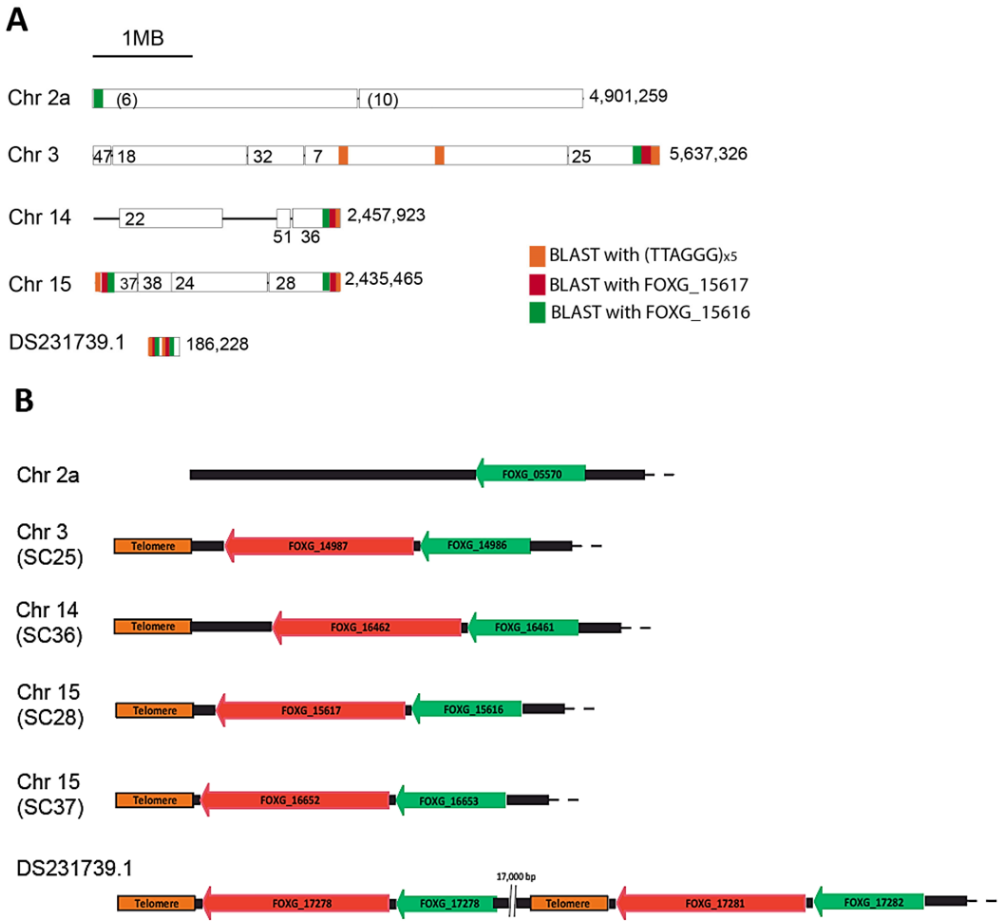

Figure 26. Structural organization of subtelomeric regions in Fol4287. (A) Chromosomal localization of homologs to *FOXG_15616* (green boxes) and *FOXG_15617* (red boxes). **(B)** Schematic representation of the identified subtelomeric regions. Note that in the unpositioned contig DS231739.1, the two ORFs are now represented as independent genes.

Note that in the case of the unpositioned contig DS231739.1, the database annotation has been corrected to represent both ORFs as independent genes while maintaining the same FOXG number. This unpositioned contig thus contains two complete sets of telomere-associated genes that probably correspond to two different chromosome ends.

2.1.2 Molecular analysis confirms structural conservation of subtelomeric regions in Fol4287

To further investigate the existence of the conserved subtelomeric region on all chromosomes, Southern blot analysis was performed (together with Gustavo Bravo Ruiz) using gDNA of *Fol4287* treated with different restriction enzymes and hybridized with the following probes: (A) telomeric repeat sequence, (B) the region located next to the telomeric repeat (NextTel), (C) gene *FOXG_15617*, and (D) gene *FOXG_15616* (Figure 27A). After *Pst*I treatment, hybridization with probes B, C and D, provided a single 10 Kb band identical to that obtained with probe A, confirming that this 10 kb region is highly conserved across all chromosomes (Figure 27A). Moreover, treatment with the enzymes *Eco*RI, *BamH*I and *Hind*III also provided identical hybridization patterns for probes A-C. As mentioned above the presence of more than one hybridizing band suggests that these restriction sites are located in variable regions of the subtelomere. We noted that the observed sizes of the different hybridizing fragments were 1-1.5 Kb larger than expected based on the genomic sequence. This suggests that the telomeric repeats in Fol4287 have a length of 1-1.5 Kb. Treatment of gDNA with *Xba*I, which cleaves outside the conserved 10 Kb region, also generated an identical pattern of hybridization with the four probes used, although the presence of multiple bands indicates a higher variability. The presence of additional hybridizing bands obtained with probe D upon treatment of gDNA with *BamH*I, *Eco*RI or *Hind*III confirmed the higher variability of the sequence adjacent to the conserved 10 Kb region (Figure 27A). Chromosome separation by CHEF electrophoresis and hybridization with probes A, B or C showed a signal in all chromosomes indicating that the conserved subtelomeric region is present in all of them (Figure 27B).

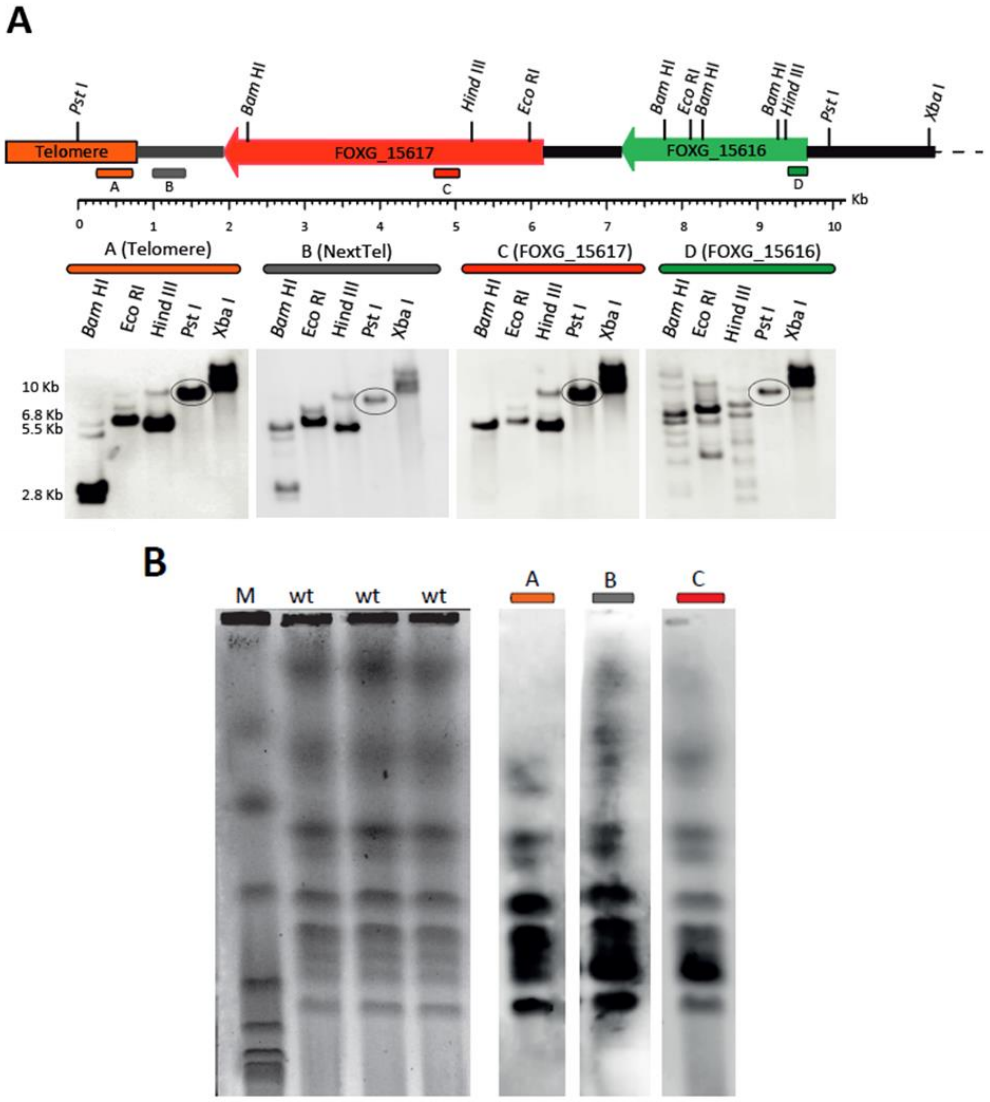

Figure 27. Structural conservation of subtelomeric regions on Fol4287 chromosomes. (A) Southern blot of Fol4287 gDNA treated with the indicated restriction enzymes and hybridized with probes A to D located at increasing distances from the telomere. The positions of the probes and the recognition sites of restriction enzymes are indicated on the top. **(B)** Chromosomes of Fol4287 separated by CHEF electrophoresis were visualized by ethidium bromide staining (left). Subsequently the lanes from the gel were cut and submitted to Southern blot analysis with the indicated probes (right). M: chromosomes of *Schizosaccharomyces pombe* and *Saccharomyces cerevisiae* used as molecular size markers. Note that an identical hybridization pattern is observed with probes A, B and C, suggesting that the regions located close to the telomere are structurally conserved in all chromosomes. CHEF analysis performed by Gustavo Bravo-Ruiz.

2.2. The subtelomeric region contains a LTR retrotransposon with a high number of copies in the Fol4287 genome

A *BLASTn* search with the sequence contiguous to the subtelomeric conserved 10 Kb region of chromosome 15 delimited by the *Pst*I site provided a high number of hits in the Fol4287 genome (data not shown). Using the "*NCBI conserved domains*" and "*Pfam*" search engines combined with a manual sequence comparison (with Gustavo Bravo Ruiz), we

detected homology in this region with retrotransposon-like elements from other organisms and were able to reconstruct a retrotransposable element named FoRS (*Fusarium oxysporum Repeated Sequence*) (Figure 28).

FoRS shows similarity to *copia*-like retrotransposons with a predicted ORF of 4,300 bp containing the two genes *gag* and *pol* (Figure 28A). The *gag* gene comprises approximately 1 Kb and encodes group-specific antigens (GAGs) which include the nucleic acid binding domain (NA) composed of zinc fingers. The *pol* gene of approximately 3,200 bp in length encodes the protease (PR), integrase (INT), reverse transcriptase (RT) and ribonuclease-H (RH) domains essential for the retrotransposition mechanism. In this family of retrotransposons, the Gag and Pol proteins are flanked by two long terminal repeats sequences (5' and 3'-LTRs). After a detailed sequence analysis, only the 5'-LTR region of the FoRS retrotransposon could be identified, including the three essential sections unique 3' (U3), repeat (R), and unique 5' (U5). The U3 domain contains the promoter and enhancer sequences that drive retrotransposon transcription while the R domain is required for initiation of reverse transcription and the U5 domain for complete cDNA synthesis. The PBS (primer binding site) and PPT (polypurine tract) sites are also essential for the replication process. The U3 region of the FoRS retrotransposon contains two near identical sequences as previously described in other *copia*-like retrotransposons (Figure 28B).

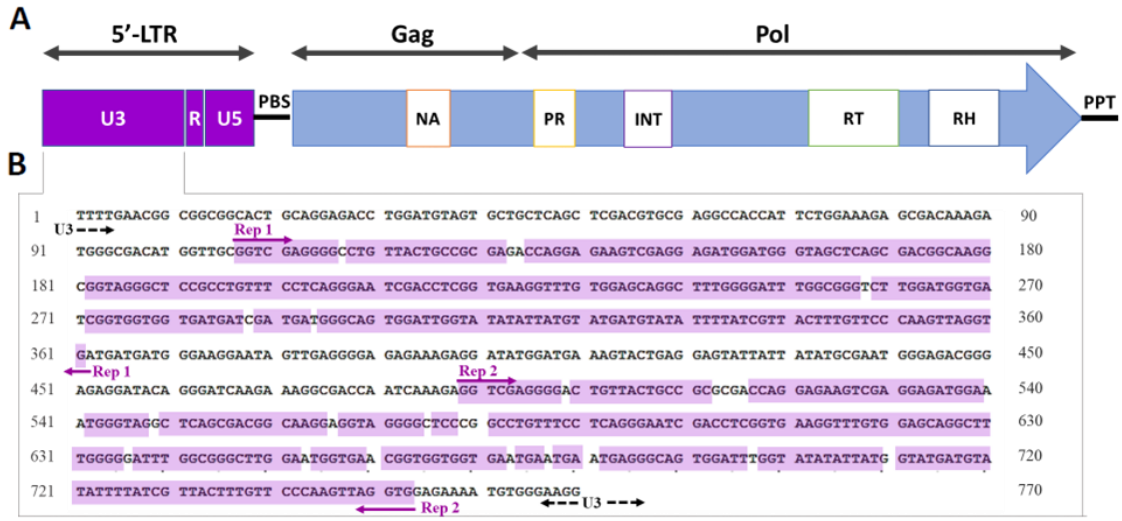

Figure 28. Schematic structure of the FoRS retrotransposon. (A) The 5' long-terminal repeat (5'-LTR) subdivided into U3, R and U5 regions. Gag, group-specific antigen with the nucleic acid binding domain (NA). Pol, polymerase comprising four domains: the aspartic protease (PR), integrase (INT), reverse transcriptase (RT) and ribonuclease-H (RH). PBS, primer binding site; PPT, polypurine tract. **(B)** Partial nucleotide sequence of the U3 domain located in the 5'-LTR region, comprising the two repeated sequences (Rep1, Rep2) with the matching nucleotides highlighted in purple.

A *BLASTn* search using only the FoRS ORF sequence retrieved 88 hits in the *Fol4287* genome. Figure 29 shows their distribution on the chromosome map considering only the hits with a coverage higher than 95%, corresponding to 45 *FoRS* copies in different regions of the genome. The highest copy number of this retrotransposable element was detected on the accessory chromosomes 3, 6, 14 and 15.

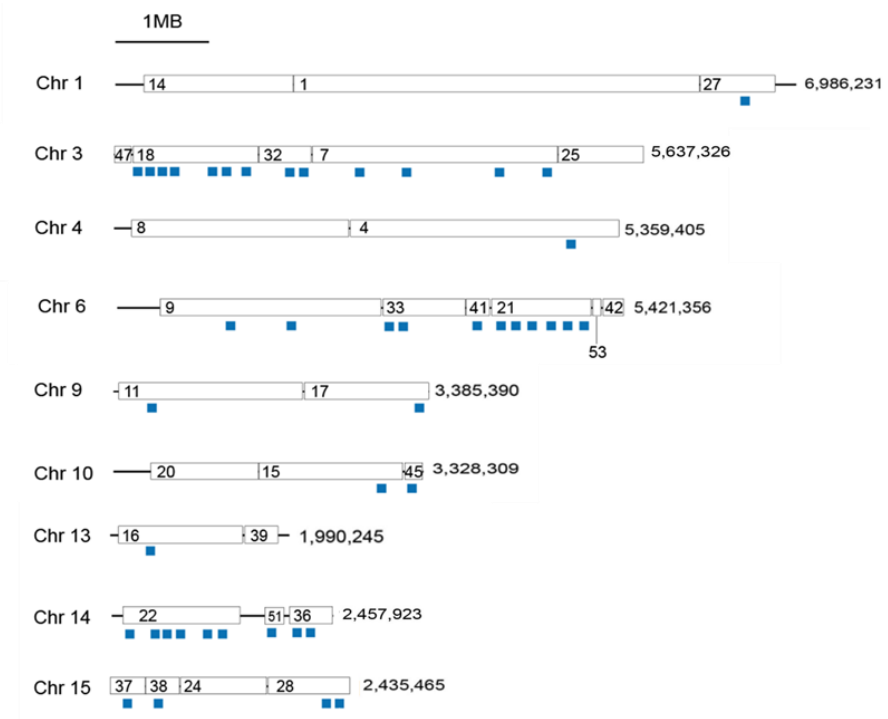

Figure 29. Chromosomal location of FoRS retrotransposon copies in Fol4287. A *BLASTn* search with the predicted ORF of the FoRS retrotransposon against the Fol4287 genome was performed in FungiDB. The chromosome map (modified from Ma *et al.,* 2010) shows the position of the identified FoRS retrotransposons (blue boxes).

2.3. Quantitative determination of the copy number of the conserved subtelomeric region in the Fol4287 genome

To experimentally determine the number of repeats of the conserved 10 kb subtelomeric region in the Fol4287 genome, qPCR analysis was performed with specific primer pairs of the two subtelomeric genes (*FOXG_15616* and *FOXG_15617*) as well as of the FoRS retrotransposon and the NexTel region. The average value obtained from four known single copy genes (*actin*, *FOXG_21450*, *gph, pg5*) were used as standards (Figure 30). Because Fol4287 has 15 chromosomes, we expected to detect approximately 30 copies of the conserved subtelomeric region. However, we calculated around 45 copies of the *FOXG_15617* gene, suggesting that additional copies of this gene are located in other regions of the genome. In contrast, qPCR analysis of the NextTel region and the *FOXG_15616* gene generated lower copy numbers than expected, 19 and 23 copies, respectively. In case of the

NexTel region, we speculate that the area in which the primer pair used for qPCR is located may not present in all the subtelomeric regions. This may generate shorter versions of the subtelomere and would explain the presence of the smaller hybridizing band observed in the Southern analysis after *BamH*I treatment (see Figure 27A). Another possible explanation is that the NextTel region is not identical on all chromosomes. On the other hand, the lower copy number of the *FOXG_15616* gene detected could indicate that this gene is not present on all chromosome ends. Finally, the copy number of the FoRS retrotransposon in the genome was estimated to be 37, which is close to the 45 full-length copies detected in the *in silico* analysis (see Figure 29).

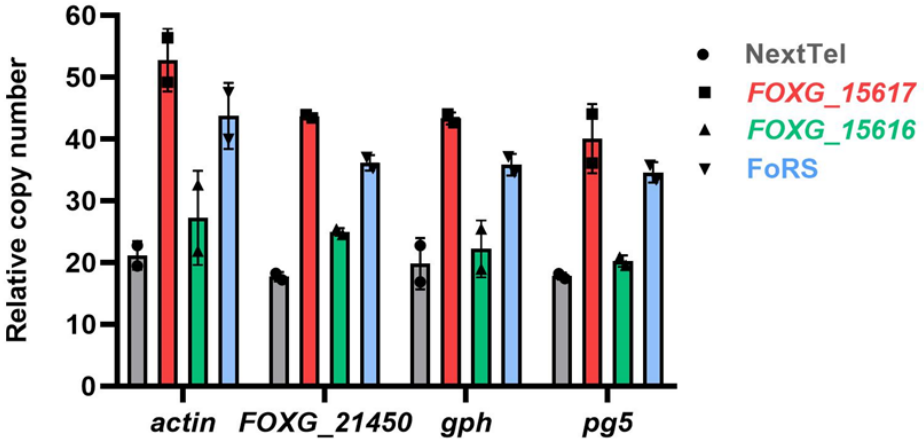

Figure 30. Copy number quantification of the conserved subtelomeric regions in Fol4287. qPCR with primer pairs specific for the NextTel region, FoRS, *FOXG_15616* or *FOXG_15617* was performed on Fol4287 gDNA. Results are indicated as copy numbers relative to the average value obtained using primers from four different single copy reference genes. Data shown represent the mean and standard deviations of two biological replicates, each including three technical replicates.

2.4. Expression of *FOXG_15617* and the FoRS retrotransposon is upregulated during tomato plant infection

To follow expression of the subtelomeric genes, we performed qRT-PCR analysis on cDNA of Fol4287 obtained from different growth conditions (Figure 31). In liquid PDB medium, the transcript levels of *FOXG_15616* and *FOXG_15617* were practically null, while the expression level of the FoRS retrotransposon was similar to that of the single copy actin gene used as a reference. During tomato root infection, the expression of FoRS and *FOXG_15617* was up to 7- and 25-fold higher at 10 days post-inoculation compared to the level in PDB.

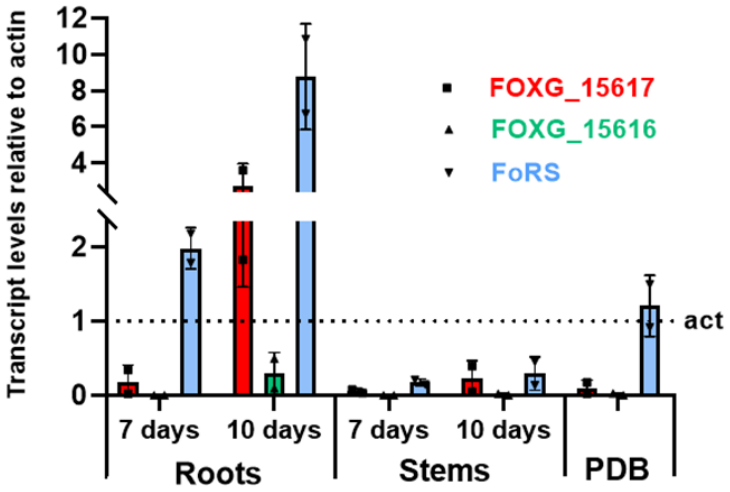

Figure 31. Expression of FOXG_15617 and the FoRS retrotransposon is upregulated during tomato plant infection. Microconidia of Fol4287 were inoculated in liquid PDB medium or on roots of tomato plants. After 14 hours growth in PDB or after 7 or 10 days after root inoculation, RNA was isolated and reverse transcribed to cDNA. RT-qPCR with specific primers of subtelomeric genes *FOXG_15616, FOXG_15617* and the FoRS retrotransposon was performed. Transcript levels are indicated relative to those of the actin gene. Data shown represent the mean and standard deviations of two biological replicates, each including three technical replicates.

2.5. Overexpression of the subtelomeric gene *FOXG_15617* in Fol4287

2.5.1 Generation of the Pact::FOXG_15617 overexpression construct

We focused on the subtelomeric gene *FOXG_15617* due to its significant increase in its expression observed during the infection process. Since generation of a knockout mutant was not feasible due to the high number of copies present in the genome, we decided to overexpress *FOXG_15617* from the strong constitutive P*act* promoter using two different fusion strategies.

In the first approach, the restriction enzyme cloning method was employed (Figure 32). First, the actin promoter of *Fol4287* (*Pact*) and the ORF of the *FOXG_15617* gene together with its terminator region were amplified using primer pairs Pact-2P/Pact-3 and subtel-11/subtel-30, respectively. The resulting PCR products were cloned into the pGEMT vector and the plasmid DNA was isolated from the resulting white colonies, selecting in a first round those that presented an increase in size due to the insertion of these fragments (Figure 32A). Plasmids P*act*/pGEMT and *FOXG_15617*/pGEMT were cut with the restriction enzymes *Pst*I and *Sal*I, respectively, to check if the fragments had been inserted in the desired orientation. Clones #21 and #23 carrying the P*act*/pGEMT plasmid were positive by generating two bands of the expected size (3 Kb and 0.9 Kb) after enzymatic treatment. Clone #9 carrying the *FOXG_15617*/pGEMT plasmid was also positive by generating three bands of 6 Kb, 0.8 Kb and 0.6 Kb (Figure 32A, bottom image). Once both plasmids were

confirmed, they were treated with *Pst*I and *Spe*I. In the case of P*act*/pGEMT, the treatment generated two bands, with the 0.9 Kb band corresponding to the P*act* fragment purified from the gel. The *FOXG_15617*/pGEMT plasmid was first cut with *Pst*I and *Spe*I to open it at the start of the ORF, then dephosphorylated to prevent self-ligation and finally the P*act* fragment was ligated into the dephosphorylated vector, obtaining the P*act*::*FOXG_15617*/pGEMT plasmid (Figure 32B). As in the previous case, the correct insertion and orientation of the fragments was checked by treatment with *Pst*I or *Sal*I, all of them being positive according to the banding pattern observed (Figure 32B, bottom image).

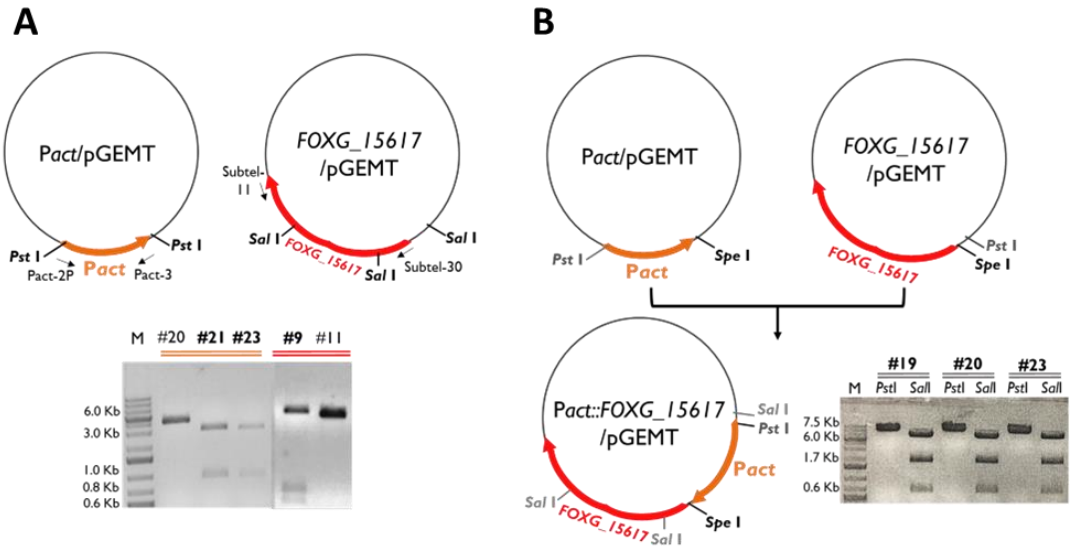

Figure 32. Generation of the Pact::FOXG_15617 overexpression construct by restriction enzyme cloning. (A) The Fol4287 actin promoter (P*act*) and the ORF and terminator region of the *FOXG_15617* gene were amplified with the indicated primers and independently cloned into the pGEMT vector. The resulting plasmids P*act*/pGEMT and *FOXG_15617*/pGEMT were cut with *Pst*I and *Sal*I, respectively, to confirm the correct insertion and orientation of the fragments (bottom left image). **(B)** Both plasmids were cut with *Pst*I and *Spe*I and, in the case of P*act*/pGEMT, the band of interest was purified from the gel. The promoter fragment was then ligated into the previously dephosphorylated *FOXG_15617*/pGEMT plasmid. The resulting plasmid P*act*::*FOXG_15617*/pGEMT was treated with *Pst*I or *Sal*I to confirm the correct insertion and orientation of the construct (bottom right image). Band sizes are indicated in Kb.

In the second approach the fusion PCR method was employed (Figure 33). For this, the previously obtained *Pact*/pGEMT and *FOXG_15617*/pGEMT plasmids were used as templates to amplify the P*act* and *FOXG_15617* regions by PCR using two pairs of primers in which Pact-4 and Subtel-36 share a complementary 5' tail. The resulting PCR fragments were fused and a second round of PCR was performed using nested primers (Pact-2P/Subtel-11) to obtain the final P*act*::*FOXG_15617* construct.

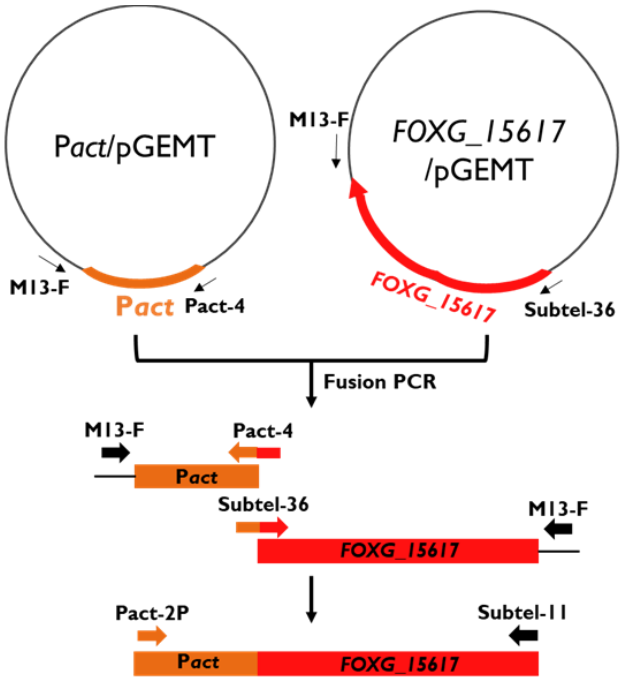

Figure 33. Generation of the Pact::FOXG_15617 overexpression construct by fusion PCR. The Fol4287 actin promoter (P*act*) and the ORF and terminator region of the *FOXG_15617* gene were amplified from plasmid DNA using the indicated pairs of primers, with Pact-4 and Subtel-36 sharing a complementary 5'-tail. The resulting PCR fragments with overlapping ends were fused and amplified with the indicated nested primers to obtain the final P*act*::*FOXG_15617* construct.

2.5.2 Generation and analysis of transformants carrying the Pact::FOXG_15617 construct

The fragment of approximately 5.5 Kb obtained by fusion PCR was used to co-transform protoplasts of the wild type strain Fol4287 with the Hyg^R cassette. In parallel, the plasmid P*act*::*FOXG_15617*/pGEMT was also amplified by PCR using the same pair of primers and the resulting fragment was also co-transformed into the genome of the wild type strain (Figure 34A). The resulting Hyg^R transformants were analyzed by PCR with a primer pair (Pact-5/Subtel-29) that binds inside the P*act* and *FOXG_15617* regions. Except for the P*act*::*FOXG_15617* #3, #4 and #5, all the other transformants were positive showing an amplification band of the expected size of 0.75 Kb (Figure 34B).

Selected candidate transformants were analyzed by Southern blot to determine the number of copies of the construct that had integrated into the genome (Figure 34C). The gDNAs of the wild type strain and the different transformants were treated with the restriction enzyme *Eco*RI. Hybridization with a probe located in the ORF of the *FOXG_15617* gene generated a 6.9 Kb hybridizing band corresponding to the endogenous copy of *FOXG_15617*. In addition, two additional bands were observed in the transformants, except for #7 which exhibited multiple bands. The additional band with a size larger than 6.9 Kb,

which was present both in the wild type strain and in the P*act*::*FOXG_15617* transformants, could correspond to a slightly different subtelomeric version as previously mentioned.

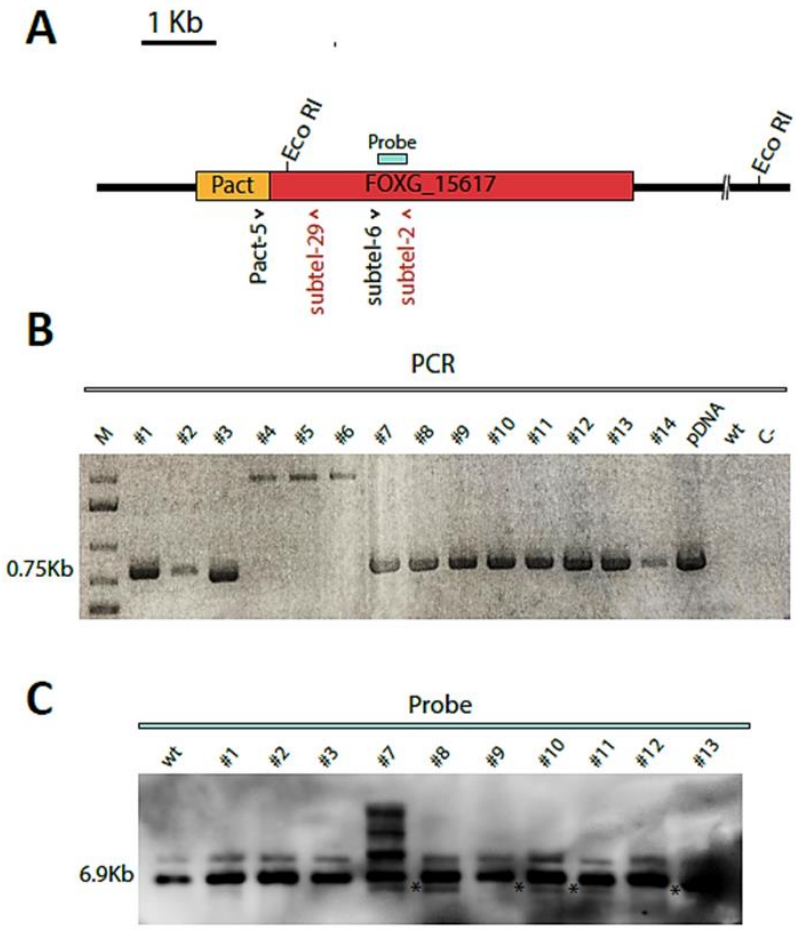

Figure 34. Analysis of transformants carrying the Pact::FOXG_15617 overexpression construct. (A) Schematic representation of the DNA construct used for co-transformation of Fol4287 protoplasts with the Hyg^{R} cassette as selective marker. Positions of *Eco*RI restriction sites are shown. Black (forward) and red (reverse) arrowheads indicate the positions of primers used for PCR and RT-qPCR analysis of the transformants as well as for obtaining the probe used for Southern blot analysis (blue bar). Scale bar, 1Kb. **(B)** PCR analysis with the primers Pact-5/subtel-29. The presence of a 0.75 kb band indicates the insertion of the P*act*::*FOXG_15617* construct into the genome. **(C)** Identification of P*act*::*FOXG_15617* transformants by Southern blot analysis. gDNAs of the wild type strain and putative transformants were treated with *Eco*RI, separated in an agarose gel, transferred to a nylon membrane and hybridized with the probe indicated in (A). The size of the hybridizing band corresponding to the endogenous copy of *FOXG_15617* is indicated on the left. The additional hybridizing band corresponding to the integrated P*act*::*FOXG_15617* construct is indicated with asterisks. The largest band may correspond to other subtelomeric versions

However, the band with a size smaller than 6.9 Kb (indicated with asterisks) was only present in some transformants but not in the wild type suggesting that it corresponds to the integrated P*act*::*FOXG_15617* construct. Transformants #8, #10, #11 and #13 exhibiting this additional band were selected for subsequent analysis. The transformant #3

was selected as a negative control since it appeared to have integrated no copy of the construct into its genome. Due to the high number of copies of the *FOXG_15617* gene in the genome, and since the chromosome ends are practically identical, it was not possible to establish with this analysis how many copies of the construct had been inserted into the *Fol4287* genome (Figure 34C).

2.5.3 Pact::FOXG_15617 transformants show increased expression levels of the FOXG_15617 gene

To check if the expression level of the *FOXG_15617* gene was increased in the selected P*act*::*FOXG_15617* transformants, a qRT-PCR analysis was performed. Total RNA isolated from germlings after 14 hours of growth in PDB medium was reverse transcribed to cDNA and the transcript levels were measured using a pair of primers flanking an intron (Subtel-17/Subtel-18). The four selected transformants #8, #10, #11 and #13 showed 20-30 fold higher transcript levels of the *FOXG_15617* gene respect to transcript level of this gene in the wild type strain (Figure 35). In contrast, in the P*act*::*FOXG_15617* #3 transformant the transcript levels of this gene were practically identical to those of the wild type strain.

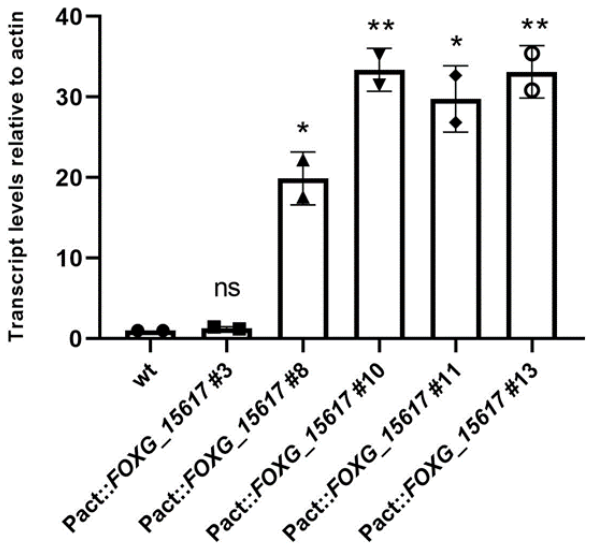

Figure 35. FOXG_15617 overexpression in the Pact::FOXG_15617 transformants. Microconidia of the indicated fungal strains were inoculated in liquid PDB medium. After 14 hours, total RNA was isolated from the obtained germlings and reverse transcribed to cDNA. RT-qPCR was performed with specific primers of the *FOXG_15617* gene (subtel-17/subtel-18). Transcript levels are indicated relative to those of the actin gene. Data shown represent the mean and standard deviations of two biological replicates, each including three technical replicates. * $p<0.05$, ** $p<0.01$ versus wild type according to t-test; ns, non-significant.

2.6. Phenotypic characterization of FOXG_15617 overexpressing strains

We first tested the effect of *FOXG_15617* overexpression in response to cell wall stress. Serial dilutions of conidia of the wild type strain and the different P*act*::*FOXG_15617* transformants were spot-inoculated on MM plates with or without the cell wall-perturbing agents Calcofluor White (CFW; 40 µg/ml) or Congo Red (CR; 100 µg/ml) and scanned after 3 days of growth at 28 °C. Of all the tested transformants, only P*act*::*FOXG_15617* #8 showed a slightly increased sensitivity to both cell wall-damaging agents although the difference to the wild type strain was not statistical significant (Figure 36). These results indicate that overexpression of the *FOXG_15617* gene has no effect on the response to cell wall damaging agents.

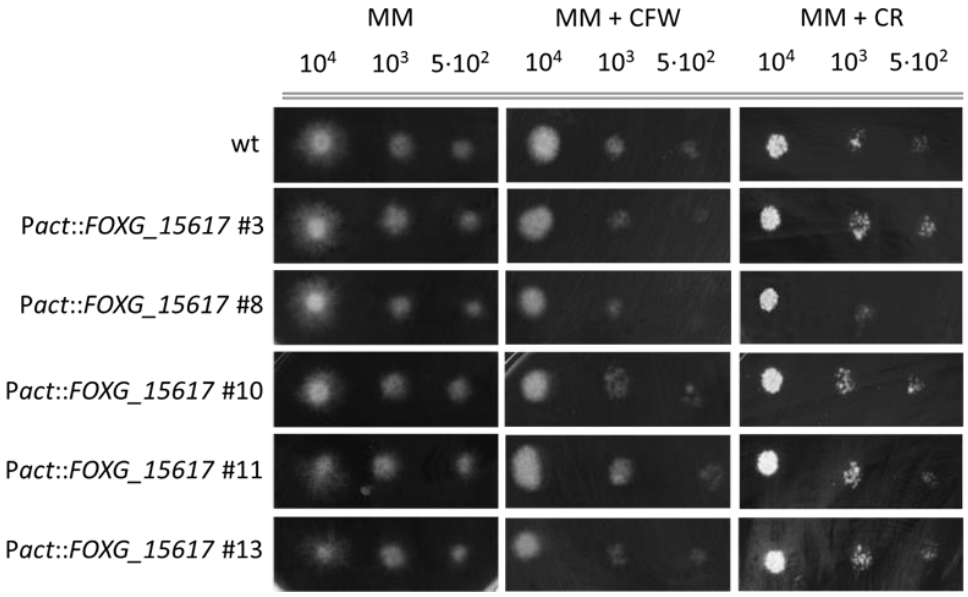

Figure 36. Sensitivity of FOXG_15617-overexpressing transformants to cell wall-damaging agents. Droplets from serial dilutions containing 10^4, 10^3 and $5{\cdot}10^2$ fresh microconidia of the indicated strains were spot-inoculated on MM plates with or without Calcofluor White (CFW; 40 µg/ml) or Congo Red (CR; 100 µg/ml). Plates were incubated at 28 °C for 3 days and scanned. Representative images from two independent replicates are shown.

It was previously described in other organisms that the telomeric and subtelomeric regions play an essential role in maintaining genomic stability. To determine the effect of *FOXG_15617* overexpression on genomic stability, an assay to quantify the frequency of colony growth sectors was performed (Díaz *et al.,* 2022) (Figure 37). Microconidia of the wild type strain and the different P*act*::*FOXG_15617* transformants were spread along a 5 cm line on Puhalla's Minimal Medium (PMM) supplemented with 50 mM methionine and the colony growth sectors were counted 3, 4, and 5 days after inoculation (Figure 37A). Quantitative analysis revealed that only the P*act*::*FOXG_15617* #11 transformant had a

slightly higher frequency of sector formation than the wild type strain. The rest of the tested transformants exhibited a frequency similar to that of the wild type strain, including the P*act*::*FOXG_15617* #3 transformant that does not overexpress this gene (Figure 37B). Collectively, these data indicate that the *FOXG_15617* gene is not related to the formation of colony growth sectors.

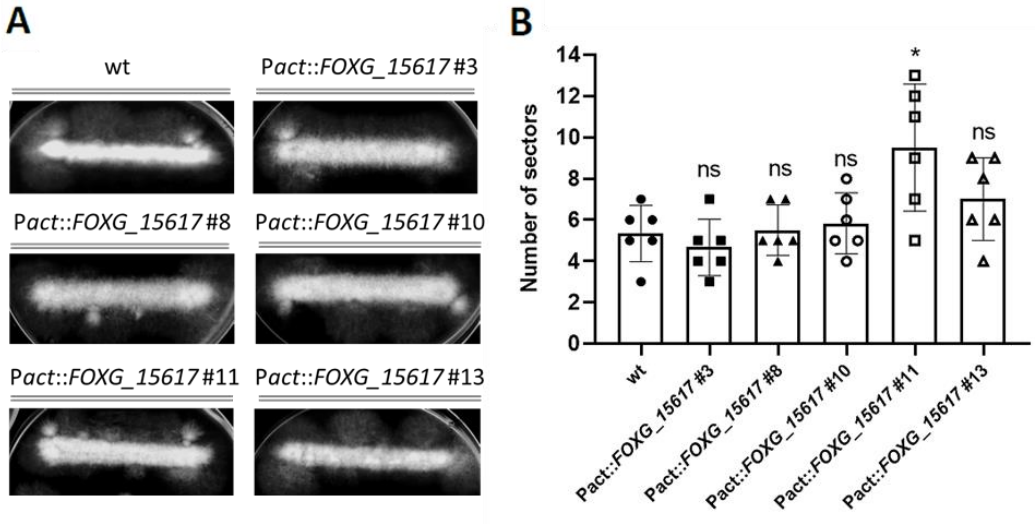

Figure 37. Frequency of colony growth sectors in FOXG_15617-overexpressing transformants. (A) 2.5x10^4 fresh microconidia of the indicated strains were spread along a 5 cm line on Puhalla's Minimal Medium (PMM) supplemented with 50 mM methionine as nitrogen source. Plates were incubated at 28 °C for 5 days and scanned. **(B)** Emerging colony growth sectors were counted starting at day 3 until day 5. The results show the mean number of colony growth sectors counted in the indicated strains. Error bars represent the standard deviation of six independent replicates per strain. * $p<0.05$ versus wild type according to t-test; ns, non-significant.

Since expression of the *FOXG_15617* gene is significantly increased during tomato plant infection, we performed a pathogenicity assay by dip-inoculating the roots of tomato plants with microconidia of the wild type strain or the P*act*::*FOXG_15617* transformants. No significant differences in mortality rates were observed between the wild type strain and the different transformants, except for P*act*::*FOXG_15617* #10 which showed a slight delay in the appearance of wilt symptoms (Figure 38).

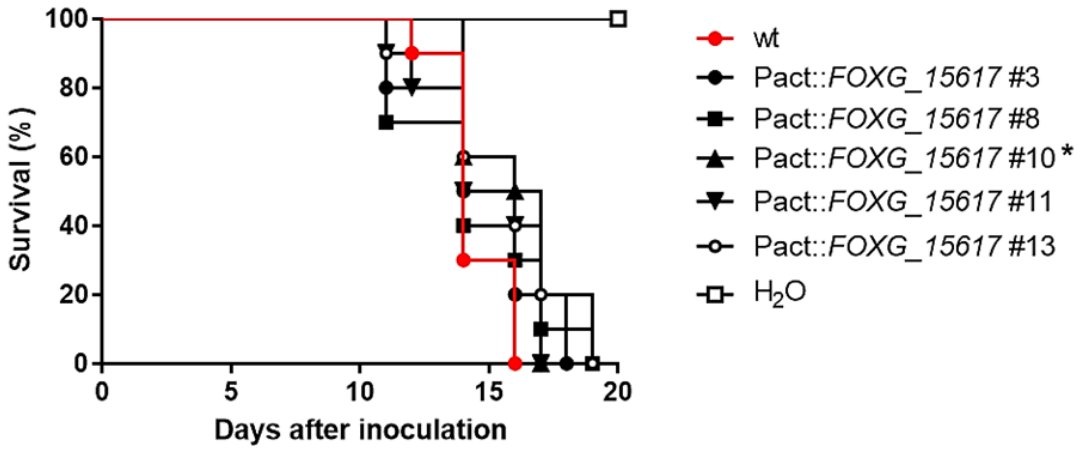

Figure 38. Virulence of FOXG_15617-overexpressing transformants on tomato plants. Groups of 10 two-week-old tomato plants (cv. Monika) were inoculated by dipping roots into a suspension of $5 \cdot 10^6$ freshly obtained microconidia mL^{-1} of the indicated fungal strains. Tomato plants were planted in vermiculite and maintained in a growth chamber with the conditions previously described. The Kaplan-Meier plot of the percentage survival of tomato plants for 20 days post-inoculation is shown. The Mantel–Cox method was used to assess the statistical significance of differences in survival among groups (* $p<0.05$ versus wild type). Experiments were performed two times with similar results. Data shown are from one representative experiment.

2.7. Overexpression of the *FOXG_15617* gene in *S. cerevisiae*

Since the overexpression of the *FOXG_15617* gene in Fol4287 did not have any detectable effect, we decided to express the *FOXG_15617* gene in *S. cerevisiae* using the self-replicating yeast expression vector p426 under control of the inducible P*gal* promoter (Figure 39). The full-length cDNA was obtained by fusion PCR of six overlapping fragments obtained from a P*act*::*FOXG_15617* transformant that overexpresses the *FOXG_15617* gene in Fol4287 (data not shown). The *FOXG_15617* cDNA and the p426 plasmid were then amplified with two pairs of primers sharing complementary 5' tails (Figure 39A). Co-transformation of the yeast strain BY4741 with both fragments resulted in cloning of the *FOXG_15617* cDNA into the p426 plasmid. As a control, a transformation was carried out using only with the plasmid p426. Positive clones that had incorporated the *FOXG_15617*/p426 plasmid were selected for their ability to grow on SD/-Ura medium and subsequently analyzed by PCR using the primer pair M13-F/M-13R, confirming that all of them had incorporated the plasmid according to the 5 Kb band size obtained (Figure 39B).

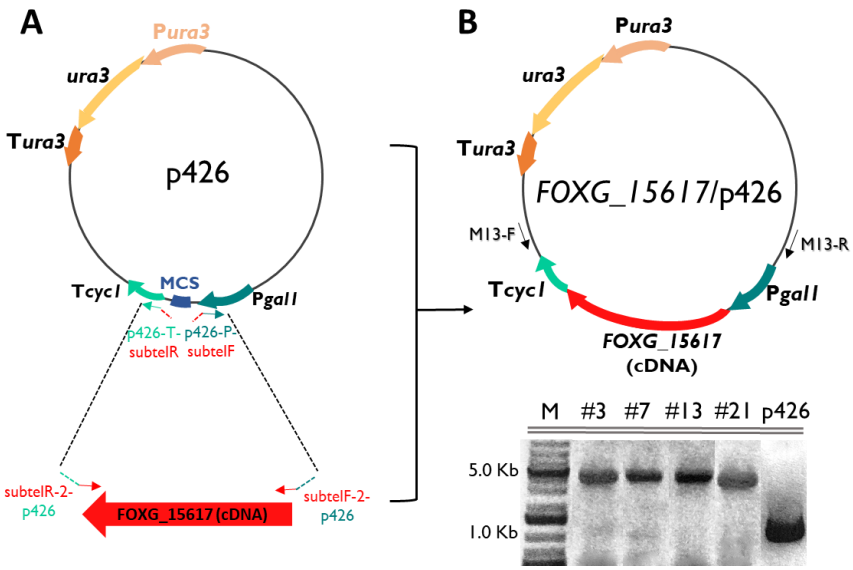

Figure 39. Generation of S. cerevisiae transformants harbouring the Pgal::FOXG_15617 fusion in the self-replicating vector p426. (A) The *FOXG_15617* cDNA and the p426 plasmid were amplified with two pairs of primers sharing complementary 5'-tails and the *FOXG_15617* cDNA was cloned into the linearized plasmid by co-transformation of the yeast strain BY4741 deficient in the URA3 gene. The transformation control was the p426 plasmid without the cDNA fragment. **(B)** For the screening of positive clones that had integrated the *FOXG_15617* cDNA into plasmid p426, a PCR analysis with the primers M13-F/M-13R was performed. Band sizes are indicated in Kb.

In addition to the *S. cerevisiae* transformants carrying the P*gal*::*FOXG_15617* construct in a self-replicating plasmid (not inserted in the chromosome), we also generated transformants harboring chromosomal integrations of the P*gal*::*FOXG_15617* construct. The rationale for this was that insertion of the *FOXG_15617* gene into a chromosome may be required for its function (Figure 40). For this, the yeast plasmid *FOXG_15617*/p426 was used to transform competent *E. coli* cells. Characterization of plasmid DNA isolated from the resulting colonies identified only one positive colony (#30-3) according to the band size observed (Figure 40A). This plasmid was subjected to PCR with primers Pura3(Sc)-1/M13-R and the resulting fragment was used to transform yeast strain BY4741. Transformation with the PCR-amplified p426 construct without the cDNA fragment was performed as control. Screening of the positive clones was carried out with two different primer pairs, confirming that all the transformants had inserted the linear construct into their genome (Figure 40B).

From now on, transformants carrying the self-replicating plasmid will be called replicative transformants (indicated with an "r" at the end of the name: P*gal*::*FOXG_15617* #3 r) and transformants with the construct inserted into the genome will be called integrative transformants (indicated without any extra letters: P*gal*::*FOXG_15617* #3).

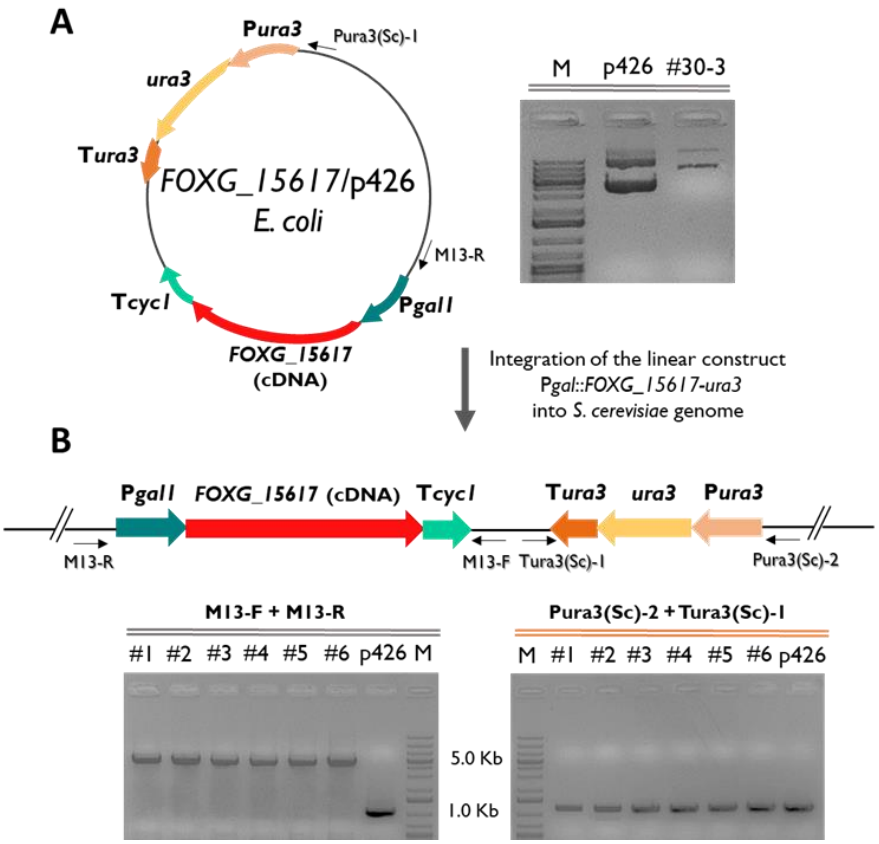

Figure 40. Generation of S. cerevisiae transformants harboring chromosomal integrations of the Pgal::FOXG_15617 construct. (A) Competent *E. coli* cells were transformed with the yeast plasmid *FOXG_15617*/p426 (see Fig. 16). Plasmid DNA was isolated from the resulting transformant #30-3 (left upper image), PCR-amplified with the primers Pura3(Sc)-1 and M13-R and the obtained fragment was transformed into the yeast strain BY4741 lacking the *URA3* gene. The transformation control was the PCR-amplified p426 construct without the cDNA fragment. **(B)** Screening of positive yeast transformants that had integrated the linear construct into the genome was performed by PCR analysis with the primers pairs M13-F/M-13R and Pura3(Sc)-2/Tura3(Sc). Band sizes are indicated in Kb.

2.8. Phenotypic characterization of *S. cerevisiae* transformants harboring the P*gal*::*FOXG_15617* construct

2.8.1 Effect of antimicrobial agents

We hypothesized that the *FOXG_15617* gene could be involved in chromosomal stability. For this reason, we determined the growth of the yeast transformants in the presence of different antimicrobial agents that can induce DNA damage and genomic instability (Figure 41). Since the assay was performed prior to obtaining the integrative transformants, only the replicative transformants were analysed. Strains were aliquoted into 96-well Microtiter™ plates supplemented with kanamycin (120 µg/ml), hygromycin (75 µg/ml) or canavanine (75 µg/ml) and the analysis was performed under inducing (2% Galactose + 0.1% glucose) or repressing (2% glucose) conditions. We found that the

transformants carrying plasmid *FOXG_15617*/p426 (#3r, #7r, #13r and #21r) and the control transformant containing plasmid p426 without the *FOXG_15617* cDNA (BY4741-p426r) showed similar growth under both inducing and repressing conditions. This indicates that *FOXG_15617* is not involved in the response to antimicrobial stress.

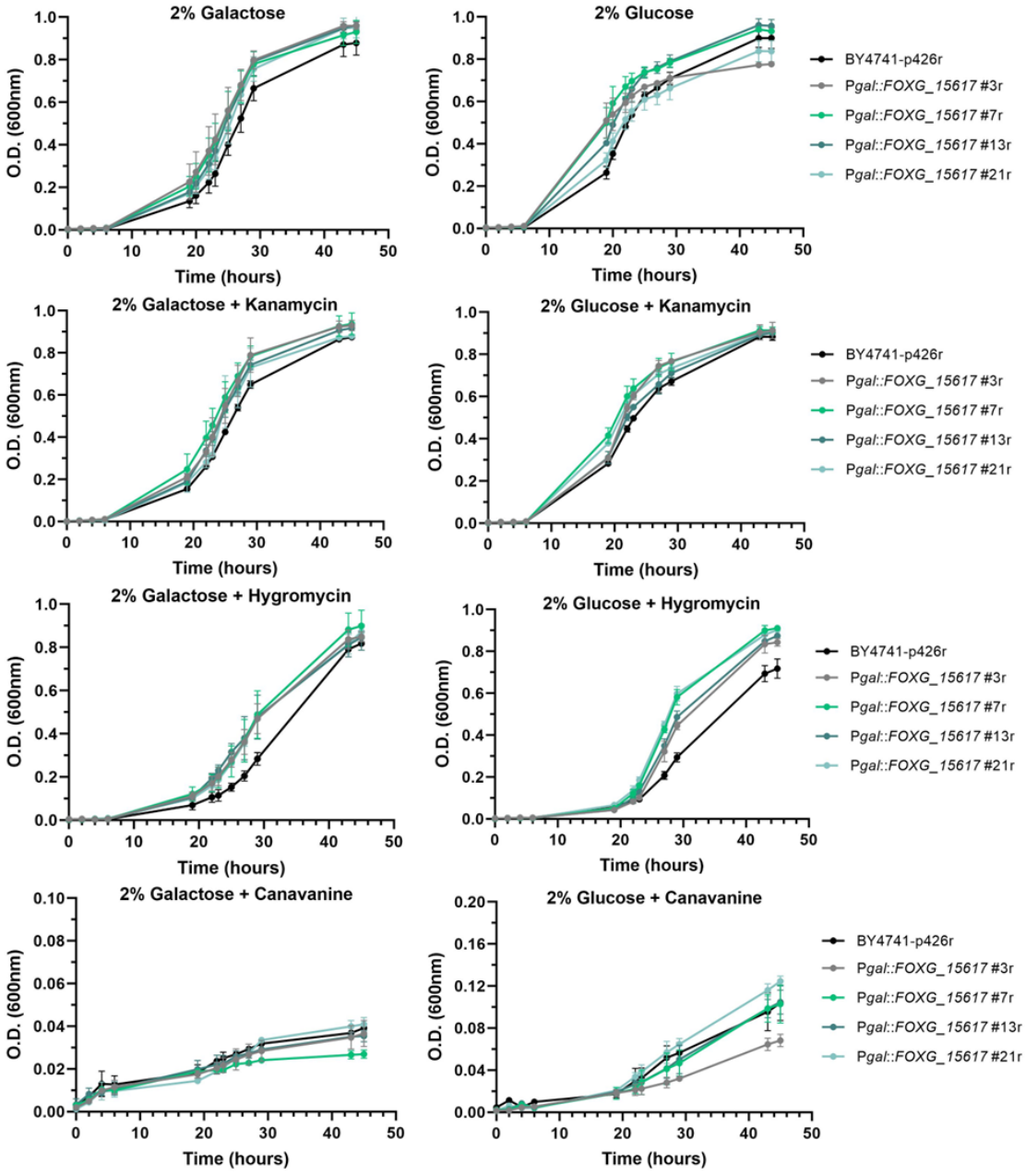

Figure 41. Growth curves of yeast transformants carrying the Pgal::FOXG_15617 construct in the presence of different antibiotics. A single colony of the indicated strains was inoculated and grown O/N at 30 °C and 200 rpm in selective synthetic medium (SD/-Ura). After 14 hours, the optical density (OD_{600}) of the cultures was measured and adjusted to 0.03. Aliquots were added to wells of Microtiter™ plates containing SD/-Ura medium supplemented with different antibiotics: kanamycin (120 µg/ml), hygromycin (75 µg /ml) or canavanine (75 µg /ml); under P*gal*::*FOXG_15617*-inducing (2% Galactose + 0.1% Glucose) or repressing (2% Glucose) conditions. The optical density at 600nm was recorded over time.

2.8.2 Effect of 5-fluoroorotic acid

Another method to test genomic stability of an organism is to quantify the rate of spontaneous mutations after exposure to toxic compounds such as 5-fluoroorotic acid (5-FOA). Because only Ura$^-$ cells can grow in the presence of 5-FOA since the product of the *ura3* gene converts 5-FOA into 5-FU (5-fluorouracil), a highly toxic compound, growth in the presence of 5-FOA indicates spontaneous loss or mutation of the *ura3* gene, thus establishing an indirect measurement of mutation rate and genomic instability.

Using this assay, we asked if the mutation rate (Ura$^-$ revertants and FOA^R) increases after inducing *F0XG_15617* expression in yeast. First, the effect of 5-FOA on growth of P*gal*::*F0XG_15617* yeast transformants was evaluated on solid medium (Figure 42). In the positive control (+Ura-FOA) all the strains grew because of the presence of uracil in the medium. By contrast, in the negative control (-URA+FOA), none of the strains grew because Ura$^-$ strains need uracil and Ura$^+$ strains convert 5-FOA into toxic 5-FU. In the absence of both compounds (-URA-FOA), the Ura$^+$ strains grew while the wild type strain BY4741 did not grow. Finally, in the +URA+FOA a medium only the auxotrophic BY4741 strain grew since it fails to convert 5-FOA to 5-FU, while the rest of the Ura$^+$ strains died due to the toxicity of this compound (Figure 42).

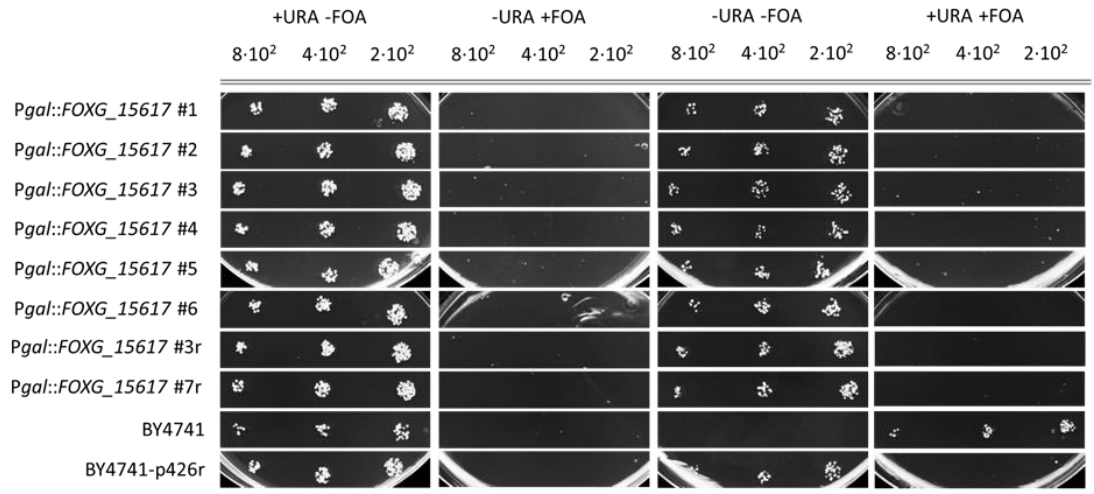

Figure 42. Effect of 5-Fluoroorotic acid on the growth of yeast transformants carrying the Pgal::FOXG_15617 construct. Droplets from serial dilutions containing $8{\cdot}10^2$, $4{\cdot}10^2$ and $2{\cdot}10^2$ cells of the indicated yeast strains were spot-inoculated on SD medium plates under P*gal::F0XG_15617*-inducing conditions (2% Galactose + 0.1% Glucose) with or without Ura (0.005%) and 5-FOA (0.1%). Plates were incubated at 30 °C for 2 days and scanned.

In parallel, growth curves were established in liquid medium under the different conditions (Figure 43). In the first three conditions analyzed (+URA-FOA, -URA-FOA and -URA+FOA) the results were identical to those observed on solid medium. However, in the

+URA+FOA medium, where only the BY4741 strain was expected to grow, we also observed growth of the Ura+ strains, although to a lesser degree. This result suggest that these cells have undergone spontaneous mutations in the *ura3* gene to become Ura-/FOA^R. The increased growth in the presence of +URA+FOA was independent of whether the P*gal*::*FOXG_15617* construct had integrated into the chromosome or was self-replicating. However, the BY4741-p426r control strain, which lacks the *FOXG_15617* cDNA, also showed increased growth that was even higher than in the strains expressing the the cDNA (Figure 43).

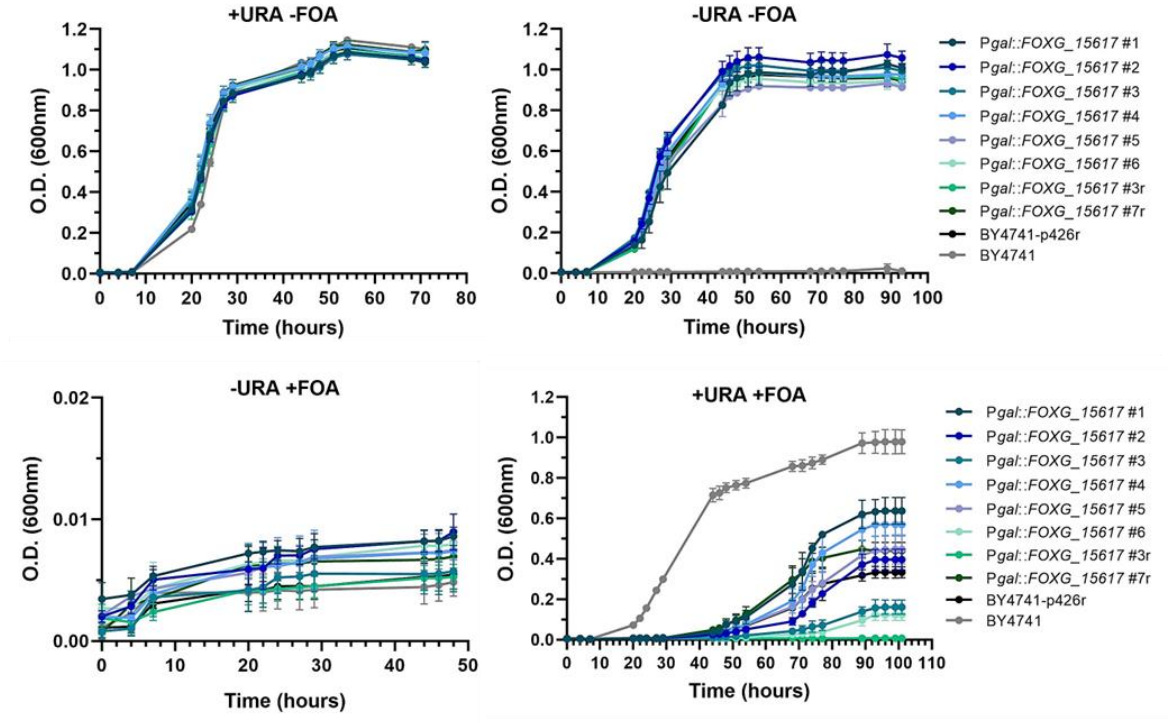

Figure 43. Effect of 5-Fluoroorotic acid on the growth of yeast transformants carrying the Pgal::FOXG_15617 construct. A single colony of each of the indicated strains was inoculated and grown O/N at 30 °C and 200 rpm in selective synthetic liquid medium (SD/-Ura or SD/-Trp). After 14 hours, the optical density (OD_{600}) of the cultures was measured and adjusted to 0.03. Aliquots were added to wells of Microtiter™ plates containing SD medium supplemented with Ura (0.005%) and/or 5-FOA (0.1%) under P*gal*::*FOXG_15617*-inducing condition (2% Galactose + 0.1% Glucose). The optical density at 600nm was recorded over time.

We reasoned that in some of the P*gal*::*FOXG_15617* strains the *ura3* gene could have been inactivated due to point mutations. We therefore established an assay to measure the frequency of spontaneous 5-FOA resistant uracil auxotrophs under inducing and repressing conditions (Table 22). After 14 hours of growth, aliquots of each strain were inoculated in SD medium with 2% galactose + 0.1% glucose (inducing condition) or 2% glucose (repressing condition). After 7 hours, aliquots were plated on SD medium with or without uracil or 5-FOA. Cell viability determined in +URA and -URA media revealed a lower value in the -

URA condition where only Ura+ cells can grow. The viability of the BY4741 strain in -URA media was 0%, as expected due to absence of the *ura3* gene. The frequency of spontaneous 5-FOA resistant uracil auxotrophs (FOA^R) was calculated by dividing the number of colonies on +URA+FOA (Ura- cells) by the number of colonies on -URA (Ura+ cells that could potentially undergo point mutations to become FOA^R). The P*gal*::*FOXG_15617* #1 and #2 transformants exhibited a higher FOA^R rate under inducing conditions than under repressing conditions (Table 22). However, the same was true for the negative control transformant BY4741-p426 #1, which lacks the *FOXG_15617* cDNA and showed an even higher FOA^R rate. We thus conclude that the appearance of spontaneous FOA^R mutants is independent of the overexpression of the *FOXG_15617* gene.

Table 22. Frequency of spontaneous 5-FOA resistant uracil auxotrophs in the different strains under Pgal::FOXG_15617-inducing or repressing conditions. After 14 hours of growth in selective synthetic medium (SD/-Ura or SD/-Trp), aliquots of each of the cultures were grown for additional 7 hours under P*gal*::*FOXG_15617*-inducing (2% Galactose + 0.1% Glucose) or repressing (2% Glucose) conditions. Aliquots of each of the indicated strains were then plated on SD medium plates with or without Ura (0.005%) and 5-FOA (0.1%) and the number of spontaneous 5-FOA resistant uracil auxotrophs was counted after 3 days. The frequency of spontaneous 5-FOA resistant uracil auxotrophs (FOA^R) was calculated by dividing the number of colonies on +URA+FOA (Ura- cells) by the number of colonies on -URA (Ura+ cells that could potentially undergo point mutations to become FOA^R).

2% GALACTOSE + 0.1% GLUCOSE					
STRAIN	INITIAL CELL DENSITY	CELL VIABILITY +URA	CELL VIABILITY -URA	CELL VIABILITY +URA +FOA	FOA^R frequency
P*gal*::*FOXG_15617* #1	$7.3x10^6$	$6x10^6$	$3.5x10^6$	832	$2.38x10^{-4}$
P*gal*::*FOXG_15617* #2	$7.4x10^6$	$6x10^6$	$3.5x10^6$	462	$1.32x10^{-4}$
P*gal*::*FOXG_15617* #3	$6.6x10^6$	$3.5x10^6$	$3.5x10^6$	23	$0.066x10^{-4}$
BY4741-p426 #1	$8.1x10^6$	$6x10^6$	$4x10^6$	987	$2.46x10^{-4}$
BY4741-p426 #4	$7x10^6$	$6x10^6$	$3.5x10^6$	144	$0.41x10^{-4}$
BY4741-p426 #6	$7.3x10^6$	$6x10^6$	$6x10^6$	21	$0.035x10^{-4}$
BY4741	$8x10^6$	$6x10^6$	$0x10^6$	∞	$6x10^6$ (100%)
2% GLUCOSE					
STRAIN	INITIAL CELL DENSITY	CELL VIABILITY +URA	CELL VIABILITY -URA	CELL VIABILITY +URA +FOA	FOA^R frequency
P*gal*::*FOXG_15617* #1	$1.46x10^7$	$1.3x10^7$	$8.7x10^6$	286	$0.33x10^{-4}$
P*gal*::*FOXG_15617* #2	$1.51x10^7$	$1.5x10^7$	$8.9x10^6$	135	$0.15x10^{-4}$
P*gal*::*FOXG_15617* #3	$1.3x10^7$	$1.2x10^7$	$9x10^6$	26	$0.028x10^{-4}$
BY4741-p426 #1	$1.65x10^7$	$1.6x10^7$	$1.3x10^7$	770	$0.59x10^{-4}$
BY4741-p426 #4	$1.28x10^7$	$1x10^7$	$6.2x10^6$	223	$0.36x10^{-4}$
BY4741-p426 #6	$1.44x10^7$	$1x10^7$	$9.5x10^6$	369	$0.39x10^{-4}$
BY4741	$1.61x10^7$	$1.5x10^7$	$0x10^6$	∞	$1.5x10^7$ (100%)

2.9. Presence of putative homologs of *FOXG_15616* and *FOXG_15617* genes in other fungal genomes

To ask if the subtelomeric region present in *Fol4287* is conserved in other *Fusarium spp.* or fungal species, we performed *BLASTp* analyses with the amino acid sequences of *FOXG_15616* and *FOXG_15617* genes. Predicted homologs of *FOXG_15617* were identified in different *F. oxysporum* isolates including, among others, the human isolate NRRL32931 and the non-pathogenic strain *Fo47* (Table 23). All the proteins encoded by these homologs exhibit more than 70% identity to *FOXG_15617*.

Table 23. Identification of putative homologs of FOXG_15617 in the genomes of Fusarium spp. using BLASTp analysis.

SPECIE	GENE	LENGTH	Nº aa	IDENTITY	COVERAGE	SCORE
F. oxysporum f.sp. *conglutinans* NRRL54008	*FOPG_19389*	2,876 bp	915	82%	60%	1,327
	FOPG_18306	2,135 bp	655	76%	54%	943
F. oxysporum f.sp. *raphani* NRRL54005	*FOQG_18682*	4,031 bp	1,270	72%	100%	1,736
	FOQG_18269	2,549 bp	832	99%	64%	1,516
F. oxysporum NRRL32931	*FOYG_17561*	4,071 bp	1,356	80%	99%	1,920
	FOYG_17594	2,538 bp	845	99%	73%	1,722
F. oxysporum Fo47	*FOZG_17462*	2,912 bp	952	83%	69%	1,365
F. poae	*FPOA_14090*	4,323 bp	1,285	82%	99%	1,967
	FPOA_12498	4,316 bp	1,322	79%	99%	1,932
	FPOA_13940	3,685 bp	1,138	82%	90%	1,798
	FPOA_12157	2,253 bp	698	89%	60%	1,247
F. mangiferae	*FMAN_14123*	4,185 bp	1,394	80%	90%	1,777
F. fujikuroi MRC2276	*FFMR_08828*	3,054 bp	947	92%	76%	1,736

Homologs with high identity to *FOXG_15617* were also identified in the genomes of other species of the genus *Fusarium* such as *F. poae*, *F. mangiferae* and *F. fujikuroi*. Interestingly, however, no matches were found in the species *F. graminearum* or *F. verticilloides*.

We next asked if there are homologs of the other subtelomeric gene *FOXG_15616* in the genome of these fungal species and if yes, whether they are located next to the *FOXG_15617* homologs. *BLASTp* analysis identified homologs of *FOXG_15616* in the genome of all the species mentioned above except for the non-pathogenic strain *Fo47* and *F. mangiferae* (Table 24). All these homologs exhibited an identity higher than 80% with *FOXG_15616*, except for the *F. fujikuroi* protein which has an identity of 56%.

Table 24. Identification of putative homologs of *FOXG_15616* in the genomes of *Fusarium* spp. using *BLASTp* analysis

SPECIE	GENE	LENGTH	N° aa	IDENTITY	COVERAGE	SCORE
F. oxysporum f.sp. *conglutinans* NRRL54008	*FOPG_19225*	3,115 bp	952	99%	100%	1,664
	FOPG_18980	3,131 bp	961	78%	100%	1,246
F. oxysporum f.sp. *raphani* NRRL54005	*FOQG_19563*	1,329 bp	339	100%	39%	664
	FOQG_19242	1,298 bp	410	81%	44%	594
F. oxysporum NRRL32931	*FOYG_17562*	2,814 bp	937	83%	99%	1,272
F. poae	*FPOA_13939*	3,099 bp	951	95%	99%	1,497
	FPOA_14091	3,098 bp	949	90%	99%	1,437
	FPOA_12021	3,098 bp	949	90%	99%	1,428
	FPOA_12497	3,098 bp	949	90%	99%	1,425
	FPOA_12156	2,755 bp	844	88%	86%	1,059
F. fujikuroi MRC2276	*FFMR_08829*	3,482 bp	1,084	56%	88%	756

To determine if the *FOXG_15616* and *FOXG_15617* homologs are contiguous in these genomes, we checked for consecutive numbering and position within the contig. In the *F. oxysporum* isolate NRRL32931, *F. poae* and *F. mangiferae*, the homologs of

FOXG_15616 and *FOXG_15617* showed consecutive numbering nomenclature consistent with an adjacent position, confirming that the gene structure is conserved in these organisms. Whether these putative homologs are located in subtelomeric regions could not be established since the contigs in these species are currently not positioned on the chromosomes.

We also detected homologs of the two genes in the fungal pathogens *Magnaporthe oryzae*, *Claviceps purpurea*, *Metarhizium majus* as well as in *Chaetomium globosum*, all belonging to the Sordariomycete group as *F. oxysporum* (Tables 25 and 26). In *C. globosum,* the two ORFs are annotated in the database as a single gene, as was the case for the *FOXG_17278* gene of *Fol4287*. In *M. majus*, the genes show consecutive numbering and a contiguous position, although it could not be established if they are located in the subtelomeric region.

Table 25. Identification of putative homologs of FOXG_15617 in the genomes of different fungal species using BLASTp analysis.

SPECIE	GENE	LENGTH	N° aa	IDENTITY	COVERAGE	SCORE
Magnaporthe oryzae 70-15	*MGG_15976*	2,652 bp	883	35%	54%	382
	MGG_14341	2,448 bp	815	35%	63%	369
	MGG_15975	963 bp	320	40%	22%	193
Claviceps purpurea 20.1	*CPUR_08690*	3,810 bp	1,201	33%	80%	410
	CPUR_08727	3,858 bp	1,249	31%	79%	338
Metarhizium majus ARSEF 297	*MAJ_09911*	3,992 bp	1,208	44%	84%	591
Chaetomium globosum	*CHGG_10724*	5,706 bp	1,901	38%	87%	479

Table 26. Identification of putative homologs of FOXG_15616 in the genomes of different fungal species using BLASTp analysis.

SPECIE	GENE	LENGTH	Nº aa	IDENTITY	COVERAGE	SCORE
Magnaporthe oryzae 70-15	*MGG_15792*	1,607 bp	535	34%	57%	238
	MGG_15974	1,317 bp	438	39%	39%	217
	MGG_10898	1,317 bp	438	38%	41%	215
Claviceps purpurea 20.1	*CPUR_03361*	2,050 bp	608	33%	55%	248
	CPUR_08849	3,640 bp	837	32%	51%	242
Metarhizium majus ARSEF 297	*MAJ_09910*	2,530 bp	783	38%	66%	336
Chaetomium globosum	*CHGG_10724*	5,076 bp	1,901	39%	65%	355

2.10. The rice blast fungus Magnaporthe oryzae and F. oxysporum share a similar structure of the chromosome ends

In the rice blast pathogen *M. oryzae* the contigs are assembled and associated to chromosomes, allowing to establish the genomic location of the identified homologs. The *FOXG_15616* and *FOXG_15617* homologs identified in the previous *BLASTp* analysis are located on chromosomes 1 and 2 of *M. oryzae*, while no homologs were identified on the remaining five chromosomes (Figure 44). This could either be due to missing sequences of the chromosome ends or the absence of homologs on these chromosomes. Although the *M. oryzae* homologs have shorter ORFs than the corresponding genes in Fol4287, their location close to the telomeric region is conserved demonstrating that the chromosome ends of *M. oryzae* have a similar structure to those of Fol4287. Note that the structure of chromosome 2 is slightly different due to the presence of two contiguous *FOXG_15616* homologs (Figure 44). *MGG_15975* likely represents a non-functional pseudogene given its small size. In addition, at more than 3 Mb from the *MGG_15974* gene, another *FOXG_15617* homolog (*MGG_15792*) was identified with a similar length as the other homologs.

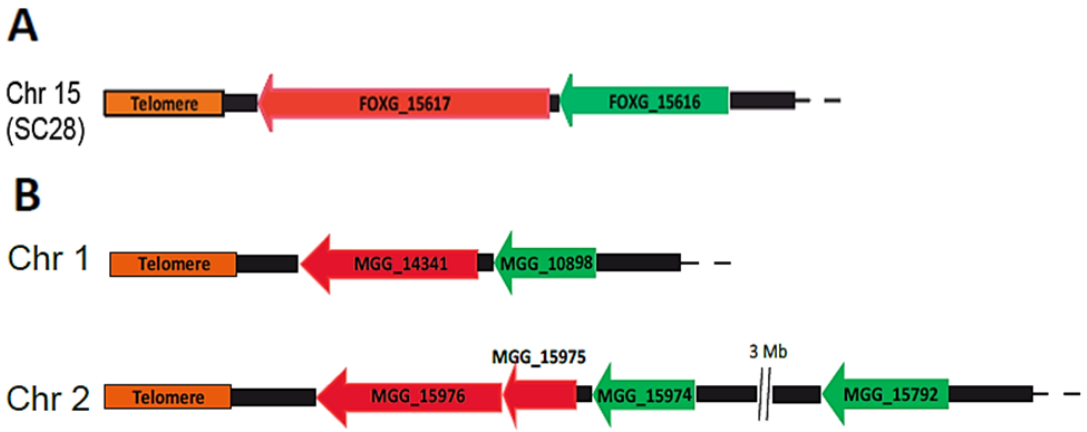

Figure 44. The fungal plant pathogens M. oryzae and F. oxysporum share a similar structure of the chromosome ends. (A) Schematic representation of the subtelomeric localization of *FOXG_15616* and *FOXG_15617* in Fol4287 **(B)** Schematic representation of chromosomal localization of the homologs genes in *M. oryzae*.

Interestingly, an analysis of the adjacent subtelomeric sequence in *M. oryzae* revealed the presence of a *gypsy*-like LTR retrotransposon that differs from the *FoRS* retrotransposon of *Fol4287* (*copia* family) in the position of the integrase domain relative to the ribonuclease-H domain (data not shown). In summary, these findings reveal a striking structural conservation of the chromosome ends of the two fungal pathogens and suggest that the presence of this conserved region could have a biological relevance for chromosome maintenance and stability.

3. Discussion

3.1. Fol4287 telomeres are made up of the highly conserved repeat sequence (TTAGGG)n

Telomeres are specialized structures located at the ends of chromosomes that are essential for maintaining chromosome integrity and genome stability (O'Sullivan and Karlseder, 2010). Telomeric DNA consists of tandem arrays of 5- to 8-bp direct repeats that are highly conserved among organisms from vertebrates to fungi (McEachern *et al.,* 2000). The isolation and analysis of telomeric DNA from numerous filamentous fungi, such as *Neurospora crassa* (Schechtman, 1987), *Magnaporthe grisea* (Farman and Leong, 1995), and *Fusarium oxysporum* f.sp. *lycopersici* (Powell and Kistler, 1990) among others, has revealed that all have the same TTAGGG repeat.

When we searched this canonical telomere repeat sequence $(TTAGGG)_{x5}$ against the Fol4287 genome database, the number of hits obtained was much lower than the actual number of chromosome ends, with identities found exclusively on 4 of the 15 chromosomes. Interestingly, two of these are on contigs apparently located in an internal region of chromosomes 3 and 6, possibly reflecting an ancestral chromosomal fusion event. Indeed, comparative genome analysis revealed that the low number of only four chromosomes in *F. graminearum* are the result of multiple chromosome fusion events (Cuomo *et al.,* 2007; Ma *et al.,* 2010).

Due to sequence-related problems caused by the high number of tandem repeats of this hexamer, most of the chromosome ends of Fol4287 are not sequenced. In most organisms, the sequencing of highly repetitive regions of the genome represents a major challenge. Recently, the use of long read-sequencing technologies like Oxford Nanopore has allowed to explore the content of these repeated regions by obtaining the complete sequence of chromosomes from telomere to telomere in diverse organisms ranging from fungi (Sonnenberg, 2020) to humans (Nurk *et al.,* 2022).

Despite the unsuccessful *in silico* identification of all Fol4287 telomeres, molecular analyses by CHEF electrophoresis of entire chromosomes and Southern blot using a telomeric probe containing several copies of the hexamer confirmed the presence of this region in all chromosomes. Previous reports suggested that although the telomeres are highly conserved between organisms, there is significant diversity in their length (Cohn, 2005). Based on our analysis, we estimate that the telomeres in Fol4287 have a total length of 1-1.5 Kb, which is in line with the size 0.9 Kb and 1.7 Kb telomeres previously described in *G. intraradices* and *G. geosporum*, respectively (Hijri *et al.,* 2007).

3.2. Fol4287 carries a highly conserved subtelomeric region on all chromosomes

In many organisms, telomeres are flanked by subtelomeric sequences that are conserved at many, sometimes all chromosome ends (Louis, 2014). These sequences in the subtelomeric region of chromosomes typically exhibit a domain structure, with proximal segments containing gene families that are duplicated at multiple chromosome ends, and more distal segments exhibiting short tandem repeats (Pryde *et al.,* 1997).

In *Fol4287* we detected the presence of a proximal subtelomeric region that meets these characteristics. Southern blot results using specific restriction enzymes revealed the presence of a single 10 Kb hybridizing band with the telomeric probe rather than a maximum of 30 bands corresponding to each of the ends of the 15 chromosomes. This finding demonstrates that this subtelomeric region is structurally conserved across all the chromosomes of *Fol4287*. This result was subsequently confirmed by Southern blot analysis at the gDNA and chromosome level, using additional probes located in this conserved subtelomeric region.

Further *in silico* analysis suggested that this highly conserved subtelomeric region also contains two putative open reading frames (*FOXG_15616* and *FOXG_15617*). Similar to the *BLAST* search for the telomeric repeat region, this search generated very few matches in the genome sequence and these were also located on accessory chromosomes and unpositioned contigs. However, karyotype analysis by CHEF and Southern blot with a probe located in the ORF of the *FOXG_15617* gene revealed that this gene is present on all chromosome ends. Although we did not perform karyotype and Southern blot analysis for the other subtelomeric gene *FOXG_15616* gene the number of copies estimated by qPCR was lower than expected (23 versus 30 expected copies), which could indicate that the *FOXG_15616* gene is not present at all chromosome ends. In contrast, for the *FOXG_15617* gene, a higher number of copies than expected (45 versus 30 expected) was estimated by qPCR, indicating that this gene may also be located in other genomic regions in addition to the subtelomeres. A third qPCR analysis with a primer pair for the NextTel region located between the telomere and the *FOXG_15617* gene, gave the lowest number of estimated copies (19 versus 30 expected). We speculate that this region may not be present at all chromosome ends, thus generating slightly shorter subtelomeric versions as suggested by the results of Southern blot analysis (see Figure 27).

3.3. The retrotransposable element FoRS triggers variability in the contiguous subtelomeric region

Our molecular analyses revealed that outside of the region delimited by the restriction site of the enzyme *Pst*I, the structural conservation of the subtelomeres was not maintained. This could be due to the presence of a retrotransposon-like element named FoRS which displayed a high degree of polymorphism reflected by the appearance of multiple hybridizing bands, suggesting that this element resides in different genomic locations. This hypothesis was confirmed by *in silico* analysis, which revealed a high copy number of the FoRS retrotransposon both at the ends and at internal chromosome regions, with a higher representation on accessory chromosomes (Ma *et al.,* 2010; Yang *et al.,* 2020). We therefore hypothesized that the FoRS retrotransposon was also present in a higher number of copies than that of chromosome ends, similar to *FOXG_15616* and *FOXG_15617*. Indeed, qPCR analysis estimated a number of 37 copies, which is close to the 45 full-length copies identified by *in silico* analysis.

An *in silico* search with the FoRS retrotransposon across the *F. oxysporum* species complex detected hits in numerous *formae speciales,* including f.sp. *raphani*, f.sp. *conglutinans* or f.sp. *cubense*, among other, with identity values higher than 97%, and a sequence coverage of 100%. The low level of polymorphism between isolates with different host specificity suggests that the presence of FoRS is either due to a recent event or that it is subject to selective pressure. Within the *Fusarium* genus, the FoRS element was also identified in species such as *F. poae* and *F. nygamai* with a coverage and identity higher than 90%. However, no hits were found in other *F. graminearum* or *F. verticillioides,* indicating a diversification during the process of pathogenic specialization. It may also be due to the presence of fewer accessory regions where TEs are enriched.

The hits obtained from *in silico* searches indicated homology of the *FoRS* retrotransposase with the Tnt1 element, which was first characterized in *Nicotiana tabacum* (Grandbastien *et al.,* 1989). The Tnt1 superfamily comprises *copia*-like retrotransposons from *Nicotiana* (Tnt1 and Tto1) and *Lycopersicon* (Retrolyc1 and Tlc1) including *Lycopersicon esculentum*, the main host of *Fol4287* (Manetti *et al.,* 2007). A detailed analysis of the *FoRS* retrotransposon sequence identified in our strain confirmed that it has the typical domains of this family, although we could not identify the 3'-LTR region (Alzohairy *et al.,* 2014).

Outside of the *Fusarium* genus, homologs of this element were identified in fungal species such as *Metarhizium majus*, *Ustilago trichophora* and *Globisporangium splendens*, as well as in bacteria such as *Chitinophagia bacterium*. In all cases, the identity was below 35%, with

the highest degree of conservation in the retrotransposase domain. Although most studies have reported the presence of this class of retrotransposons in plants, we found that this domain is widely distributed in prokaryotes and eukaryotes. Similar findings were reported for Hop, the first active transposon of the MULE (Mutator-like element) family identified in the genome of *F. oxysporum* and that was found outside of plants, which shared the transposase domain with other filamentous fungi as well as bacteria (Chalvet *et al.,* 2003).

3.4. Conservation of chromosome end structure between *F. oxysporum* and *M. oryzae*

Blastp analysis with the deduced amino acid sequences of genes *FOXG_15616* and *FOXG_15617* identified homologs in the genome of the rice blast fungus *M. oryzae*. Among the 7 chromosomes of this specie, identities were only found on chromosomes 1 and 2, possibly due to sequencing gaps at some chromosome ends or the absence of homologs on the other chromosomes. Interestingly, the two homologs found in *M. oryzae* were also located in the subtelomeric regions, demonstrating that the chromosome ends between both fungal species have a similar structure. In addition, the distance of the genes from the chromosome end was 30-70 Kb, slightly higher than *Fol4287*.

Another common characteristic that demonstrates the nature and structure of the subtelomeric regions was the presence of a transposable element in the adjacent sequence, as we identified in *Fol4287*. A detailed analysis of its sequence revealed that it was also an LTR-like retotransposon in which, surprisingly, we were also unable to identify the 3'-LTR region as was the case with *FoRS* retrotransposon. Its structure resembled a *gypsy*-like retrotransposon, which differs from *FoRS* (*copia* family) in the position of the integrase domain with respect to the ribonuclease-H domain.

It was previously reported that the chromosome ends of *M. oryzae* are enriched in transposable elements, that are found at the 14 ends of the seven chromosomes within 40 Kb of the chromosome tip. These elements are of a different nature, including DNA transposons such as Pot2 and Occan, LTR-retrotransposons such as Pyret and MAGGY, and SINE-type elements such as Mg-SINE (Rehmeyer *et al.,* 2006). It has also been reported that non-LTR retrotransposons (MoTeRs - *M. oryzae* Telomeric Retrotransposons) are inserted in the telomeric regions and may constitute a source of genome instability.

3.5. Biological significance of the Fol4287 subtelomeric regions

The presence of a highly conserved region next to the telomere in most *Fol4287* chromosomes suggests a biological significance. Expression analysis of these subtelomeric

genes and of the FoRS retrotransposon revealed that the expression of FoRS and *FOXG_15617* during tomato root infection was 7- and 25-fold higher at 10 days post-inoculation compared to axenic culture. This indicates a potential role of this region during tomato plant infection. However, transformants overexpressing the subtelomeric *FOXG_15617* gene did not show significant differences with the wild type strain during virulence assays on tomato plants.

A possible explanation for the increased transcription of these subtelomeric elements may reside in a change in chromatin status. Gene silencing is a critical mechanism in fungi, as subtelomeric regions are frequent targets of transcriptional repression through the presence of epigenetic markers, such as H3K27me3, associated with heterochromatin formation (Jamieson et al., 2013; Galazka and Freitag, 2014; Schotanus *et al.,* 2015; Möller *et al.,* 2019). The subtelomeric genes *FOXG_15616* and *FOXG_15617* analyzed in this work show barely detectable levels of expression during growth in PDB medium and in other conditions such as temperature stress, different pH or lack of carbon sources (data not shown), suggesting transcriptional silencing of the subtelomeric region in these conditions. However, an increase in expression was observed in response to the host environment. This fact has also been observed in other pathogenic fungi such as *F. graminearum*, *V. dahliae* and *F. oxysporum* where many genes carrying H3K27me3 marks are derepressed *in planta* (Connolly et al., 2013; Wang *et al.,* 2017; Cook *et al.,* 2020; Fokkens *et al.,* 2018). This suggests that pathogenic fungi must redistribute this epigenetic marker to relax transcriptional gene repression and favor the development of the pathogen within the host. We thus speculate that the observed increase in the transcription levels of the subtelomeric elements during plant infection could be associated with optimizing and enhancing the growth and development of the fungus within the tomato host.

It has been proposed that some organisms could use transposable elements to regulate effector gene expression and escape host immunity (Gijzen *et al.,* 2014). The finding that the *FoRS* retrotransposon of *Fol4287* increases its transcription during infection may be indicative of the expression of the adjacent subtelomeric gene and of effectors located in the subtelomeric regions.

Another possible role associated with the telomeric and subtelomeric regions is their involvement in the maintenance of genome stability. Telomeres are the structures that guarantee the integrity of chromosome ends. Alterations in these regions lead to increased instability, as reported in *M. oryzae*, where the insertion of MoTeRs retrotransposons inside the telomeric repeats generates interstitial telomeric regions that lead to break-induced

rearrangements (Starnes *et al.,* 2012; Rahnama *et al.,* 2020). But not only transposable elements are the cause of chromosome instability. There are other types of homologous repeat sequences, including subtelomeric gene families, which can also contribute to genome instability (Rudd Gao *et al.,* 2002; Chen *et al.,* 2018).

As the *Fol4287* subtelomeric region includes two genes of unknown function that are highly represented at the chromosome ends, we speculated that they could play a role in genome stability. although the best strategy to study the function of these genes would be their deletion, this approach is hampered by the high number of copies present in the genome. Therefore, we opted for overexpression of the subtelomeric gene *FOXG_15617*. Furthermore, this gene was also cloned in the yeast *S. cerevisiae* under the control of an inducible promoter to study its possible function.

The results obtained in various genomic instability tests in either of the two organisms were not fully conclusive, since its involvement in genomic instability could not be demonstrated. A study in *Schizosaccharomyces pombe* revealed the importance of repeated homologous sequences (SH) in chromosome homeostasis (Tashiro *et al.,* 2017). The SH region which is the most adjacent to the telomeres contains multiple segments of homologous sequences spanning 50 Kb in length. The fact that this organism has only 3 chromosomes and 6 subtelomeric regions made it possible to eliminate all SH sequences, revealing that although they are dispensable for mitosis and meiosis, their presence is required to avoid deleterious inter-chromosomal end fusion when telomeres are lost, helping to maintain chromosome stability (Tashiro *et al.,* 2017). Based on the results, we could speculate that these conserved genes at the chromosomal ends could contribute to genome stability in *F. oxysporum*.

CHAPTER 3

Dynamics of accessory chromosomes of Fol4287

CHAPTER 3: Dynamics of accessory chromosomes of Fol4287

SUBCHAPTER 3.1: Characterisation of karyotypic changes in *Fol4287*

1. Introduction

To investigate genomic plasticity and adaptation of *Fol4287* to different environmental conditions, experimental evolution was carried out by Dr. Cristina López Díaz using this isolate (from now on called the parental isolate) (López-Díaz, 2019). For this purpose, the wild type strain *Fol4287* was subjected to ten serial passages through the plant host tomato (*Solanum lycopersicum*), minimal (MMA) or rich (YPDA) medium plates (Figure 45). For plate passages, microconidia were spot-inoculated on MMA or YPDA plates. After one week the conidia were harvested from the whole colony, stored at -80°C and an aliquot was used to inoculate a new plate for the next passage. For plant passages, conidia were dip-inoculated on roots of tomato plants. After two weeks, the fungus was re-isolated from the stem and subjected to a brief growth stage in PDB medium to obtain sufficient conidia for storage and for the next plant passage. In each condition, five independent lines were passaged.

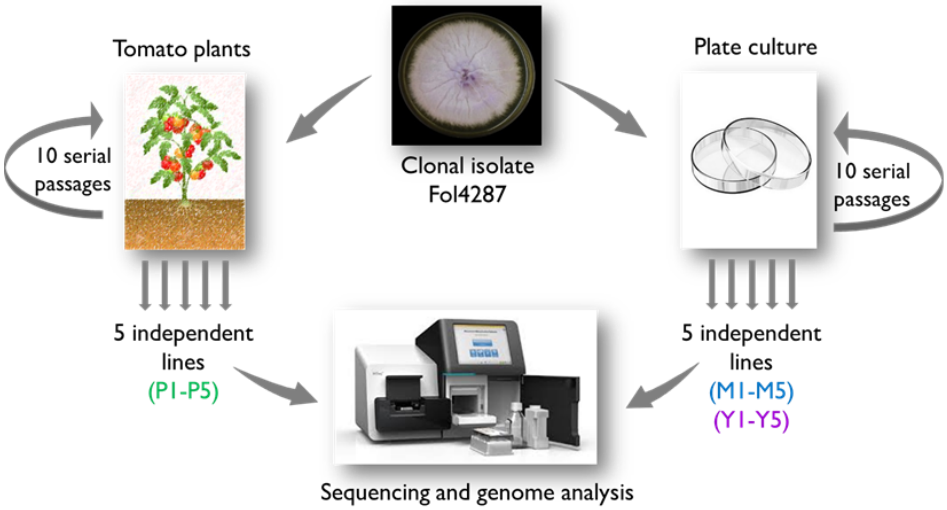

Figure 45. Schematic diagram of the experimental evolution approach with Fol4287 in different environmental conditions. Experiment conducted by Cristina López-Díaz (López-Díaz, 2019). Starting with the clonal isolate Fol4287, ten serial passages through tomato plants (P), YPDA plates (Y) and MMA plates (M) were performed. For plant passages, $5x10^5$ fungal microconidia were dip-inoculated on roots of tomato plants and, after 12-14 days, the fungus was re-isolated from the apical zone of the stem and used to produce conidia for inoculation of the next passage. For plate passages, 10^6 microconidia were spot-inoculated on the center of YPDA or MMA plates and incubated at 28 °C for 7 days. Total microconidia from the colony were harvested and aliquots were used for inoculation of the next passage. In each condition, five independently passaged lines were obtained (1-5). Evolved populations obtained from the 10^{th} passage were analyzed by Illumina Next-Generation Sequencing (NGS) and compared with the genomic sequence of the initial wild type strain (wt). From each passaged population, ten independent monoconidial isolates were obtained for further analysis.

To analyze the genetic variations that might have occurred during serial passaging, whole-genome *Next Generation Sequencing (NGS)* of populations obtained from passage 10 was performed using the Illumina HiSeq 2500 or NextSeq 500 platforms. The genome of the parental isolate used at the start of the passaging experiment was also re-sequenced (Ayhan *et al.,* 2018) and compared with the Fol4287 reference genome sequence originally deposited in the NCBI database (Ma *et al.,* 2010). This revealed copy number divergences between the reference genome and that of the Fol4287 parental isolate which affected some of the accessory regions that were analyzed throughout this work by CHEF analysis with specific probes (Figure 46).

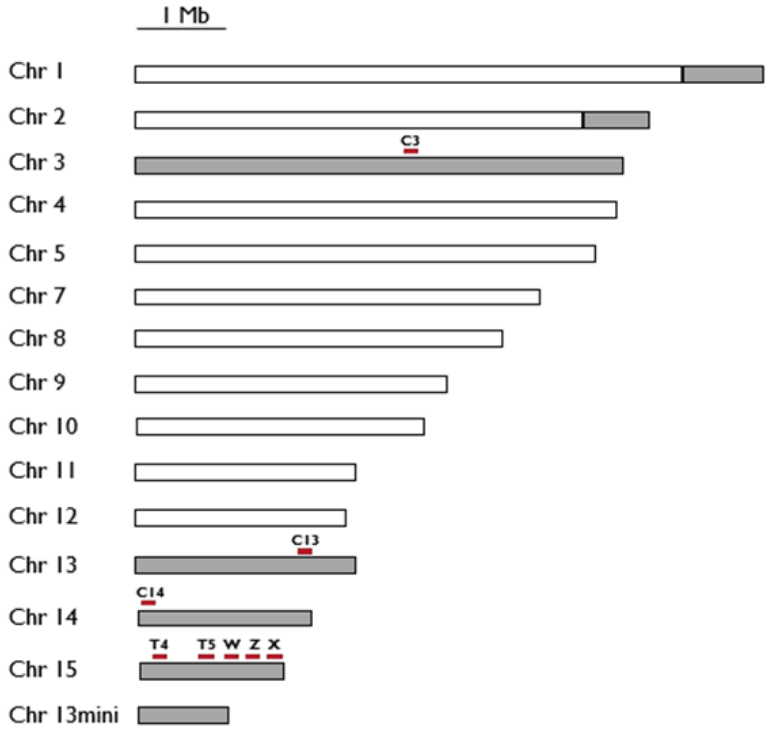

Figure 46. Chromosome map of the Fol4287 isolate. Adaptation of the previous map (Ma *et al.,* 2010) based on the latest improved assembly of the *Fol4287* strain (Ayhan *et al.,* 2018). Core genomic regions are in white while accessory regions are in gray. The putative position of the probes used for Southern analyses of CHEF gels are indicated (red boxes). Note that chromosome 6 is not present in the genome of the Fol4287 parental isolate.

Therefore, the NGS data obtained from the passaged populations were compared directly with the parental isolate. This led to the identification of four types of genetic variants: single nucleotide variations (SNVs), insertions or deletions (INDELs), transposon insertion variations (TIVs) and large-scale copy number variations (CNVs). While the first three types were analyzed previously (López-Díaz, 2019), the detailed analysis of the CNVs as well as their frequencies and underlying mechanisms were investigated in the present study.

2. Results

2.1. Copy number variations detected in experimentally evolved populations of Fol4287 by whole-genome sequencing

Detection of CNVs was performed by Dr. Dilay Hazal Ayhan at University of Massachusetts, Amherst, US, using the whole-genome read depth method (Ayhan, 2021). First, the single-base resolution read depth for the evolved populations and wild type strain was calculated. Then, the median read depth was obtained using a predefined 10 kb-window and normalized first to the median read coverages of the samples and then to wild type to remove potential biases mainly due to GC content and repeated regions. Finally, an algorithm was applied to identify contiguous genomic windows allowing to position the different contigs. The results of this analysis were represented in form of a read depth plot showing to scale the core and accessory chromosomes of the wild type strain and the 15 final populations evolved in the different environmental conditions (Figure 47).

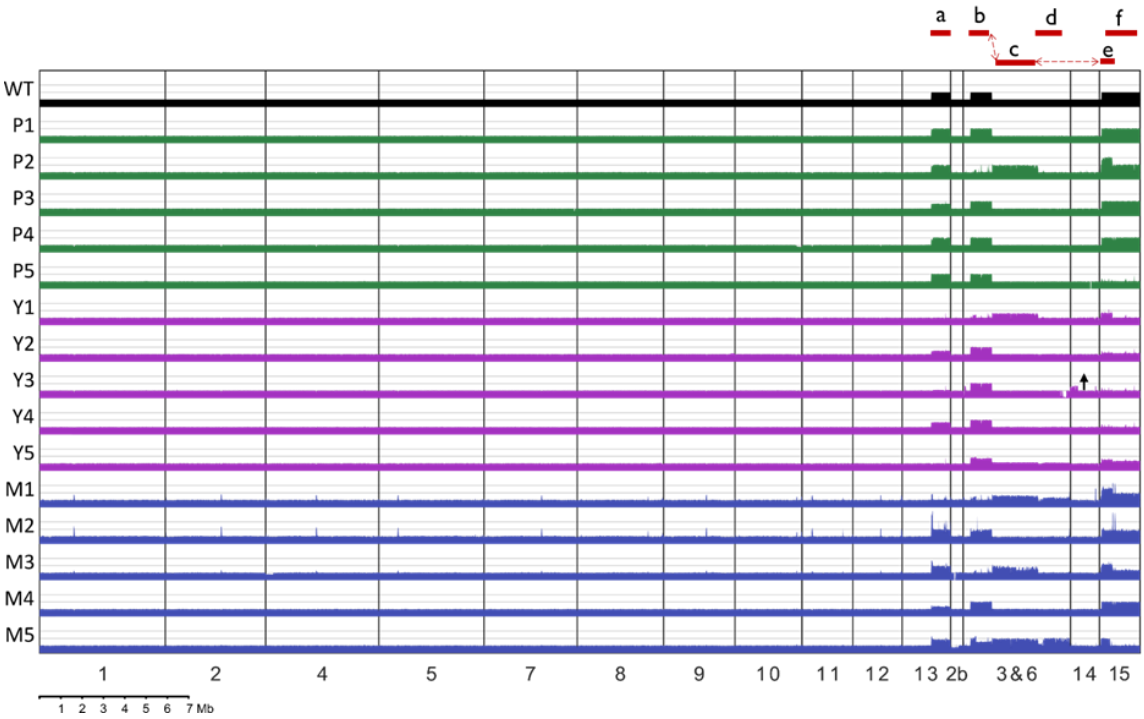

Figure 47. Copy number variations (CNVs) detected in experimentally evolved lines. Core chromosomes and accessory regions are drawn to scale in the reference strain (wt) and in the populations obtained after ten serial passages through tomato plants (P), YPDA (Y) and MMA (M) plates. Median Illumina read depths calculated over 10 kb-window regions were normalized first to the median read coverage of the sample and then, to wt. Duplicated regions are shown as 2x coverage. CNVs present in more than one evolved population are represented by letters and red lines in the upper part of the diagram. The dashed arrows indicate events that appear to be linked (b, c, e). The arrow pointing up represents a partial duplication of Chr14 observed only in the Y3 line (adapted from Ayhan, 2021).

This analysis revealed that large-scale CNVs were exclusively present in accessory regions of the genome. Almost all CNVs were detected in more than one independent lines passaged through different environmental conditions:

a) The right end of chromosome 13 is duplicated in the original wild type strain, detecting the loss of one of the copies in all rich media-passaged populations and the minimal media-passaged M1 and M4 populations with variable loss frequencies.
b) The 1Mb duplicated region located in the 3&6 shared region is deleted in P2, Y1, M1 and M3 evolved populations. This event seems to be linked with "c" and "e" events.
c) Duplication of a 2 Mb region of chromosome 3 in P2, Y1, M1, M3 and M5 evolved populations. This duplication always appears accompanied by two other CNVs ("b" and "e") that seem to be part of the same event.
d) Duplication of an additional 1Mb region of chromosome 3 occurs in M1 and M5 populations.
e) Duplication of a 0.5 Mb region located at the end of chromosome 15 associated with "b" and "c" events in P2, Y1, M1, M3 and M5 populations.
f) A region corresponding to chromosome 15, which is duplicated in the original wild type strain, loses a copy in all rich media-passaged lines and also in P5, M3 and M5 populations.

Besides the recurrent CNVs described above, a CNV involving a partial duplication of chromosome 14 was detected only in the Y3 population.

2.2. Karyotype and Southern blot analysis of the main CNVs detected in passaged populations

To experimentally confirm the CNVs detected by whole-genome sequencing, we carried out Contour-Clamped Homogeneous Electric Field (CHEF) electrophoresis and Southern blot analysis (together with Cristina López Díaz) using monoconidial isolates obtained from passage 10 populations.

2.2.1 The duplicated region of chromosome 13 lost in passaged populations corresponds to an independent mini-chromosome

Coverage analysis of Illumina sequencing reads indicated the presence of a duplicated region at the right end of chromosome 13 in the parental isolate (see Figure 47). To determine the exact location of this second copy in the genome, the chromosomes of the parental and three monoconidial isolates from YPDA-passaged populations were separated by CHEF electrophoresis. Subsequent Southern blot analysis with a probe located in the

duplicated region of chromosome 13 revealed the presence of a small independent chromosome in the parental isolate, which had not been detected previously and which we named chromosome 13mini (Figure 48). Importantly, 13mini had been lost in the three passaged isolated showing the CNV. By contrast, in none of these isolates loss of the full size chromosome 13 was detected.

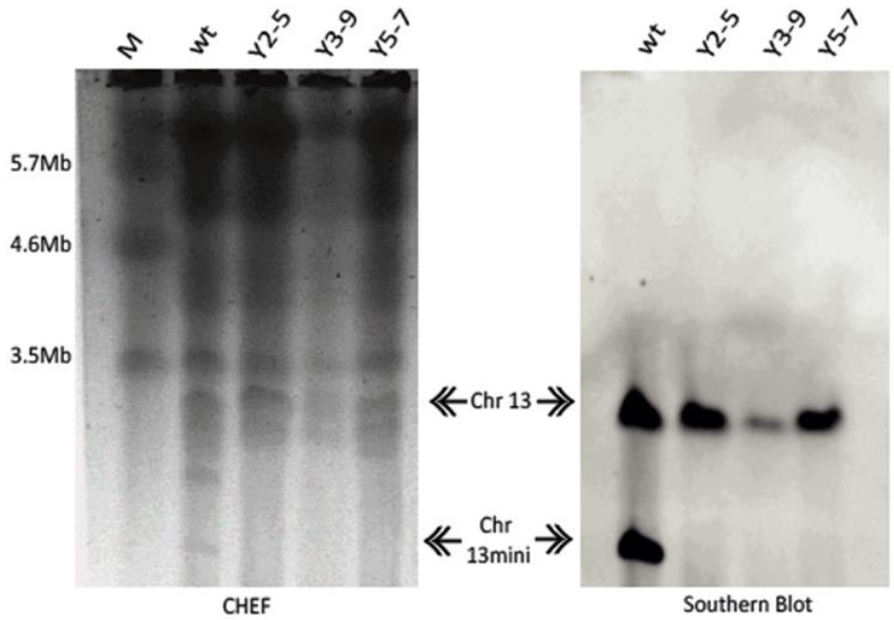

Figure 48. Southern analysis of CHEF gel reveals the presence of an independent mini-chromosome containing a duplicated region of chromosome 13, that is spontaneously lost in passaged lines. Separation of chromosome bands by CHEF electrophoresis and visualization by ethidium bromide staining (left) and Southern blot analysis (right) of the parental strain and three passaged isolates. The left lane (M) shows the chromosome pattern of *S. pombe* used as molecular size marker. Hybridization with probe C13 located in the duplicated region of chromosome 13 (see Fig. 46) confirms the presence of an additional partial copy in form of a mini-chromosome (named Chr 13mini) that undergoes spontaneous loss in the passaged isolates.

To test whether chromosome 13mini is an exact duplication of the right end of chromosome 13 end or whether it contains additional sequences from other chromosomes, the 1Mb band corresponding to 13mini was excised from a CHEF gel (Figure 49).

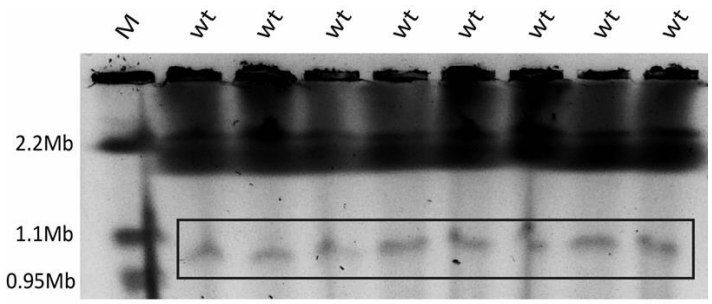

Figure 49. Recovery of DNA from chromosome 13mini for sequencing by cutting the band from a CHEF gel. Blocks of protoplasts of the Fol4287 wild type strain were subjected to CHEF electrophoresis following the protocol for separation of small chromosomes used for *S. cerevisiae*. The bands corresponding to Chr 13mini were cut from the gel, the DNA was re-isolated and sent for Illumina sequencing. The left lane (M) shows part of the chromosome pattern of *S. cerevisiae* used as molecular size marker.

Illumina NovaSeq 6000 sequencing of the DNA isolated from the excised gel pieces produced a total of 23,446,092 paired end reads with a mean length of 150 bp, which were mapped to the most recently Fol4287 reference genome by Dr. Dilay Hazal Ayhan, obtaining a median coverage of 10.5X. This revealed that chromosome 13mini is highly enriched for sequences homologous to the right end of chromosome 13 (named Chr13p) as well as to the unmapped contigs U2 and U3 (Figure 50A).

The regions with high read mapping to the reference assembly were artificially joined, yielding the putative structure of the new chromosome 13mini. For further confirmation, the PacBio reads from the whole-genome sequencing of the parental isolate were mapped to this artificially constructed chromosome. The new assembly includes 13 contigs, 11 of which cover the expected size of around 1 Mb. Among these, 6 align with Chr13p, 4 with U2 and U3, while 2 correspond to subtelomeric sequences and the remaining contig has a rRNA-like sequence (Figure 50B).

While the regions linking the Chr13p region with the U2 and the U3 contigs have not been identified yet, the finding that chromosome 13mini is made up of the right end of chromosome 13 plus U2 and U3, and that 13mini is an exact duplication of the right end of chromosome 13, strongly suggests that contigs U2 and U3 are located contiguous on the right end of chromosome 13. This establishes a new proposed structure of chromosome 13, increasing its size from 1.8 Mb to 2.3 Mb, which is in agreement with karyotype analysis by CHEF electrophoresis (Figure 50C).

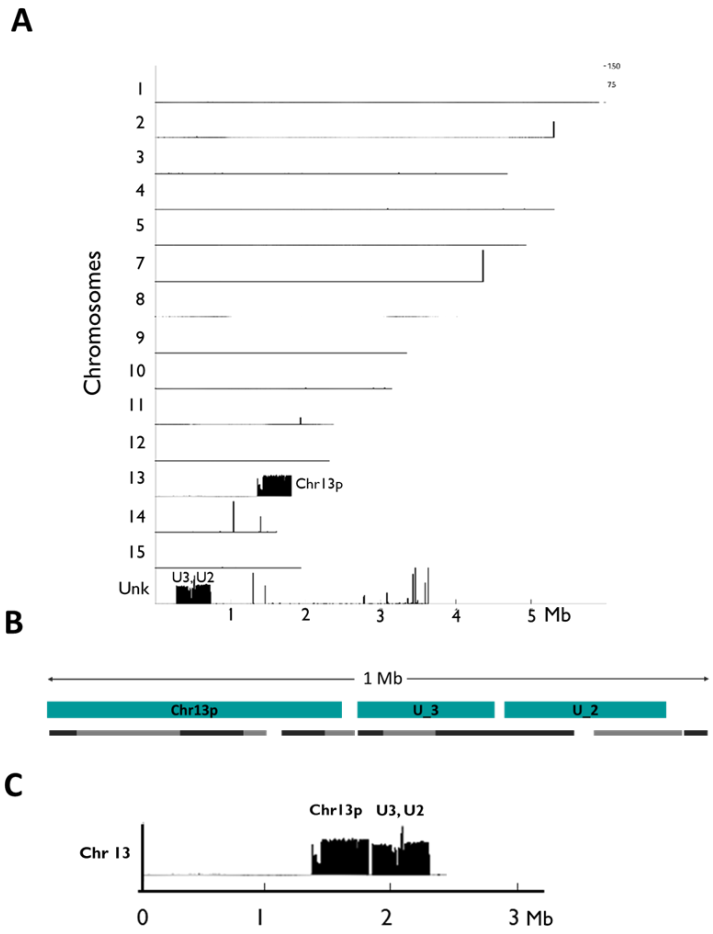

Figure 50. Single chromosome DNA sequencing confirms that Chr 13mini is a partial duplication of Chr13. (A) Normalized coverage of Illumina sequencing reads from chromosome 13mini recovered from the CHEF gel (see Fig. 49) mapped to the Fol4287 genome assembly. Chr13mini is highly enriched for sequences of the small arm of Chr13 (Chr13p) and unmapped contigs U2 and U3. Enrichment is also observed for the rRNA sequence on Chr2, the subtelomeric sequence of Chr7, the retrotransposon Skippy on Chr11 and subtelomeric sequence and Skippy on Chr14. **(B)** Representation of the contigs arrangements for the Chr 13mini assembly. Green boxes are the scaffolds from the Fol4287 genome assembly (Ma *et al.,* 2010) and the alternating dark and grey lines show the contigs of the assembled enriched PacBio reads (Ayhan *et al.,* 2018). No connection was detected between the unmapped contigs and Chr13p. **(C)** Genomic reconstitution of the end of Chr 13. The unmapped contigs U2 and U3 were artificially located contiguous to Chr13p, thus showing the putative composition of Chr 13 (modified from Ayhan, 2021).

2.2.2 Partial duplication of the pathogenicity chromosome 14 involves additional chromosomal rearrangements

Illumina sequencing analysis of the passaged Y3 population revealed an increase in read depth indicative of a partial duplication of chromosome 14 (see Figure 47). To determine if this region corresponds to a tandem partial duplication of chromosome 14 or whether it is attached to another chromosome, we performed CHEF and Southern blot analyses of the parental and a monoconidial isolate from the Y3 population. This revealed the absence of chromosome 14 and the presence of two new bands in the passaged Y3 isolate, observed both in the CHEF gel and the Southern blot using a specific probe for this

region, suggesting that the partial duplication involves a rearrangement of chromosome 14 leading to an increase in size. The second hybridizing band observed in the Y3 isolate suggests a more complex chromosomal rearrangement. Based on the pattern of chromosomal bands of the parental and the Y3 isolates in the CHEF gel, we hypothesize that chromosomes 11 and 12 may also be involved in this rearrangement (Figure 51).

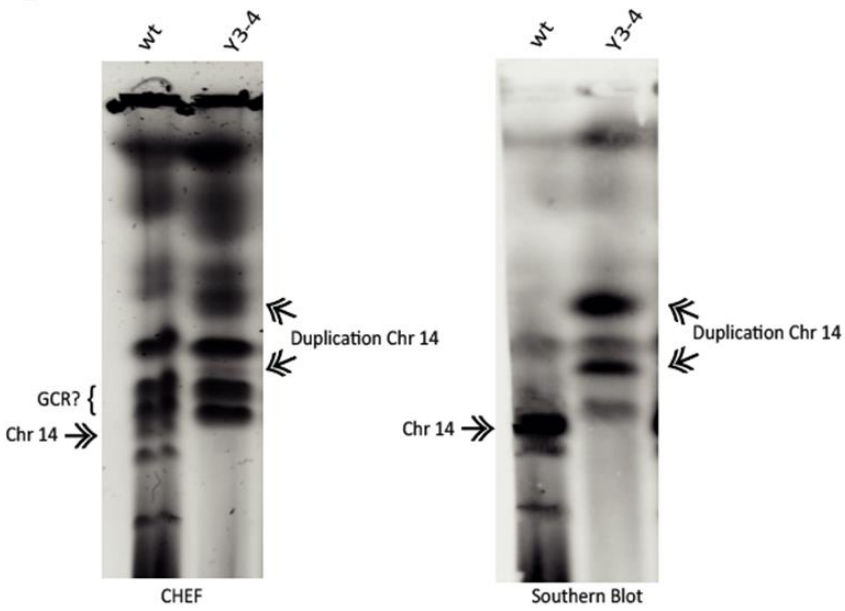

Figure 51. Southern analysis of CHEF gel reveals the duplication of a region of chromosome 14. CHEF (left) and Southern blot analysis (right) with a probe specific for Chr14 (C14; see Fig. 46) confirm that the duplication of this region leads to a loss of the band corresponding to Chr14 and the appearance of two new bands in the passaged isolate. These bands are larger than expected, suggesting a spontaneous rearrangement involving additional chromosomes (indicated as GCR).

2.2.3 The duplicated region shared between chromosome 15 and the accessory part of chromosome 1 is lost in some passaged lines

Illumina whole-genome sequencing revealed a high degree of homology between the accessory region located at the right end of chromosome 1 and a 0.7 Mb region of chromosome 15, annotated as region 1&15 (see Figures 46 and 47). CHEF and Southern blot analysis of the parental and four monoconidial isolates from YPDA-passaged populations with specific probes T5 and W located in the shared 1&15 region (see Figure 46) confirmed that the accessory region of chromosome 1 shares homology with chromosome 15 (Figure 52). Additionally, lack of a hybridizing band in some of the YPDA-passaged isolates at the position of chromosome 15 suggested that this small chromosome had been lost in these isolates (Figure 52A).

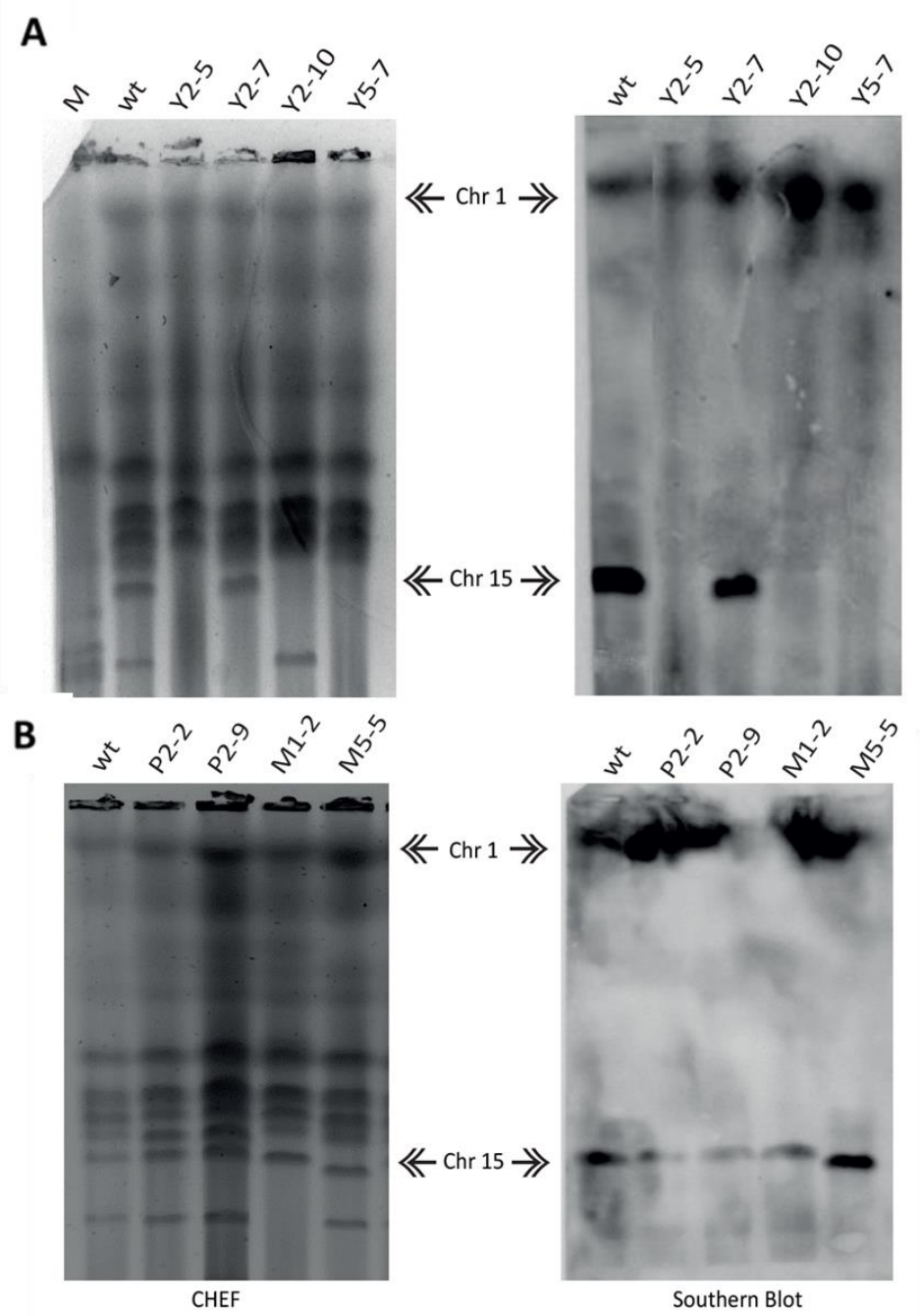

Figure 52. Southern analysis of CHEF gels with two different probes confirms the presence of a shared region on chromosomes 1 and 15. Separation of chromosome bands by CHEF electrophoresis (left) and Southern blot analysis (right) of the parental and the indicated passaged isolates. The left lane (M) shows the chromosome pattern of *S. pombe* and *S. cerevisiae* used as molecular size markers. Hybridization with probes T5 **(A)** and W **(B)** (see Fig. 46) shows a signal on both chromosome 1 and 15 confirming the presence of a region shared between Chr15 and Chr1. Note that some of the passaged isolates in (A) have lost Chr15. Note also the reduced size of Chr15 in passaged line M5 in (B), suggesting a partial deletion. CHEF experiment (B) performed by Cristina López-Díaz.

CHEF and Southern blot analysis with the probe "Z", located in the 1&15 region validated the previous results and showed that the area where this probe is located is also conserved between both chromosomes (Figure 53).

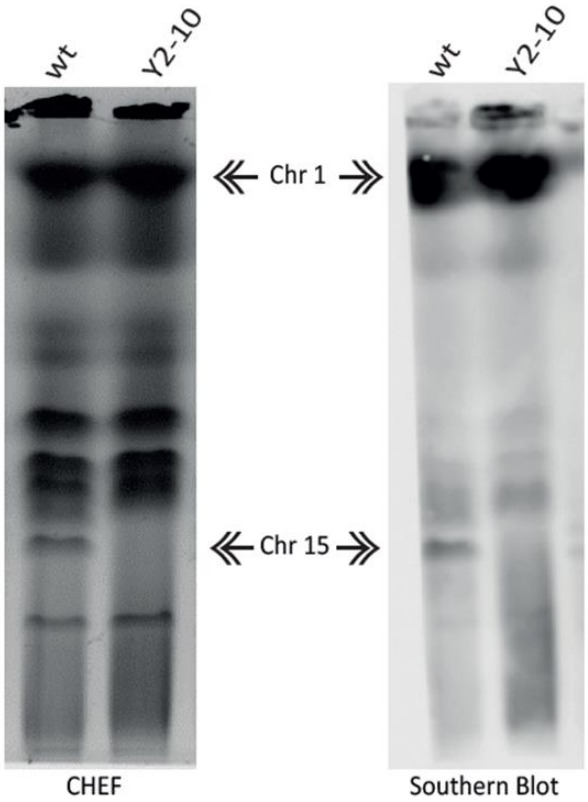

Figure 53. Southern analysis of CHEF gel with yet another probe reaffirms the existence of a region shared between chromosomes 1 and 15. CHEF (left) and Southern blot analysis (right) with a different probe (Z) located in 1&15 region (see Fig. 46) shows a signal on both chromosome 1 and 15. Note that the passaged isolate has lost Chr15.

CHEF and Southern blot analysis with the probe from region "X" further confirmed the existence of a shared 1&15 region and revealed that some of the passaged isolates had lost the signal corresponding to the region present on chromosome 1 (Figure 54). Importantly, simultaneous loss of both copies (on chr 15 and 1) was never detected, suggesting the possible presence of essential genes on this shared DNA region. In the case of the MMA-passaged line M5, a slightly reduced size of chromosome 15 was observed indicating a putative deletion in this chromosome in these isolates (Figures 52B and 54).

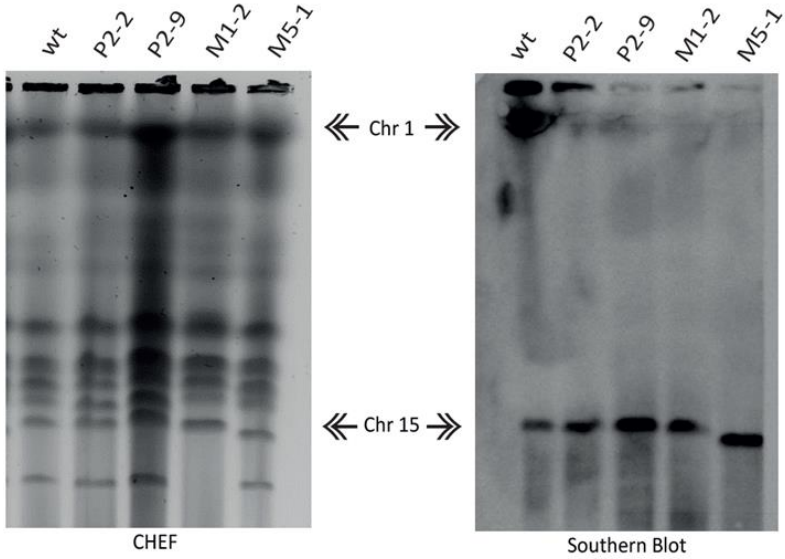

Figure 54. Southern analysis of CHEF gel with a different probe reveals spontaneous loss of a region on chromosome 1 sharing homology with chromosome 15. Separation of chromosome bands by CHEF electrophoresis (left) and Southern blot analysis (right) of the parental and the indicated passaged isolates. Hybridization with a different probe (X) located in 1&15 region (see Fig. 46) confirms the existence of a shared region. Note that the passaged isolates lack the region of Chr1 sharing homology with Chr 15. Note also the reduced size of Chr15 in passaged line M5 suggesting a partial deletion. CHEF experiment performed by Cristina López-Díaz.

While Southern blot analysis of the same passaged lines with the probes "X" and "W" confirmed that this sequence is duplicated on chromosomes 1 and 15 region, unexpectedly the region corresponding to probe "W" was apparently not lost in these passaged isolates. although the hybridization bands on chromosome 1 were somewhat diffuse, possibly due to previous stripping. Taken together, these results suggest that not the entire shared 1&15 region is lost in this CNV event.

2.2.4 Accessory chromosomes 3 and 15 also share a region of homology

Unexpectedly, CHEF electrophoresis and Southern blot analysis using yet another probe (T4) supposedly located on the 1&15 region, revealed hybridization bands at the position of chromosomes 15 and 3 (Figure 55). This suggests that, in addition to the region homologous to chromosome 1, chromosome 15 also contains an additional region shared with chromosome 3. Analysis with the T4 probe further confirmed the loss of chromosome 15 in the passaged isolate Y2.

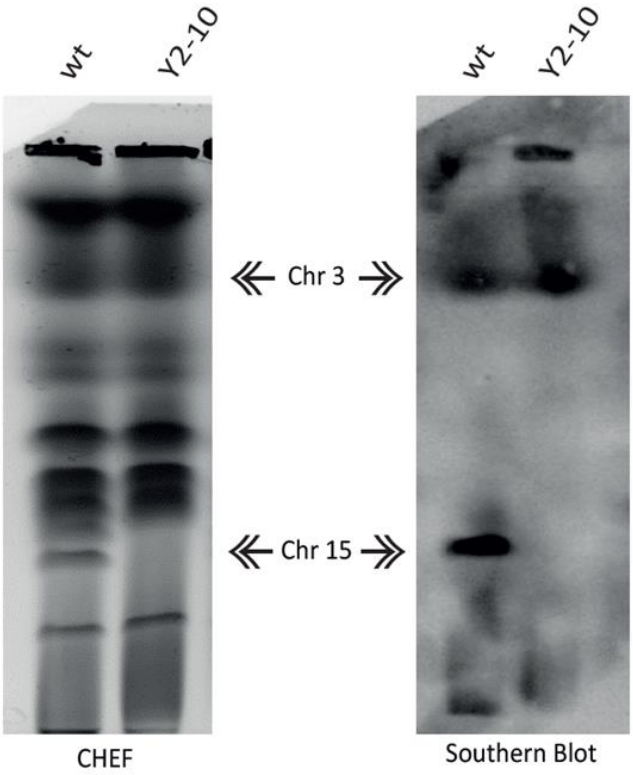

Figure 55. Southern analysis of CHEF gel demonstrates that accessory chromosome 3 shares homology with a region of chromosome 15. CHEF (left) and Southern blot analysis (right) with probe T4, supposedly specific for the 1&15 region (see Fig. 46) demonstrates that part of Chr15 shares homology with Chr3. Note that the band corresponding to Chr15 is lacking in the passaged isolate, confirming spontaneous loss of this chromosome.

2.2.5 A new accessory chromosome 6 is generated by partial duplication of chromosome 3

Karyotype analysis of passaged lines P2 and M1, which carry duplication event "c" (see Figure 47), by CHEF and Southern blot with probe "C3" specific for the 3&6 region (see Figure 46), revealed that they carry a new accessory chromosome called 6 which is absent from the parental isolate and was likely generated through partial duplication of chromosome 3 (Figure 56). By contrast, in line M5 which carries both duplication events "c" and "d" (see Figure 47), a much larger new chromosome similar in size to chromosome 1 was detected which shares homology with chromosome 3 (Figure 56).

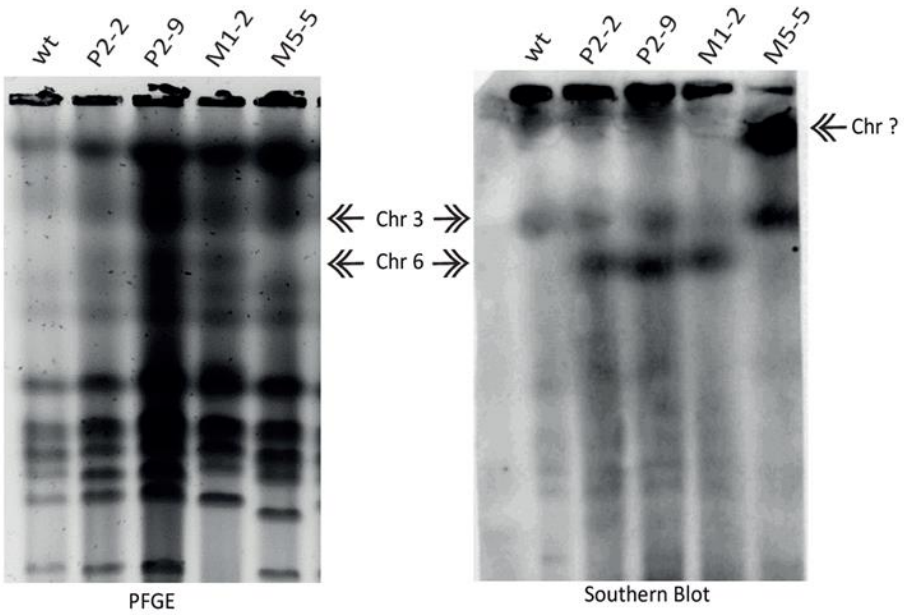

Figure 56. Southern analysis of CHEF gel confirms the existence of a shared region between chromosomes 3 and 6. CHEF (left) and Southern blot analysis (right) with probe C3 located in the 3&6 region (see Fig. 46) reveals the presence of a newly generated chromosome (named Chr6), resulting from a partial duplication of Chr3, in monoconidial isolates derived from passaged lines P2 and M1. Note the presence of a distinct duplication of Chr3 in the M5 line resulting in a new chromosome/region with a larger size indicated by a question mark (see also Fig. 47). CHEF experiment performed by Cristina López-Díaz.

Interestingly, the duplication events "d" was only detected together with duplication "c", but never independently (Figures 47 and 56). Although further studies are needed, this finding suggests that either both duplications occurred simultaneously in these passaged lines or that duplication "c" resulting in generation of chromosome 6 represents an intermediate structure that can then undergo additional rearrangements to generate an even larger new chromosome.

2.2.6 Summary of the main CNVs detected in passaged lines of Fol4287

To obtain an overview of the main CNVs observed in the passaged populations of *Fol4287*, a single CHEF gel was run with different passaged isolates (Figure 57). In this Figure, the chromosomes involved in CNVs are indicated by arrows of different colors. All passaged lines shown here, except M5, have lost the small chromosome 13mini (CNV event "a", see Figure 47). Moreover, all Y lines show loss of chromosome 15 (CNV event "f"), whereas M5 carries a partial deletion on this chromosome. Line Y1 has CNV event "c" involving the generation of chromosome 6 via duplication of chromosome 3, while monoconidial isolates M5-3 and M5-5 from line M5 carry both CNV events "c" and "d", resulting in generation of a much larger new chromosome running at a similar level to chromosome 1. Finally, line Y3

carries a partial duplication of chromosome 14 involving additional chromosome rearrangements (Figure 57).

Interestingly, we detected the presence of an apparently new mini-chromosome in two monoconidial isolates derived from line Y1. According to the read depth map, no CNV events were observed in line Y1 that could be linked to the formation of this new mini-chromosome. Due to its size, we hypothesized that it could correspond to a partial deletion in chromosome 15 similar to, but larger than the deletion observed in line M5. However, Southern blot analysis with probe "T5" located on chromosome 15 failed to produce a hybridization signal suggesting that this new mini-chromosome must have a different origin (data not shown).

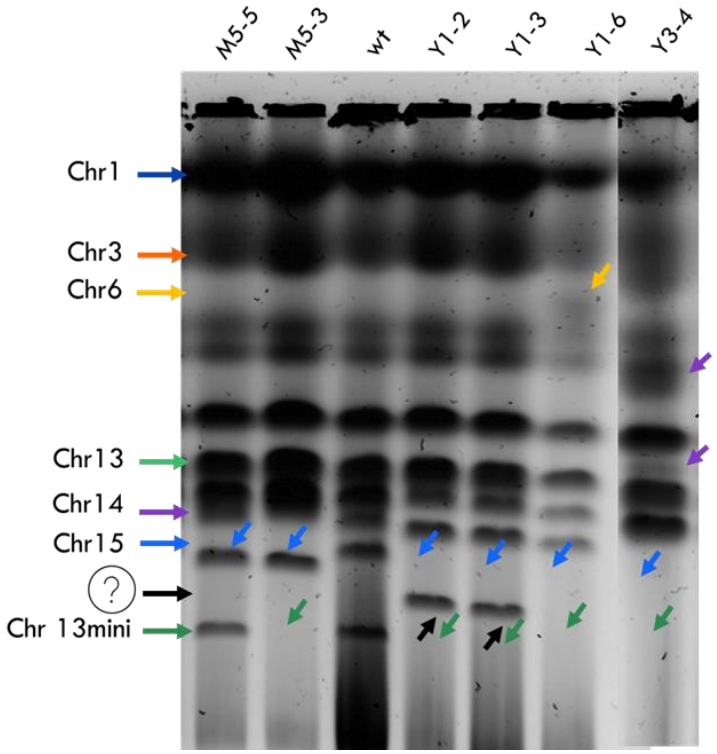

Figure 57. CHEF gel analysis summarizing the main chromosomal rearrangements detected in passaged lines of Fol4287. Chromosomes of the parental strain and of monoconidial isolates derived from the indicated passaged lines were resolved by CHEF. Chromosomes involved in rearrangements are indicated by arrows of different colors (see also Fig. 58). The position of a new mini-chromosome of unknown identity detected in some monoconidial isolates derived from passaged line Y1 (black arrows) is indicated by a question mark. Note that the last lane has been pasted from a separate gel.

2.3. Proposed model of the structure and dynamics of Fol4287 accessory chromosomes

Based on the previously published chromosome map of *Fol4287* (Ma *et al.*, 2010), and considering the new results obtained through sequencing and karyotype analyses in this study, we propose a working model of the structure and dynamics of the accessory chromosomes in *Fol4287* showing the main CNVs and chromosomal rearrangements detected in passaged populations (Figure 58).

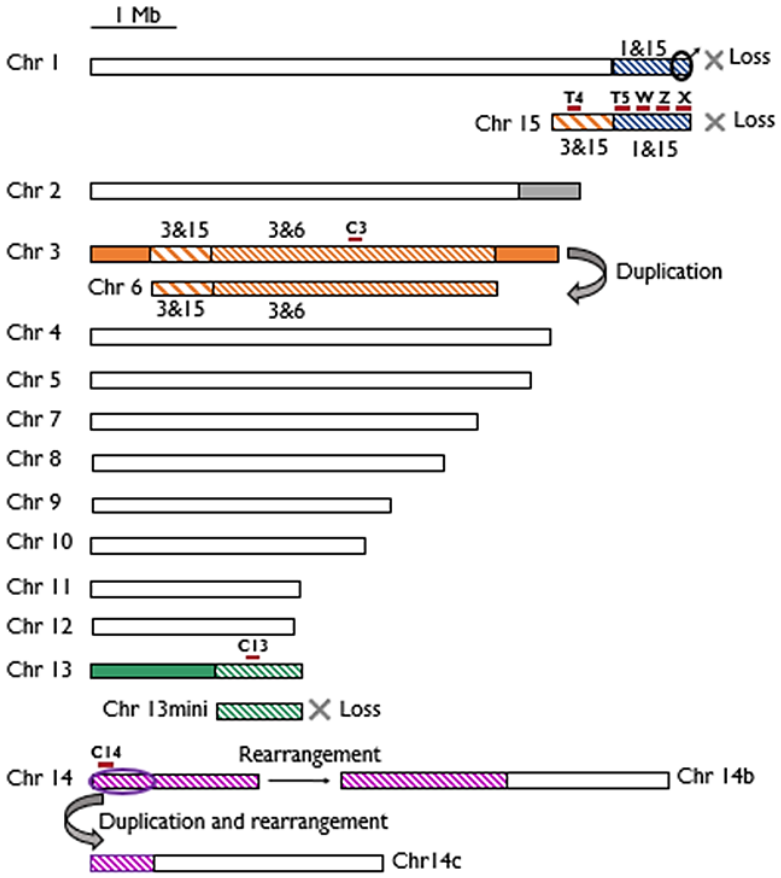

Figure 58. Proposed working hypothesis of the main chromosomal rearrangements observed in experimentally evolved lines of Fol4287. Adaptation of the chromosome map of the parental Fol4287 isolate (see Fig. 46) based on the karyotype/Southern analysis results obtained in the present study. Core genomic regions are in white while accessory regions are in different colors. Duplicated regions are hatched. The putative position of the probes used for Southern analyses of CHEF gels is indicated (red boxes). Spontaneous loss of chromosomal regions or entire chromosomes is indicated by a cross while regions undergoing duplication are indicated by an arrow. In the case of the duplicated region of Chr15 located on Chr1 (named 1&15), only the circled region appears to be lost. Note that the partial duplication of a region of Chr14 involves subsequent fusion to an unknown chromosome.

According to current evidence, part of chromosome 15 (named 1&15) is shared with the accessory region of chromosome 1. Either of these two copies may be spontaneously lost during serial passaging (indicated by a cross), although only part of the shared region

located on chromosome 1 appears to be lost (see Figure 54). Previously unrecognized, we found here that chromosome 15 also contains a region of homology with chromosome 3 (called 3&15). The partial duplication process of chromosome 3 to generate chromosome 6 (CNV event "c") is also reflected in this map. The associated event "d" involving the formation of a larger chromosome is not included in this schematic representation due to the currently unknown origin of this rearrangement.

The map also includes the new discovery of an independent mini-chromosome named 13mini, corresponding to a partial duplication of the right end of chromosome 13, and which can be spontaneously lost during serial passaging. Finally, the CNV affecting chromosome 14 was also included in this hypothetical model, showing that the region of chromosome 14 that is duplicated during experimental evolution appears to fuse to an unknown chromosome generating a new structure (Chr 14c), while it also involves rearrangement of chromosome 14 itself (Chr 14b), which may also imply its fusion to another chromosomal region as indicated by the increase in size detected in karyotype analysis.

SUBCHAPTER 3.2: Development of methodologies for quantitative determination of chromosome loss frequency in Fol4287

1. Introduction

Quantitative estimation of chromosome losses cannot be performed using karyotype analysis by CHEF and Southern blot techniques. The fluorescence signal of the label can be measured as a function of its concentration, so quantitative measurements can be easily performed. Flow cytometry and fluorescence-activated cell sorting (FACS) measure the presence and/or fluorescence particles. With this later technique, many hundreds of particles or more can be determined simultaneously, which considerable increases the sample throughput. The use of the FACS technique to quantify chromosome losses had already been previously reported in other fungi such as *Colletotrichum higginsianum* (Plaumann *et al.,* 2018) and *F. oxysporum f.sp. lycopersici* (Vlaardingerbroek *et al.,* 2016). To estimate the accessory regions loss frequency in Fol4287, we used the FACS technique during a stay in the group of Prof. Martijn Rep at the University of Amsterdam, Netherlands, where this technique had previously been fine-tuned (Vlaardingerbroek *et al.,* 2016). The main issue is the achievement of proper fluorescent signals, which can be distinguishable from the background signal. Thus, the use of adequate promoters that enhance the expression of the gene, so that the fungal pathogen can produce the fluorescent protein is necessary. Other methods were also developed to quantify chromosome loss, such as qPCR, which makes it possible to determine the copy number of a certain genomic region, although it has the disadvantage that it does not allow a large number of individuals to be analysed simultaneously. A third technique previously developed in our group consisting of labelling one of the chromosome duplicate region with a restriction fragment length polymorphism (RFLP) marker, was used to assess the dynamics of chromosome loss.

2. Results

2.1. Use of Fluorescence-Activated Cell Sorting (FACS) to measure chromosome loss frequency

2.1.1 Differential fluorescent labeling of the duplicated regions of chromosome 13

We reasoned that the availability of a strain carrying the GFP gene in one and the ChFP gene in the other repeated region of chromosome 13 would allow us to use FACS to readly detect conidia that have lost either green or red fluorescence to estimate chromosome loss frequency. To create such a strain, and to avoid homologous insertion of both constructs in the same repeated chromosome region, a physical gap was created between the two insertions into the Δ1 and Δ2 regions of chromosome 13. To this aim, the

region deleted in one construct (Δ1) was used as a flank (Flank 3) for the other construct and *vice versa* (Figure 59A). Previously obtained fluorescent strains (Ruiz-Roldán *et al.,* 2010) carrying histone H1 or H2 fused to the fluorescent proteins ChFP of GFP, respectively, were used to amplify these regions which were subsequently fused to the specific flanks of the Δ1 and Δ2 regions (Figure 59B). Both constructs were used together to co-transform protoplasts of the wild type strain *Fol4287* with the neomycin resistance (*Neo*^{R}) cassette. Neo^R transformants were then screened by fluorescence microscopy to verify the presence of GFP and ChFP nuclear signals (data not shown).

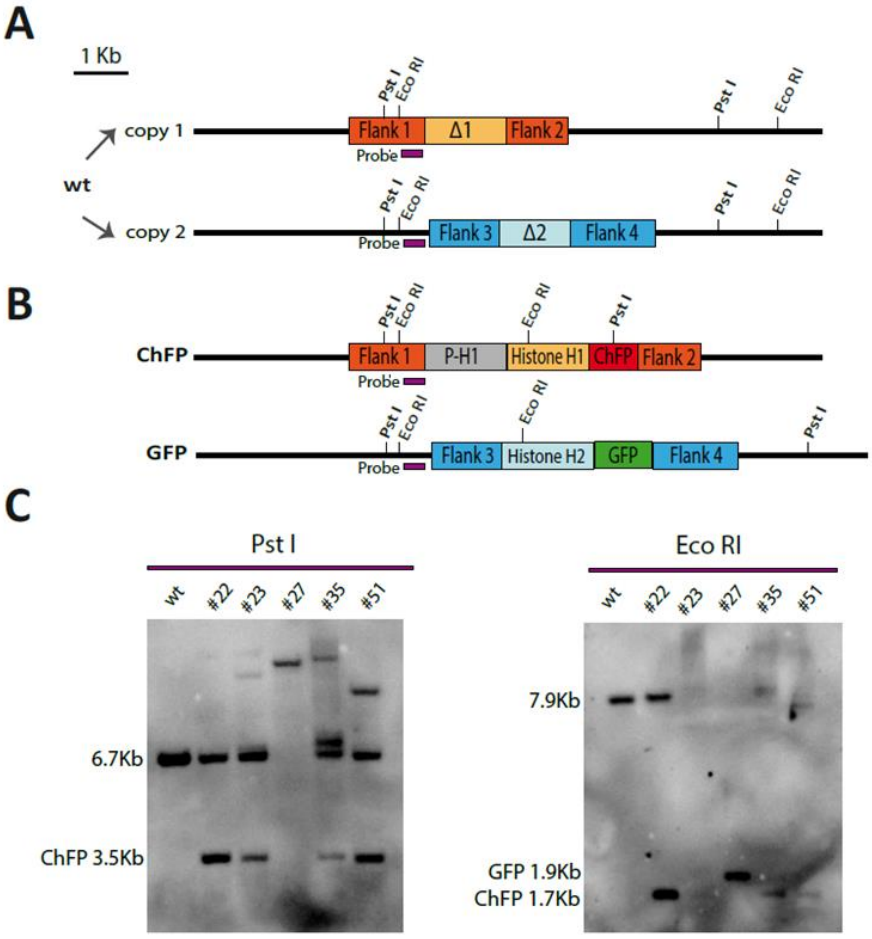

Figure 59. Construction of a strain carrying GFP and ChFP in the duplicated region of chromosome 13. (A) Schematic representation of the strategy followed for differential fluorescent labeling of the two copies of the repeated region of chromosome 13. To avoid homologous insertion of both constructs in the same repeated chromosome region, a physical gap was created between the two insertions into the Δ1 and Δ2 regions of chromosome 13. To this aim, the region deleted in one construct (Δ1) was used as a flank (Flank 3) for the other construct and vice versa. **(B)** The H1::ChFP and H2::GFP regions were amplified from previously obtained strains (Ruiz-Roldán *et al.,* 2010) and fused to the specific flanks of the Δ1 and Δ2 regions, respectively. Positions of restriction sites *Pst*I and *Eco*RI are shown. The probe used for Southern blot analysis is indicated (purple bar). Scale bar, 1kb. **(C)** Identification of Chr13::GFP-ChFP transformants by Southern blot analysis. gDNAs of the wild type strain and putative transformants were treated with *Pst*I (left panel) or *Eco*RI (right panel), separated in an agarose gel, transferred to a nylon membrane and hybridized with the probe. Sizes of hybridizing bands are indicated on the left.

Molecular analysis of the selected candidate transformants by Southern blot was performed to check for homologous insertion of either one or both constructs in the duplicated regions of chromosome 13 (Figure 59C). Upon enzymatic treatment with *Pst*I, transformants #22, #23, #35 and #51 presented a hybridizing band of 3.5 Kb consistent with homologous insertion of the ChFP construct in one of the duplicated regions. However, the presence of the 6.7 Kb hybridizing band expected in the wild type strain suggesting that the other duplicated region of chromosome 13 was not targeted in these transformants. Indeed, these transformants lacked the hybridizing band indicative of homologous insertion of the GFP construct, suggesting insertion of this construct into an ectopic region of the genome. Transformant #27 was the only one lacking the wild type bands corresponding to both regions, since the hybridization band corresponding to the wild type allele was absent in this transformant (Figure 59C). However, in this transformant neither of the two bands indicative of the homologous insertion of the GFP and ChFP constructs were observed. The additional bands observed in some transformants are due to multiple insertions in ectopic regions of the genome. Treatment of the gDNA with the restriction enzyme *Eco*RI confirmed these results and demonstrated that transformant #27 has a hybridization band of smaller size than expected, suggesting some non-canonical event during the homologous insertion of the GFP construct.

Chr13::GFP-ChFP transformants #22, 23 and #35 were selected for further analysis because, even though only one of the chromosome 13 copies was fluorescently labeled, we should be able to determine if that copy has been lost during passaging. Since in transformant #27 loss of one of the duplicated regions of chromosome 13 (chromosome 13mini) appeared to have already occurred (data not shown) and transformant #51 displayed a low level of fluorescence, these two strains were not included in subsequent analyses.

Analysis by fluorescence microscopy revealed the presence of non-fluorescent nuclei in the selected transformants, suggesting a possible admixture with the wild type strain. Therefore, a third round of monoconidial purification was performed to remove the remaining wild type nuclei and obtain pure labelled transformants. Five monoconidial isolates obtained from each transformant were analyzed by fluorescence microscopy (Figure 60), and finally two isolates from each were select that showed a nuclear signal of both GFP and ChFP.

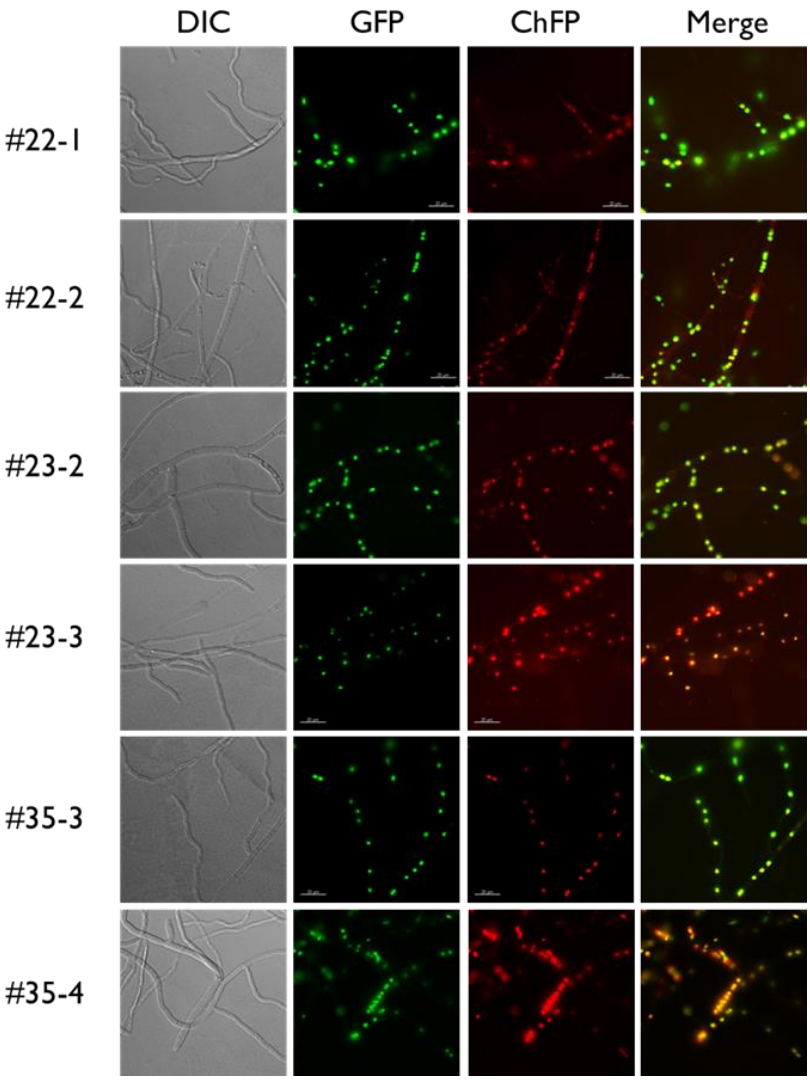

Figure 60. Fluorescence microscopy analysis of Chr13::GFP-ChFP strains. Hyphae of the indicated strains show nuclear signal of GFP and ChFP. DIC, differential interference contrast; scale bar = 20 µm.

2.1.2 GFP and ChFP signals are lost in some Chr13::GFP-ChFP strains during serial passaging experiment on YPDA plates

To assess the stability of the duplicated regions of chromosome 13, we conducted serial passaging experiments. Microconidia of the Chr13::GFP-ChFP strains were spot-inoculated on the center of rich medium plates (YPDA) and allowed to grow for 7 days at 28 °C. After this time, the conidia were collected from the whole colony and an aliquot was spot-inoculated on a new plate for the next passage. The process was repeated for 5 passages and 3 independently passaged lines were obtained. After the five passages, fluorescence microscopy and qPCR analyses were performed with different monoconidial isolates of the passaged lines to assess whether loss of one of the duplicated regions of chromosome 13 had occurred (Figure 61).

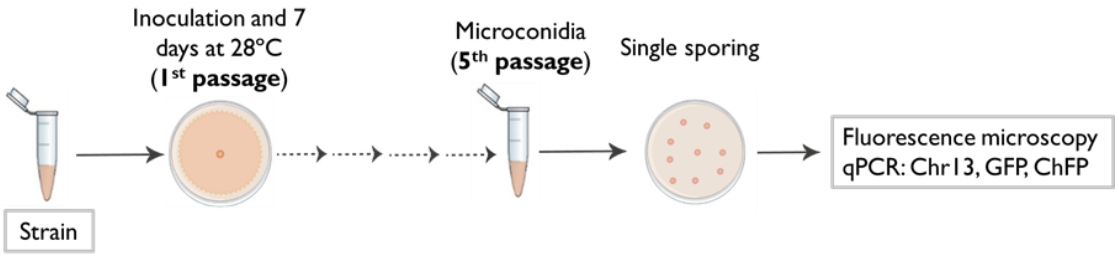

Figure 61. Schematic diagram of the serial passaging experiment performed with the Chr13::GFP-ChFP strains. An aliquot containing 10^6 microconidia was spot inoculated on the center of a YPDA plate, incubated at 28 °C for 7 days, total microconidia from the colony were collected and a new aliquot of 10^6 microconidia was inoculated on a new plate. Aliquots from the microconidia obtained after the 5th passage were plated on YPDA plates and incubated for 2 days at 28 °C. Single colonies were picked for fluorescence microscopy and qPCR analyses. For each strain, three independently passaged lines were obtained (A, B, C).

Fluorescence microscopy analysis revealed that, after the 5th passage, some of the evolved isolates had lost both the GFP and ChFP signals (Figure 62). For example, all the passaged lines from Chr13::GFP-ChFP #22 lacked both green and red fluorescence, whereas lines with or without green and red fluorescence were detected among those derived from Chr13::GFP-ChFP #23. We noted that hyphae of lines derived from Chr13::GFP-ChFP #22 showed some residual autofluorescence, which was absent in those derived from Chr13::GFP-ChFP #23. For Chr13::GFP-ChFP #35, all tested evolved isolates had maintained both green and red fluorescence.

The lack of both green and red fluorescence in some passaged lines did not fit our initial hypothesis, since we expected to see lack of only one fluorescent signal, as a consequence of loss of one of the duplicated regions of chromosome 13. Therefore, we resorted to previous passages to analyse the dynamics of fluorescence. Surprisingly, we found that both fluorescent signals were lost simultaneously, suggesting that the GFP and ChFP genes might have inserted into the same duplicated region of chromosome 13 (data not shown).

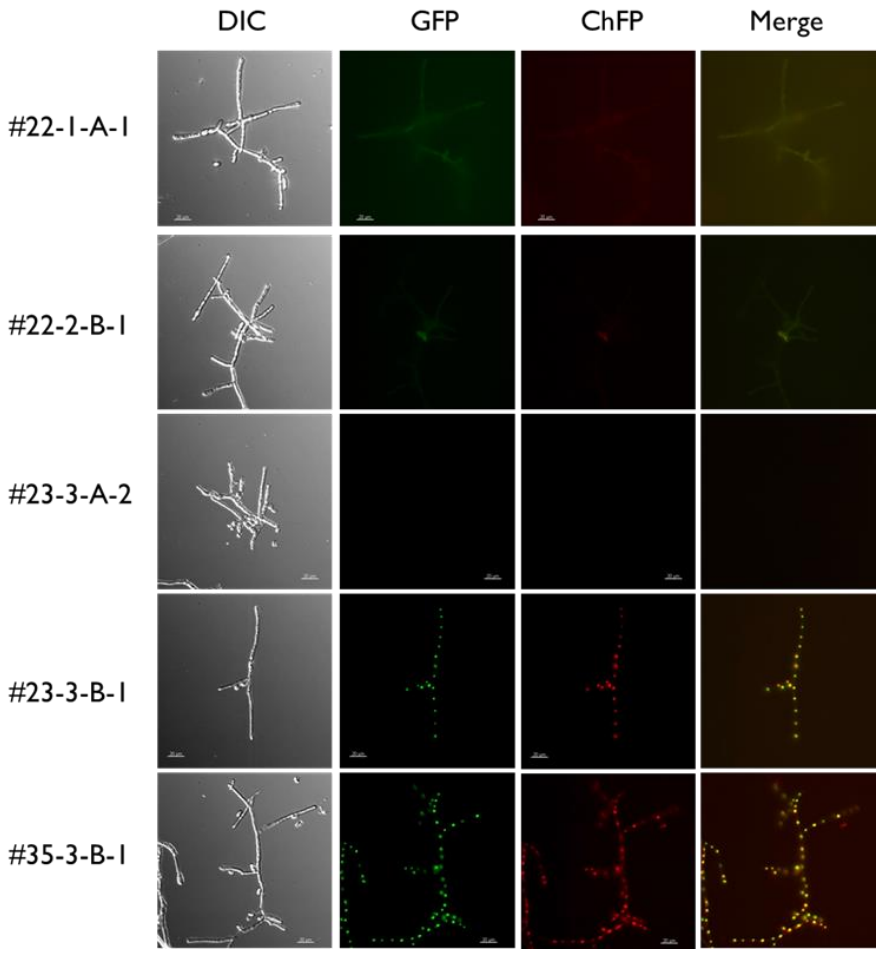

Figure 62. Fluorescence microscopy analysis of passaged Chr13::GFP-ChFP strains. Strains obtained after five serial passages on YPDA medium were cultured in PDB for 2 days and imaged by fluorescence microscopy. Note that some of the evolved strains have lost both the GPF and ChFP fluorescent signal. DIC, differential interference contrast; scale bar = 20 µm.

2.1.3 Lack of both fluorescent signals is not associated with loss of one of the duplicated regions of chromosome 13

To verify the possible correlation between lack of fluorescence observed in some passaged isolates and the loss of one of the duplicated regions of chromosome 13, a qPCR analysis with specific primers of this region was performed (Figure 63). As expected, the progenitor strains had both copies of the duplicated region. However, after the 5th passage one of the copies had been lost in all passaged isolates analyzed. Unexpectedly, loss of one of the copies of the duplicated regions of chromosome 13 was also detected in those lines that still showed both GFP and ChFP signals, suggesting that it did not correlate with the fluorescence pattern detected in the passaged lines.

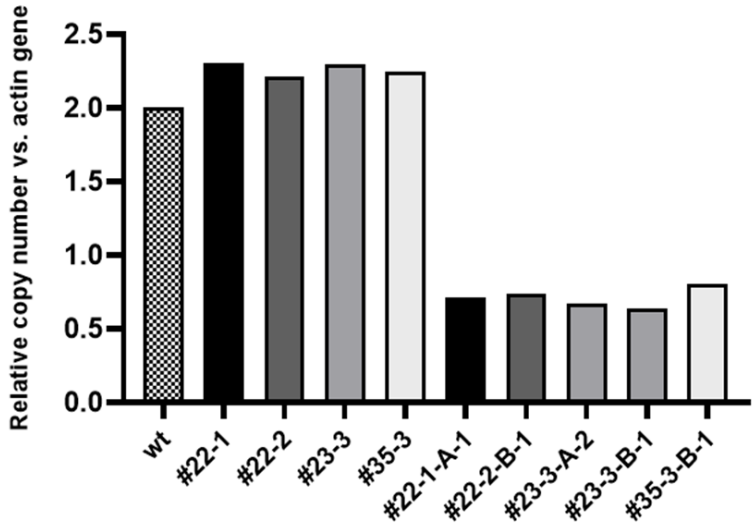

Figure 63. Relative copy number of the duplicated region of chromosome 13 in the progenitor and the passaged Chr13::GFP-ChFP strains. gDNA obtained from the indicated strains (see Fig. 62) either before (left columns) or after (right columns) five serial passages on YPDA medium was subjected to qPCR using specific primers from the duplicated region of Chr13 and normalized to the actin gene. Results are indicated as copy numbers relative to the wild type strain carrying two copies of the duplicated region of Chr13.

In view of these results, we performed a second qPCR analysis using specific primers for either the *GFP* or the *ChFP* genes (Figure 64).

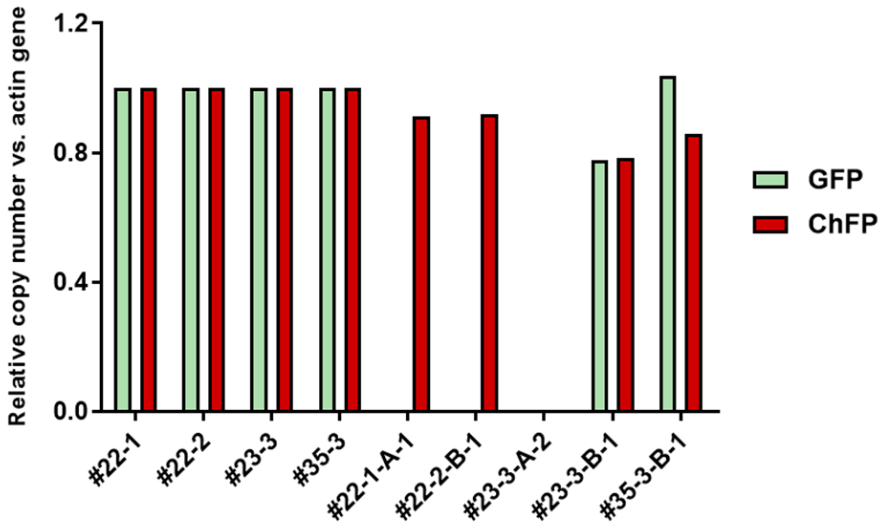

Figure 64. Relative copy number of the gfp and chfp genes in the progenitor and passaged Chr13::GFP-ChFP strains. gDNA obtained from the indicated strains (see Fig. 4) either before (left columns) or after (right columns) five serial passages on YPDA medium was subjected to qPCR using specific primers for each fluorescent marker and normalized to the actin gene. Results are indicated as copy number relative to the respective progenitor strain.

As expected, the progenitor strains had both fluorescent markers. The same was true for passaged isolates #23-3-B-1 and #35-3-B-1, whereas in isolate #23-3-A-2 none of the two markers was detected, consistent with the fluorescence microscopy results. However, the two isolates derived from Chr13::GFP-ChFP #22 that appeared to have lost both fluorescent signals according to microscopy analysis, showed presence of the *ChFP* gene, suggesting a possible mutation or silencing of the *ChFP* marker gene.

To determine in which region of the genome the *ChFP* and *GFP* genes had been inserted, the chromosomes of the wild type strain, the progenitor strains and some of the passaged Chr13::GFP-ChFP lines were separated by PFGE (Figure 65A) and subjected to Southern blot analysis with three different probes. Hybridization with a specific probe for the duplicated region of chromosome 13 demonstrated that the loss of the copy detected by qPCR in all cases corresponded to the chromosome 13mini, whereas the copy located on chromosome 13 was still present (Figure 65B). Hybridization with specific probes for *ChFP* and *GFP* genes revealed that neither of the two fluorescence markers had integrated into chromosome 13mini (Figure 65C-D). In the progenitor strains #22-1 and #23-3, both markers had inserted into chromosome 13, whereas for progenitor strain #35-3, the size of the hybridizing band suggests that both markers had inserted ectopically into chromosome 1. PCR tests suggest that both GFP and ChFP constructs may have inserted *in tandem* at the same chromosomal region (data not shown). This karyotype analysis confirmed previous results, showing that the passaged isolate #23-3-A-2 lacks both fluorescent markers while isolate #22-1-A-1 still carries the *ChFP* gene in its genome although no red fluorescence signal is observed by microscopy. The remaining passaged isolates showed both GFP and ChFP hybridization signals.

The fact that the passaged isolate #23-3-A-2 derived from progenitor #23-3 had lost the fluorescence-labelled region integrated on chromosome 13, allowed us to use it for optimization of the protocol for quantification of chromosomal regions loss by the FACS technique.

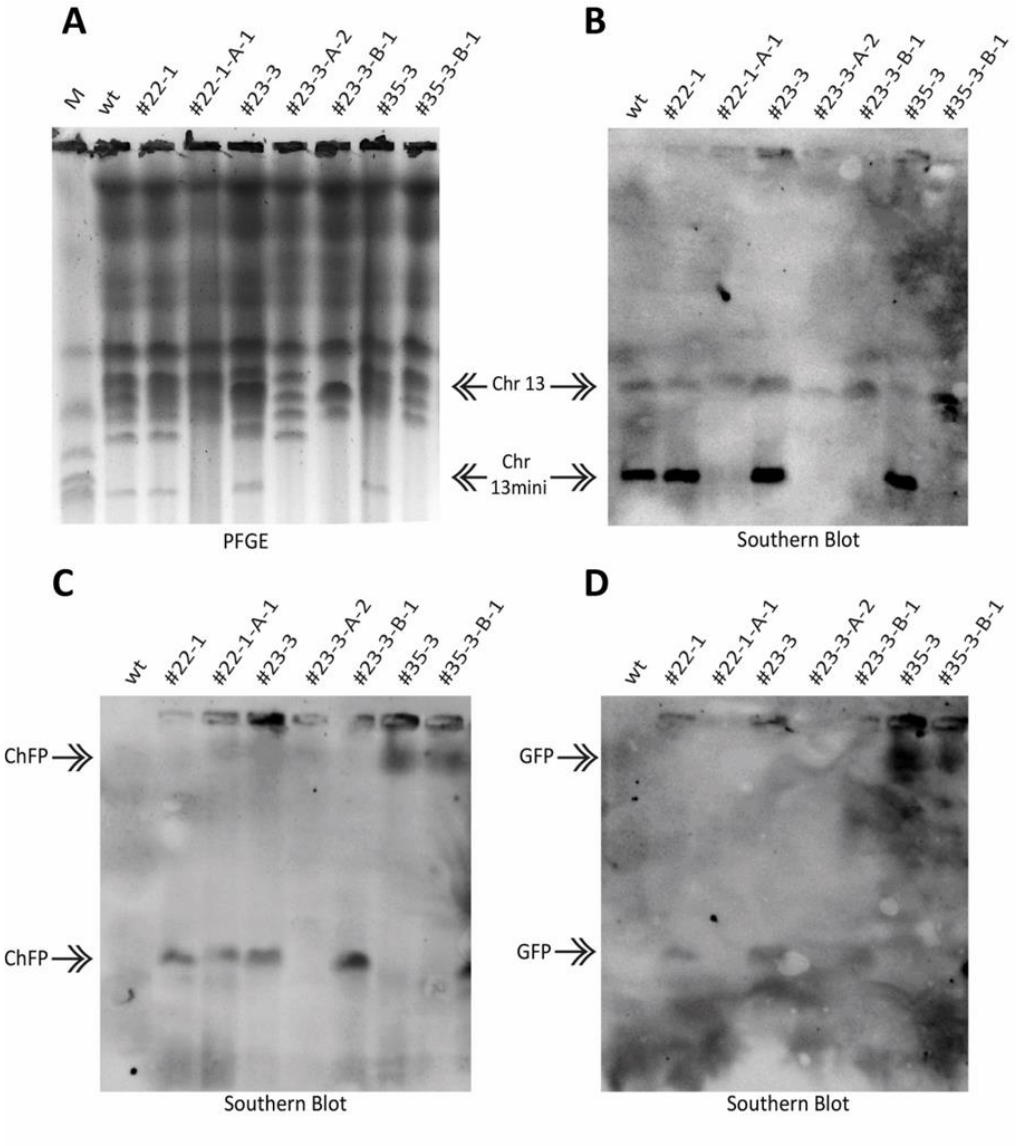

Figure 65. Pulsed-field gel electrophoresis and Southern blot of Chr13::GFP-ChFP strains. (A) PFGE of the wild type as well as progenitor and passaged Chr13::GFP-ChFP strains (see Fig. 4) to visualize chromosome bands by ethidium bromide staining. The left lane (M) shows the chromosome pattern of *S. cerevisiae* used as molecular size marker. **(B)** Southern blot analysis with a probe located in the duplicated region of Chr13 confirms that some of the passaged lines have lost the chromosome 13mini. **(C-D)** Hybridization with specific probes for the ChFP (left panel) or GFP (right panel) genes confirms the loss of the fluorescence marker in some of the passaged strains.

2.1.4 Testing the accuracy of flow cytometry-based discrimination of fluorescent and non-fluorescent Fol4287 microconidia

Fluorescence-based identification of chromosomal loss in *F. oxysporum* by FACS method was reported previously by the group of Prof. Martijn Rep at the University of Amsterdam, Netherlands (Vlaardingerbroek *et al*., 2016). We therefore decided to use the FACS method to quantify the loss of fluorescence-labelled region of chromosome 13 (work performed during a stay in the group of Prof. Rep). We first tested the accuracy of the flow

cytometry protocol to separate conidia based on the presence or absence of fluorescent signal. The first approach consisted in mixing microconidia of the wild type strain (non-fluorescent) and the Chr13::GFP::ChFP #35-3 strain (both green and red fluorescence) in different known proportions (Figure 66). The Chr13::GFP::ChFP #35-3 strain was chosen based on the fact that both fluorescence markers are integrated into a stable core region of the genome (chromosome 1) and that no loss of fluorescence had been detected during the previous serial passaging experiment (see Figures 62 and 65). This should ensure that non-fluorescent conidia detected by FACS correspond to the wild type strain and not to conidia of the fluorescent strain that had spontaneously lost fluorescence. Fresh conidial suspensions from the two strains were mixed at the desired ratios to obtain a final concentration of $2x10^6$ microconidia mL^{-1} and used directly for FACS analysis.

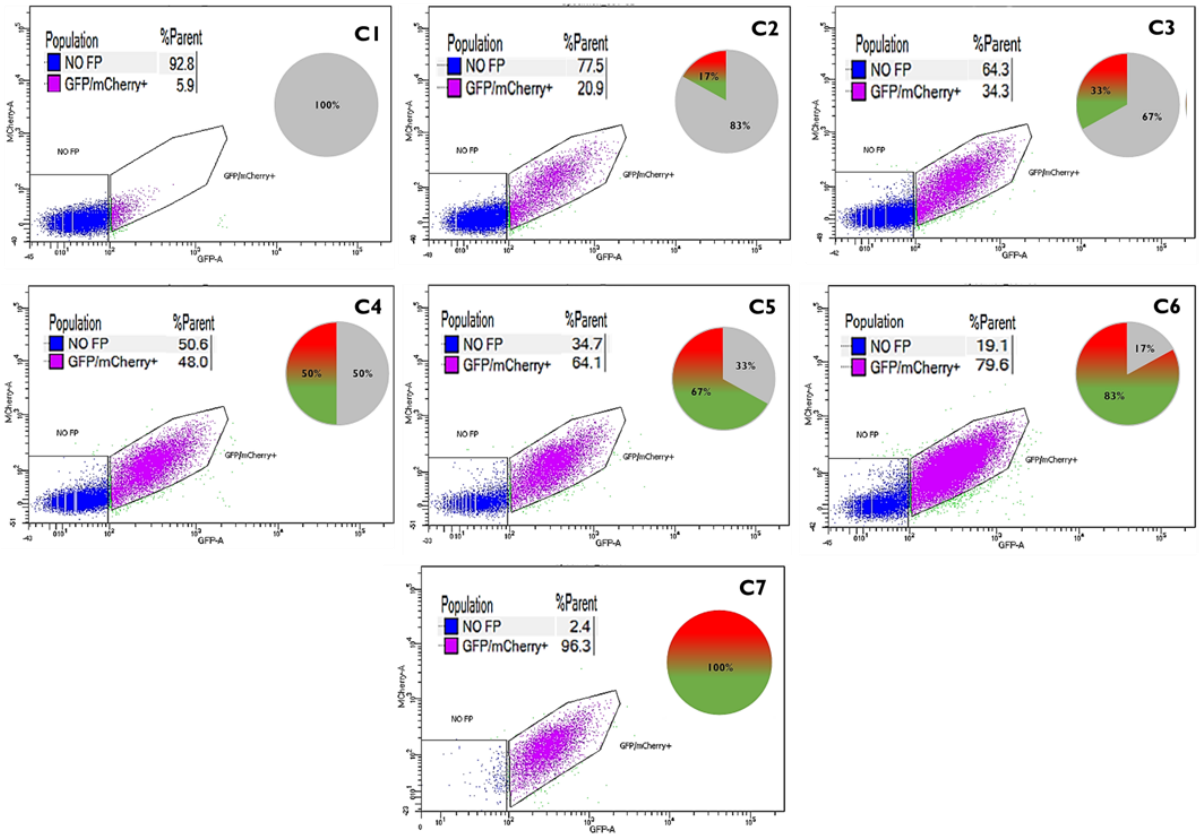

Figure 66. Validation of the accuracy of flow cytometry for discrimination of fluorescent and non-fluorescent microconidia. Pie charts C1-C7: Microconidia from the wild type strain (without fluorescence, in grey) and of the Chr13::GFP-ChFP #35-3 strain (with red and green fluorescence) were mixed at the indicated ratios. Experiment to validate the accuracy of the flow cytometer in discriminating between the fluorescent and non-fluorescent conidia. Results are represented as dot plots. Populations of conidia with fluorescence are shown in purple (GFP/mCherry+) and those without fluorescence in blue (NO FP). Percentages detected by the flow cytometer are shown in the upper left corner of each plot. Axis labels indicate the detection channel used (*x*-axis: λ=488nm; *y*-axis: λ =561nm).

Figure 66 shows the classification of the conidial populations by FACS represented as dot plots, with the non-fluorescent population in blue and the fluorescent one in purple. The C5 sample (67% fluorescent/33% non-fluorescent conidia) was used to establish the division between conidia with and without fluorescence, and the remaining samples were analyzed using the same settings. In general, the percentages detected by the FACS were very close to the expected percentages, particularly when the proportions of fluorescent and non-fluorescent conidia were similar (samples C3-C5). The variations between the two methods observed were slightly more notable in conditions C7 and C1 where there were only conidia with or without fluorescence. In condition C1, 6% fluorescent conidia were detected by FACS even though this sample contained only non-fluorescent wild type conidia. A possible explanation could be a strong autofluorescence of some conidia. On the opposite side, in sample C7 a low percentage of putatively non-fluorescent conidia was detected by FACS, although it contained exclusively conidia with fluorescence. This could be due to different reasons: 1) dead conidia having lost fluorescence; 2) conidia that had simultaneously lost both the GFP and ChFP markers which were inserted in the same genomic region; 3) heterogeneity in conidia exhibiting differences in fluorescence intensity. Taken together these results suggest that perhaps the division line was not optimally set. However, moving the line towards the right would also alter the percentages detected in the other mixtures by increasing the proportion of non-fluorescent conidia.

From this initial analysis we concluded that the FACS method was not adequate to reliably discriminate between the presence and absence of the two markers genes. One reason could be that the intensity of the GFP and ChFP signals was not high enough when compared to the autofluorescence, with both types of conidial populations being located too close to each other. This represents a severe limitation for the optimal separation of conidia based on their fluorescence pattern.

The presence of both *GFP* and *ChFP* genes in the same genomic region where they would undergo simultaneous loss during the serial passaging experiment made it difficult to distinguish dead non-fluorescent conidia from live non-fluorescent conidia that had undergone loss of both fluorescent signals. Based on the possibility that the autofluorescence exhibited by live conidia that had lost both fluorescent markers was greater than the autofluorescence of dead conidia, the initial protocol of fluorescence-activated cell sorting (Figure 67A) was replaced by an alternative sorting protocol (Figure 67B), in which the non-fluorescent conidial population (NO FP) was divided into two subpopulations: dead conidia (group A) and conidia that had supposedly lost *GFP* and *ChFP* genes (group B). To confirm

the correctness of this model, in subsequent analyses we performed control plating of the different conidial populations classified by FACS (groups A-C) to check viability based on the presence or absence of growth.

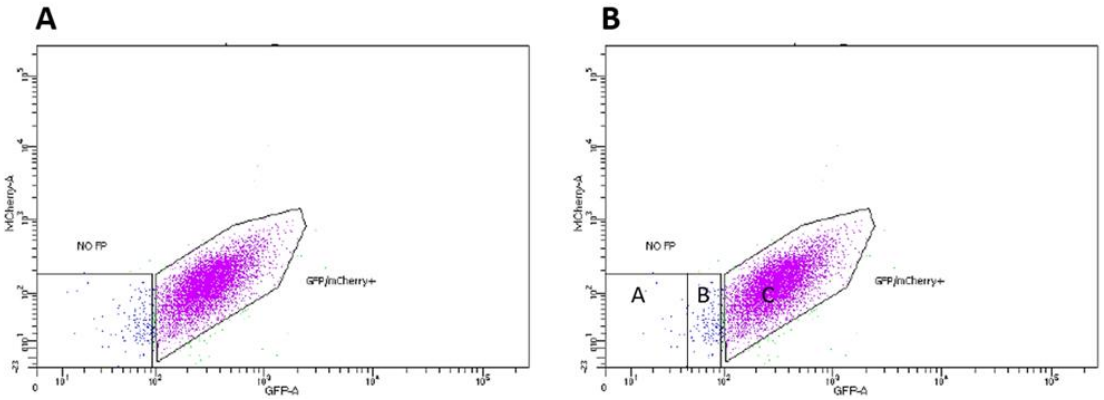

Figure 67. Two protocols for fluorescence-activated cell sorting. (A) Dot plot showing the initial protocol of conidia separation during the optimization of the cytometer with two conidial populations. **(B)** Final protocol used for cell classification. The non-fluorescent spore population (NO FP) was further separated into dead cells (group A) and cells with loss of GFP/ChFP signal (group B). Axis labels indicate the detection channel used (*x*-axis: λ=488nm; *y*-axis: λ =561nm).

2.1.5 Use of FACS to measure the loss of GFP and ChFP markers during serial passaging

To test the usefulness of FACS in quantification of fluorescence marker loss, we conducted a serial passaging experiment on YPDA medium plates (Figure 68).

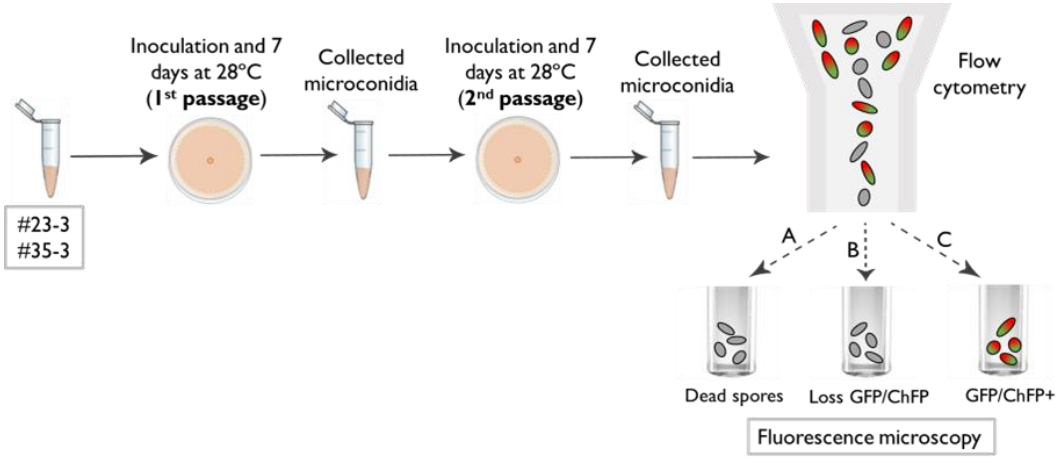

Figure 68. Schematic representation of the fluorescence-activated cell sorting experiment with Chr13::GFP-ChFP strains. Two serial passages on YPDA plates were performed with the #23-3 and #35-3 transformants. The microconidia obtained from the last passage were introduced in the flow cytometer and separated according to the previous model: dead cells (A), cells with loss of GFP/ChFP signal (B) and GFP/ChFP+ fluorescent cells (C). Aliquots from the different conidial populations were plated on YPDA, incubated for 2 days at 28 °C to obtain individual colonies and analyzed by fluorescence microscopy. For each strain, three independently passaged lines were obtained (R1, R2, R3).

The Chr13::GFP::ChFP #23-3 strain was used as a positive control, since the loss of both fluorescent signals had been detected in the previous passaging experiment (see Figure 62), while the Chr13::GFP::ChFP #35-3 strain was used as a negative control because no loss of any of the fluorescence markers had been previously observed in this isolate. In addition, this strain allowed estimating the death rate of conidia, based on absence of fluorescence.

After two serial passages, the conidia obtained were used directly for FACS to separate them into three different populations (A-C), according to the previously described cell sorting model. In parallel, dilutions of each of the collected conidial populations were plated on YPDA and after 2 days the single colonies were analyzed by fluorescence microscopy for presence or absence of GFP and ChFP signals. This process was performed for 3 independently passaged lines per parental strain (R1-R3) (Figure 68).

The results of the flow-cytometric separation are represented as dot plots, showing one of the three independently passaged lines as representative (Figure 69). For passaged lines from both parental strains, most of the conidial population analyzed was in group C (exhibiting both GFP and ChFP signals) (Table 27).

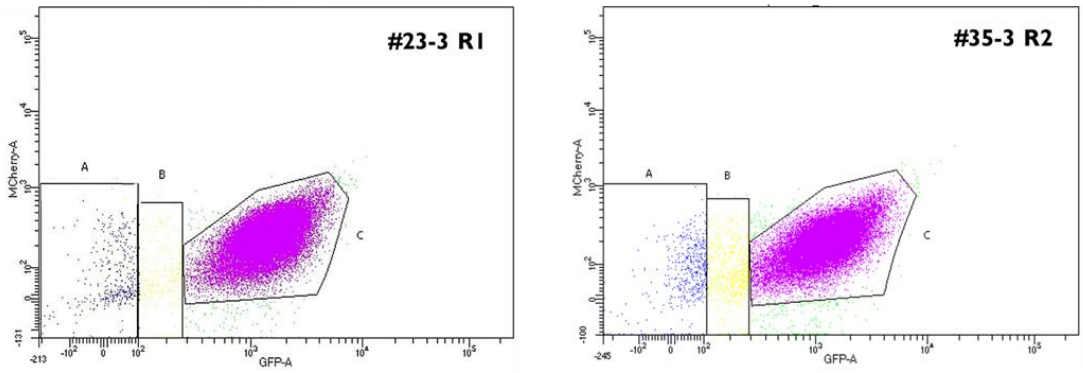

Figure 69. Flow-cytometric separation of fluorescent conidial populations passaged on YPDA plates. Dot plots showing the flow cytometry analysis of conidial populations obtained after the 2nd serial passage on YPDA medium of fluorescent strains #23-3 and #35-3 (see Fig. 68). For each strain, the plot from one representative of three independently passaged lines is shown. Axis labels indicate the detection channel used (*x*-axis: λ=488nm; *y*-axis: λ =561nm).

Moreover, in group A (dead conidia) a similar number of individuals was detected in both strains, suggesting that the ratio of dead conidia is relatively stable. However, in group B, that should contain that lost both fluorescent markers, we observed a higher proportion in the passaged line obtained from the (supposedly more stable) #35-3 strain (Figure 69, Table 27). This result contrasts with the initial hypothesis, as it indicates that in #35-3 the ratio of loss of the *GFP* and *ChFP* genes was higher than in #23- 3. In the dot plots there was

no clear separation between the different groups, suggesting a certain variability in the intensity of GFP and ChFP signals in the microconidial population of *Fol4287*.

Table 27. Percentages of different conidial populations detected by flow cytometry. Dead cells (population A), cells with loss of GFP/ChFP signal (B) and GFP/ChFP+ fluorescent cells (C).

	Population A	Population B	Population C
#23-3 R1	1.0 %	0.5 %	98.1 %
#23-3 R2	1.6 %	0.8 %	97.1 %
#23-3 R3	1.7 %	1.2 %	96.4 %
#35-3 R1	1.3 %	1.9 %	95.8 %
#35-3 R2	1.4 %	2.0 %	96.0 %
#35-3 R3	1.6 %	2.3 %	94.4 %

Dilutions of the different conidial populations classified by the flow cytometer were plated to check both viability and presence or absence of fluorescence (Table 28). In total, 180 monoconidial isolates were analyzed, 30 from each of the FACS-sorted populations. As expected, in group C a 100% of the conidia analyzed were GFP and ChFP positive. However, in contrast to our hypothesis, almost the entire population of conidia in groups A and B were also fluorescent.

Table 28. Frequencies of fluorescent (FP+) or non-fluorescent (FP-) conidia detected by fluorescence microscopy analysis. Dead cells (population A), cells with loss of GFP/ChFP signal (B) and GFP/ChFP+ fluorescent cells (C).

	Population A	Population B	Population C
#23-3 R1+R2+R3	100 % FP+	96.7 % FP+ 3.4 % FP-	100 % FP+
#35-3 R1+R2+R3	96.7 % FP+ 3.4 % FP-	96.7 % FP+ 3.4 % FP-	100 % FP+

Based on these unexpected results, two hypotheses were established:

1. Due to the low rate of loss of *GFP* and *ChFP* genes during the two serial passages, there were very few conidia without fluorescence. Due to heterogeneity of fluorescence in the population, groups A and B contain conidia that for some reason show a lower intensity of fluorescence signal.

2. The intensity of the GFP and ChFP signals is insufficient for FACS to reliably discriminate between the presence and absence of the fluorescence markers, resulting in a high error rate.

To test the two hypotheses, we used our initial experimental approach of mixing fluorescent and non-fluorescent conidia using low proportions of non-fluorescent wild type conidia: 10% (A), 5% (B) and 1% (C) (Figure 70). For each proportion, two technical replicates were performed (R1, R2). In this experiment, only two populations were collected (NO FP and FP). After FACS, the percentages of conidia in the two populations were very close to the expected numbers. However, we still observed a continuous and homogeneous dot plot, making it difficult to establish the separation between the two types of populations, even after removing a fraction of conidia on the borderline that was not classified in any group (Figure 70).

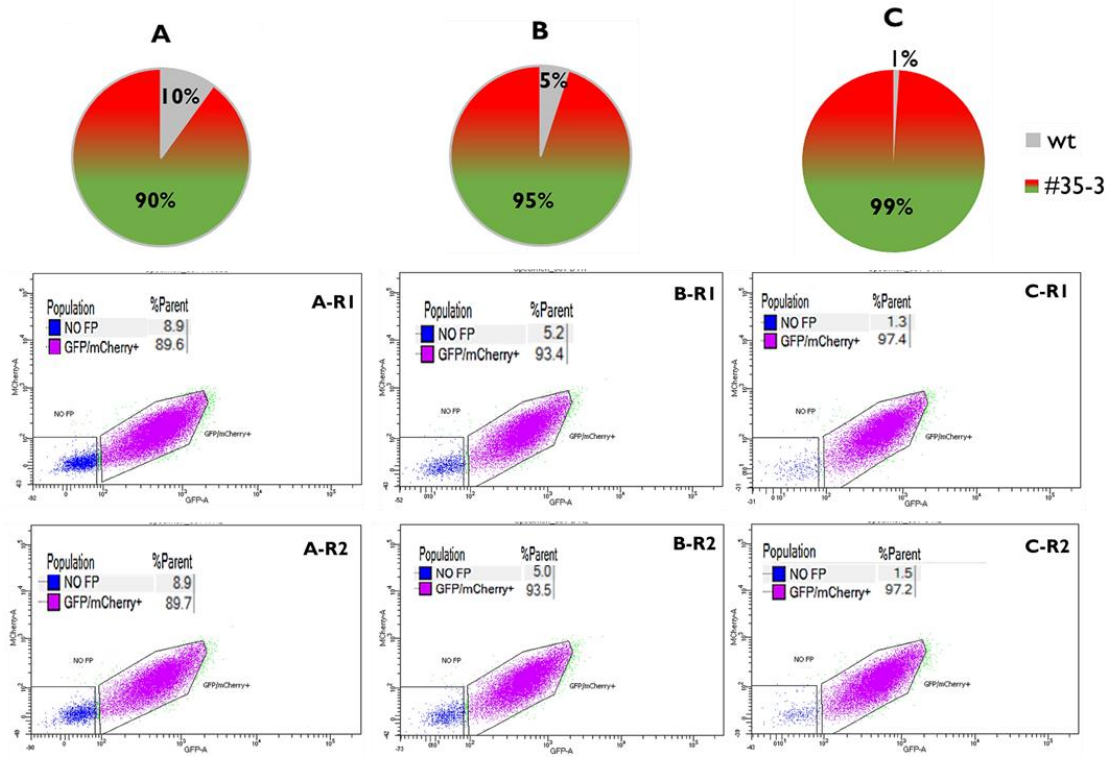

Figure 70. Testing the capacity of the flow cytometer to discriminate non-fluorescent from fluorescent conidia. Pie charts A-C: Low percentages of wild type conidia (without fluorescence, in grey) were mixed at the indicated proportions with conidia of the Chr13::GFP-ChFP #35-3 strain (red and green fluorescence, see pie chart) to test the capacity of the flow cytometer to accurately discriminate non-fluorescent from fluorescent conidia. Discrimination of conidial populations by flow cytometry is represented as dot plots. Populations of conidia with fluorescence are shown in purple (GFP/mCherry+) and those without fluorescence in blue (NO FP). Percentages detected by the flow cytometer are shown in the upper left corner of each plot. For each condition, two technical replicates were made (R1, R2). Axis labels indicate the detection channel used (*x*-axis: λ=488nm; *y*-axis: λ =561nm).

The NO FP population was subsequently analyzed by fluorescence microscopy to confirm whether indeed all conidia were GFP and ChFP negative (Table 29). In the sample where the percentage of non-fluorescent conidia was the highest (10%), almost all conidia analyzed (96.4%) were non-fluorescent as expected, while 3.6% were false negatives that showed both GFP and ChFP signals in fluorescence microscopy. In the sample with a lower proportion of non-fluorescent conidia (5%), the percentage of false negatives in the NO FP population increased to 13%, while in the sample with the 1% proportion more than half of the NO FP conidial population (54%) were false negatives (Table 29).

Table 29. Frequency of fluorescent and non-fluorescent conidia in the NO FP previously population separated by the flow cytometer, as determined by fluorescence microscopy.

	Non-fluorescent	Fluorescent
A R1+R2	96.4 %	3.6 %
B R1+R2	87 %	13 %
C R1+R2	46 %	54 %

These results suggest that a low percentage of conidia (around 0.5%) are sorted by FACS to the left of the dividing line in the NO FP population when they are really FP positive. One possible explanation is that the intensity of the fluorescent signal in these conidia falls below the detection limit of FACS due to the heterogeneity of the fluorescence level in the population. As the percentage of this type of conidia is very low and appears to be constant in the population, their interference is greater when the percentage of non-fluorescent conidia is less than 5%. Based on this, the loss rate of GFP and ChFP genes during the serial passaging experiment should be sufficiently high to prevent the percentage of false negatives from distorting the quantitative measurement.

In summary, we concluded that although the FACS technique is useful for detecting conidia that have lost fluorescence, it failed to accurately quantify the loss rate of a fluorescence marker inserted in a genomic region under the conditions used in this study.

2.2. Use of real-time Quantitative PCR to measure the frequency of chromosome loss

Although the FACS technique has the advantage of allowing rapid analysis of a high number of conidia, the accurate quantification of the loss of a genomic region with this

technique was not possible. We therefore decided to use quantitative PCR (qPCR) as an alternative.

2.2.1 Dynamics of loss of chromosomes 15 and 13mini during serial passaging on YPDA plates

We conducted a serial passaging experiment with the *Fol4287* wild type strain on YPDA plates, because previous studies established that chromosomes 15 and 13mini were frequently lost under these conditions (López-Díaz, 2019). A total of 4 passages were performed with two independently lines (wt-A, wt-B) (Figure 71), In parallel, serial dilutions of the conidia collected from each passage were plated on YPDA, and 10 of the resulting colonies were transferred to liquid PDB medium for isolation of gDNA. The gDNA was then subjected to qPCR using specific primers for the duplicated regions of chromosomes 13 and 15, to measure the frequency of chromosome loss in the passaged populations.

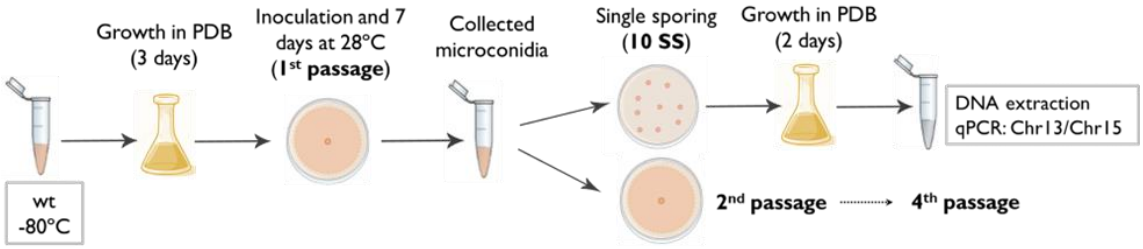

Figure 71. Schematic diagram of the serial passaging experiment on YPDA plates. Aliquots of 10^6 fresh microconidia of the wild type strain Fol4287 obtained from PDB were spot-inoculated on the center of YPDA plates and incubated at 28 °C for 7 days. Total conidia from the colony were collected and an aliquot of 10^6 microconidia was spot-inoculated on a new YPDA plate for the next passage. Four serial passages were performed with two independently passaged lines (wt-A, wt-B). In parallel, dilutions of the collected microconidia were plated on YPDA and incubated for 2 days at 28 °C. gDNA was isolated from 10 individual colonies and analyzed by qPCR using specific primers of the duplicated regions of chromosomes 13 and 15.

The results of the quantitative analysis allowed to establish the dynamics of loss of chromosomes 15 and 13mini in Fol4287 during serial passaging (Figure72). In the two independently passaged lines, an early appearance of both CNVs types after one or two passaged was observed. In the wt-B line, a gradual loss of chromosome 13 was observed reaching a loss frequency of 44% after the 4th passage. Similarly, the loss frequency of chromosome 15 gradually increased after an initial lag phase to a value of 33% after the last passage.

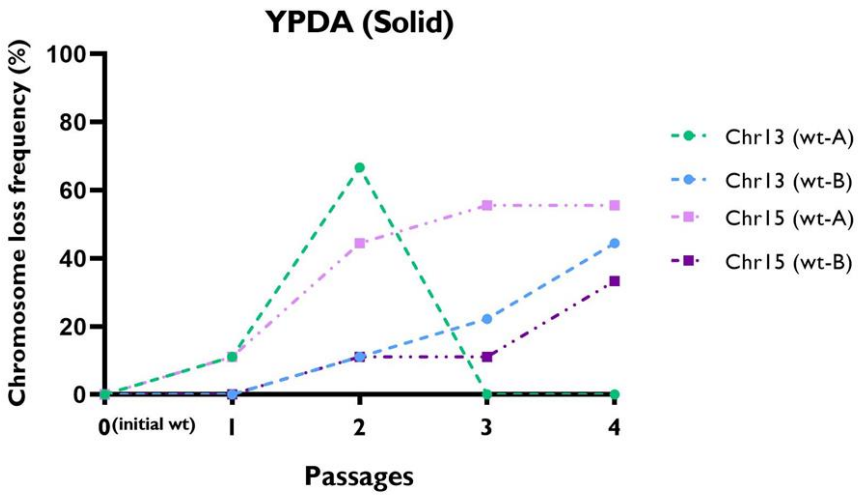

Figure 72. Dynamics of spontaneous loss of chromosomes 13mini and 15 detected during four serial passages of Fol4287 on YPDA plates. The wild type strain Fol4287 was subjected to four serial passages on YPDA medium (see Fig. 71). After each passage dilutions of collected microconidia were plated on YPDA and incubated for 2 days at 28 °C. gDNA from 10 individual colonies for each independent line (wt-A, wt-B) was isolated and subjected to qPCR using specific primers of the duplicated regions of chromosomes 13 and 15 against the actin gene as a reference.

A different trajectory was observed in the wt-A line. Between the first and second passage, the loss frequency of one of the duplicated regions of chromosome 13 (most likely 13mini) and 15 increased considerably, reaching 66% and 44%, respectively. However, after the third passage, the loss frequency of chromosome 13mini had returned to the starting point (0%) and no further loss was detected in the subsequent passages (Figure 72). This event was associated with a visible change in colony phenotype observed after the third passage, including a more branched appearance and increased growth speed (data not shown). These phenotypic characteristics were previously shown to entail a fitness gain in this environmental condition (YPDA), resulting in the individuals carrying this mutation outcompeting those showing wild type growth (López-Díaz, 2019). Based on the dynamics of chromosome loss, we hypothesize that the adaptive growth mutation in this line occurred in a genetic background that had both duplicated regions of chromosome 13, and consequently, when this lineage became fixed in the population the frequency of loss for chromosome 13mini went back to 0. By contrast, the loss frequency of chromosome 15 remained rather constant at a value around 50% until the last passage (Figure 72). The most likely explanation for these results is the occurrence of advantageous mutations in two different genetic backgrounds, one with two copies of the duplicated region from chromosomes 13 and 15, and the other in a background with two copies of the duplicated

region from chromosome 13 and a single copy of chromosome 15. Both mutations would compete without displacing each other.

2.2.2 Dynamics of loss of chromosomes 15 and 13mini during serial passaging in liquid YPD medium

In an attempt to avoid the distorting effect of gain-of-fitness mutations on the trajectory of chromosome losses, an experiment with three serial passages in liquid YPD medium was performed (Figure 73). In parallel, serial dilutions of the collected conidia were plated on YPDA, and gDNA isolated directly from 50 colonies per passage (to avoid an additional step of growth in liquid culture) was subjected to qPCR with specific primers for the duplicated regions of chromosomes 13 and 15. As initial control, conidia of the wild type strain were plated on YPDA directly from stock at -80 °C. (Figure 73).

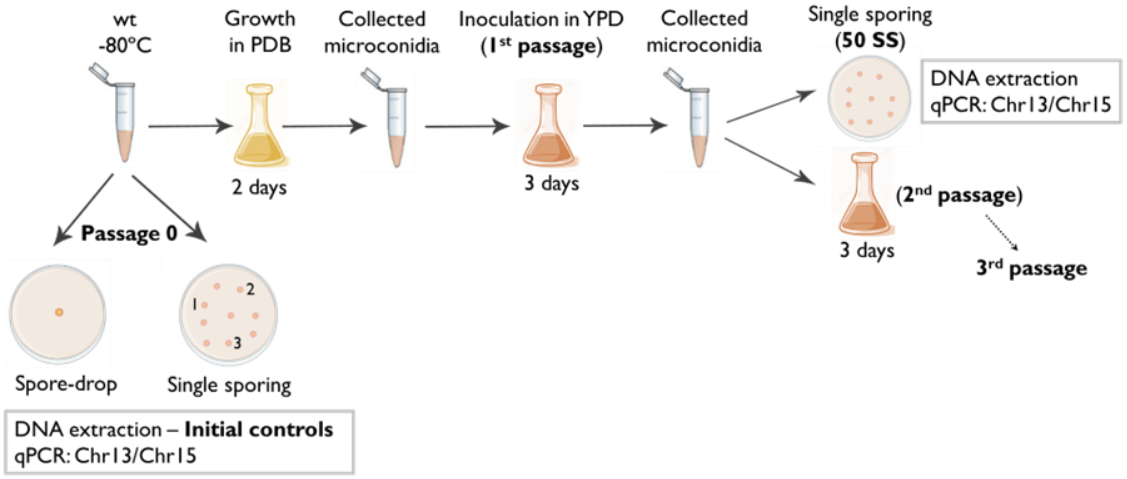

Figure 73. Schematic diagram of the serial passaging experiment in liquid YPD medium. $1.25x10^7$ fresh microconidia of the wild type strain *Fol4287* obtained from PDB were cultured during 3 days at 28 °C in liquid YPD medium. Microconidia were collected by filtration and centrifugation and $1.25x10^7$ microconidia were inoculated in a new flask with YPD (next passage). In parallel, dilutions of collected microconidia were plated on YPDA and incubated for 2 days at 28 °C. gDNA from 50 individual colonies was isolated and subjected to qPCR using specific primers of the duplicated regions of chromosomes 13 and 15. For the passage 0 control, the microconidia used for the starting inoculum of the experiment were directly spot-inoculated or plated on YPDA for colony DNA extraction.

Figure 74 shows the dynamics of loss of chromosomes 15 and 13mini during the serial passaging experiment in liquid YPD medium. The frequency of loss for both chromosomes increased steadily during the first two passages and then appeared to stabilize at around 5%. Thus, although the number of generations in the two passaging conditions remains to be determined, the rate of chromosome loss detected in liquid medium appears to be lower than on solid medium.

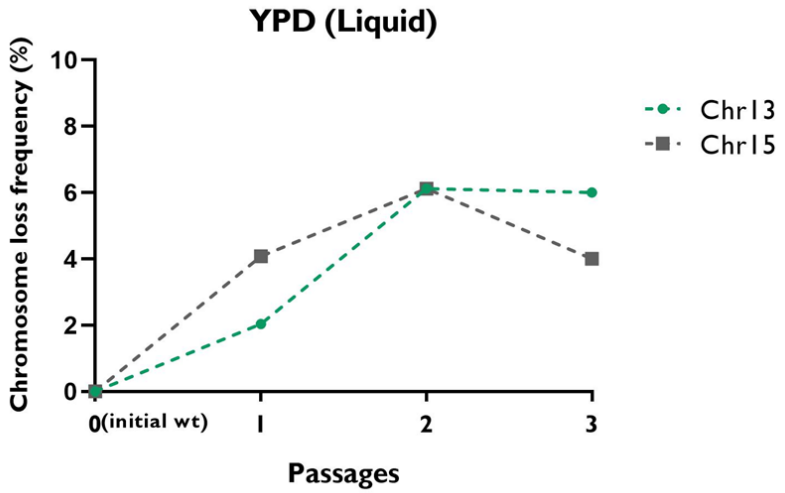

Figure 74. Dynamics of spontaneous loss of chromosomes 13mini and 15 detected during three serial passages of Fol4287 in liquid YPD medium. The wild type strain Fol4287 was subjected to three serial passages in liquid YPD medium (see Fig. 73). After each passage, dilutions of collected microconidia were plated on YPDA and incubated for 2 days at 28 °C. gDNA from 50 individual colonies was isolated and subjected to qPCR using specific primers of the duplicated regions of chromosomes 13 and 15 against the actin gene as a reference. to determine absence or presence of chromosome loss.

2.2.3 A long-term serial passaging experiment on YPDA plates reveals a high rate of chromosome loss

In a previous experimental evolution process (López-Díaz, 2019) a significant rate of loss of chromosomes 15 and 13mini was detected after 10 passages on YPDA plates, although considerable variability was observed between the 5 independently passaged lines analyzed. Based on this, we decided to repeat this assay increasing the number of independent lines to more reliably establish the rate of loss for both chromosomes. Moreover the entire serial passaging experiment was performed three times (biological replicates A, B, C), each time with 10 independently passaged lines (Figure 75).

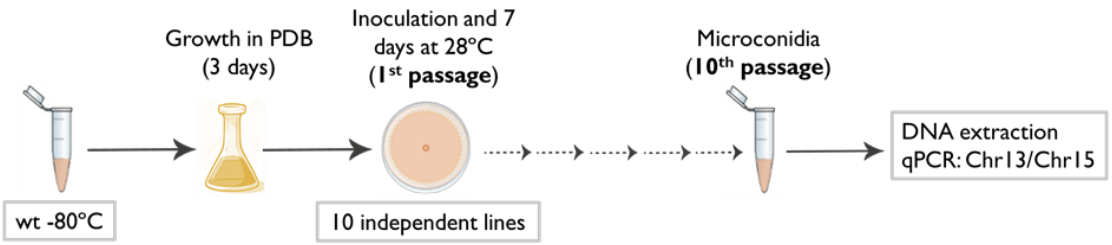

Figure 75. Schematic diagram of the long-term serial passaging experiment on YPDA plates. Aliquots of 10^6 fresh microconidia of the wild type strain Fol4287 obtained from PDB were spot-inoculated on the center of YPDA plates and incubated at 28 °C for 7 days. Total conidia from the colony were collected and an aliquot of 10^6 microconidia was spot-inoculated on a new YPDA plate for the next passage. gDNA from the mycelium of the evolved lines after the 10^{th} passage was

isolated and subjected to qPCR using specific primers of the duplicated regions of chromosomes 13 and 15. Three independent serial passaging experiments (A, B, C) were performed, each including ten independently passaged lines.

The results from qPCR analysis of the passaged populations after the 10th passage are shown in Figure 18. The mean rates of loss for chromosomes 13mini and 15 were 70% and 89%, respectively, which is similar to the results of the previous assay (76% and 93%, respectively; López-Díaz, 2019). Thus, in spite the natural variability that exists during the evolution process, the rate of chromosome loss under this particular environmental condition (YPDA plates) appears to be remarkably reproducible.

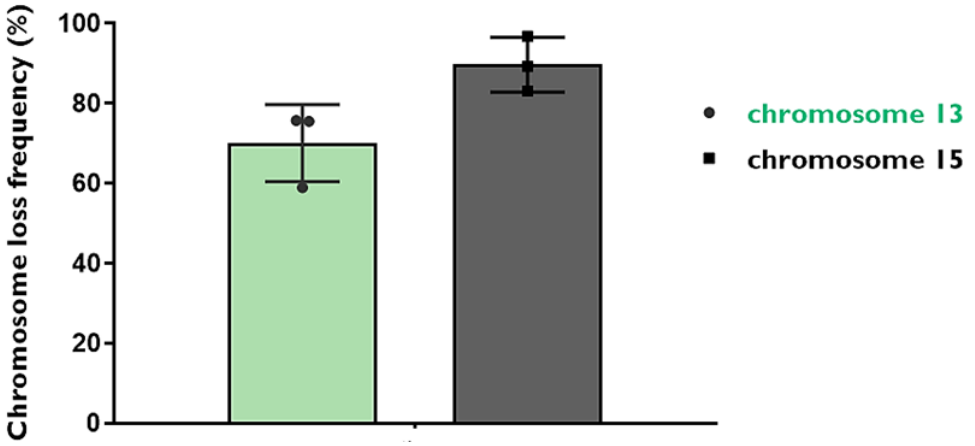

Figure 76. Frequency of spontaneous loss of chromosomes 13mini and 15 in Fol4287 after ten serial passages on YPDA plates. The wild type strain Fol4287 was subjected to ten serial passages on YPDA medium (see Figure 75). After the 10th passage, gDNA was isolated from passaged populations and subjected to qPCR using specific primers of the duplicated regions of each chromosome against the actin gene as a reference. Frequency of chromosome loss was calculated. Data shown represent the mean and standard deviation of three independent passaging experiments, each including ten independently passaged lines.

2.3. Use of an RFLP marker in chromosome 13mini to measure chromosome loss frequency

As mentioned above, the effect of selection by the environment increases with multiple passaging steps, making it difficult to determine the "real" frequency of spontaneous loss of accessory chromosomes. In addition, the loss rate in the wild type strain detected in the long-term passaging experiment was already very high, leaving little space for detecting a possible increase in the rate that could be expected in mutants affected in chromosome stability.

In an attempt to solve these issues, we decided to conduct a very short passaging experiment. Since the frequency of chromosome loss was expected to be very low, we reasoned that it would be necessary to analyze a high number of passaged isolates resulting

in an elevated cost of qPCR reactions. We therefore considered using restriction fragment length polymorphism (RFLP) as an alternative that would be cheaper and more feasible for large-scale analysis. A further advantage of the RFLP technique over qPCR is that it allows rapid and unequivocal detection of the presence/absence of chromosome copies based on the differential banding pattern obtained after enzymatic treatment.

2.3.1 Generation of a strain carrying an RFLP marker in one of the duplicated regions of chromosome 13

To assess the dynamics of loss of chromosomes 15 and 13mini, we initially intended to tag one of the duplicated regions for both chromosomes by introducing a new restriction site as an RFLP marker via homologous recombination (Franco-Cano, 2021). To this aim, a linear construct was generated in which an SNP was artificially introduced to generate a recognition site for the *Xho*I restriction enzyme (Figure 77). This construct was used to co-transform protoplasts of Fol4287 together with the nourseothricin resistance (*Nat*^{R}) cassette. Nat^{R} transformants were screened for homologous insertion of the RFLP marker into one of the two duplicated regions of chromosome 13 by PCR with primers flanking the newly introduced restriction site and subsequent treatment with *Xho*I. Transformants carrying an RFLP in one copy of the duplicated region of chromosome 13 were expected to produce an electrophoretic pattern consisting of three bands: a 1.4 Kb band corresponding to the wild type allele without the RFLP site and two bands of 0.8 Kb and 0.6 Kb corresponding to the allele cut by *Xho*I (Figure 77A). We identified three transformants showing the expected banding pattern and used transformant C4-10 for subsequent assays (Figure 77B). Subsequent experiments showed that the RFLP site had inserted in chromosome 13 (Figure 77A). We also attempted to also generate an RFLP site in one of the repeated copies of chromosome 15. However, these efforts have so far remained unsuccessful (Franco-Cano, 2021).

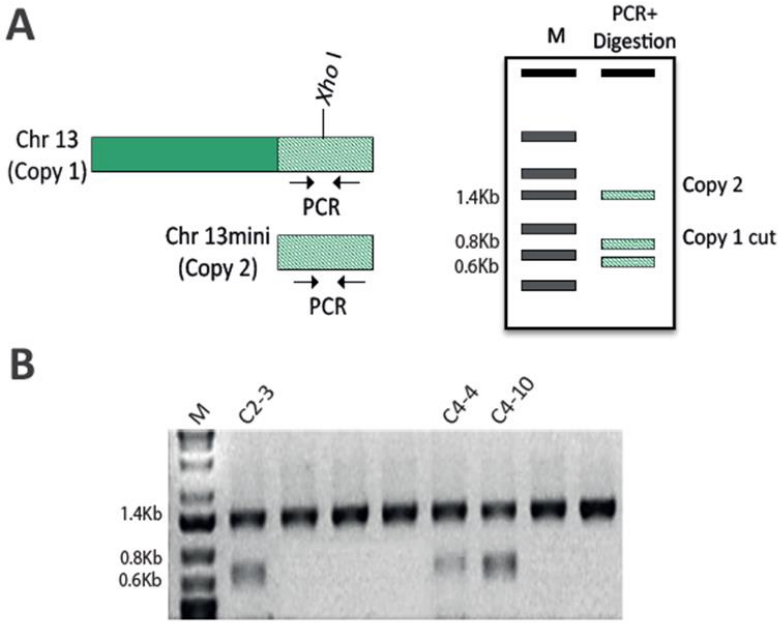

Figure 77. Generation of the RFLP13 strain carrying an RFLP marker in the duplicated region of chromosome 13. (A) Schematic representation of the insertion of an RFLP marker (*Xho*I recognition site) in the duplicated region of Chr13. The expected banding pattern after PCR and *Xho*I treatment, followed by agarose gel electrophoresis is shown on the right. **(B)** RFLP analysis of obtained transformants. gDNA was amplified by PCR using a pair of primers flanking the RFLP site and the PCR product was treated with the enzyme *Xho*I. The indicated transformants show a banding pattern consistent with insertion of the *Xho*I recognition site in one of the two copies of the duplicated region of Chr13.

2.3.2 A short-term serial passaging experiment on YPDA plates to measure chromosome loss frequency using the RFLP strategy

Once the RFLP strain for chromosome 13 (RFLP13) was obtained, we performed a short- term experiment to quantify the loss rate of chromosome 13mini in the near-absence of selection (Figure 78). Briefly, conidia of RFLP13 were plated on YPDA directly from the -80 °C stock. After two days, conidia were picked from three randomly chosen colonies (P1, P2, P3), resuspended in water and serial dilutions were plated on YPDA. After an additional two days, gDNA was isolated directly from 200 individual colonies derived from each progenitor (P1, P2, P3) and subjected to PCR and subsequent treatment with *Xho*I to determine presence/absence of chromosome 13mini.

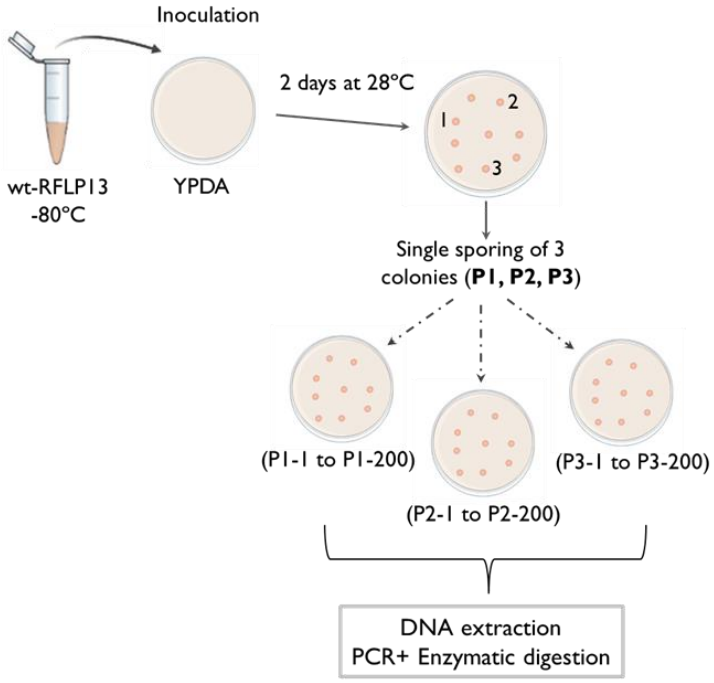

Figure 78. Schematic diagram of the short-term serial passaging experiment on YPDA plates. Microconidia of strain RFLP13 were directly plated from -80 °C onto YPDA plates and incubated at 28 °C for 2 days**.** Conidia from three randomly chosen colonies (clones P1-P3) were taken with a toothpick, diluted, plated on YPDA and incubated for 2 days at 28 °C. gDNA from 200 individual colonies of each clone was isolated and analyzed by PCR and *Xho*I treatment to determine loss of one copy of the duplicated region of chromosome 13.

We first confirmed that the three progenitor colonies (P1, P2, P3) still had both copies of the duplicated region (Figure 79A). Moreover, the wild type strain was also included as a negative control where only the 1.4 Kb band was detected due to the absence of the RFLP marker (Figure 79A). Among the 600 total colonies analysed from the derivatives of P1, P2 and P3, four (P2-73, P2-132, P3-17 and P3-55) had lost chromosome 13mini as indicated by the absence of the 1.4 Kb band. As controls we included the wild type strain (showing a single band) and colony P3-56 that has both duplicated regions of chromosome 13 (3 bands). While none of the colonies derived from P1 showed loss of chromosome 13mini (0%), the loss frequency in P2 and P3 was 1% each (2 positive colonies out of 200) Altogether, the average loss frequency for chromosome 13mini in this experimental condition and under near-absence of selection was estimated at 0.66% (bar graph).

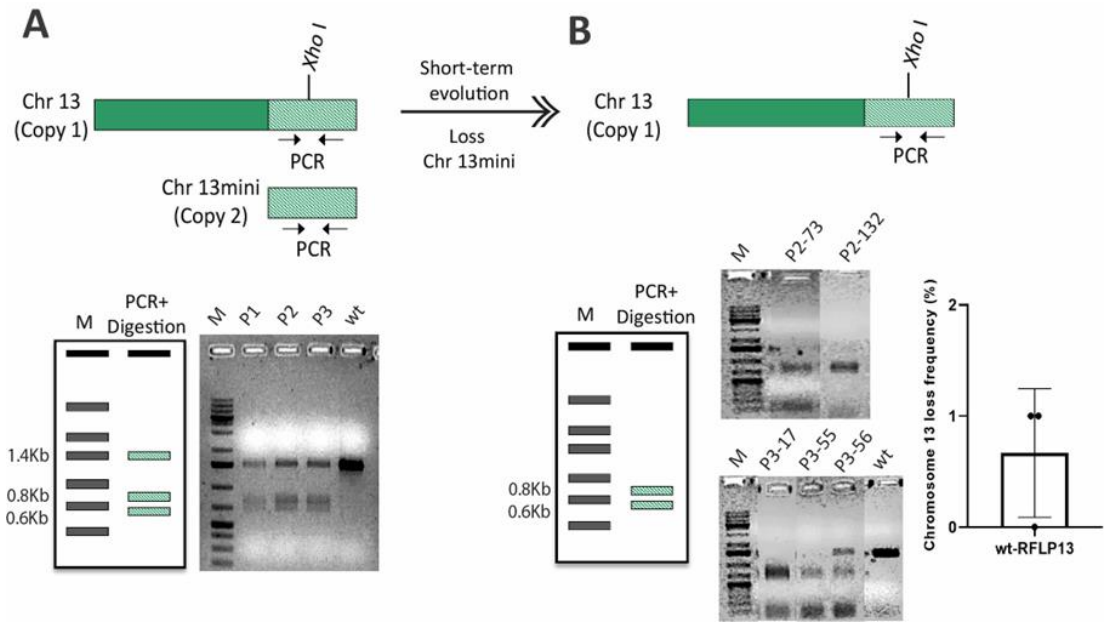

Figure 79. Determination of the rate of spontaneous loss of chromosome 13mini in the RFLP13 strain after the short-term serial passaging experiment. (A) Schematic diagram showing the strategy used for determining the copy number of the duplicated region of Chr13 in the progenitor colonies (clones P1-P3). PCR was performed with a pair of primers flanking the RFLP site followed by treatment with *Xho*I and agarose gel electrophoresis (see gel image). **(B)** Detection of spontaneous loss of Chr13mini after short-term serial passaging experiment using PCR and *Xho*I treatment of monoconidial isolate colonies derived from progenitor clones P1-P3. Gel images show the banding pattern of four colonies derived from progenitor clones P2 or P3 that have lost Chr13mini, (P2-73, P2-132, P3-17, P3-55), as well as of one colony (P3-56) derived from clone P3 which maintains both duplicated regions and the wild type as controls. The graph shows the mean and standard deviation of spontaneous chromosome loss calculated from 200 colonies analysed for each of the three independent passaged lines (P1, P2, P3).

SUBCHAPTER 3.3: Mechanisms involved in chromosomal rearrangements of Fol*4287*

1. Introduction

Fungal pathogens show high genome variability that is frequently manifested in copy number variations and chromosomal rearrangements. There is a growing interest in elucidating the mechanisms underlying these rearrangements. Recent results obtained in other fungal pathogens and yeasts seem to indicate that DNA repair pathways and chromatin structure are involved in maintaining chromosome stability (Argueso *et al.,* 2008; Möller *et al.,* 2019). This chapter describes the obtaining of knockout mutants in genes involved in both processes, their phenotypical characterization, and their possible involvement in the processes of loss of accessory chromosomes in *Fol4287*.

2. Results

2.1. In silico identification of the *rad1*, *ku70* and *lig4* orthologs in Fol4287

A *BLASTp* search in the *Fol4287* genome was performed (together with Cristina López Díaz) with the amino acid sequences of Rad1, Ku70 and Dnl4 of *S. cerevisiae*, involved in different double strand DNA break repair pathways (Table 30). *In silico* analysis with the *S. cerevisiae* Rad1 sequence identified a single ortholog in Fol4287 (*FOXG_03142*) annotated as "DNA excision repair protein ERCC-4". This gene, located on chromosome 8, encodes a predicted 937 amino acid protein that exhibits 35% identity with Rad1 of *S. cerevisiae* and more than 50% identity with Rad1 proteins from the ascomycete fungi *N. crassa* (*NCU_07440*, 77%), *M. oryzae* (*MGG_02804*, 73%) and *A. nidulans* (*AN_8713*, 57%). Similarly, *BLASTp* search with the *S. cerevisiae* Ku70 sequence resulted in the identification of a single ortholog in Fol4287 (*FOXG_06386*) annotated as "ATP-dependent DNA helicase II subunit 1". This gene, located on chromosome 2, encodes a 644 amino acid protein with 23% identity with Ku70 of *S. cerevisiae* and more than 50% identity with the ascomycete fungi *N. crassa* (*NCU_08290*, 64%), *M. oryzae* (*MGG_01512*, 61%) and *A. nidulans* (*AN_7753*, 55%). Finally, BLASTp analysis with *S. cerevisiae* Dnl4 sequence identified a single ortholog in Fol4287 (*FOXG_11480*) annotated as "DNA ligase 4". This gene, located on chromosome 10, encodes a 984 amino acid protein that exhibits 29% identity with Dnl4 of *S. cerevisiae* and more than 50% identity with Lig4 proteins from the ascomycete fungi *M. oryzae* (*MGG_12899*, 62%), *N. crassa* (*NCU_06264*, 59%) and *A. nidulans* (*AN_0097*, 57%).

Table 30. Identities between the deduced amino acid sequences of the rad1, ku70 and lig4 genes of Fol4287 and their orthologs in other ascomycete fungi using BLASTp analysis. *N. crassa* (NCU), *M. oryzae* (MGG), *A. nidulans* (AN), and *S. cerevisiae* (YPL, YMR , YOR).

PROTEIN	GENE	Nº aa	IDENTITY
DNA excision repair protein ERCC-4 (Rad1)	*FOXG_03142*	937	*NCU_07440* (77%) *MGG_02804* (73%) *AN_8713* (57%) *YPL022W* (35%)
ATP-dependent DNA helicase II subunit 1 (Ku70)	*FOXG_06386*	644	*NCU_08290* (64%) *MGG_01512* (61%) *AN_7753* (55%) *YMR284W* (23%)
DNA ligase 4 (Lig4)	*FOXG_11480*	984	*NCU_06264* (59%) *MGG_12899* (62%) *AN_0097* (57%) *YOR005C* (29%)

2.2. Targeted deletion of *rad1*, *ku70* and *lig4* genes involved in repairing damaged DNA

To investigate a possible role of double strand DNA break repair mechanisms in accessory chromosome stability of *Fol4287*, previously obtained knockout mutants in *rad1*, *ku70* and *lig4* genes were used (López-Díaz, unpublished). The mutants had been generated by replacing the ORF of each gene by the *Hyg*^{R} cassette using the "Split-Marker" technique (Figures 80A-82A). The two constructs obtained, each containing a flanking region of the gene and 75% of the *Hyg*^{R} cassette, were used to transform protoplasts of the wild type strain *Fol4287*. PCR analysis of the Hyg^R transformants with a primer pair that hybridizes inside of the ORF was performed to confirm if homologous insertion and consequent gene deletion had occurred (Figures 80B-82B). We also attempted to generate knockout mutants in the rad52 gene, involve in homologous recombination DNA repair pathway, but failed to detect any transformants carrying a homologous insertion of the deletion construct (results not shown).

PCR analysis of the DNA of the knockout strains revealed a minor contamination with the wild type strain. We therefore performed a third round of monoconidial purification and conducted further PCR analysis to confirm the purity of these mutants including both, the primary transformants and the monoconidial isolates purified thereof, and in all cases the absence of mixing with the wild type strain was subsequently confirmed.

Selected candidate knockout strains were further analyzed by Southern blot to confirm the insertion of a single copy of the construct into the genome. The gDNA of the wild type strain and putative knockouts in *rad1*, *ku70* and *lig4* genes were treated with the restriction enzymes *BamH*I, *Sal*I or *Nco*I, respectively. Hybridization with a probe located in the terminator region of the *rad1* gene showed replacement of the 2.7 Kb hybridizing band of the wild type *rad1* allele by a 7.0 Kb band in the Δ*rad1* transformants #2.1 #3.1 and #8.2, indicating that a single homologous replacement event had occurred (Figure 80C). For its part, hybridization with a probe located in the promoter region of the *ku70* gene also confirmed the homologous insertion of the deletion construct in transformants Δ*ku70* #7.2 and #9.2, as indicated by replacement of the 2.7 Kb hybridizing band of the wild type *ku70* allele by a band of the expected size of 4.6 Kb (Figure 81C). Finally, the correct deletion of the *lig4* gene was confirmed in the Δ*lig4* transformants #3.1 and #6.1 as shown by replacement of the 8.0 Kb hybridizing band of the wild type *lig4* allele by a band of 3.0 Kb (Figure 82C).

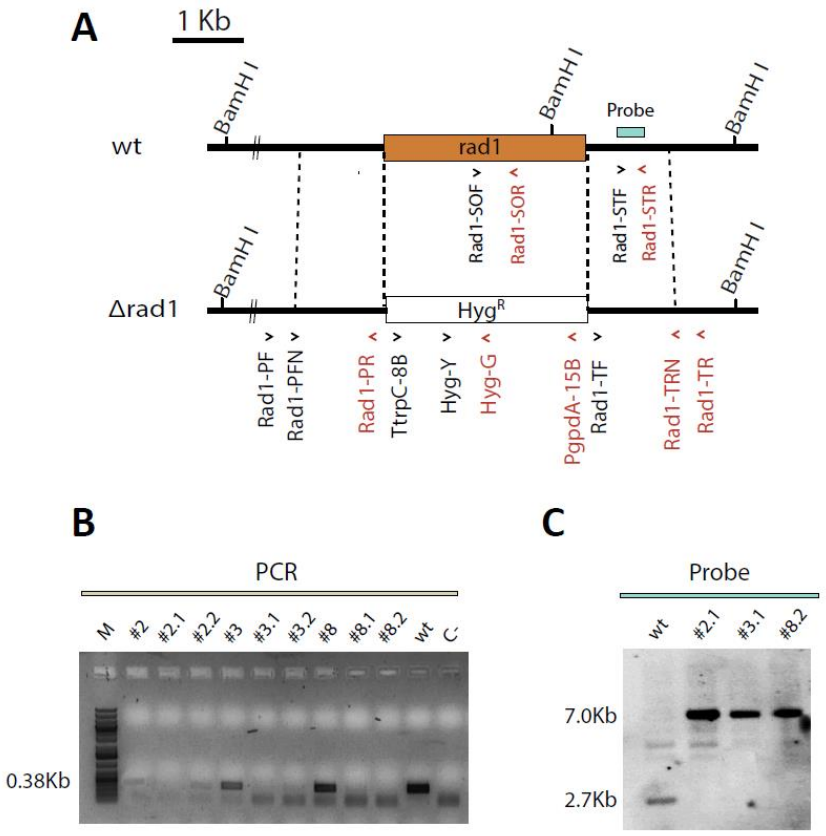

Figure 80. Targeted deletion of the F. oxysporum rad1 gene. (A) Physical structure of the *rad1* locus and strategy for the replacement of the coding region with the split-marker method using the *Hyg*^{R} cassette as selective marker. Positions of *BamH*I restriction sites are shown. Black (forward) and red (reverse) arrowheads indicate the positions of primers used for generation of the gene disruption constructs and for PCR analyses of the transformants; the probe used for Southern blot analysis is indicated (blue bar). Scale bar indicates 1kb. **(B)** PCR analysis to confirm the deletion of

the open reading frame (ORF) using the primers Rad1-SOF/Rad1-SOR. **(C)** Identification of deletion mutants by Southern blot analysis. gDNAs of wild type strain and putative Δ*rad1* transformants were treated with *BamH*I, separated in an agarose gel, transferred to a nylon membrane and hybridized with the probe. Sizes of hybridizing bands are indicated on the left.

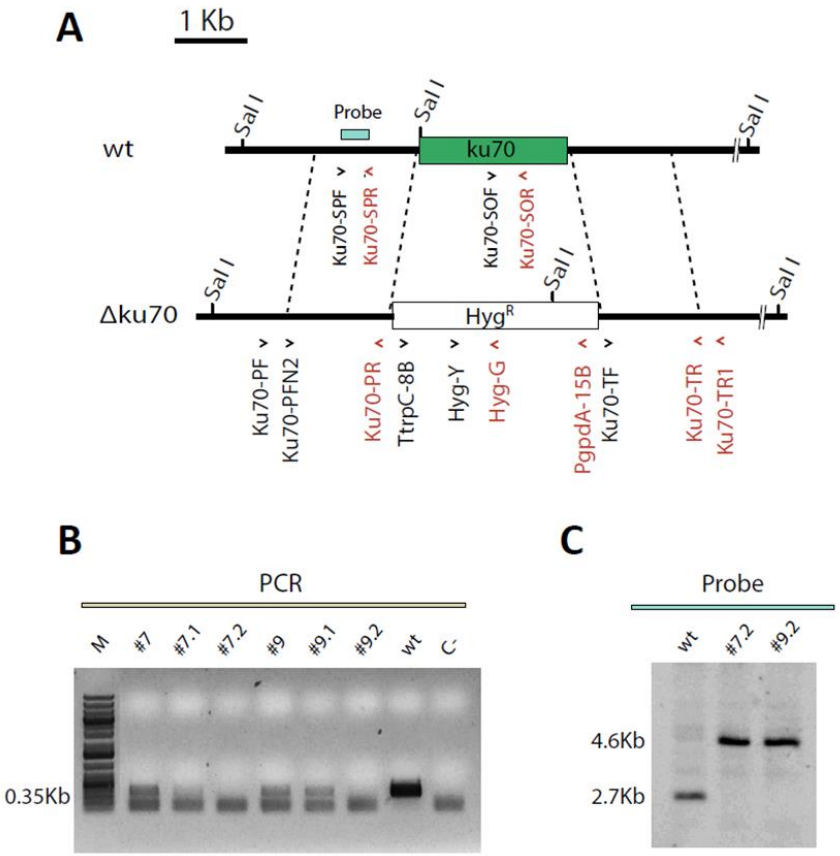

Figure 81. Targeted deletion of the F. oxysporum ku70 gene. (A) Physical structure of the *ku70* locus and strategy for the replacement of the coding region with the split-marker method using the *Hyg*^{R} cassette as selective marker. Positions of *Sal*I restriction sites are shown. Black (forward) and red (reverse) arrowheads indicate the positions of primers used for generation of the gene disruption constructs and PCR analyses of the transformants; the probe used for Southern blot analysis is indicated (blue bar). Scale bar indicates 1kb. **(B)** PCR analysis to confirm the deletion of the open reading frame (ORF) using the primers Ku70-SOF/Ku70-SOR. **(C)** Identification of deletion mutants by Southern blot analysis. gDNAs of wild type strain and putative Δ*ku70* transformants were treated with *Sal*I, separated in an agarose gel, transferred to a nylon membrane and hybridized with the probe. Sizes of hybridizing bands are indicated on the left.

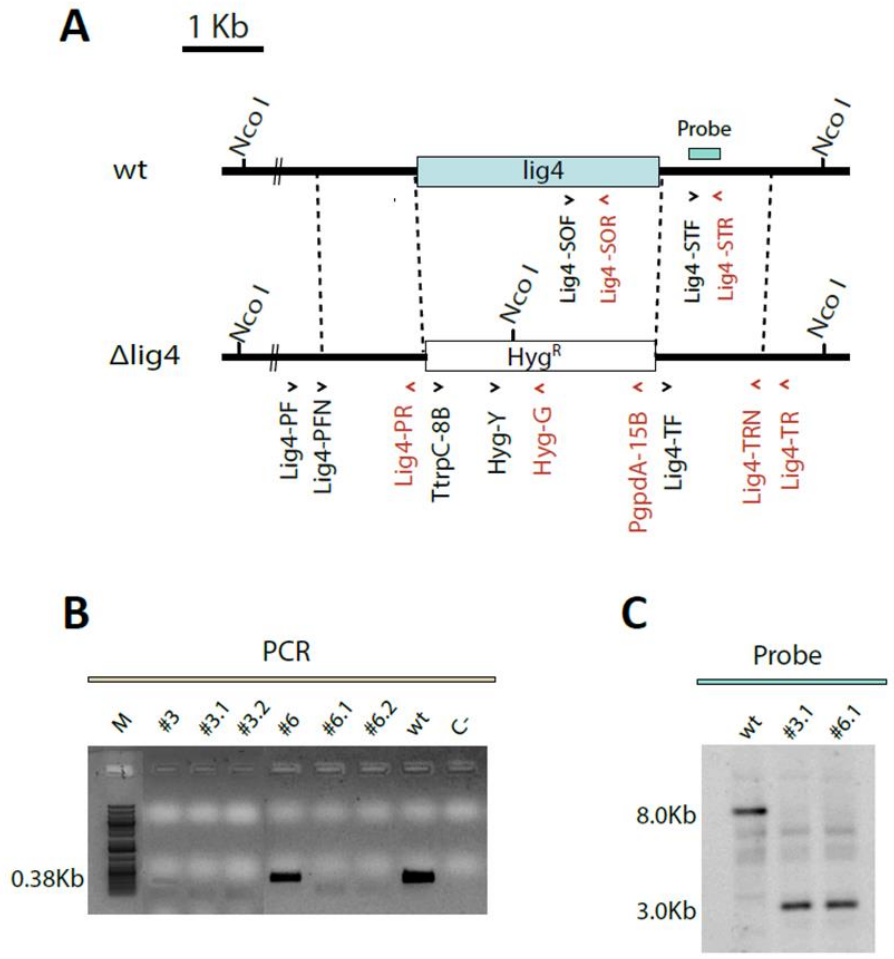

Figure 82. Targeted deletion of the F. oxysporum lig4 gene. (A) Physical structure of the *lig4* locus and strategy for the replacement of the coding region with the split-marker method using the *Hyg*^{R} cassette as selective marker. Positions of *Nco*I restriction sites are shown. Black (forward) and red (reverse) arrowheads indicate the position of primers used for generation of the gene disruption constructs and PCR analyses of the transformants; the probe used for Southern blot analysis is indicated (blue bar). Scale bar indicates 1kb. **(B)** PCR analysis to confirm the deletion of the open reading frame (ORF) using the primers Lig4-SOF/Lig4-SOR. **(C)** Identification of deletion mutants by Southern blot analysis. gDNAs of wild type strain and putative Δ*lig4* transformants were treated with *Nco*I, separated in an agarose gel, transferred to a nylon membrane and hybridized with the probe. Sizes of hybridizing bands are indicated on the left.

2.3. Phenotypic characterization of Δrad1, Δlig4 and Δku70 mutants

2.3.1 Deletion of rad1 severely impacts growth and conidiation on solid medium

To investigate if the deletion of the *rad1*, *ku70* and *lig4* genes influences vegetative hyphal growth, 10^6 conidia of the wild type strain and the different mutants were spot-inoculated at the center of YPDA plates and incubated at 28 °C. Plates were scanned after 48h and 72h and growth rate was calculated by measuring the increase in colony area between the two time points referenced to that of the wild type strain (Figure 83A). Both Δ*rad1* mutants exhibit greatly reduced growth compared to the wild type strain, while no

significant differences in growth speed were detected for the Δ*lig4* and Δ*ku70* mutants (Figure 83B).

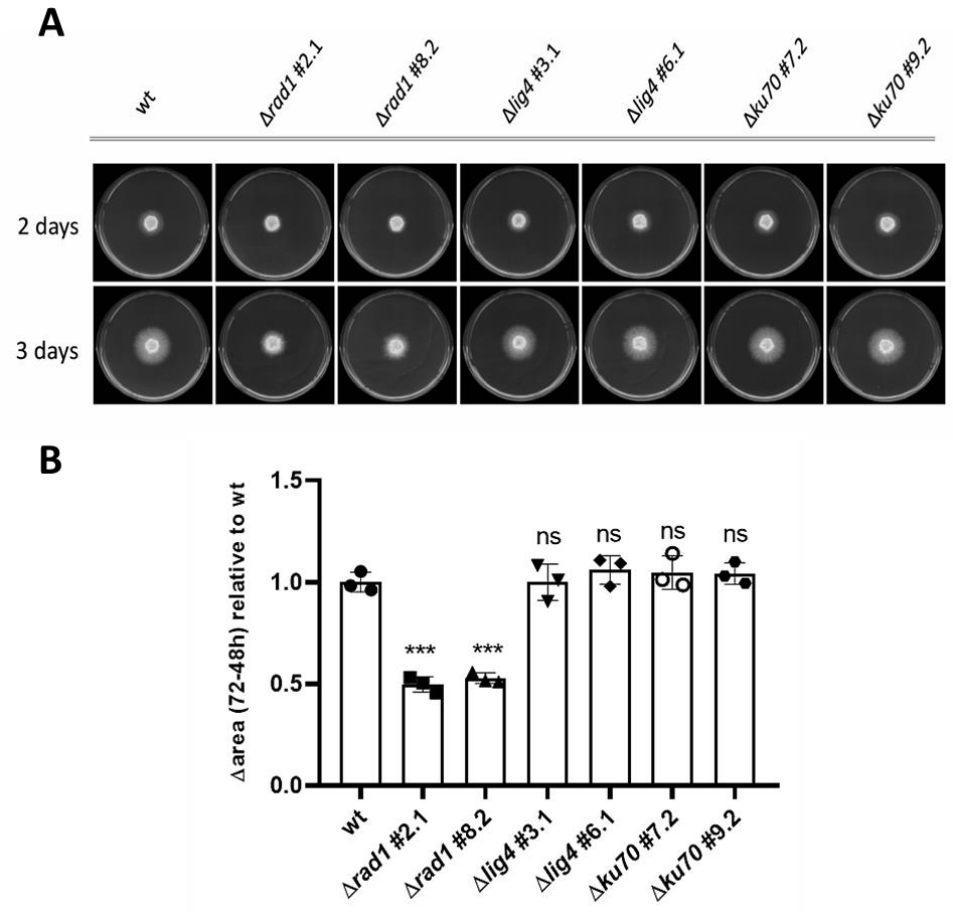

Figure 83. Colony growth speed of Δrad1, Δlig4 and Δku70 mutants. (A) Aliquots of 10^6 microconidia were spot inoculated on the center of YPDA plates and incubated at 28 °C for 3 days. **(B)** Increase in colony area relative to wild type strain. Plates were scanned at 48h and 72h and the growth rate was calculated by measuring the increase in the colony area between the two time points. Data shown represent the mean and standard deviations of three independent replicates for each strain. *** $p<0.001$ versus wild type according to t-test; ns, non-significant.

The role of Rad1, Lig4 and Ku70 in conidiation of *Fol4287* was investigated by spot-inoculating 10^6 conidia on the center of YPDA plates. After 7 days the conidia were collected from the entire colony and counted. Both Δ*rad1* mutants produced significantly fewer conidia than the wild type strain, whereas the conidiation of the Δ*lig4* and Δ*ku70* mutants was not significantly affected (Figure 84). These observations indicate that Rad1 is required for normal hyphal growth and conidiation in *Fol4287*.

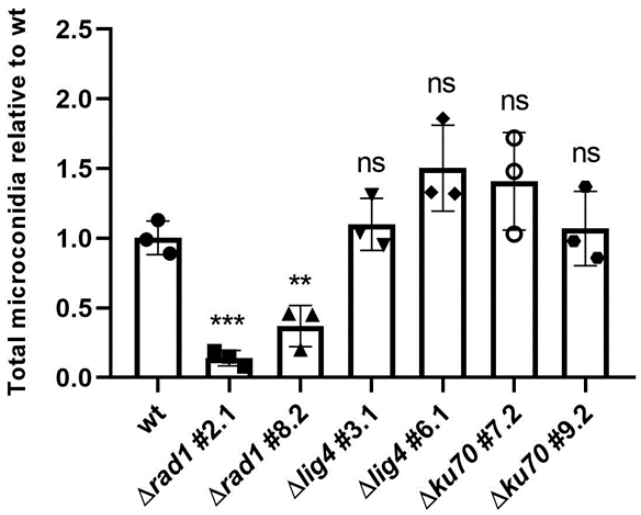

Figure 84. Conidiation rate of Δrad1, Δlig4 and Δku70 mutants. Aliquots of 10^6 microconidia were spot inoculated on the center of YPDA plates and incubated at 28 °C for 7 days. Microconidia were collected from the entire colony and counted to calculate the total amount of conidia relative to wild type strain. Data shown represent the mean and standard deviations of three independent replicates for each strain. ** p<0.01, *** p<0.001 versus wild type according to t-test; ns, non-significant.

2.3.2 Sensitivity of Δrad1, Δlig4 and Δku70 mutants to the DNA-damaging agent methyl methanesulfonate

To explore the role of Rad1, Lig4 and Ku70 in DNA damage responses, $1x10^7$ conidia of the wild type strain and the different mutants were treated with 0.1% MMS or water (control) for 1 or 2 hours, heated for 5 minutes at 50 °C to promote the rupture of the thermolabile sites formed during MMS treatment, and serial dilutions were spot-inoculated on PDA plates and scanned after 2 days. The MMS treatment produced a detectable decrease in colony growth of the wild type strain (Figure 85). Both *Δrad1* mutants showed reduced survival after MMS treatment compared to the wild type strain. This effect was more pronounced after 2 hours of exposure to the DNA-damaging agent. The rest of the mutants analyzed only showed a slight increase in sensitivity after the 2 hour treatment.

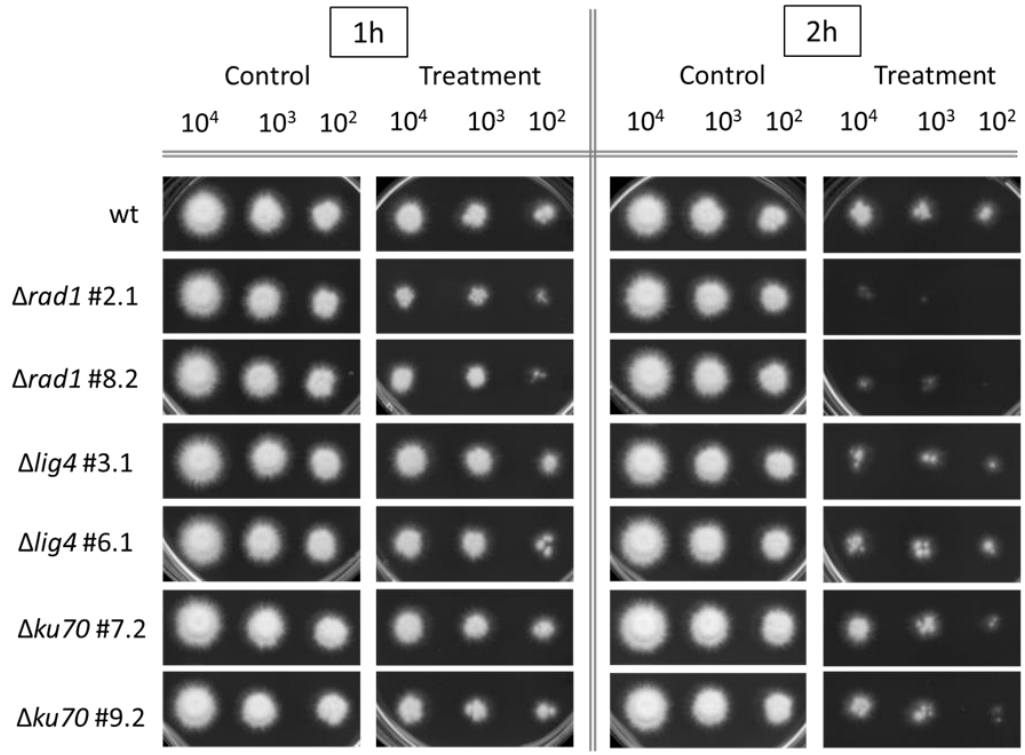

Figure 85. Sensitivity of Δrad1, Δlig4 and Δku70 mutants to the DNA-damaging agent methyl methane sulfonate. Aliquots of 10^7 microconidia were suspended in Milli-Q water, either supplemented or not (control) with 0.1% MMS, incubated for 1 or 2 hours at 28 °C and transferred for 5 minutes to 50 °C. Droplets from serial dilutions containing 10^4, 10^3 and 10^2 microconidia were spot inoculated on PDA plates, incubated at 28 °C for 2 days and scanned. Three independent replicates were made. images show the results from one representative replicate.

2.4. Both duplicated regions of chromosomes 13 and 15 are still present in Δ*rad1*, Δ*lig4* and Δ*ku70* mutants

As our main objective was to compare the frequency of loss of chromosomes 15 and 13mini in the Δ*rad1, Δlig4 and Δku70* mutants with the wild type strain, we first needed to confirm that these mutants still carried both copies of the duplicated regions. A qPCR analysis with two specific primer pairs of the duplicated regions of chromosomes 13 and 15 revealed that all the tested mutants had two copies of both regions, except for the Δ*rad1* #3.1 mutant that hat had lost the copy corresponding to chromosome 13mini during the purification process (Figure 86). This mutant was therefore excluded from subsequent analyses.

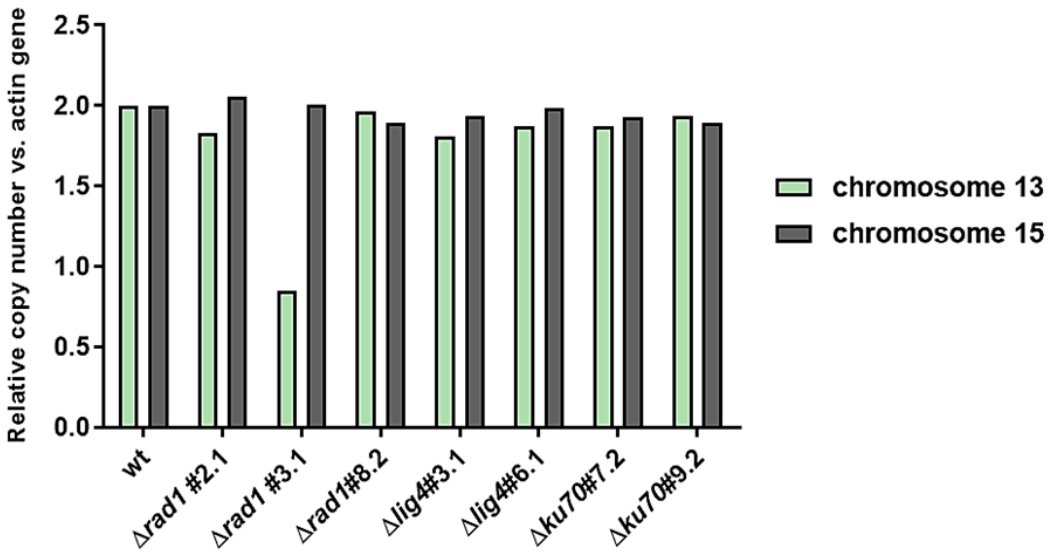

Figure 86. Determination of copy numbers of the duplicated regions of chromosomes 13 and 15 in the obtained knockout mutants. qPCR with specific primers of the duplicated regions of chromosomes 13 and 15 was performed on gDNA of the wild type strain Fol4287 and of the Δ*rad1*, Δ*lig4* and Δ*ku70* mutants. Copy numbers were calculated relative to the actin gene and wild type strain which has two copies of both regions.

To further confirm that the selected mutants had both duplicated regions of chromosomes 13 and 15, a karyotype analysis was performed by separating the chromosomes of the Δ*rad1*, Δ*lig4* and Δ*ku70* mutants by CHEF electrophoresis (Figure 87A) and carrying out subsequent Southern blot analysis with specific probes for the duplicated regions of chromosomes 13 and 15. In agreement with the results of the previous qPCR analysis, we found that these mutants still carry the chromosomes 15 and 13mini (Figure 87B).

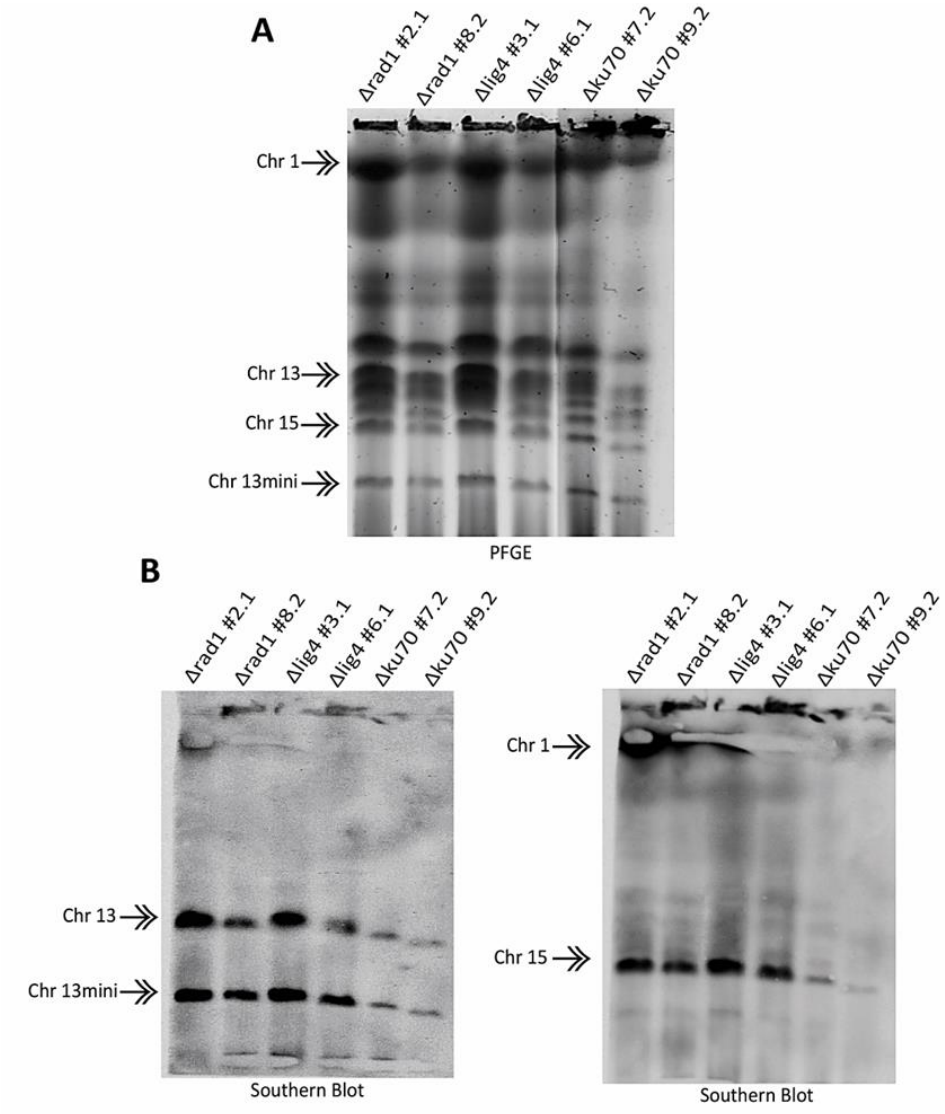

Figure 87. Karyotype analysis confirms the presence of duplicated regions of chromosomes 13 and 15 in the knockout mutants. Contour-clamped homogeneous electric field (CHEF) electrophoresis of Δ*rad1*, Δ*lig4* and Δ*ku70* mutants was performed. **(A)** Visualization of chromosome bands after CHEF electrophoresis by gel red staining. **(B)** Southern blot analysis with specific probes for chromosomes 13 (left) or 15 (right) validates the presence of the duplicated regions of both chromosomes in all the tested mutants.

2.5. Δrad1, Δlig4 and Δku70 mutants show a high loss rate of chromosomes 15 and 13mini in a long-term serial passaging experiment

To investigate the possible role of DNA damage repair mechanisms in accessory chromosome stability of *Fol4287*, the Δ*rad1*, Δ*lig4* and Δ*ku70* mutants were subjected to both long-term and short-term serial passaging experiments, as described previously for the wild type strain (subchapter 3.2, Figures 75 and 78). For the long-term experiment, 30 independent lines from each of the tested strains were subjected to ten serial passages on YPDA medium. The gDNA obtained from the mycelium collected from the last passage was

subjected to qPCR analysis with primers specific for the duplicated regions of chromosomes 13 and 15 to measure the frequency of chromosome loss (Figure 88 and table S1). All the tested mutants showed a higher loss rate of chromosome 13mini than the wild type strain (increase of 12% to 23%). However, due to the relatively high loss frequency of the wild type strain and the fact that the loss frequency in some of the mutants was close to 100%, the observed increase was statistically not significant (P values 0.13 to 0.23). In the case of chromosome 15, the differences between the wild type strain and the different mutants were less clear. All the mutants except Δ*lig4* #6.1, showed a reduced loss rate of chromosome 15 than the wild type strain, although the difference was only significant for the Δ*rad1* #2.1 mutant (P value = 0.031) due to the lower variability between the evolved lines. In summary, these results did not reveal a direct and unequivocal link between loss of the accessory chromosomes to a specific DNA repair pathway.

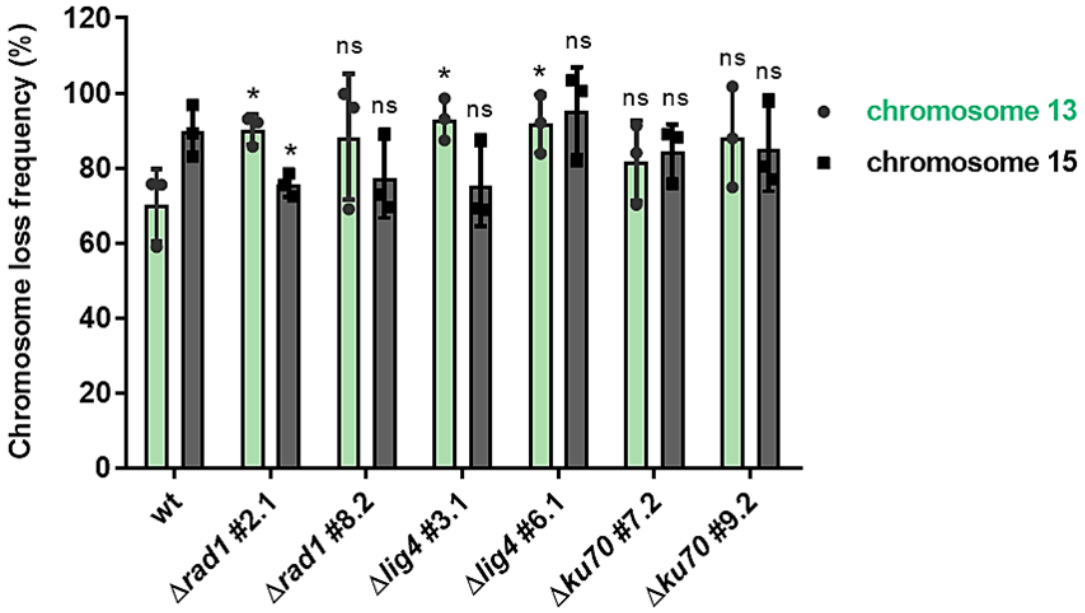

Figure 88. Frequency of spontaneous loss of chromosomes 13mini or 15 in mutants in DNA damage repair genes after ten serial passages on YPDA plates. The wild type strain Fol4287 and Δ*rad1*, Δ*lig4* and Δ*ku70* mutants were subjected to ten serial passages on YPDA medium. After the 10th passage, gDNA was isolated from passaged populations and subjected to qPCR using specific primers of the duplicated regions of both chromosomes against the actin gene as a reference, to determine the rate of chromosome loss in the population. Data shown represent the mean and standard deviations of three independent passaging experiments, each including ten independently passaged lines. * $p<0.05$ versus wild type according to t-test; ns, non-significant.

2.6. Measuring loss frequency of chromosome 13mini in knockout mutants affected in DNA repair or chromatin structure

One of the drawbacks of long-term serial passaging experiments is that selection can lead to the emergence of beneficial mutations that may distort the observed frequencies of chromosome loss, thereby masking the effect of DNA repair gene mutations on chromosomal stability (see subchapter 3.2). Therefore, we decided to conduct a short-term serial passaging experiment which minimizes the effect of selection, using the RFLP technique to measure spontaneous loss of chromosome 13mini (see Figure 78). To this aim, we generated again the knockout mutants in the *rad1*, *lig4* and *ku70* genes in the RFLP13 genetic background. Several candidate knockout mutants were identified obtained for each of the three genes of interest, although only the Δ*rad1*-RFLP13 strain was analyzed in this study.

In addition to these genes involved in repairing damaged DNA, a mutant in the *kmt1* gene was obtained. This gene encodes a methyltransferase responsible for introducing the heterochromatin epigenetic mark H3K9me3 into the DNA. This methylation mark contributes to genomic stability, with *Z. tritici* Δ*kmt1* mutants showing a higher frequency of rearrangements and chromosomal losses (Möller *et al.,* 2019). Through *BLASTp* analysis with the amino acid sequences of the Kmt1 proteins from *Z. tritici* and DIM-5 from *N. crassa*, we identified the ortholog protein in *Fol4287* encoded by the *FOXG_10263* gene with an identity of 34.5% and 61.3%, respectively.

2.6.1 Generation of a Δrad1-RFLP13 strain

To delete the *rad1* gene in the RFLP13 background (see Fig. 77), the split marker technique was used (Figure 89A). To confirm insertion of the construct at the homologous region, the Hyg^R transformants were analyzed by PCR using two different pairs of primers that hybridize outside of the fragments used for transformation and inside of the resistance cassette (Figure 89B). Almost all transformants analyzed showed an amplification band of the expected size for both the promoter (1.5 Kb) and terminator (1.6 Kb) regions. These transformants were further analyzed by Southern blot to confirm the insertion of a single copy into the genome. The gDNA of the wild type strain and the different transformants was treated with the restriction enzyme *BamH*I. Hybridization with a probe located in the terminator region of the *rad1* gene showed replacement of the 2.7 Kb hybridizing band of the wild type *rad1* allele by a 7.0 Kb band in the Δ*rad1*-RFLP13 #2, #3, #4, #5, #6 and #11 transformants, indicating that homologous recombination had occurred (Figure 89C). Finally, we performed PCR analysis with primers flanking the RFLP site and subsequent treatment with *Xho*I to verify the presence of both duplicated regions of chromosome 13. Although all

mutants had the RFLP13 allele (0.8 Kb and 0.6 Kb bands resulting from the *Xho*I cut), the Δ*rad1*-RFLP13 #2 mutant had lost the chromosome 13mini during the purification process (absence of the 1.4 Kb band) (Figure 89D) and was thus discarded from further analysis.

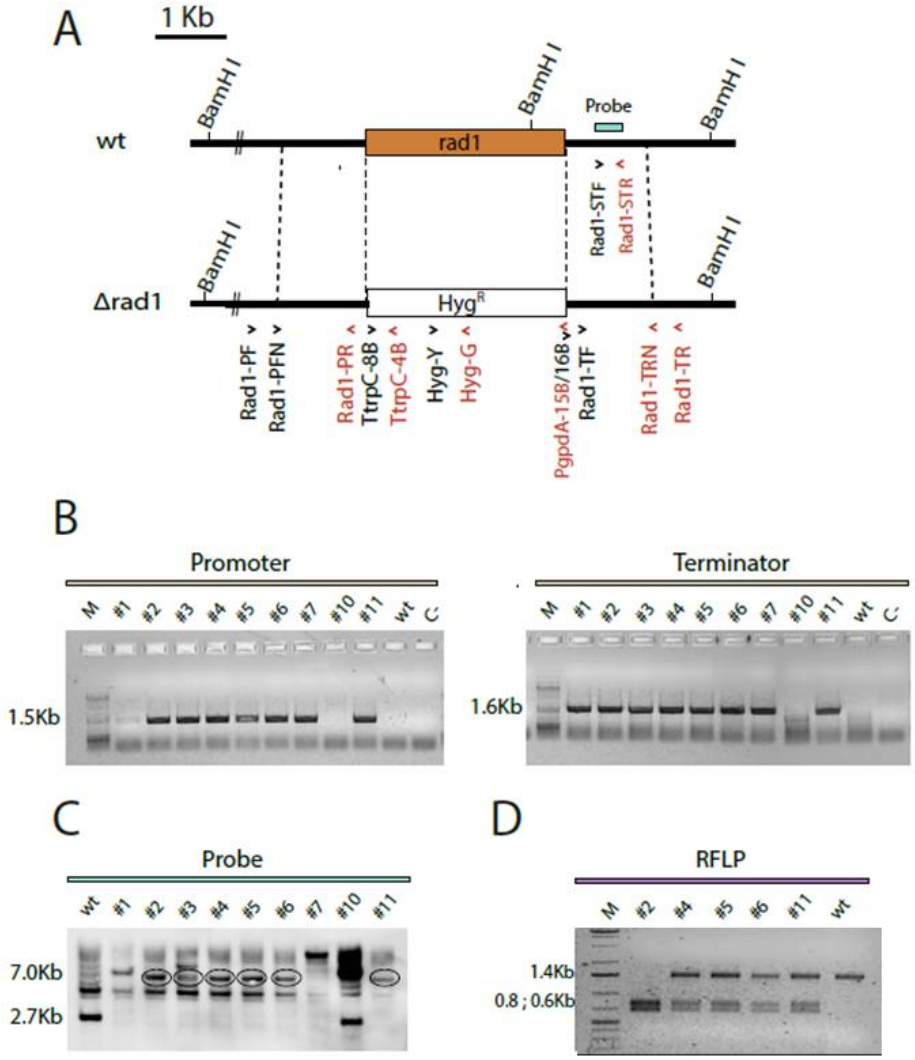

Figure 89. Generation of a Δrad1 gene deletion mutant in the RFLP13 genetic background carrying an RFLP marker in the duplicated region of chromosome 13. (A) Physical structure of the *rad1* locus and strategy for the replacement of the coding region with the split-marker method using the *Hyg*^{R} cassette as selective marker. Positions of *BamH*I restriction sites are shown. Black (forward) and red (reverse) arrowheads indicate the position of primers used for generation of the gene disruption constructs and PCR analyses of the transformants; the probe used for Southern blot analysis is indicated (blue bar). Scale bar indicates 1kb. **(B)** PCR analysis to confirm homologous integration of the construct into the genome of the transformants using the primer pairs: Rad1-PF/TtrpC-4B (promoter region) and PgpdA-16B/Rad1-TR (terminator region). **(C)** Identification of deletion mutants by Southern blot analysis. gDNAs of wild type strain and putative Δ*rad1*-RFLP13 transformants were treated with *BamH*I, separated in an agarose gel, transferred to a nylon membrane and hybridized with the probe. **(D)** Analysis of Δ*rad1*-RFLP13 transformants by RFLP technique. gDNA of the wild type strain (control) and transformants was amplified by PCR using a pair of primers flanking the RFLP site and the PCR product was treated with the *Xho*I enzyme, to determine the presence or absence of both copies of the duplicated region of chromosome 13.

2.6.2 Δrad1-RFLP13 transformants are significantly affected in growth on solid medium

We next performed a growth assay on solid YPDA medium to confirm the phenotype of the Δ*rad1*-RFLP13 mutants as described above. The Δ*rad1* #2.1 mutant obtained in the wild type background was included as a positive control. The growth speed of the Δ*rad1*-RFLP13 transformants was approximately half that of the wild type strain, except for Δ*rad1*-RFLP13 #1 which showed a similar growth rate as the wild type, confirming the absence of gene deletion in this transformant (Figure 90).

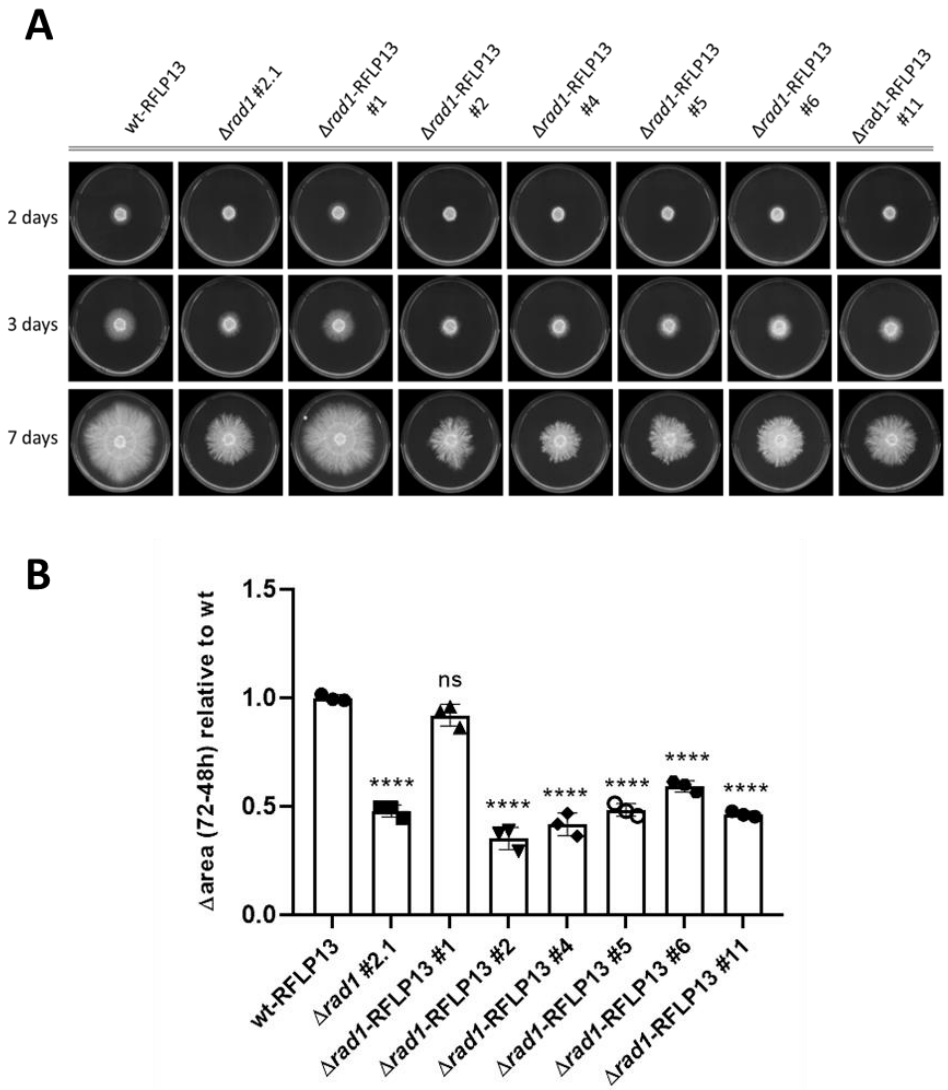

Figure 90. Colony growth speed of Δrad1-RFLP13 transformants. (A) Aliquots of 10^6 microconidia were spot inoculated on the center of YPDA plates and incubated for 7 days at 28 °C. The mutant Δ*rad1* #2.1 obtained in the wild type background was included as a positive control. **(B)** Increase in colony area relative to wild type strain. Plates were scanned at 48h and 72h and the growth rate was calculated by measuring the increase in the colony area between the two time points normalized relative to the wild type. Data shown represent the mean and standard deviations of three independent replicates for each strain. **** $p<0.0001$ versus wild type according to t-test; ns, non-significant.

2.6.3 Generation of a Δkmt1-RFLP13 strain

Using the "Split-marker" technique, the ORF of *kmt1* gene was replaced by the *Hyg*^{R} cassette in protoplasts of the RFLP13 strain (Figure 91A). PCR analysis of the Hyg^R transformants with two different pairs of primers that hybridize outside of the fragments used for transformation and inside of the resistance cassette was performed to confirm if homologous insertion and consequent gene deletion had occurred (Figure 91B).

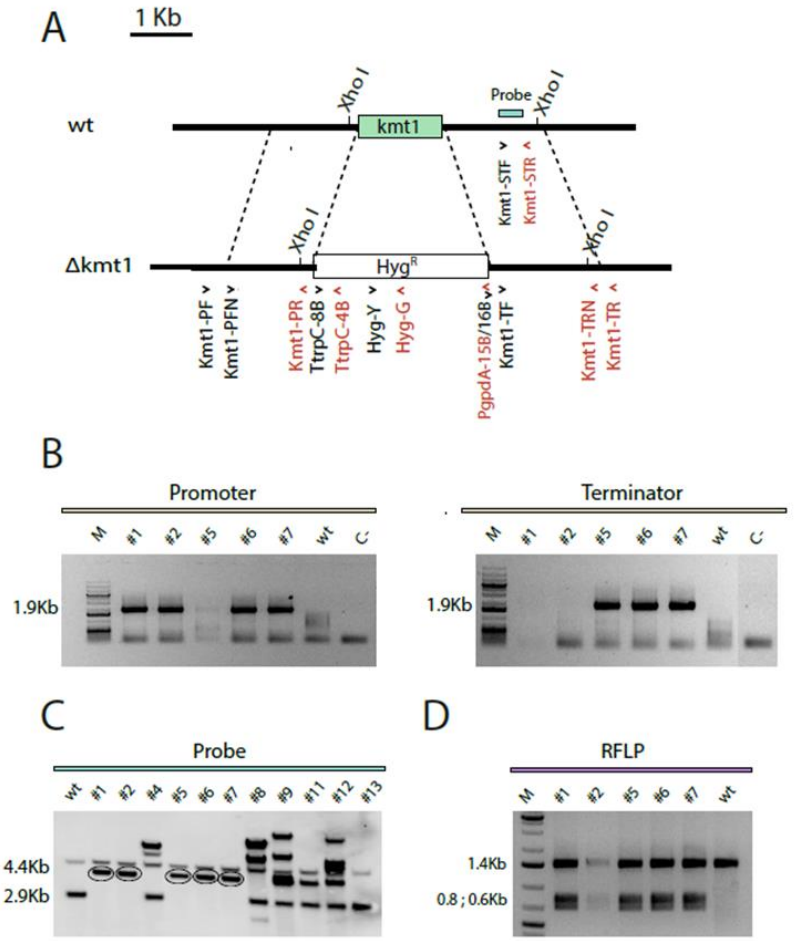

Figure 91. Generation of a Δkmt1 gene deletion mutant in the RFLP13 genetic background carrying an RFLP marker in the duplicated region of chromosome 13. (A) Physical structure of the *kmt1* locus and strategy for the replacement of the coding region with the split-marker method using the *Hyg*^{R} cassette as selective marker. Positions of *Xho*I restriction sites are shown. Black (forward) and red (reverse) arrowheads indicate the position of primers used for generation of the gene disruption constructs and PCR analyses of the transformants; the probe used for Southern blot analysis is indicated (blue bar). Scale bar indicates 1kb. **(B)** PCR analysis to confirm homologous integration of the construct into the genome of the transformants using the primer pairs: Kmt1-PF/TtrpC-4B (promoter region) and PgpdA-16B/Kmt1-TR (terminator region). **(C)** Identification of deletion mutants by Southern blot analysis. gDNAs of wild type strain and putative Δ*kmt1*-RFLP13 transformants were treated with *Xho*I, separated in an agarose gel, transferred to a nylon membrane and hybridized with the probe. **(D)** Analysis of Δ*kmt1*-RFLP13 transformants by RFLP technique. gDNA of the wild type strain (control) and transformants was amplified by PCR using a pair of primers flanking the RFLP site and the PCR product was treated with the *Xho*I enzyme to determine the presence or absence of both copies of the duplicated region of chromosome 13.

Subsequent Southern blot analysis of gDNAs treated with the restriction enzyme *Xho*I and hybridized with a probe located in the terminator region of the *kmt1* gene revealed that the 2.9 Kb hybridizing band of the wild type *kmt1* allele had been replaced by a hybridizing band of the expected size of 4.4 Kb band in Δ*kmt1*-RFLP13 #1, #2, #5, #6 and #7 transformants, confirming that homologous insertion of the deletion construct had occurred (Figure 91C). PCR analysis using primers flanking the RFLP site and subsequent treatment with *Xho*I revealed that all the tested transformants carried the RFLP marker as well as both duplicated regions of chromosome 13 according to the banding pattern obtained (Figure 91D).

2.6.4 The Δkmt1, but not the Δrad1 mutant shows a higher loss rate of chromosome 13mini

To test the effect of *rad1* or *kmt1* deletion on accessory chromosome stability, the Δ*rad1*-RFLP13 #5 and the Δ*kmt1*-RFLP13 #7 mutants were used for a short-term serial passaging experiment as previously described for the wild type strain (Figure 78). Conidia of the two strains were plated on YPDA and allowed to grow for 2 days at 28 °C. The gDNA of three random colonies (clones P1-P3) was isolated to verify the presence of both copies of chromosome 13 in its genome, and serial conidial dilutions from each colony were plated on YPDA. After 2 days gDNA from 200 individual colonies per clone were tested for loss of 13mini using the RFLP technique. Previously, in the wild type strain, a total of 4 of the 600 colonies analyzed had shown loss of chromosome 13mini, resulting in an average loss frequency of 0.66% (see Figure 79).

The Δ*rad1*-RFLP13 #5 transformant showed the same overall loss frequency as the wild type strain (0.66%), since in clones P1 and P2 2 out of 200 colonies tested had lost the 13mini chromosome whereas none of the colonies derived from P3 showed loss of chromosome 13mini (0%), obtaining the same average loss frequency (Table 31 and Figure 92). In contrast, the Δ*kmt1*-RFLP13 #7 transformant showed an increased average loss frequency (2.38%) with a total of 14 colonies having lost chromosome 13mini. Although the difference is not statistically significant (P value = 0.13) due to the relatively high fluctuations between the 3 clones P1-P3. This represents a considerable increase compared to the wild type, suggesting a possible role of H3K9me3 methylation in the stability of accessory chromosome 13mini.

Table 31. Number of colonies showing loss of chromosome 13mini detected in three separate clones (P1-P3) of the wt, Δrad1 and Δkmt1 strains during a short-term serial passaging experiment (see Fig. 92).

Replicate	wt-RFLP13	Δ*rad1*-RFLP13	Δ*kmt1*-RFLP13
P1	0	2	3
P2	2	2	3
P3	2	0	8
Total loss	4	4	14
Total tested	600	599	588
Loss rate (%)	0.666	0.667	2.38

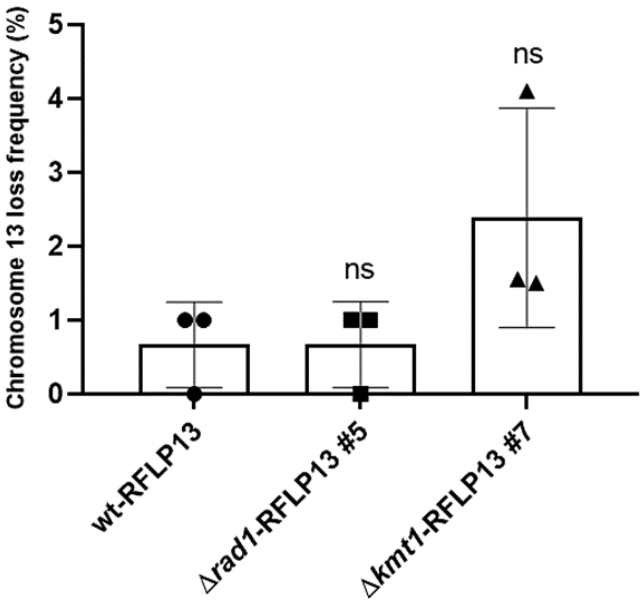

Figure 92. Rate of spontaneous loss of chromosome 13mini in wt, Δrad1 and Δkmt1 strains carrying the RFLP13 marker after short-term serial passaging experiment. Microconidia were directly inoculated from -80 °C on YPDA plates and incubated at 28 °C for 2 days. Conidia collected from three randomly chosen single colonies (clones P1, P2, P3) of each strain were plated on a fresh YPDA plate and incubated for an additional 2 days. gDNA obtained from 200 randomly chosen colonies from each clone was RFLP analysis was performed as described in Fig. 10D to determine the presence or absence of chromosome 13mini. The graph shows the mean and standard deviation of spontaneous chromosome loss calculated from 200 colonies analyzed for each of the three independent passaged lines (P1, P2, P3) per strain. ns, non-significant versus wild type according to t-test.

Discussion

3.1. Copy number variations in accessory regions as a mechanism of genome plasticity of Fol4287

Despite lacking a known sexual cycle, we find here that the fungal pathogen *F. oxysporum* displays a high genomic and phenotypic plasticity, which is likely to contribute to its evolutionary success, allowing it to cause vascular wilt on more than a hundred different crops. Moreover, a single isolate such as *Fol4287* can kill tomato plants, immunodepressed mice and the model insect host *Galleria mellonella* (Ortoneda *et al.,* 2004; Velasco-Navarro *et al.,* 2013). To analyze the genetic mechanisms underlying fungal adaptation, Dr. Cristina López Díaz subjected a clonal isolate of *Fol4287* to serial passages through different environmental conditions, including the host plant tomato as well as plates with complete or minimal media (López-Díaz, 2019).

The combination of experimental evolution with next-generation sequencing is an essential tool to identify, at the full-genome scale, the genetic changes in the passaged lines compared to the parental strain (Lang *et al.,* 2013; Schlötterer *et al.,* 2015). Genome sequencing of evolved *Fol4287* populations revealed four types of genetic variants, three of which (INDELs, TIVs and SNVs) were rather homogeneously distributed across all genomic regions (López-Díaz, 2019). However, the last type of genetic variation, large-scale CNVs, were exclusively observed in accessory or lineage specific (LS) regions of the genome as described in other pathogenic fungi like *Zymoseptoria tritici* (Fouché *et al.,* 2018) or *Verticillium dahliae* (Hartmann *et al.,* 2017; Shi-Kunne *et al.,* 2018). The high rate of CNVs and genomic rearrangements in these regions has been attributed to structural characteristics such as distinct chromatin status or presence of transposons and repeats, among others, which set them apart from the core regions (Bertazzoni e*t al.,* 2018; Yang *et al.,* 2020). It has been suggested that these features associated with accessory regions result in a more rapid accumulation of mutations and structural variations compared to core chromosomes, making accessory regions major drivers of genome plasticity. Consequently, it is generally accepted that the accessory genome evolves more rapidly, which gave rise to the "two-speed genome" concept (Croll *et al.,* 2012; Dong *et al.,* 2015).

3.2. The chromosome Chr13mini is a partial duplication of the end of chromosome 13

In this work we have discovered the presence, in the genome of *Fol4287*, of a new mini-chromosome called Chr13mini, which undergoes spontaneous loss during under certain environmental conditions. Previously, the existence of a duplicated region of

chromosome 13, whose location in the genome was unknown., had been reported (López-Díaz, 2019). In the present work, karyotype analysis by CHEF electrophoresis and Southern analysis with a specific probe revealed that one of the duplications was an independent chromosome that was not linked to another region. To further elucidate its composition and possible origin, single chromosome sequencing was performed on DNA of 13mini extracted from the corresponding band in the CHEF gel. It has previously been suggested that accessory chromosomes could originate from partial duplications of core chromosome regions, followed by degradation via breakage-fusion-bridge cycles (BFB) (Croll *et al.,* 2013). Here we confirmed that chr13mini it is a duplication of the end of core chromosome 13. Comparative sequence analysis of did not reveal significant SNPs between the two copies, suggesting either a very recent origin of this mini-chromosome or the presence of strong purifying selection. Our results are in agreement with a recent study in *M. oryzae* reporting the generation of mini-chromosomes via structural rearrangement and segmental duplication of chromosome ends (Langner *et al.,* 2021).

3.3. Other recurrent losses and gains of accessory chromosomes and regions in Fol4287

Besides chromosome losses, we also detected CNVs involving the spontaneous generation of new chromosomes in the passaged populations. One of these recurrent events involves the generation of chromosomes 6 by partial duplication of a region from chromosome 3. The originally sequenced strain of *Fol4287* contained both inter- and intra-chromosomal segmental duplications on chromosomes 3 and 6 (Ma *et al.,* 2010). Chromosome 3 has two divergent duplicated regions and, in addition, a region of this chromosome is duplicated in the reverse direction on chromosome 6. These segmental duplications showed 99% sequence identity indicating that they were recent duplication events (Ma *et al.,* 2010). Subsequently, this spontaneous generation of chromosome 6 from chromosome 3 could be confirmed during the experimental evolution experiments carried out in our group (López-Díaz *et al.,* 2019), suggesting that the first sequenced strain of Fol4287 had undergone a duplication event with respect to the original *Fol4287* strain stored in our laboratory. Since this original isolate was used as parental for serial passaging, Illumina sequencing and Southern blot analysis of the parental strain and the evolved lines revealed that the parental strain only carries chromosome 3 and that partial duplication had given rise to the new accessory chromosome 6.

In addition to this CNV (event "c"), we detected a second duplication event (event "d") in the region 3&6 in some of the passaged lines, that caused the disappearance of the

band corresponding to chromosome 6 and generated a new band with a size similar to that of chromosome 1. Interestingly, this event "d" was always detected in lines that also had undergone duplication event "c", but never independently. This finding gives rise to two hypotheses: 1) both events arise simultaneously, or 2) event "c" resulting in generation of chromosome 6 acts as an intermediate structure for the subsequent formation of the larger chromosome during event "d". Preliminary results by Southern blot analysis seem to indicate that the two events are independent from each other and that additional core chromosomes could be involved, although this hypothesis remains to be confirmed.

The original genome sequence of strain *Fol4287* revealed the presence of an accessory region attached to the core chromosome 1, which shares homology with part of the small accessory chromosome 15 (Ma *et al.,* 2010). Later it was found that chromosome 15 can be spontaneously lost during vegetative growth (Vlaardingerbroek *et al.,* 2016). Our study confirms these data and provides new results on the structure, dynamics and potential origin of chromosome 15. Using probes located in different areas of the 1&15 shared region, we detected that besides loss of the entire chromosome 15, a part of the 1&15 duplicated region attached to chromosome 1 can be spontaneously lost during growth. Interestingly, the loss of this particular region was always detected in passaged lines that previously had generated chromosome 6, indicating a possible relationship between these two CNVs. To further investigate this hypothesis, it would be necessary to analyse passaged lines lacking chromosome 6.

Furthermore, we discovered that chromosome 15 also shares a region of high homology with chromosome 3. This result was unexpected since the duplicated region on chromosome 15 was considered to belong exclusively to the 1&15 region. Based on the read depth map shown in Figure 47, we hypothesized that the region shared between chromosomes 15 and 3 could correspond to the first duplication peak observed in region 3&6 of the parental isolate (event “b” in Figure 47). To better understand the link between these CNVs, the read depth of passaged line P2 was analyzed as a representative. The results suggest that the region duplicated in event “b” is included in the formation of the new chromosome 6 (see contiguous duplication event "c"), as indicated by the reduced coverage assigned to this region after formation of chromosome 6. Moreover, after the first 3&6 duplication event, which supposedly involves the region shared between chromosomes 3 and 15, the subsequent event "c" also results in an increase of coverage in this shared region (event "e"). We suspect that the apparent increase in coverage of the chromosome 15 region could be an artifact of the assembly and that it may be already represented in the "c" event.

This hypothesis need to be further tested by analyzing, for example, the passaged line Y1, which still shows an apparent increased coverage on chromosome 15, even though chromosome 15 was shown to be lost in this line (see Figure 57). Moreover, it could be confirmed experimentally by karyotyping and Southern blot analysis of monoconidial isolates derived from the P2 population using specific probes. Taken together, the above results indicate a link between CNVs 3&6 and 1&15, although further analyses will be required to fully elucidate the molecular events involved in these recurrent CNVs.

Unlike the previously mentioned events, partial duplication of chromosome 14 was only detected once, in evolved line Y3. The banding pattern obtained after hybridization with a probe from this region revealed that this partial duplication produced both an increase in the size of chromosome 14 itself as well as the presence of another larger hybridizing band. To elucidate, which of these two bands is derived from the original chromosome 14, it will be necessary to perform CHEF and Southern blot analysis with a probe located in the non-duplicated region of this chromosome. Furthermore, our results indicate that chromosomes 11 and 12 (according to size in CHEF gel) may also be involved in this chromosome rearrangement. This needs to be confirmed by Southern blot analysis with probes specific for these two chromosomes. Partial duplication of pathogenicity chromosome 14 in *Fol4287* has been previously reported (Vlaardingerbroek *et al.,* 2016). While in this previous study, partial as well as complete loss of chromosome 14 was recurrently selected, in our work we never observed complete loss under the passaging conditions used.

3.4. Are chromosome CNVs reversible?

In this study we detected both loss and gain of new accessory chromosomes in *Fol4287*, albeit in different regions. This led us to speculate on the possible reversibility of these rearrangements. The basis of the hypothesis would be in the existence of duplicated copies of accessory chromosome regions in the genome. For example, we repeatedly observed that chromosome 13mini is spontaneously lost during vegetative growth in certain conditions, but is it possible that this mini-chromosome could be generated again by partial duplication of the end of chromosome 13? Under the conditions tested we failed to detect such reversibility, which indicates that the presence of two copies of this region is not required for growth of the fungus under these conditions. However, it is possible that the regeneration of Chr13mini could take place under other environmental conditions, where the presence of two copies of this region could provide an adaptive advantage. For example, reversibility of chromosome rearrangements has been previously reported in yeast populations (Chang *et al.,* 2013). Under stress conditions, partial duplication of chromosomal

regions was observed, that carry genes conferring increased tolerance to the toxic compound. However, when the cells carrying the chromosomal rearrangements were cultured in the absence of selection, the wild type configuration was re-established via loss of the previously duplicated chromosomes.

3.5. Usefulness of the FACS technique for chromosome loss quantification

The FACS technique was previously employed to detect the loss of accessory chromosomal regions in *Fol4287* as well as in other fungal pathogens (Plaumann *et al.,* 2018; Vlaardingerbroek *et al*., 2016). We originally planned to quantify the loss rate of Chr13mini by tagging each of the duplicated regions of chromosome 13 with a different fluorescence marker, GFP or ChFP, respectively. However, fluorescence microscopy and karyotype analysis revealed that none of the transformants obtained had integrated the fluorescence marker in the Chr13mini region, with both GFP and ChFP being located *in tandem* in chromosome 13 or chromosome 1. The lack of integration in Chr13mini could be due to a more compact chromatin state in this mini-chromosome, which difficult insertion of the fluorescence transformation constructs. Interestingly, that the region on chromosome 13 in which both fluorescent markers had inserted in tandem, was also susceptible to loss and could thus be used to test the FACS protocol for quantifying loss frequency.

After trying several approaches, no efficient separation between fluorescent and non-fluorescent conidia could be achieved in this study, mainly due to the presence of false negatives that distorted the quantitative measurement. The most likely explanation is that the intensity of the GFP and ChFP signals was not high enough to guarantee inequivocal discrimination between fluorescent and non-fluorescent populations based on fluorescence intensity. We hypothesize this issue could be solved by obtaining higher expression and improved fluorescence marked genes such as codon optimized 3X-Clover fused to the strong P*tef* promoter.

3.6. Studying accessory chromosome loss frequency and the underlying mechanisms in Fol4287

One of the main goals of this study was to address the mechanisms underlying the frequent loss of accessory chromosome detect in *Fol4287*. Recent studies on genome instability in yeast suggest that DNA repair pathways and epigenetic mechanisms may play a central role in chromosome stability (Myung *et al.,* 2001; Argueso *et al.,* 2008; Putnam *et al.,* 2009; Möller *et al.,* 2019). Based on this, knockout mutants in genes involved in these two processes were generated and tested for a possible effect on chromosome loss frequency.

Mutants in DNA damage repair genes were reported to be more sensitive to compounds that induce DNA double-strand breaks such as MMS. Here we found that *Fol4287* knockout mutants in Δ*rad1*, which functions in the nucleotide excision repair (NER) pathway, show reduced survival in the presence of MMS compared to the wild type strain. This result was somewhat unexpected, since *rad1* functions mainly in single-strand DNA break repair and it was previously reported that mutations in the *rad1* gene did not increase sensitivity to MMS (Hwang *et al.,* 2005). However, successful repair of DSBs not only requires processes specific for this type of breaks, but also other mechanisms including the nucleotide excision repair pathway where *rad1* functions (Zhang *et al.,* 2009), providing a possible explanation for the MMS-sensitive phenotype of the *Fol4287* Δ*rad1* mutants.

On the other hand, we did expect increased sensitivity of the Δ*ku70* and Δ*lig4* mutants, since both genes are involved in DSBs repair by the non-homologous end joining (NHEJ) pathway. However, these mutants only showed a slight increase in MMS sensitivity. In other fungi, deletion of these genes had differential effects. While *N. crassa* mutants lacking *ku70* or *lig4* were more sensitive to MMS (Ninomiya *et al.,* 2004; Ishibashi *et al.,* 2006), *M. oryzae* mutants in *lig4* and *ku70* showed similar sensitivity to MMS as the wild type strain (Kito *et al.,* 2008). The Δ*rad1* mutants also were the only ones that showed a significant reduction in colony growth rate and conidiation with respect to the wild type strain. A reduction in the sporulation rate of Δ*rad1* mutants were also detected in *S. cerevisiae* (Resnick *et al.,* 1983; Marston *et al.,* 2004). Similar to *M. oryzae*, deletion of the *lig4* gene in Fol4287 did not result in a reduction in growth rate or conidiation capacity (Kito *et al.,* 2008).

Once the DNA repair mutants were phenotypically characterized, we carried out two experimental approaches, short- and long-term serial passaging experiments, to elucidate if these genes could be involved in the chromosomal losses detected in Fol4287. Previously, a high frequency of loss of chromosomes 13mini (76%) and 15 (93%) was detected during a long-term serial passaging experiment in YPDA medium (López-Díaz, 2019). In the present work, we were able to confirm these results demonstrating that the frequency of loss of these two small chromosomes in this particular environmental condition is remarkably reproducible. Interestingly, the Δ*rad1*, Δ*lig4* and Δ*ku70* mutants showed an increased loss frequency of chromosome 13mini. The fact that mutants in two different DNA repair pathways exhibit similar behaviour indicates that both pathways may contribute to the stability of this chromosome in Fol4287. In a previous study in *S. cerevisiae*, it was shown that these two different DNA damage repair pathways can act synergistically to

suppress chromosome rearrangements (Myung *et al.,* 2001). By contrast, in mutants lacking chromosome 15, a slight reduction in its loss frequency was observed compared to the wild type strain, although these differences were not statistically significant. This could indicate that the mechanisms underlying the loss of these two small chromosomes differ in Fol4287. It is possible that the mechanism underlying loss of chromosome 15 may be more complex than that of 13mini, because both the chromosome itself as well as part of the duplicated region on chromosome 1 can be lost. In conclusion, our experiments did not reveal a direct unequivocal link between the loss of accessory chromosomes and a specific DNA repair pathway.

Given these results, we consider that the high frequency of loss observed for chromosomes 13mini and 15 could be due to the passaging condition rather than to the inactivation of these genes. Furthermore, the number of passages is an influential factor because it increases the probability of other mutations arising as the selective pressure increases. In fact, we could confirm this fact since the appearance of an uncharacterized mutation in one of the passaged lines conferred an adaptive advantage during growth on YPDA plates, thereby altering the frequency of loss of chromosome 13mini from 66% to 0% in a single passage.

To minimize the effect of selection and more accurately measure the "real" rate of accessory chromosome loss, we performed short-term serial passaging experiments using an RFLP strategy for determining presence or absence of 13mini. With this type of assay, the real frequency of chromosome loss in Fol4287 in the absence of selection can be more accurately calculated. Using this assay, we found that Δ*rad1* mutants were unaffected in the frequency of Chr13mini loss, with an average value of 0.66% which is similar to the wild type. By contrast, we observed a considerable increase in the frequency of loss of 13mini in the Δ*kmt1* mutant, suggesting that H3K9me3 may contribute to the stability of chromosome 13mini. In other organisms, loss of the H3K9me3 mark has also been associated with genome instability (Peters *et al.,* 2001; Kondo *et al.,* 2008; Peng and Karpen, 2009). The importance of H3K9me3 methylation in genomic and chromosome stability was also demonstrated in the pathogenic fungus *Z. tritici* (Möller *et al.,* 2019). Thus, a Δ*kmt1* mutant lacking H3K9me3 methylation caused a relocation of another heterochromatin marker, H3K27me3, which destabilized the accessory chromosomes and increasing their loss frequency, as observed in our study. A higher rate of mutation and activation of transposable elements has also been reported in Akmt1 mutants, while in Akmt6 mutants, responsible for the heterochromatic marker H3K27me3, the stability of the genome is greater. Further

analyzes are needed to truly understand how chromatin status influences genomic and chromosomal stability in the pathogenic fungus *Fol4287*.

KEY QUESTIONS AND FUTURE OUTLOOKS

KEY QUESTIONS AND FUTURE OUTLOOKS

1) What is the evolutionary origin of accessory genomic regions?

Currently, there are two hypotheses to explain the origin of accessory genomic regions: **1)** acquisition by horizontal transfer or **2)** generation from core chromosomes (Mehrabi *et al.,* 2017). Previously, in *F. oxysporum* it was proposed that accessory chromosomes could have been acquired from an exogenous donor by horizontal transfer (Ma *et al.,* 2010). This process was experimentally demonstrated for *Fol* accessory chromosome 14 that was transferred to a non-pathogenic strain, making it pathogenic on tomato plants. Later studies revealed that horizontal transfer is not exclusively restricted to accessory chromosomes since regions or even full core chromosomes can also be transferred between strains (Vlaardingerbroek *et al.*, 2016), although with a lower frequency4. An interesting finding is that the transfer of these core regions was linked to that of the accessory chromosome 14. This seems to suggest that accessory chromosomes have a higher capacity to be horizontally transferred than the core chromosomes, and that this process could occurr under natural conditions, providing a possible mechanism for the acquisition of accessory chromosomes.

The second hypothesis is that accessory regions they originate from partial duplications of the ends of core chromosomes which subsequently diverge through repeated breakage-fusion-bridge cycles (BFB) as reported in *Z. tritici* (Croll *et al.,* 2013). In line with this hypothesis, we identified a partial duplication of the end of chromosome 13 resulting in a mini-chromosome named Chr 13mini, which could represent a new accessory chromosome in *Fol4287*. Interestingly, chromosome 13 is considered a core chromosome, although recent studies have shown that it presents features reminiscent of accessory regions such as a high number of repeated elements, lower gene content and specific patterns of histone modifications, leading to its classification as a "fast-core" chromosome (Fokkens *et al.,* 2018). We propose that these features make the chromosome more dynamic and prone to rearrangements. Furthermore, an in-depth analysis revealed an enrichment of retroelements at the border of the region of chromosome 13 that undergoes duplication (Ayhan, 2021). We propose that the partial duplication at the end of chromosome 13 could be mediated by the activity of transposable elements, generating the recent accessory chromosome 13mini. These findings shed open new directions for future research on the possible mechanisms responsible for the origin of accessory regions.

2) Why does *F. oxysporum* carry duplicated accessory regions and what is the function of chromosomal gains and losses?

The first question that comes to mind is why almost all accessory regions in the *Fol4287* genome are duplicated and why these duplications are maintained in spite of the increased energetic cost for the fungus. Most of the studies carried out in yeast suggest that segmental duplications arise as an adaptative mechanism to stress situations (e.g. the presence of an antifungal), and that they represent a temporary solution, with copy numbers returning to the original level as soon as the stress disappears (Yona *et al.,* 2012; Chang *et al.,* 2013; Berman, 2016). Based on our results it appears that *Fol4287* never loses both copies of the duplicated accessory regions. The fact that it always maintains one of the copies may suggest that these regions encode essential functions. Moreover, the frequent changes in copy numbers indicate that these regions may participate in evolutionary processes, with dynamic of gain and loss of copies representing an adaptive mechanism to changes in the environmental conditions. The impact of these CNVs on the fitness of Fol4287 has been evaluated in monoconidial isolates obtained after a long-term passaging experiment (López Díaz, 2019). However, in contrast to other mutations such as single nucleotide variants (SNVs) or TE insertions, the recurrent CNVs observed in the passaged isolates could so far not be associated directly with a gain or loss in fitness as they emerged in all the conditions tested. Our monoconidial isolates that have lost chromosome 13mini, obtained after a short-term passaging experiment in the near absence of selection, could be suitable candidates to study the fitness effect from the loss of this chromosome under different environmental conditions, both *in vitro* and during infection of tomato plants. Because in these lines the probability of other mutations is expected to be very low due to the reduced number of mitotic generations, a more direct relationship between chromosome loss and fitness should be obtained.

CONCLUSIONS
CONCLUSIONES

CONCLUSIONS

1) Nit1 is the main nitrate reductase synthesized under induction conditions in *Fol4287*.
2) Upon mutation of *nit1*, *Fol4287* activates a compensatory mechanism by regulating gene expression to optimize nitrate assimilation.
3) During growth in the presence of different nitrogen sources, we detected the recurrent appearance of colony variant sectors indicated genomic instability.
4) The structure of the subtelomeric regions is highly conserved in *Fol4287* chromosomes.
5) Chromosome ends of *Fol4287* and *Magnaporthe oryzae* are highly similar, suggesting that they play a role in chromosome maintenance and stability.
6) Copy number variations and chromosome rearrangements occur exclusively in accessory regions of *Fol4287* and affect specific positions of the chromosome.
7) Chromosome rearrangements have been successfully tracked using CHEF karyotyping, which allows the detection of structural changes by using region specific probes.
8) A new mini chromosome (Chr 13mini) has been identified, which corresponds to a partial duplication of the right end of chromosome 13. The elucidation of the duplication mechanism needs further work.
9) The epigenetic mark H3k9me3 appears to contribute the stability of the accessory chromosome Chr 13 mini.

CONCLUSIONES

1) Nit1 es la principal nitrato reductasa sintetizada en condiciones de inducción en Fol4287.
2) Tras la mutación de *nit1*, Fol4287 activa un mecanismo compensatorio mediante la regulación de la expresión génica para optimizar la asimilación de nitrato.
3) Durante el crecimiento en presencia de diferentes fuentes de nitrógeno, detectamos la aparición recurrente de sectores variantes de colonias indicados con inestabilidad genómica.
4) La estructura de las regiones subteloméricas está muy conservada en los cromosomas Fol4287.
5) Los extremos de los cromosomas de *Fol4287* y *Magnaporthe oryzae* son muy similares, lo que sugiere que desempeñan un papel en el mantenimiento y la estabilidad de los cromosomas.
6) Las variaciones del número de copias y los reordenamientos cromosómicos ocurren exclusivamente en regiones accesorias de *Fol4287* y afectan posiciones específicas del cromosoma.
7) Los reordenamientos cromosómicos se han rastreado con éxito mediante el cariotipo CHEF, que permite la detección de cambios estructurales mediante el uso de sondas específicas de la región.
8) Se ha identificado un nuevo mini-cromosoma (Chr 13mini), que corresponde a una duplicación parcial del extremo derecho del cromosoma 13. La aclaración del mecanismo de duplicación necesita más trabajo.
9) La marca epigenética H3k9me3 parece contribuir a la estabilidad del cromosoma accesorio Chr 13 mini.

REFERENCES

REFERENCES

Alzohairy, A. M., Sabir, J., Gyulai, G. B., Younis, R., Jansen, R. K., & Bahieldin, A. (2014). Environmental stress activation of plant long-terminal repeat retrotransposons. Functional plant biology : FPB, 41(6), 557–567. https://doi.org/10.1071/FP13339

Amaar, Y. G., & Moore, M. M. (1998). Mapping of the nitrate-assimilation gene cluster (crnA-niiA-niaD) and characterization of the nitrite reductase gene (niiA) in the opportunistic fungal pathogen Aspergillus fumigatus. *Current genetics*, *33*(3), 206–215. https://doi.org/10.1007/s002940050328

Argueso JL, Westmoreland J, Mieczkowski PA, Gawel M, Petes TD, Resnick MA. Double-strand breaks associated with repetitive DNA can reshape the genome. (2008) Proceedings of the National Academy of Sciences of the United States of America. 105(33), 11845-11850. https://doi.org/10.1073/pnas.0804529105.

Arst, H. N., Jr, & Cove, D. J. (1973). Nitrogen metabolite repression in Aspergillus nidulans. *Molecular & general genetics: MGG*, *126*(2), 111–141. https://doi.org/10.1007/BF00330988

Arst, H. N., Jr, MacDonald, D. W., & Cove, D. J. (1970). Molybdate metabolism in Aspergillus nidulans. I. Mutations affecting nitrate reductase and-or xanthine dehydrogenase. *Molecular & general genetics: MGG*, *108*(2), 129–145. https://doi.org/10.1007/BF02430519

Barry, J. D., Ginger, M. L., Burton, P., & McCulloch, R. (2003). Why are parasite contingency genes often associated with telomeres?. International journal for parasitology, 33(1), 29–45. https://doi.org/10.1016/s0020-7519(02)00247-3

Bhattacharyya, A., & Blackburn, E. H. (1997). Aspergillus nidulans maintains short telomeres throughout development. Nucleic acids research, 25(7), 1426–1431. https://doi.org/10.1093/nar/25.7.1426

Bell, B.P., Khabbaz, R.F. (2013). Responding to the Outbreak of Invasive Fungal Infections: The Value of Public Health to Americans. Journal of American Medical Association 309, 883. https://doi.org/10.1001/jama.2013.526

Bennett, R. J., & Johnson, A. D. (2003). Completion of a parasexual cycle in *Candida albicans* by induced chromosome loss in tetraploid strains. *The EMBO journal*, 22(10), 2505–2515. https://doi.org/10.1093/emboj/cdg235

Berger, H., Basheer, A., Böck, S., Reyes-Dominguez, Y., Dalik, T., Altmann, F., & Strauss, J. (2008). Dissecting individual steps of nitrogen transcription factor cooperation in the Aspergillus nidulans nitrate cluster. *Molecular microbiology*, 69(6), 1385–1398. https://doi.org/10.1111/j.1365-2958.2008.06359.x

Berman J. (2016). Ploidy plasticity: a rapid and reversible strategy for adaptation to stress. FEMS yeast research, 16(3), fow020. https://doi.org/10.1093/femsyr/fow020

Bertazzoni S., Williams A.H., Jones D.A., Syme R.A., Tan K.C., Hane, J.K. (2018), Accessories Make the Outfit: Accessory Chromosomes and Other Dispensable DNA Regions in

Plant-Pathogenic Fungi. Molecular Plant Microbe Interactions. 31(8), 779-788. https://doi.org/10.1094/MPMI-06-17-0135-FI.

Bhargava, R., Onyango, D. O., & Stark, J. M. (2016). Regulation of Single-Strand Annealing and its Role in Genome Maintenance. *Trends in genetics*: TIG, 32(9), 566–575. https://doi.org/10.1016/j.tig.2016.06.007

Biju, V.C., Fokkens, L., Houterman, P.M., Rep, M., Cornelissen, B.J.C. (2017). Multiple Evolutionary Trajectories Have Led to the Emergence of Races in *Fusarium oxysporum* f. sp. *lycopersici*. Applied Environmental Microbiology, 83, e02548-16. https://doi.org/10.1128/AEM.02548-16

Blackburn E. H. (2001). Switching and signaling at the telomere. Cell, 106(6), 661–673. https://doi.org/10.1016/s0092-8674(01)00492-5

Bravo Ruiz, G., Di Pietro, A., Gonzalez Roncero, M.I. (2016) Combined action of the major secreted exo- and endopolygalacturonases is required for full virulence of Fusarium oxysporum, Molecular Plant Pathology, 17(3), 339-353. https://doi.org/10.1111/mpp.12283.

Burger, G., Tilburn, J., & Scazzocchio, C. (1991). Molecular cloning and functional characterization of the pathway-specific regulatory gene nirA, which controls nitrate assimilation in Aspergillus nidulans. *Molecular and cellular biology*, *11*(2), 795–802. https://doi.org/10.1128/mcb.11.2.795-802.1991

Buscaino A. (2019). Chromatin-Mediated Regulation of Genome Plasticity in Human Fungal Pathogens. Genes, 10(11), 855. https://doi.org/10.3390/genes10110855

Capper, R., Britt-Compton, B., Tankimanova, M., Rowson, J., Letsolo, B., Man, S., Haughton, M., & Baird, D. M. (2007). The nature of telomere fusion and a definition of the critical telomere length in human cells. *Genes & development*, *21*(19), 2495–2508. https://doi.org/10.1101/gad.439107

Cardona-Piedrahita, L.F., Castaño-Zapata, J. (2019). Comparación de métodos de inoculación de *Fusarium oxysporum* f. sp. *lycopersici* (Sacc.) Snyder & Hansen, causante del marchitamiento vascular del tomate, Revista de la Academia Colombiana de Ciencias de Ciencias Exactas, Físicas y Naturales. 43(167), 227 – 263. doi: http://dx.doi.org/10.18257/raccefyn.854.

Catlett, N. L., B. Lee, O.C. Yoder, & B.G. Turgeon (2003) "Split-Marker Recombination for Efficient Targeted Deletion of Fungal Genes," *Fungal Genetics Reports*: Vol. 50, Article 4. https://doi.org/10.4148/1941-4765.1150

Chalvet, F., Grimaldi, C., Kaper, F., Langin, T., & Daboussi, M. J. (2003). Hop, an active Mutator-like element in the genome of the fungus Fusarium oxysporum. Molecular biology and evolution, 20(8), 1362–1375. https://doi.org/10.1093/molbev/msg155

Chang, S. L., Lai, H. Y., Tung, S. Y., & Leu, J. Y. (2013). Dynamic large-scale chromosomal rearrangements fuel rapid adaptation in yeast populations. *PLoS genetics*, 9(1), e1003232. https://doi.org/10.1371/journal.pgen.1003232.

Chen, N., Thareau, V., Ribeiro, T., Magdelenat, G., Ashfield, T., Innes, R. W., Pedrosa-Harand, A., & Geffroy, V. (2018). Common Bean Subtelomeres Are Hot Spots of Recombination and Favor Resistance Gene Evolution. *Frontiers in plant science*, 9, 1185. https://doi.org/10.3389/fpls.2018.01185

Cohn, M., Liti, G., Barton, D.B. (2005), Telomeres in fungi. In: Sunnerhagen, P., Piskur, J. (eds) Comparative Genomics. Topics in Current Genetics, vol 15. Springer, Berlin, Heidelberg. https://doi.org/10.1007/4735_108

Connolly, L. R., Smith, K. M., & Freitag, M. (2013). The Fusarium graminearum histone H3 K27 methyltransferase KMT6 regulates development and expression of secondary metabolite gene clusters. PLoS genetics, 9(10), e1003916. https://doi.org/10.1371/journal.pgen.1003916

Cook, D. E., Kramer, H. M., Torres, D. E., Seidl, M. F., & Thomma, B. (2020). A unique chromatin profile defines adaptive genomic regions in a fungal plant pathogen. eLife, 9, e62208. https://doi.org/10.7554/eLife.62208

Correll, J.C., Klitt, C.JR., Leslie, J.F. (1987) Nitrate nonutililizing mutants of Fusarium oxysporum and their use in vegetative compatibility tests. *Phytopathology* 77, 1640–1646.

Covo, S. (2020). Genomic Instability in Fungal Plant Pathogens. Genes 11, 421. https://doi.org/10.3390/genes11040421

Craig, N.L., Craigie, R., Gellert, M., Lambowitz., A.M. (2002). Mobile DNA II. American Society for Microbiology, Washington, DC, pp. 3–11. ISBN: 1–55581–209–0. 2002.

Croll D, Zala M, McDonald BA. (2013). Breakage-fusion-bridge cycles and large insertions contribute to the rapid evolution of accessory chromosomes in a fungal pathogen. PLoS Genetics 9(6) e1003567. https://doi.org/10.1371/journal.pgen.1003567.

Croll, D., & McDonald, B. A. (2012). The accessory genome as a cradle for adaptive evolution in pathogens. PLoS pathogens, 8(4), e1002608. https://doi.org/10.1371/journal.ppat.1002608

Crous, P.W., Hawksworth, D.L., Wingfield, M.J. (2015). Identifying and Naming Plant-Pathogenic Fungi: Past, Present, and Future. Annual Review of Phytopathology, 53, 247–267. https://doi.org/10.1146/annurev-phyto-080614-120245

Cuomo, C. A., Güldener, U., Xu, J. R., Trail, F., Turgeon, B. G., Di Pietro, A., Walton, J. D., Ma, L. J., Baker, S. E., Rep, M., Adam, G., Antoniw, J., Baldwin, T., Calvo, S., Chang, Y. L., Decaprio, D., Gale, L. R., Gnerre, S., Goswami, R. S., Hammond-Kosack, K., … Kistler, H. C. (2007). The *Fusarium graminearum* genome reveals a link between localized polymorphism and pathogen specialization. Science (New York, N.Y.), 317(5843), 1400–1402. https://doi.org/10.1126/science.1143708

de Jonge, R., Bolton, M. D., Kombrink, A., van den Berg, G. C., Yadeta, K. A., & Thomma, B. P. (2013). Extensive chromosomal reshuffling drives evolution of virulence in an asexual pathogen. *Genome research*, 23(8), 1271–1282. https://doi.org/10.1101/gr.152660.112

Di Pietro, A., & Roncero, M. I. (1998). Cloning, expression, and role in pathogenicity of pg1 encoding the major extracellular *endopolygalacturonase* of the vascular wilt pathogen *Fusarium oxysporum*. *Molecular plant-microbe interactions*, 11(2), 91–98. https://doi.org/10.1094/MPMI.1998.11.2.91

Di Pietro, A., & Roncero, M.I.G. (1996a) *Endopolygalacturonase* from *Fusarium oxysporum* f. sp. *lycopersici:* purification, characterization, and production during infection of tomato plants. *Phytopathology*, 86(12), 1324-1330.

Di Pietro, A., García-Maceira, F.I., Méglecz, E., Roncero, M.I.G. (2004). A MAP kinase of the vascular wilt fungus *Fusarium oxysporum* is essential for root penetration and pathogenesis: *Fusarium* MAPK is essential for pathogenesis. Molecular Microbiology 39, 1140–1152. https://doi.org/10.1111/j.1365-2958.2001.02307.x

Di Pietro, A., Roncero, M.I.G. (1996). Purification and characterization of a pectate lyase from *Fusarium oxysporum* f. sp. *lycopersici* produced on tomato vascular tissue. Physiological and Molecular Plant Pathology 49, 177–185. https://doi.org/10.1006/pmpp.1996.0047

Díaz, C. L., Gómez-Gil, L., Pérez-Nadales, E., Velasco, G. N., & Di Pietro, A. (2022). Quantification and Isolation of Spontaneous Colony Growth Variants. *Methods in molecular biology* (Clifton, N.J.), 2391, 55–62. https://doi.org/10.1007/978-1-0716-1795-3_5

Ayhan, D.H. (2021) Discovering mechanisms driving adaptive evolution in the cross-kingdom fungal pathogen Fusarium oxysporum. Dissertation. University of Massachusetts.

Dong, S., Raffaele, S., Kamoun, S. (2015). The two-speed genomes of filamentous pathogens: waltz with plants. Current Opinion in Genetics and Development 35, 57-65. https://doi.org/10.1016/j.gde.2015.09.001.

Downey, R. J., Cook, J. A., & Brumfield, A. M. (1987). Monoclonal antibody probes for the niaD specified subunit in the NADPH-nitrate reductase from *Aspergillus nidulans*. *Microbios*, *52*(212-213), 137–150.

Dyakov, Yu.T., Zinovyeva, S.V. (2007). Plant parasite microorganisms, in: Comprehensive and Molecular Phytopathology. Elsevier, pp. 19–47. https://doi.org/10.1016/B978-044452132-3/50004-3

Featherstone, C., & Jackson, S. P. (1999). DNA double-strand break repair. *Current biology* : CB, 9(20), R759–R761. https://doi.org/10.1016/S0960-9822(00)80005-6

Fedorova, N. D., Khaldi, N., Joardar, V. S., Maiti, R., Amedeo, P., Anderson, M. J., Crabtree, J., Silva, J. C., Badger, J. H., Albarraq, A., Angiuoli, S., Bussey, H., Bowyer, P., Cotty, P. J., Dyer, P. S., Egan, A., Galens, K., Fraser-Liggett, C. M., Haas, B. J., Inman, J. M., … Nierman, W. C. (2008). Genomic islands in the pathogenic filamentous fungus Aspergillus fumigatus. PLoS genetics, 4(4), e1000046. https://doi.org/10.1371/journal.pgen.1000046

Ferrari, T. E., & Varner, J. E. (1971). Intact tissue assay for nitrite reductase in barley aleurone layers. *Plant physiology*, 47(6), 790–794. https://doi.org/10.1104/pp.47.6.790

Ferreira, R.B., Monteiro, S., Freitas, R., Santos, C.N., Chen, Z., Batista, L.M., Duarte, J., Borges, A., & Teixeira, A.R. (2006) Fungal Pathogens: The Battle for Plant Infection. Critical Reviews in Plant Sciences, 25(6), 505-524, https://doi.org/10.1080/07352680601054610

Fidalgo, M., Barrales, R. R., Ibeas, J. I., & Jimenez, J. (2006). Adaptive evolution by mutations in the FLO11 gene. *Proceedings of the National Academy of Sciences of the United States of America*, 103(30), 11228–11233. https://doi.org/10.1073/pnas.0601713103

Finnegan D. J. (1989). Eukaryotic transposable elements and genome evolution. Trends in genetics : TIG, 5(4), 103–107. https://doi.org/10.1016/0168-9525(89)90039-5

Fokkens, L.; Shahi, S.; Connolly, L.R.; Stam, R.; Schmidt, S.M.; Smith, K.M.; Freitag, M.; Rep, M. (2018) The multi-speed genome of Fusarium oxysporum reveals association of histone modifications with sequence divergence and footprints of past horizontal chromosome transfer events. bioRxiv 2018.

Fouché, S., Badet, T., Oggenfuss, U., Plissonneau, C., Francisco, C. S., & Croll, D. (2020). Stress-Driven Transposable Element De-repression Dynamics and Virulence Evolution in a Fungal Pathogen. Molecular biology and evolution, 37(1), 221–239. https://doi.org/10.1093/molbev/msz216

Fouché, S., Oggenfuss, U., Chanclud, E., Croll, D. (2022). A devil's bargain with transposable elements in plant pathogens. Trends in Genetics 38, 222–230. https://doi.org/10.1016/j.tig.2021.08.005

Franco-Cano, F. (2021). Desarrollo de marcadores RFLP para detección de la dinámica cromosómica en el hongo patógeno *Fusarium oxysporum*. Trabajo Fin de Máster. Universidad de Córdoba.

Freitag M. (2017). Histone Methylation by SET Domain Proteins in Fungi. Annual review of microbiology, 71, 413–439. https://doi.org/10.1146/annurev-micro-102215-095757

Froeliger, E. H., & Carpenter, B. E. (1996). NUT1, a major nitrogen regulatory gene in Magnaporthe grisea, is dispensable for pathogenicity. *Molecular & general genetics: MGG*, *251*(6), 647–656. https://doi.org/10.1007/BF02174113

Fu, Y. H., & Marzluf, G. A. (1987). Characterization of nit-2, the major nitrogen regulatory gene of Neurospora crassa. *Molecular and cellular biology*, *7*(5), 1691–1696. https://doi.org/10.1128/mcb.7.5.1691-1696.1987

Fujii, T., & Takaya, N. (2008). Denitrification by the fungus *Fusarium oxysporum* involves NADH-nitrate reductase. *Bioscience, biotechnology, and biochemistry*, 72(2), 412–420. https://doi.org/10.1271/bbb.70538

Galazka, J. M., & Freitag, M. (2014). Variability of chromosome structure in pathogenic fungi--of 'ends and odds'. Current opinion in microbiology, 20, 19–26. https://doi.org/10.1016/j.mib.2014.04.002

Gámez-Arjona, F.M., Vitale, S., Voxeur, A., Dora, S., Müller, S., Sancho-Andrés, G., Montesinos, J.C., Di Pietro, A., Sánchez-Rodríguez, C. (2022). Impairment of the

cellulose degradation machinery enhances *Fusarium oxysporum* virulence but limits its reproductive fitness. Sci. Adv. 8, eabl9734. https://doi.org/10.1126/sciadv.abl9734

Gao-Rubinelli, F., & Marzluf, G. A. (2004). Identification and characterization of a nitrate transporter gene in Neurospora crassa. *Biochemical genetics*, *42*(1-2), 21–34. https://doi.org/10.1023/b:bigi.0000012141.51114.23

Garcia-Bastidas, F., Ordonez, N., Konkol, J., Al-Qasim, M., Naser, Z., Abdelwali, M., Salem, N., Waalwijk, C., Ploetz, R.C., Kema, G.H.J. (2014). First report of *Fusarium oxysporum* f.sp. cubense Tropical Race 4 associated with Panama Disease of banana outside Southeast Asia, Plant Disease, 98, 694-694. https://doi.org/10.1094/PDIS-09-13-0954-PDN

Garcia-Pedrajas, M. D., & Roncero, M. I. (1996). A homologous and self-replicating system for efficient transformation of Fusarium oxysporum. Current genetics, 29(2), 191–198. https://doi.org/10.1007/BF02221584

Gemble, S., Wardenaar, R., Keuper, K., Srivastava, N., Nano, M., Macé, A. S., Tijhuis, A. E., Bernhard, S. V., Spierings, D., Simon, A., Goundiam, O., Hochegger, H., Piel, M., Foijer, F., Storchová, Z., & Basto, R. (2022). Genetic instability from a single S phase after whole-genome duplication. *Nature*, 604(7904), 146–151. https://doi.org/10.1038/s41586-022-04578-4

Gijzen, M., Ishmael, C., & Shrestha, S. D. (2014). Epigenetic control of effectors in plant pathogens. Frontiers in plant science, 5, 638. https://doi.org/10.3389/fpls.2014.00638

Gomez-Gil, L., Camara Almiron, J., Rodriguez Carrillo, P. L., Olivares Medina, C. N., Bravo Ruiz, G., Romo Rodriguez, P., Corrales Escobosa, A. R., Gutierrez Corona, F., & Roncero, M. I. (2018). Nitrate assimilation pathway (NAP): role of structural (nit) and transporter (ntr1) genes in Fusarium oxysporum f.sp. lycopersici growth and pathogenicity. *Current genetics*, *64*(2), 493–507. https://doi.org/10.1007/s00294-017-0766-8

Gorfer, M., Blumhoff, M., Klaubauf, S., Urban, A., Inselsbacher, E., Bandian, D., Mitter, B., Sessitsch, A., Wanek, W., & Strauss, J. (2011). Community profiling and gene expression of fungal assimilatory nitrate reductases in agricultural soil. *The ISME journal*, 5(11), 1771–1783. https://doi.org/10.1038/ismej.2011.53

Gorkovskiy, A., & Verstrepen, K. J. (2021). The Role of Structural Variation in Adaptation and Evolution of Yeast and Other Fungi. *Genes*, 12(5), 699. https://doi.org/10.3390/genes12050699

Grandbastien, M. A., Spielmann, A., & Caboche, M. (1989). Tnt1, a mobile retroviral-like transposable element of tobacco isolated by plant cell genetics. Nature, 337(6205), 376–380. https://doi.org/10.1038/337376a0

Gray Y. H. (2000). It takes two transposons to tango: transposable-element-mediated chromosomal rearrangements. Trends in genetics: TIG, 16(10), 461–468. https://doi.org/10.1016/s0168-9525(00)02104-1

Grewal, S. I., & Jia, S. (2007). Heterochromatin revisited. *Nature reviews. Genetics*, 8(1), 35–46. https://doi.org/10.1038/nrg2008

Habig, M., Lorrain, C., Feurtey, A., Komluski, J., & Stukenbrock, E. H. (2021). Epigenetic modifications affect the rate of spontaneous mutations in a pathogenic fungus. Nature communications, 12(1), 5869. https://doi.org/10.1038/s41467-021-26108-y

Harr, J. C., Gonzalez-Sandoval, A., & Gasser, S. M. (2016). Histones and histone modifications in perinuclear chromatin anchoring: from yeast to man. *EMBO reports*, 17(2), 139–155. https://doi.org/10.15252/embr.201541809

Hartmann F.E., Sánchez-Vallet A., McDonald B.A., Croll D. (2017). A fungal wheat pathogen evolved host specialization by extensive chromosomal rearrangements. International Society of Microbial Ecology Journal, 11(5), 1189-1204. https://doi.org/10.1038/ismej.2016.196

Heacock, M. L., Idol, R. A., Friesner, J. D., Britt, A. B., & Shippen, D. E. (2007). Telomere dynamics and fusion of critically shortened telomeres in plants lacking DNA ligase IV. *Nucleic acids research*, *35*(19), 6490–6500. https://doi.org/10.1093/nar/gkm472

Heasley, L. R., & Argueso, J. L. (2022). Genomic characterization of a wild diploid isolate of Saccharomyces cerevisiae reveals an extensive and dynamic landscape of structural variation. *Genetics*, *220*(3), iyab193. https://doi.org/10.1093/genetics/iyab193

Hedges, D. J., & Deininger, P. L. (2007). Inviting instability: Transposable elements, double-strand breaks, and the maintenance of genome integrity. Mutation research, 616(1-2), 46–59. https://doi.org/10.1016/j.mrfmmm.2006.11.021

Hernández-Chávez, M. J., Pérez-García, L. A., Niño-Vega, G. A., & Mora-Montes, H. M. (2017). Fungal Strategies to Evade the Host Immune Recognition. Journal of fungi (Basel, Switzerland), 3(4), 51. https://doi.org/10.3390/jof3040051

Hijri, M., Niculita, H., & Sanders, I. R. (2007). Molecular characterization of chromosome termini of the arbuscular mycorrhizal fungus Glomus intraradices (Glomeromycota). Fungal genetics and biology: FG & B, 44(12), 1380–1386. https://doi.org/10.1016/j.fgb.2007.03.004

Hoff, G., Bertrand, C., Piotrowski, E., Thibessard, A., & Leblond, P. (2018). Genome plasticity is governed by double strand break DNA repair in *Streptomyces*. *Scientific reports*, 8(1), 5272. https://doi.org/10.1038/s41598-018-23622-w

Hull, C. M., Raisner, R. M., & Johnson, A. D. (2000). Evidence for mating of the "asexual" yeast *Candida albicans* in a mammalian host. *Science* (New York, N.Y.), 289(5477), 307–310. https://doi.org/10.1126/science.289.5477.307

Hwang J.Y., Smith S., Myung K. (2005). The Rad1-Rad10 complex promotes the production of gross chromosomal rearrangements from spontaneous DNA damage in Saccharomyces cerevisiae. Genetics. 169(4), 1927-37. https://doi.org/10.1534/genetics.104.039768.

Ishibashi K., Suzuki K., Ando Y., Takakura C., Inoue H. (2006) Nonhomologous chromosomal integration of foreign DNA is completely dependent on MUS-53 (human Lig4 homolog) in Neurospora. Proceedings of the National Academic of Sciences of the United ates of America, 103(40), 14871-14876. https://doi.org/10.1073/pnas.0604477103.

Jamieson, K., Rountree, M. R., Lewis, Z. A., Stajich, J. E., & Selker, E. U. (2013). Regional control of histone H3 lysine 27 methylation in Neurospora. Proceedings of the National Academy of Sciences of the United States of America, 110(15), 6027–6032. https://doi.org/10.1073/pnas.1303750110

Jashni, M.K., Dols, I.H.M., Iida, Y., Boeren, S., Beenen, H.G., Mehrabi, R., Collemare, J., de Wit, P.J.G.M., 2015. Synergistic Action of a Metalloprotease and a Serine Protease from *Fusarium oxysporum* f. sp. *lycopersici* Cleaves Chitin-Binding Tomato Chitinases, Reduces Their Antifungal Activity, and Enhances Fungal Virulence. MPMI 28, 996–1008. https://doi.org/10.1094/MPMI-04-15-0074-R

Joergensen, R.G., & Wichern, F. (2008). Quantitative assessment of the fungal contribution to microbial tissue in soil. *Soil Biology and Biochemistry*, 40(12), 2977-2991. https://doi.org/10.1016/j.soilbio.2008.08.017

Johnstone, I. L., McCabe, P. C., Greaves, P., Gurr, S. J., Cole, G. E., Brow, M. A., Unkles, S. E., Clutterbuck, A. J., Kinghorn, J. R., & Innis, M. A. (1990). Isolation and characterisation of the crnA-niiA-niaD gene cluster for nitrate assimilation in *Aspergillus nidulans*. *Gene*, *90*(2), 181–192. https://doi.org/10.1016/0378-1119(90)90178-t

Kashiwa, T., Kozaki, T., Ishii, K., Turgeon, B.G., Teraoka, T., Komatsu, K., Arie, T., 2017. Sequencing of individual chromosomes of plant pathogenic *Fusarium oxysporum*. Fungal Genetics and Biology 98, 46–51. https://doi.org/10.1016/j.fgb.2016.12.001

Kenny, N. J., Chan, K. W., Nong, W., Qu, Z., Maeso, I., Yip, H. Y., Chan, T. F., Kwan, H. S., Holland, P. W., Chu, K. H., & Hui, J. H. (2016). Ancestral whole-genome duplication in the marine *chelicerate horseshoe* crabs. *Heredity*, 116(2), 190–199. https://doi.org/10.1038/hdy.2015.89

Kito H., Fujikawa T., Moriwaki A., Tomono A., Izawa M., Kamakura T., Ohashi M., Sato H., Abe K., Nishimura M. (2008), *MgLig4*, a homolog of *Neurospora crassa Mus-53* (DNA ligase IV), is involved in, but not essential for, non-homologous end-joining events in *Magnaporthe grisea*. Fungal Genetics Biology, 45(12), 1543-1551. https://doi.org/10.1016/j.fgb.2008.09.005

Klittich, C., & Leslie, J. F. (1988). Nitrate reduction mutants of fusarium moniliforme (gibberella fujikuroi). *Genetics*, *118*(3), 417–423. https://doi.org/10.1093/genetics/118.3.417

Kobayashi, M., Matsuo, Y., Takimoto, A., Suzuki, S., Maruo, F., & Shoun, H. (1996). Denitrification, a novel type of respiratory metabolism in fungal mitochondrion. *The Journal of biological chemistry*, *271*(27), 16263–16267. https://doi.org/10.1074/jbc.271.27.16263

Kondo, Y., Shen, L., Ahmed, S., Boumber Y., Sekido Y., Haddad B.R., Issa J.P. (2008) Downregulation of *histone H3 lysine 9 methyltransferase G9a* induces centrosome disruption and chromosome instability in cancer cells. PLoS One. 3(4), e2037. https://doi.org/10.1371/journal.pone.0002037.

Kopke, K., Hoff, B., & Kück, U. (2010). Application of the *Saccharomyces cerevisiae* FLP/FRT recombination system in filamentous fungi for marker recycling and construction of knockout strains devoid of heterologous genes. *Applied and environmental microbiology*, 76(14), 4664–4674. https://doi.org/10.1128/AEM.00670-10

Korolev, N., Mamiev, M., Zahavi, T., Elad, Y. (2011). Screening of *Botrytis cinerea* isolates from vineyards in Israel for resistance to fungicides. European Journal of Plant Pathology, 129, 591–608. https://doi.org/10.1007/s10658-010-9723-9

Krejci, L., Altmannova, V., Spirek, M., & Zhao, X. (2012). Homologous recombination and its regulation. *Nucleic acids research*, 40(13), 5795–5818. https://doi.org/10.1093/nar/gks270

Kudla, B., Caddick, M. X., Langdon, T., Martinez-Rossi, N. M., Bennett, C. F., Sibley, S., Davies, R. W., & Arst, H. N., Jr (1990). The regulatory gene areA mediating nitrogen metabolite repression in *Aspergillus nidulans*. Mutations affecting specificity of gene activation alter a loop residue of a putative zinc finger. *The EMBO journal*, *9*(5), 1355–1364. https://doi.org/10.1002/j.1460-2075.1990.tb08250.x

Laemmli U. K. (1970). Cleavage of structural proteins during the assembly of the head of bacteriophage T4. *Nature*, 227(5259), 680–685. https://doi.org/10.1038/227680a0

Lang, G. I., Rice, D. P., Hickman, M. J., Sodergren, E., Weinstock, G. M., Botstein, D., & Desai, M. M. (2013). Pervasive genetic hitchhiking and clonal interference in forty evolving yeast populations. Nature, 500(7464), 571–574. https://doi.org/10.1038/nature12344

Langner, T., Harant, A., Gomez-Luciano L.B., Shrestha R.K., Malmgren A., Latorre, S.M., Burbano, H.A., Win, J., Kamoun, S. (2021). Genomic rearrangements generate hypervariable mini-chromosomes in host-specific isolates of the blast fungus. PLoS Genetics, 17(2), e1009386. https://doi.org/10.1371/journal.pgen.1009386.

Langner, T., Harant, A., & Kamoun, S. (2019). Isolation of supernumerary minichromosomes from fungi for enrichment sequencing. https://doi.org/10.17504/protocols.io.9t7h6rn.

Langner, T., Harant, A., Gomez-Luciano, L. B., Shrestha, R. K., Malmgren, A., Latorre, S. M., Burbano, H. A., Win, J., & Kamoun, S. (2021). Genomic rearrangements generate hypervariable mini-chromosomes in host-specific isolates of the blast fungus. *PLoS genetics*, 17(2), e1009386. https://doi.org/10.1371/journal.pgen.1009386

Li, J., Cornelissen, B., Rep, M. (2020a). Host-specificity factors in plant pathogenic fungi. Fungal Genetics and Biology 144, 103447. https://doi.org/10.1016/j.fgb.2020.103447

Li, J., Fokkens, L., Conneely, L.J., Rep, M. (2020b). Partial pathogenicity chromosomes in *Fusarium oxysporum* are sufficient to cause disease and can be horizontally transferred. Environmental Microbiology 22, 4985–5004. https://doi.org/10.1111/1462-2920.15095

Lieber M. R. (2010). The mechanism of double-strand DNA break repair by the nonhomologous DNA end-joining pathway. *Annual review of biochemistry*, 79, 181–211. https://doi.org/10.1146/annurev.biochem.052308.093131

Liu, D., O'Connor, M. S., Qin, J., & Songyang, Z. (2004). Telosome, a mammalian telomere-associated complex formed by multiple telomeric proteins. *The Journal of biological chemistry*, *279*(49), 51338–51342. https://doi.org/10.1074/jbc.M409293200

Longhese M. P. (2008). DNA damage response at functional and dysfunctional telomeres. Genes & development, 22(2), 125–140. https://doi.org/10.1101/gad.1626908

Lõoke, M., Kristjuhan, K., & Kristjuhan, A. (2011). Extraction of genomic DNA from yeasts for PCR-based applications. *BioTechniques*, 50(5), 325–328. https://doi.org/10.2144/000113672

López-Berges, M. S., Rispail, N., Prados-Rosales, R. C., & Di Pietro, A. (2010). A nitrogen response pathway regulates virulence functions in Fusarium oxysporum via the protein kinase TOR and the bZIP protein MeaB. *The Plant cell*, *22*(7), 2459–2475. https://doi.org/10.1105/tpc.110.075937

López-Díaz, C. (2019) Molecular and genetic mechanisms underlying genome plasticity in Fusarium oxysporum. Tesis doctoral. University of Córdoba. Available: https://helvia.uco.es/xmlui/bitstream/handle/10396/18865/2019000001959.pdf?sequence=1&isAllowed=y

Lorrain, C., Feurtey, A., Möller, M., Haueisen, J., & Stukenbrock, E. (2021). Dynamics of transposable elements in recently diverged fungal pathogens: lineage-specific transposable element content and efficiency of genome defenses. G3 (Bethesda, Md.), 11(4), jkab068. https://doi.org/10.1093/g3journal/jkab068

Louis, E. J. (2014). "Introduction," in Subtelomeres, eds E. J. Louis and M. M. Becker (Berlin: Springer Verlag), 1–12. doi: 10.1093/actrade/9780199589944.003.0001

M L Farman, S A Leong, Genetic and physical mapping of telomeres in the rice blast fungus, Magnaporthe grisea., Genetics, Volume 140, Issue 2, 1 June 1995, Pages 479–492, https://doi.org/10.1093/genetics/140.2.479

Ma, L.-J., Geiser, D.M., Proctor, R.H., Rooney, A.P., O'Donnell, K., Trail, F., Gardiner, D.M., Manners, J.M., Kazan, K. (2013). *Fusarium* Pathogenomics. Annual Reviews of Microbiology 67, 399–416. https://doi.org/10.1146/annurev-micro-092412-155650

Ma, L.-J., van der Does, H.C., Borkovich, K.A., Coleman, J.J., Daboussi, M.-J., Di Pietro, A., Dufresne, M., Freitag, M., Grabherr, M., Henrissat, B., Houterman, P.M., Kang, S., Shim, W.-B., Woloshuk, C., Xie, X., Xu, J.-R., Antoniw, J., Baker, S.E., Bluhm, B.H., Breakspear, A., Brown, D.W., Butchko, R.A.E., Chapman, S., Coulson, R., Coutinho, P.M., Danchin, E.G.J., Diener, A., Gale, L.R., Gardiner, D.M., Goff, S., Hammond-Kosack, K.E., Hilburn, K., Hua-Van, A., Jonkers, W., Kazan, K., Kodira, C.D., Koehrsen, M., Kumar, L., Lee, Y.-H., Li, L., Manners, J.M., Miranda-Saavedra, D., Mukherjee, M., Park, G., Park, J., Park, S.-Y., Proctor, R.H., Regev, A., Ruiz-Roldan, M.C., Sain, D., Sakthikumar, S., Sykes, S., Schwartz, D.C., Turgeon, B.G., Wapinski, I., Yoder, O., Young, S., Zeng, Q., Zhou, S.,

Galagan, J., Cuomo, C.A., Kistler, H.C., Rep, M. (2010). Comparative genomics reveals mobile pathogenicity chromosomes in *Fusarium*. Nature 464, 367–373. https://doi.org/10.1038/nature08850

Malardier, L., Daboussi, M. J., Julien, J., Roussel, F., Scazzocchio, C., & Brygoo, Y. (1989). Cloning of the nitrate reductase gene (niaD) of *Aspergillus nidulans* and its use for transformation of *Fusarium oxysporum*. *Gene*, 78(1), 147–156. https://doi.org/10.1016/0378-1119(89)90322-3

Manetti, M.E., Rossi, M., Costa, A.P. et al. Radiation of the Tnt1 retrotransposon superfamily in three Solanaceae genera. BMC Evol Biol 7, 34 (2007). https://doi.org/10.1186/1471-2148-7-34

Marston, A.L., Tham W.H., Shah, H., Amon, A. (2004). A genome-wide screen identifies genes required for centromeric cohesion. Science. 303(5662), 1367-1370. https://doi.org/10.1126/science.1094220.

Marzluf G. A. (1997). Genetic regulation of nitrogen metabolism in the fungi. Microbiology and molecular biology reviews: MMBR, 61(1), 17–32. https://doi.org/10.1128/mmbr.61.1.17-32.1997

Mat Razali, N., Cheah, B. H., & Nadarajah, K. (2019). Transposable Elements Adaptive Role in Genome Plasticity, Pathogenicity and Evolution in Fungal Phytopathogens. International journal of molecular sciences, 20(14), 3597. https://doi.org/10.3390/ijms20143597

Mattern, I. E., P.J. Punt, & C.A. Van den Hondel (1988) "A vector for Aspergillus transformation conferring phleomycin resistance.," *Fungal Genetics Reports*: Vol. 35, Article 13. https://doi.org/10.4148/1941-4765.1533

Mehrabi, R., Mirzadi Gohari, A., Kema, G.H.J. (2017). Karyotype Variability in Plant-Pathogenic Fungi. Annual Review of Phytopathology, 55, 483–503. https://doi.org/10.1146/annurev-phyto-080615-095928

Miller, J.H. (1972). Experiment in molecular genetics. Cold Spring Harbor Laboratory, New York.

Möller, M., Schotanus, K., Soyer, J. L., Haueisen, J., Happ, K., Stralucke, M., Happel, P., Smith, K. M., Connolly, L. R., Freitag, M., & Stukenbrock, E. H. (2019). Destabilization of chromosome structure by histone H3 lysine 27 methylation. PLoS genetics, 15(4), e1008093. https://doi.org/10.1371/journal.pgen.1008093

Möller, M., Stukenbrock, E.H. (2017). Evolution and genome architecture in fungal plant pathogens. Nature Reviews. Microbiology 15, 756–771. https://doi.org/10.1038/nrmicro.2017.76

Moretti, A., Susca, A. (Eds.) (2017). Mycotoxigenic Fungi: Methods and Protocols, Methods in Molecular Biology. Springer New York, New York, NY. https://doi.org/10.1007/978-1-4939-6707-0

Moyzis, R. K., Buckingham, J. M., Cram, L. S., Dani, M., Deaven, L. L., Jones, M. D., Meyne, J., Ratliff, R. L., & Wu, J. R. (1988). A highly conserved repetitive DNA sequence, (TTAGGG)n, present at the telomeres of human chromosomes. Proceedings of the National Academy of Sciences of the United States of America, 85(18), 6622–6626. https://doi.org/10.1073/pnas.85.18.6622

Muro-Pastor, M. I., Strauss, J., Ramón, A., & Scazzocchio, C. (2004). A paradoxical mutant GATA factor. *Eukaryotic cell*, *3*(2), 393–405. https://doi.org/10.1128/EC.3.2.393-405.2004

Murray, M. G., & Thompson, W. F. (1980). Rapid isolation of high molecular weight plant DNA. *Nucleic acids research*, 8(19), 4321–4325. https://doi.org/10.1093/nar/8.19.4321

Myung, K., Chen, C., Kolodner, R.D. (2001) Multiple pathways cooperate in the suppression of genome instability in Saccharomyces cerevisiae. Nature. 411(6841), 1073-1076. https://doi.org/10.1038/35082608.

Naranjo-Ortiz, M. A., & Gabaldón, T. (2020). Fungal evolution: cellular, genomic and metabolic complexity. *Biological reviews of the Cambridge Philosophical Society*, 95(5), 1198–1232. https://doi.org/10.1111/brv.12605

Ninomiya, Y., Suzuki, K., Ishii, C., Inoue, H. (2004). Highly efficient gene replacements in *Neurospora* strains deficient for nonhomologous end-joining. Proceeding of the National Academy of Sciences of the United States of America, 101(33), 12248-12253. https://doi.org/10.1073/pnas.0402780101.

Nurk, S., Koren, S., Rhie, A., Rautiainen, M., Bzikadze, A. V., Mikheenko, A., Vollger, M. R., Altemose, N., Uralsky, L., Gershman, A., Aganezov, S., Hoyt, S. J., Diekhans, M., Logsdon, G. A., Alonge, M., Antonarakis, S. E., Borchers, M., Bouffard, G. G., Brooks, S. Y., Caldas, G. V., … Phillippy, A. M. (2022). The complete sequence of a human genome. Science (New York, N.Y.), 376(6588), 44–53. https://doi.org/10.1126/science.abj6987

O'Donnell, K., Rooney, A.P., Proctor, R.H., Brown, D.W., McCormick, S.P., Ward, T.J., Frandsen, R.J.N., Lysøe, E., Rehner, S.A., Aoki, T., Robert, V.A.R.G., Crous, P.W., Groenewald, J.Z., Kang, S., Geiser, D.M. (2013). Phylogenetic analyses of RPB1 and RPB2 support a middle Cretaceous origin for a clade comprising all agriculturally and medically important fusaria. Fungal Genetics and Biology 52, 20–31. https://doi.org/10.1016/j.fgb.2012.12.004

O'Donnell, K., Sutton, D.A., Rinaldi, M.G., Magnon, K.C., Cox, P.A., Revankar, S.G., Sanche, S., Geiser, D.M., Juba, J.H., van Burik, J.-A.H., Padhye, A., Anaissie, E.J., Francesconi, A., Walsh, T.J., Robinson, J.S. (2004). Genetic Diversity of Human Pathogenic Members of the *Fusarium oxysporum* Complex Inferred from Multilocus DNA Sequence Data and Amplified Fragment Length Polymorphism Analyses: Evidence for the Recent Dispersion of a Geographically Widespread Clonal Lineage and Nosocomial Origin. Journal of Clinical Microbiology, 42, 5109–5120. https://doi.org/10.1128/JCM.42.11.5109-5120.2004

Ortoneda, M., Guarro, J., Madrid, M. P., Caracuel, Z., Roncero, M. I., Mayayo, E., & Di Pietro, A. (2004). Fusarium oxysporum as a multihost model for the genetic dissection of fungal

virulence in plants and mammals. Infection and immunity, 72(3), 1760–1766. https://doi.org/10.1128/IAI.72.3.1760-1766.2004

O'Sullivan, R. J., & Karlseder, J. (2010). Telomeres: protecting chromosomes against genome instability. Nature reviews. Molecular cell biology, 11(3), 171–181. https://doi.org/10.1038/nrm2848

Otto S. P. (2007). The evolutionary consequences of polyploidy. *Cell*, 131(3), 452–462. https://doi.org/10.1016/j.cell.2007.10.022

Pareja-Jaime, Y., Roncero, M.I.G., Ruiz-Roldán, M.C. (2008). *Tomatinase* from *Fusarium oxysporum* f. sp. *lycopersici* Is Required for Full Virulence on Tomato Plants. Molecular Plant-Microbe Interactions, 21, 728–736. https://doi.org/10.1094/MPMI-21-6-0728

Pateman, J. A., Cove, D. J., Rever, B. M., & Roberts, D. B. (1964). A common co-factor for nitrate reductase and xanthine dehydrogenase which also regulates the synthesis of nitrate reductase. *Nature*, *201*, 58–60. https://doi.org/10.1038/201058a0

Pateman, J. A., Rever, B. M., & Cove, D. J. (1967). Genetic and biochemical studies of nitrate reduction in Aspergillus nidulans. *The Biochemical journal*, *104*(1), 103–111. https://doi.org/10.1042/bj1040103

Peng, J.C., Karpen, G.H. Heterochromatic genome stability requires regulators of histone H3 K9 methylation. (2009) PLoS Genetics 5(3), e1000435. https://doi.org/10.1371/journal.pgen.1000435.

Peters AH, O'Carroll D, Scherthan H, Mechtler K, Sauer S, Schöfer C, Weipoltshammer K, Pagani M, Lachner M, Kohlmaier A, Opravil S, Doyle M, Sibilia M, Jenuwein T. (2001) Loss of the Suv39h histone methyltransferases impairs mammalian heterochromatin and genome stability. Cell. 107(3), 323-337. https://doi.org/10.1016/s0092-8674(01)00542-6

Plaumann PL, Schmidpeter J, Dahl M, Taher L, Koch C. (2018). A Dispensable Chromosome Is Required for Virulence in the Hemibiotrophic Plant Pathogen Colletotrichum higginsianum. Frontiers of Microbiology, 9. 1005. https://doi.org/10.3389/fmicb.2018.01005

Powell, W. A., & Kistler, H. C. (1990). In vivo rearrangement of foreign DNA by Fusarium oxysporum produces linear self-replicating plasmids. Journal of bacteriology, 172(6), 3163–3171. https://doi.org/10.1128/jb.172.6.3163-3171.1990

Pray, L. (2008) Transposons: The jumping genes. Nature Education 1(1):204

Price, M. N., Huang, K. H., Arkin, A. P., & Alm, E. J. (2005). Operon formation is driven by co-regulation and not by horizontal gene transfer. *Genome research*, *15*(6), 809–819. https://doi.org/10.1101/gr.3368805

Pryde, F. E., Gorham, H. C., & Louis, E. J. (1997). Chromosome ends: all the same under their caps. Current opinion in genetics & development, 7(6), 822–828. https://doi.org/10.1016/s0959-437x(97)80046-9

Puhalla J. E. (1968). Compatibility reactions on solid medium and interstrain inhibition in *Ustilago maydis*. *Genetics*, 60(3), 461–474. https://doi.org/10.1093/genetics/60.3.461

Punt, P. J., Oliver, R. P., Dingemanse, M. A., Pouwels, P. H., & van den Hondel, C. A. (1987). Transformation of *Aspergillus* based on the hygromycin B resistance marker from Escherichia coli. *Gene*, 56(1), 117–124. https://doi.org/10.1016/0378-1119(87)90164-8

Putnam CD, Hayes TK, Kolodner RD. (2009). Specific pathways prevent duplication-mediated genome rearrangements. Nature. 460(7258), 984-989. https://doi.org/10.1038/nature08217.

Qu, L., Wang, L., Ji, H., Fang, Y., Lei, P., Zhang, X., Jin, L., Sun, D., Dong, H. (2022). Toxic Mechanism and Biological Detoxification of Fumonisins. Toxins 14, 182. https://doi.org/10.3390/toxins14030182

Raffaele, S., & Kamoun, S. (2012). Genome evolution in filamentous plant pathogens: why bigger can be better. Nature reviews. Microbiology, 10(6), 417–430. https://doi.org/10.1038/nrmicro2790

Rahnama, M., Wang, B., Dostart, J., Novikova, O., Yackzan, D., Yackzan, A., Bruss, H., Baker, M., Jacob, H., Zhang, X., Lamb, A., Stewart, A., Heist, M., Hoover, J., Calie, P., Chen, L., Liu, J., & Farman, M. L. (2021). Telomere Roles in Fungal Genome Evolution and Adaptation. Frontiers in genetics, 12, 676751. https://doi.org/10.3389/fgene.2021.676751

Rana, A., Sahgal, M., Johri, B.N. (2017). *Fusarium oxysporum*: Genomics, Diversity and Plant–Host Interaction, in: Satyanarayana, T., Deshmukh, S.K., Johri, B.N. (Eds.), Developments in Fungal Biology and Applied Mycology. Springer Singapore, Singapore, pp. 159–199. https://doi.org/10.1007/978-981-10-4768-8_10

Redkar, A., Sabale, M., Zuccaro, A., Di Pietro, A. (2022). Determinants of endophytic and pathogenic lifestyle in root colonizing fungi. Current Opinion in Plant Biology 67, 102226. https://doi.org/10.1016/j.pbi.2022.102226

Rehmeyer, C., Li, W., Kusaba, M., Kim, Y. S., Brown, D., Staben, C., Dean, R., & Farman, M. (2006). Organization of chromosome ends in the rice blast fungus, Magnaporthe oryzae. Nucleic acids research, 34(17), 4685–4701. https://doi.org/10.1093/nar/gkl588

Rep, M. (2005). Small proteins of plant-pathogenic fungi secreted during host colonization. FEMS Microbiology Letters 253, 19–27. https://doi.org/10.1016/j.femsle.2005.09.014

Rep, M., Dekker, H.L., Vossen, J.H., de Boer, A.D., Houterman, P.M., de Koster, C.G., Cornelissen, B.J.C. (2003) A tomato xylem sap protein represents a new family of small cysteine-rich proteins with structural similarity to lipid transfer proteins, FEBS Letters, 534(1-3) 82 – 86. https://doi.org/10.1016/s0014-5793(02)03788-2

Rep, M., Meijer, M., Houterman, P.M., van der Does, H.C., Cornelissen, B.J.C. (2005). *Fusarium oxysporum* Evades *I-3* -Mediated Resistance Without Altering the Matching Avirulence Gene. Molecular Plant-Microbe Interactions, 18, 15–23. https://doi.org/10.1094/MPMI-18-0015

Rep, M., van der Does, H.C., Meijer, M., van Wijk, R., Houterman, P.M., Dekker, H.L., de Koster, C.G., Cornelissen, B.J.C. (2004). A small cysteine-rich protein secreted by *Fusarium oxysporum* during colonization of xylem vessels is required for I-3-mediated resistance in tomato, Molecular Microbiology, 53(5), 1373 – 1383. https://doi.org/10.1111/j.1365-2958.2004.04177.x

Resnick MA, Stasiewicz S, Game JC. Meiotic DNA metabolism in wild-type and excision-deficient yeast following UV exposure. (1983). Genetics. 104(4), 583-601. https://doi.org/10.1093/genetics/104.4.583.

Rudd, M. K., Friedman, C., Parghi, S. S., Linardopoulou, E. V., Hsu, L., & Trask, B. J. (2007). Elevated rates of sister chromatid exchange at chromosome ends. *PLoS genetics*, *3*(2), e32. https://doi.org/10.1371/journal.pgen.0030032

Sasaki, T., Lynch, K. L., Mueller, C. V., Friedman, S., Freitag, M., & Lewis, Z. A. (2014). Heterochromatin controls γH2A localization in *Neurospora crassa*. *Eukaryotic cell*, 13(8), 990–1000. https://doi.org/10.1128/EC.00117-14

Schechtman M. G. (1987). Isolation of telomere DNA from Neurospora crassa. Molecular and cellular biology, 7(9), 3168–3177. https://doi.org/10.1128/mcb.7.9.3168-3177.1987

Schinko, T., Berger, H., Lee, W., Gallmetzer, A., Pirker, K., Pachlinger, R., Buchner, I., Reichenauer, T., Güldener, U., & Strauss, J. (2010). Transcriptome analysis of nitrate assimilation in *Aspergillus nidulans* reveals connections to nitric oxide metabolism. *Molecular microbiology*, *78*(3), 720–738. https://doi.org/10.1111/j.1365-2958.2010.07363.x

Schinko, T., Gallmetzer, A., Amillis, S., & Strauss, J. (2013). Pseudo-constitutivity of nitrate-responsive genes in nitrate reductase mutants. *Fungal genetics and biology : FG & B*, *54*, 34–41. https://doi.org/10.1016/j.fgb.2013.02.003

Schlötterer, C., Kofler, R., Versace, E. et al. (2015). Combining experimental evolution with next-generation sequencing: a powerful tool to study adaptation from standing genetic variation. Heredity 114, 431–440. https://doi.org/10.1038/hdy.2014.86

Schotanus, K., Soyer, J.L., Connolly, L.R. et al. Histone modifications rather than the novel regional centromeres of Zymoseptoria tritici distinguish core and accessory chromosomes. Epigenetics & Chromatin 8, 41 (2015). https://doi.org/10.1186/s13072-015-0033-5

Segorbe, B., Di Pietro, A., Pérez-Nadales, E., Turrà, D. (2017). Three *Fusarium oxysporum* mitogen-activated protein kinases MAPKs have distinct and complementary roles in stress adaptation and cross-kingdom pathogenicity, Molecular Plant Pathology, 18(7), 912 – 924. https://doi.org/10.1111/mpp.12446

Seidl, M. F., & Thomma, B. P. (2014). Sex or no sex: evolutionary adaptation occurs regardless. BioEssays: news and reviews in molecular, cellular and developmental biology, 36(4), 335–345. https://doi.org/10.1002/bies.201300155

Seidl, M. F., Cook, D. E., & Thomma, B. P. (2016). Chromatin Biology Impacts Adaptive Evolution of Filamentous Plant Pathogens. *PLoS pathogens*, 12(11), e1005920. https://doi.org/10.1371/journal.ppat.1005920

Serero, A., Jubin, C., Loeillet, S., Legoix-Né, P., & Nicolas, A. G. (2014). Mutational landscape of yeast mutator strains. *Proceedings of the National Academy of Sciences of the United States of America*, 111(5), 1897–1902. https://doi.org/10.1073/pnas.1314423111

Shi-Kunne X, Faino L, van den Berg GCM, Thomma BPHJ, Seidl MF. (2018) Evolution within the fungal genus Verticillium is characterized by chromosomal rearrangement and gene loss. Environmental Microbiology, 20(4), 1362-1373. https://doi.org/10.1111/1462-2920.

Shoun, H., & Tanimoto, T. (1991). Denitrification by the fungus *Fusarium oxysporum* and involvement of cytochrome P-450 in the respiratory nitrite reduction. *The Journal of biological chemistry*, *266*(17), 11078–11082.

Shoun, H., Fushinobu, S., Jiang, L., Kim, S. W., & Wakagi, T. (2012). Fungal denitrification and nitric oxide reductase cytochrome P450nor. *Philosophical transactions of the Royal Society of London. Series B, Biological sciences*, *367*(1593), 1186–1194. https://doi.org/10.1098/rstb.2011.0335

Shoun, H., Kim, D. H., Uchiyama, H., & Sugiyama, J. (1992). Denitrification by fungi. *FEMS microbiology letters*, *73*(3), 277–281. https://doi.org/10.1016/0378-1097(92)90643-3

Silar P. (2019). Phenotypic instability in fungi. *Advances in applied microbiology*, *107*, 141–187. https://doi.org/10.1016/bs.aambs.2019.03.002

Silar, P., Haedens, V., Rossignol, M., & Lalucque, H. (1999). Propagation of a novel cytoplasmic, infectious and deleterious determinant is controlled by translational accuracy in Podospora anserina. *Genetics*, *151*(1), 87–95. https://doi.org/10.1093/genetics/151.1.87

Smith, S.A., Beaulieu, J.M., Donoghue, M.J. (2010). An uncorrelated relaxed-clock analysis suggests an earlier origin for flowering plants. Proceedings National Academy of Sciences of U.S.A. 107, 5897–5902. https://doi.org/10.1073/pnas.1001225107

Soltis, P. S., Marchant, D. B., Van de Peer, Y., & Soltis, D. E. (2015). Polyploidy and genome evolution in plants. *Current opinion in genetics & development*, 35, 119–125. https://doi.org/10.1016/j.gde.2015.11.003

Sonnenberg, A.S.M., Sedaghat-Telgerd, N., Lavrijssen, B. et al. Telomere-to-telomere assembled and centromere annotated genomes of the two main subspecies of the button mushroom Agaricus bisporus reveal especially polymorphic chromosome ends. Sci Rep 10, 14653 (2020). https://doi.org/10.1038/s41598-020-71043-5

Srinivas, C., Nirmala Devi, D., Narasimha Murthy, K., Mohan, C.D., Lakshmeesha, T.R., Singh, B., Kalagatur, N.K., Niranjana, S.R., Hashem, A., Alqarawi, A.A., Tabassum, B., Abd_Allah, E.F., Chandra Nayaka, S., Srivastava, R.K. (2019). *Fusarium oxysporum* f. sp. *lycopersici* causal agent of vascular wilt disease of tomato: Biology to diversity– A review. Saudi Journal of Biological Sciences 26, 1315–1324. https://doi.org/10.1016/j.sjbs.2019.06.002

Starnes, J. H., Thornbury, D. W., Novikova, O. S., Rehmeyer, C. J., & Farman, M. L. (2012). Telomere-targeted retrotransposons in the rice blast fungus *Magnaporthe oryzae*: agents of telomere instability. *Genetics*, 191(2), 389–406. https://doi.org/10.1534/genetics.111.137950

Steenwyk, J. L., & Rokas, A. (2018). Copy Number Variation in Fungi and Its Implications for Wine Yeast Genetic Diversity and Adaptation. *Frontiers in microbiology*, 9, 288. https://doi.org/10.3389/fmicb.2018.00288

Steenwyk, J., & Rokas, A. (2017). Extensive Copy Number Variation in Fermentation-Related Genes Among *Saccharomyces cerevisiae* Wine Strains. *G3* (Bethesda, Md.), 7(5), 1475–1485. https://doi.org/10.1534/g3.117.040105

Stranger, B. E., Forrest, M. S., Dunning, M., Ingle, C. E., Beazley, C., Thorne, N., Redon, R., Bird, C. P., de Grassi, A., Lee, C., Tyler-Smith, C., Carter, N., Scherer, S. W., Tavaré, S., Deloukas, P., Hurles, M. E., & Dermitzakis, E. T. (2007). Relative impact of nucleotide and copy number variation on gene expression phenotypes. Science (New York, N.Y.), 315(5813), 848–853. https://doi.org/10.1126/science.1136678

Strauss, J., Muro-Pastor, M. I., & Scazzocchio, C. (1998). The regulator of nitrate assimilation in ascomycetes is a dimer which binds a nonrepeated, asymmetrical sequence. *Molecular and cellular biology*, *18*(3), 1339–1348. https://doi.org/10.1128/MCB.18.3.1339

Stukenbrock, E.H., & Croll, D. (2014). The evolving fungal genome. Fungal Biology Reviews, 28(1), 1-12. https://doi.org/10.1016/j.fbr.2014.02.001.

Sun, L., Zhang, Y., Zhang, Z., Zheng, Y., Du, L., & Zhu, B. (2016). Preferential Protection of Genetic Fidelity within Open Chromatin by the Mismatch Repair Machinery. *The Journal of biological chemistry*, 291(34), 17692–17705. https://doi.org/10.1074/jbc.M116.719971

Takken, F., Rep, M. (2010). The arms race between tomato and *Fusarium oxysporum*. Molecular Plant Pathology 11, 309–314. https://doi.org/10.1111/j.1364-3703.2009.00605.x

Tashiro, S., Nishihara, Y., Kugou, K., Ohta, K., & Kanoh, J. (2017). Subtelomeres constitute a safeguard for gene expression and chromosome homeostasis. *Nucleic acids research*, 45(18), 10333–10349. https://doi.org/10.1093/nar/gkx780

Teunissen, H. A., Verkooijen, J., Cornelissen, B. J., & Haring, M. A. (2002). Genetic exchange of avirulence determinants and extensive karyotype rearrangements in parasexual recombinants of *Fusarium oxysporum*. Molecular genetics and genomics, 268(3), 298–310. https://doi.org/10.1007/s00438-002-0747-5

Todd, R. T., Forche, A., & Selmecki, A. (2017). Ploidy Variation in Fungi: Polyploidy, Aneuploidy, and Genome Evolution. *Microbiology spectrum*, 5(4), 10.1128/microbiolspec.FUNK-0051-2016. https://doi.org/10.1128/microbiolspec.FUNK-0051-2016

Torres, A. M., Weeden, N. F., & Martín, A. (1993). Linkage among isozyme, RFLP and RAPD markers in *Vicia faba*. *Theoretical and applied genetics*, 85(8), 937–945. https://doi.org/10.1007/BF00215032

Torres, D. E., Thomma, B., & Seidl, M. F. (2021). Transposable Elements Contribute to Genome Dynamics and Gene Expression Variation in the Fungal Plant Pathogen *Verticillium dahliae*. Genome biology and evolution, 13(7), evab135. https://doi.org/10.1093/gbe/evab135

Torres, D.E., Oggenfuss, U., Croll, D., & Seidl, M.F. (2020). Genome evolution in fungal plant pathogens: looking beyond the two-speed genome model. Fungal Biology Reviews, 34(3), 136-143. https://doi.org/10.1016/j.fbr.2020.07.001.

Toussoun, T.A., and Nelson, P.E. (1976). A Pictorial Guide to the Identification of *Fusarium* Species, Second Edition. Pennsylvania State University Press, University Park.

Turrà, D., El Ghalid, M., Rossi, F., Di Pietro, A. (2015). Fungal pathogen uses sex pheromone receptor for chemotropic sensing of host plant signals. Nature 527, 521–524. https://doi.org/10.1038/nature15516

Unkles, S. E., Heck, I. S., Appleyard, M. V., & Kinghorn, J. R. (1999). Eukaryotic molybdopterin synthase. Biochemical and molecular studies of *Aspergillus nidulans* cnxG and cnxH mutants. *The Journal of biological chemistry*, *274*(27), 19286–19293. https://doi.org/10.1074/jbc.274.27.19286

Unkles, S. E., Wang, R., Wang, Y., Glass, A. D., Crawford, N. M., & Kinghorn, J. R. (2004). Nitrate reductase activity is required for nitrate uptake into fungal but not plant cells. *The Journal of biological chemistry*, *279*(27), 28182–28186. https://doi.org/10.1074/jbc.M403974200

Unkles, S. E., Zhou, D., Siddiqi, M. Y., Kinghorn, J. R., & Glass, A. D. (2001). Apparent genetic redundancy facilitates ecological plasticity for nitrate transport. *The EMBO journal*, *20*(22), 6246–6255. https://doi.org/10.1093/emboj/20.22.6246

Untergasser A. "Preparation of Chemical Competent Cells" Untergasser's Lab. Winter 2008. http://www.untergasser.de/lab/protocols/competent_cells_chemical_v1_0.htm

van Dam, P., Fokkens, L., Schmidt, S.M., Linmans, J.H.J., Kistler, H.C., Ma, L.-J., Rep, M. (2016). Effector profiles distinguish *formae speciales* of *Fusarium oxysporum*: Effector profiles distinguish *Formae speciales* of Fo. Environmental Microbiology,18, 4087–4102. https://doi.org/10.1111/1462-2920.13445

Van Der Does, H.C., Lievens, B., Claes, L., Houterman, P.M., Cornelissen, B.J.C., Rep, M. (2008). The presence of a virulence locus discriminates *Fusarium oxysp*orum isolates causing tomato wilt from other isolates: A virulence locus defines f.sp. lycopersici. Environmental Microbiology 10, 1475–1485. https://doi.org/10.1111/j.1462-2920.2007.01561.x

Vasan, S., Deem, A., Ramakrishnan, S., Argueso, J. L., & Malkova, A. (2014). Cascades of genetic instability resulting from compromised break-induced replication. *PLoS genetics*, *10*(2), e1004119. https://doi.org/10.1371/journal.pgen.1004119

Veiga, F.F., Castro-Hoshino, L.V., Sato, F., Baesso, M.L., Silva, S., Negri, M., Svidzinski, T.I.E. (2022). Characterization of a biofilm formed by *Fusarium oxysporum* on the human nails. International Journal of Dermatology 61, 191–198. https://doi.org/10.1111/ijd.15747

Vidmar, J. J., Zhuo, D., Siddiqi, M. Y., Schjoerring, J. K., Touraine, B., & Glass, A. D. (2000). Regulation of high-affinity nitrate transporter genes and high-affinity nitrate influx by nitrogen pools in roots of barley. *Plant physiology*, *123*(1), 307–318. https://doi.org/10.1104/pp.123.1.307

Vlaardingerbroek, I., Beerens, B., Schmidt, S.M., Cornelissen, B.J.C., Rep, M. (2016). Dispensable chromosomes in *Fusarium oxysporum* f. sp. *lycopersici*. Molecular Plant Pathology 17, 1455–1466. https://doi.org/10.1111/mpp.12440

Vodenicharov, M. D., & Wellinger, R. J. (2006). DNA degradation at unprotected telomeres in yeast is regulated by the CDK1 (Cdc28/Clb) cell-cycle kinase. Molecular cell, 24(1), 127–137. https://doi.org/10.1016/j.molcel.2006.07.035

Wang, Q., Jiang, C., Wang, C., Chen, C., Xu, J. R., & Liu, H. (2017). Characterization of the Two-Speed Subgenomes of Fusarium graminearum Reveals the Fast-Speed Subgenome Specialized for Adaption and Infection. Frontiers in plant science, 8, 140. https://doi.org/10.3389/fpls.2017.00140

Wang, Q., Sun, M., Zhang, Y., Song, Z., Zhang, S., Zhang, Q., Xu, J. R., & Liu, H. (2020). Extensive chromosomal rearrangements and rapid evolution of novel effector superfamilies contribute to host adaptation and speciation in the basal ascomycetous fungi. *Molecular plant pathology*, 21(3), 330–348. https://doi.org/10.1111/mpp.12899

Wang, Y., Wu, J., Yan, J., Guo, M., Xu, L., Hou, L., Zou, Q. (2022). Comparative genome analysis of plant ascomycete fungal pathogens with different lifestyles reveals distinctive virulence strategies. BMC Genomics 23, 34. https://doi.org/10.1186/s12864-021-08165-1

Wessler S. R. (2006). Transposable elements and the evolution of eukaryotic genomes. Proceedings of the National Academy of Sciences of the United States of America, 103(47), 17600–17601. https://doi.org/10.1073/pnas.0607612103

West-Eberhard, M.J. (1989). Phenotypic Plasticity and the Origins of Diversity Annual Review of Ecology and Systematics, 20(1), 249-278.

Wicker, T., Sabot, F., Hua-Van, A., Bennetzen, J. L., Capy, P., Chalhoub, B., Flavell, A., Leroy, P., Morgante, M., Panaud, O., Paux, E., SanMiguel, P., & Schulman, A. H. (2007). A unified classification system for eukaryotic transposable elements. Nature reviews. Genetics, 8(12), 973–982. https://doi.org/10.1038/nrg2165

Wolfe, K. H., & Shields, D. C. (1997). Molecular evidence for an ancient duplication of the entire yeast genome. *Nature*, 387(6634), 708–713. https://doi.org/10.1038/42711

Wong, K. H., Hynes, M. J., & Davis, M. A. (2008). Recent advances in nitrogen regulation: a comparison between Saccharomyces cerevisiae and filamentous fungi. *Eukaryotic cell*, *7*(6), 917–925. https://doi.org/10.1128/EC.00076-08

Wrobel, Kazimierz, Wrobel, Katarzyna, Garcia Lara, B., Guerrero Esperanza, M., Roncero, M.I.G., Corrales Escobosa, A.R. (2020). Comparative evaluation of two F*usarium oxysporum* f. sp. *lycopersici* strains grown on two different carbon sources: LC-MS - based

secretome study after in vivo 15N metabolic labeling. International Journal of Mass Spectrometry 449, 116288. https://doi.org/10.1016/j.ijms.2019.116288

Wu, C., Kim, Y. S., Smith, K. M., Li, W., Hood, H. M., Staben, C., Selker, E. U., Sachs, M. S., & Farman, M. L. (2009). Characterization of chromosome ends in the filamentous fungus Neurospora crassa. Genetics, 181(3), 1129–1145. https://doi.org/10.1534/genetics.107.084392

Yang, H., Yu, H., & Ma, L. J. (2020). Accessory Chromosomes in Fusarium oxysporum. Phytopathology, 110(9), 1488–1496. https://doi.org/10.1094/PHYTO-03-20-0069-IA

Yang, L., Ukil, L., Osmani, A., Nahm, F., Davies, J., De Souza, C. P., Dou, X., Perez-Balaguer, A., & Osmani, S. A. (2004). Rapid production of gene replacement constructs and generation of a green fluorescent protein-tagged centromeric marker in *Aspergillus nidulans*. *Eukaryotic cell,* 3(5), 1359–1362. https://doi.org/10.1128/EC.3.5.1359-1362.2004

Yona, A. H., Manor, Y. S., Herbst, R. H., Romano, G. H., Mitchell, A., Kupiec, M., Pilpel, Y., & Dahan, O. (2012). Chromosomal duplication is a transient evolutionary solution to stress. *Proceedings of the National Academy of Sciences of the United States of America*, 109(51), 21010–21015. https://doi.org/10.1073/pnas.1211150109

Yu, J., Proctor, R.H., Brown, D.W., Abe, K., Gomi, K., Machida, M., Hasegawa, F., Nierman, W.C., Bhatnagar, D., Cleveland, T.E., 2004. Genomics of Economically Significant *Aspergillus* and *Fusarium Species*, in: Applied Mycology and Biotechnology. Elsevier, pp. 249–283. https://doi.org/10.1016/S1874-5334(04)80013-3

Zakian V. A. (1996). Structure, function, and replication of Saccharomyces cerevisiae telomeres. Annual review of genetics, 30, 141–172. https://doi.org/10.1146/annurev.genet.30.1.141

Zhang, F., Gu, W., Hurles, M. E., & Lupski, J. R. (2009). Copy number variation in human health, disease, and evolution. *Annual review of genomics and human genetics*, 10, 451–481. https://doi.org/10.1146/annurev.genom.9.081307.164217

Zhang, Y., Ma, L.J. (2017). Deciphering Pathogenicity of *Fusarium oxysporum* from a Phylogenomics Perspective. Advances in Genetics, Volume 100, Chapter 5. https://doi.org/10.1016/bs.adgen.2017.09.010

Zhang, Y., Rohde, L. H., & Wu, H. (2009). Involvement of nucleotide excision and mismatch repair mechanisms in double strand break repair. Current genomics, 10(4), 250–258. https://doi.org/10.2174/138920209788488544

Zumft W. G. (1997). Cell biology and molecular basis of denitrification. *Microbiology and molecular biology reviews: MMBR*, *61*(4), 533–616. https://doi.org/10.1128/mmbr.61.4.533-616.1997

ANNEXES

ANNEXES

Table S1. Loss rate (%) of chromosomes 13mini and 15 in wt, Δrad1, Δlig4 and Δku70 mutants during a long-term serial passaging experiment on YPDA plates (see Fig. 9).

wt-A	1	2	3	4	5	6	7	8	9	10
Chr13	96.5	101.9	57.3	96.5	31.2	48.4	5.9	55.9	92.6	3.4
Chr15	104.9	99.5	90.8	97.7	91.9	90.2	88.0	98.8	103.7	101.4
wt-B	1	2	3	4	5	6	7	8	9	10
Chr13	92.4	90.5	44.6	89.4	100.7	42.3	50.0	46.2	102.4	97.1
Chr15	103.6	98.5	78.0	60.1	87.1	94.2	67.4	81.1	98.3	62.4
wt-C	1	2	3	4	5	6	7	8	9	10
Chr13	32.9	99.4	95.0	76.7	60.5	78.0	79.7	101.0	32.6	101.5
Chr15	83.8	103.8	96.0	80.8	60.8	81.6	83.8	103.7	98.4	100.3
Δ*rad1* #2.1-A	1	2	3	4	5	6	7	8	9	10
Chr13	98.9	93.2	102.9	85.7	95.8	90.9	73.0	89.9	98.1	93.6
Chr15	89.0	80.1	92.1	57.3	46.7	56.1	37.2	100.8	96.2	99.1
Δ*rad1* #2.1-B	1	2	3	4	5	6	7	8	9	10
Chr13	97.9	102.1	98.0	95.4	104.3	88.9	89.8	72.1	101.3	84.1
Chr15	88.3	43.9	78.6	61.0	66.8	83.1	97.2	76.0	95.2	95.6
Δ*rad1* #2.1-C	1	2	3	4	5	6	7	8	9	10
Chr13	98.5	50.1	95.9	96.6	87.8	101.1	71.1	78.6	79.4	98.5
Chr15	98.8	63.1	85.5	61.0	65.6	90.4	47.1	80.3	98.3	34.1
Δ*rad1* #8.2-A	1	2	3	4	5	6	7	8	9	10
Chr13	101.5	98.7	103.6	98.7	103.7	103.2	88.7	102.8	100.2	97.7
Chr15	98.7	99.3	79.1	90.0	81.1	93.9	54.6	101.0	97.0	96.5
Δ*rad1* #8.2-B	1	2	3	4	5	6	7	8	9	10
Chr13	100.8	99.5	97.5	95.5	101.3	92.6	77.5	97.4	99.0	100.2
Chr15	91.8	47.4	82	82.6	76.4	46.9	25.2	81.7	86.9	84.9
Δ*rad1* #8.2-C	1	2	3	4	5	6	7	8	9	10
Chr13	47.4	23.1	93.3	96.9	86.1	54.4	53.8	90.9	82.4	72.0
Chr15	89.7	95.7	96.5	61.0	59.4	46.0	69.3	97.9	58.4	54.6

Δ*lig4* #3.1-A	1	2	3	4	5	6	7	8	9	10
Chr13	96.0	98.7	103.8	101.7	96.7	92.0	97.3	96.5	100.1	102.5
Chr15	69.8	97.1	96.8	37.9	43.6	77.0	88.2	61.9	24.1	95.7
Δ*lig4* #3.1-B	1	2	3	4	5	6	7	8	9	10
Chr13	81.9	95.7	62.7	93.07	98.8	85.0	75.1	99.0	82.9	99.5
Chr15	95.2	51.2	90.4	71.8	32.2	32.4	66.0	98.0	95.2	55.2
Δ*lig4* #3.1-C	1	2	3	4	5	6	7	8	9	10
Chr13	95.7	77.6	100.5	100.6	97.3	99.9	80.5	100.4	79.7	98.6
Chr15	98.9	100.3	94.9	97.0	56.4	92.9	96.3	93.7	97.0	48.9
Δ*lig4* #6.1-A	1	2	3	4	5	6	7	8	9	10
Chr13	81.4	85.9	98.2	96.9	75.2	85.1	99.1	95.7	100.8	102.1
Chr15	99.7	105.6	107.5	99.8	100.8	99.5	107.2	104.3	102.2	105.2
Δ*lig4* #6.1-B	1	2	3	4	5	6	7	8	9	10
Chr13	90.5	59.4	95.7	63.8	70.0	100.0	64.9	96.9	98.0	99.7
Chr15	102.0	91.3	101.7	62.9	52.9	78.5	39.6	96.5	98.4	95.7
Δ*lig4* #6.1-C	1	2	3	4	5	6	7	8	9	10
Chr13	104.2	99.2	95.2	96.6	99.6	105.6	91.0	101.2	103.3	98.1
Chr15	102.1	102.1	95.1	98.5	94.0	105.7	93.6	105.2	103.7	100.1
Δ*ku70* #7.2-A	1	2	3	4	5	6	7	8	9	10
Chr13	98.0	46.3	95.7	55.7	47.3	91.7	73.5	48.8	90.3	54.6
Chr15	96.0	99.3	97.1	80.6	82.7	79.0	55.1	97.6	95.2	97.8
Δ*ku70* #7.2-B	1	2	3	4	5	6	7	8	9	10
Chr13	95.1	98.6	54.0	81.4	59.2	94.3	97.8	95.8	65.4	98.1
Chr15	101.5	100.4	90.9	82.1	63.0	94.4	93.9	97.4	95.2	71.4

Δ*ku70* #7.2-C	1	2	3	4	5	6	7	8	9	10
Chr13	95.2	98.2	85.4	98.2	81.5	90.1	86.0	95.1	100.8	82.3
Chr15	90.9	98.4	92.3	42.2	51.8	76.7	62.2	95.2	90.3	57.4
Δ*ku70* #9.2-A	1	2	3	4	5	6	7	8	9	10
Chr13	98.9	98.4	97.2	82.1	97.3	54.3	92.5	59.7	100.1	97.4
Chr15	66.9	65.1	99.8	74.8	64.2	80.8	70.1	92.6	95.2	60.3
Δ*ku70* #9.2-B	1	2	3	4	5	6	7	8	9	10
Chr13	91.0	95.6	97.4	69.1	90.5	65.8	71.6	49.2	59.3	59.6
Chr15	93.5	95.1	87.1	71.6	77.7	70.6	31.3	95.6	90.6	91.3
Δ*ku70* #9.2-C	1	2	3	4	5	6	7	8	9	10
Chr13	103.4	105.2	99.7	103.6	98.0	105.9	98.1	100.6	99.0	103.7
Chr15	100.0	101.1	96.8	102.1	90.1	98.1	91.3	103.9	102.6	95.8